

FILM COOLING OF GAS TURBINE BLADES

by

N. W. Foster, B.Sc.

*Thesis submitted to the University of Nottingham
for the degree of Doctor of Philosophy, May 1976*

TO:

Gillian, Vera and Syd

C O N T E N T S

	<u>page</u>
ABSTRACT	i
ACKNOWLEDGEMENTS	ii
LIST OF FIGURES	iii
LIST OF PLATES	x
LIST OF TABLES	xi
NOMENCLATURE	xii

Chapter 1: Introduction

1.1 The Gas Turbine	1
1.2 Turbine Blade Cooling	3
1.3 Film Cooling	6
1.4 Film Cooling Parameters	9

Chapter 2: Literature Survey

2.1 General	12
2.2 <u>Experimental Techniques</u>	
2.2.1 Temperature Measurement	13
2.2.2 Concentration Measurement	14
2.3 Injectant to Mainstream Density Ratio	15
2.4 The Boundary Layer Displacement Thickness	17
2.5 The Pressure Gradient	20
2.6 Injection Geometry	22
2.7 Heat Transfer Coefficients	24
2.8 Theoretical Models and Correlations	25
2.9 Conclusion	28

Chapter 3: Objectives and Methods 29

Chapter 4: The Experimental Apparatus

4.1 The Wind Tunnel	39
4.2 <u>The Working Section</u>	
4.2.1 The Upstream Section	40
4.2.2 The Boundary Layer Bleed	40
4.2.3 Injection and Test Section	43
4.2.4 Downstream Sections	45
4.3 The Contours	46
4.4 The Traverse Gear	46
4.5 The Probe Traverse Gear	49
4.6 <u>The Secondary Flow Injection System</u>	49
4.6.1 Freon/Air Mixing Chamber	52
4.6.2 Plenum Chamber	52
4.6.3 Hole-Spacing Injection Plate	54

	<u>page</u>
4.7 <u>Gas Sampling and Analysis</u>	54
4.7.1 The Katharometer	57
4.7.2 The Iso-kinetic Sampling Probe	58
4.8 Boundary Layer Measurement	60
4.9 Conclusion	60
 <u>Chapter 5: The Experimental Programme</u>	 61
 <u>Chapter 6: The Experimental Procedure</u>	
6.1 Apparatus Checks	67
6.2 <u>Preliminary Adjustments</u>	
6.2.1 Boundary Layer Measurements	67
6.2.2 Pressure Gradient Measurements	68
6.3 <u>Test Procedure</u>	
6.3.1 Preliminaries	69
6.3.2 Tests	69
6.3.3 Traversing Steps	70
6.4 Tests above the Surface	71
6.5 Processing of Results	71-A
 <u>Chapter 7: Discussion of Results</u>	
7.1 <u>Injection at 90° to the Mainstream</u>	
7.1.1 The Effect of the Density Ratio	72
7.1.2 The Effect of Velocity Ratio	77
7.1.3 The Blowing and Momentum Parameters	79
7.1.4 The Effect of Pressure Gradient	87
7.1.5 The Effect of the Boundary Layer Thickness	92
7.1.6 The Effect of Hole Spacing	95
7.2 <u>Angled Injection</u>	
7.2.1 The Effect of Velocity Ratio	101
7.2.2 The Effect of Boundary Layer Thickness	108
7.2.3 The Effect of Injection Angle	111
 <u>Chapter 8: Further Discussion of Results</u>	
8.1 General	118
8.2 <u>Overall Effectiveness</u>	118
8.2.1 The Effect of Hole Spacing	119
8.2.2 The Effect of the Angle of Injection	121
8.3 <u>Distribution of Effectiveness</u>	124
8.3.1 The Effect of Hole Spacing	125
8.3.2 The Effect of Angled Injection	127
8.4 <u>The Aerodynamic Penalties</u>	
8.4.1 The Effect of Injectant Angle	127
8.5 Summary	133

Chapter 9: Models & Correlations9.1 The Bulk Mixing Models

9.1.1 Kelly's Model	136
9.1.2 Smith's Model	138

9.2 The Heat Sink Model	142
-------------------------	-----	-----	-----	-----	-----

9.3 Shaped Holes	145
------------------	-----	-----	-----	-----	-----

9.4 The J.F. Louis Correlation	150
--------------------------------	-----	-----	-----	-----	-----

9.5 Simple Jet Models	151
-----------------------	-----	-----	-----	-----	-----

9.6 <u>The Nottingham Correlation</u>	
---------------------------------------	-----	-----	-----	-----	--

9.6.1 Normal Injection	154
------------------------	-----	-----	-----	-----	-----

9.6.2 Hole Spacing	158
--------------------	-----	-----	-----	-----	-----

9.6.3 Angled Injection	160
------------------------	-----	-----	-----	-----	-----

9.6.4 Lateral Variation of Effectiveness	163
--	-----	-----	-----	-----	-----

9.7 Limitations of the Models	167
-------------------------------	-----	-----	-----	-----	-----

Chapter 10: Conclusions

10.1 Injectant to Mainstream Density Ratio	172
--	-----	-----	-----	-----

10.2 Boundary Layer Displacement Thickness	172
--	-----	-----	-----	-----

10.3 Pressure Gradients	172
-------------------------	-----	-----	-----	-----

10.4 Hole Spacing	173
-------------------	-----	-----	-----	-----

10.5 Angle of Injection	173
-------------------------	-----	-----	-----	-----

10.6 Correlations & Theories	174
------------------------------	-----	-----	-----	-----

10.7 The Applicability of the Current Work	175
--	-----	-----	-----	-----

10.8 Final Conclusion	177
-----------------------	-----	-----	-----	-----

10.9 Recommendations for Further Work	177
---------------------------------------	-----	-----	-----	-----

REFERENCES	179
------------	-----	-----	-----	-----	-----

APPENDIX 1: The Two-Dimensionality of the Flow and Repeatability of the Results	A.1
---	-----	-----	-----	-----

APPENDIX 2: Calibration of Orifice Plates	A.5
---	-----	-----	-----	-----

APPENDIX 3: Calibration and Use of the Katharometer	A.7
---	-----	-----	-----	-----

APPENDIX 4: Iso-kinetic Sampling	A.11
----------------------------------	-----	-----	-----	------

APPENDIX 5: The Experimental Data	A.15
-----------------------------------	-----	-----	-----	------

===ooOoo===

A B S T R A C T

An experimental apparatus was designed and built to study the film cooling effectiveness from a single row of holes at various angles and hole spacings, using a foreign gas technique. Mixtures of Freon 12 and air were injected into an air mainstream to give a range of density ratios encompassing the values found in a gas turbine.

The density ratio was found to be of importance and none of the commonly used parameters - e.g. blowing parameters - can be used to scale results, unless the density ratio is correctly modelled.

The boundary layer thickness was varied independently of other parameters, and an increase in thickness was found to decrease the effectiveness, for normal and angled injection geometries, for 20 hole diameters downstream. Favourable and adverse pressure gradients over the injection holes were tested and found to have little effect on the film cooling effectiveness.

Changing the hole spacing produced considerable variations, with the smallest hole spacing giving the best performance in all respects. A hole spacing of greater than 3.75 diameters was found to be the maximum to give overall coverage above 0.10 effectiveness.

The injection angle was also investigated and for low blowing rates the shallow angles gave the best results; but at high blowing rates, i.e. greater than 1.4, normal injection gave the best performance as the shallow angles rapidly became detached from the surface with increasing velocity ratio. The normal injection was also superior in terms of lateral distribution of coolant at all values of blowing rate.

A correlation was proposed that included the density and velocity ratios and hole spacing for normal injection and, in a modified form, for angled injection at 3 diameter spacings. This was found to work well for the experimental results obtained here and by other researchers.

A C K N O W L E D G E M E N T S

The author wishes to thank those who have assisted in the experimental programme and in the preparation of this thesis: Prof. A. G. Smith for the use of the laboratories and excellent facilities of the Department of Mechanical Engineering; Mr. D. Lampard for his assistance, direction and encouragement throughout the entire project; Mr. V. Hawley and his staff for their help with the construction of the experimental apparatus, and finally, Mrs. G. Foster for her patience and efforts in front of the typewriter.

L I S T O F F I G U R E S

	<u>page</u>
<u>Chapter 1</u>	
<i>Fig.1.1</i> Schematic cross-sectional view of a typical jet engine and a graph giving pressures, temperatures and velocities through the engine from reference 2.2	2
<i>Fig.1.2</i> The rise in turbine entry temperature over the last 30 years	4
<i>Fig.1.3</i> Cross-sectional drawing of an hypothetical cooled turbine blade	5
<i>Fig.1.4</i> Film cooling configurations	7
<i>Fig.1.5</i> Parameters influencing the performance of a single row of holes and the co-ordinate system used in the present work	10
<u>Chapter 2</u>	
<i>Fig.2.1a</i> Spanwise averaged effectiveness, $\bar{\eta}$, plotted against dimensionless distance downstream X/D , from Liess (2.12 fig.19)	19
<i>Fig.2.1b</i> Variation of spanwise averaged effectiveness, $\bar{\eta}$ with boundary layer displacement thickness, δ^*/D , from Liess (2.12 fig.25)	19
<u>Chapter 4</u>	
<i>Fig.4.1</i> The working section	41
<i>Fig.4.2</i> The boundary layer bleed	42
<i>Fig.4.3</i> Profiles of contours in the working section ...	47
<i>Fig.4.4</i> The injection plate traverse gear	48
<i>Fig.4.5</i> The probe traverse gear	50
<i>Fig.4.6</i> The secondary flow system	51
<i>Fig.4.7</i> Sketch of the Freon 12/air mixing chamber ...	53
<i>Fig.4.8</i> Variable hole spacing injection plate	55

	<u>page</u>
<i>Fig.4.9</i> The gas sampling system	56
<i>Fig.4.10</i> The katharometer	59
 <u>Chapter 6</u>	
<i>Fig.6.1</i> Lateral positions of downstream traverses ...	71
 <u>Chapter 7</u>	
<i>Fig.7.1</i> The effect of varying density ratio on the downstream distribution of the spanwise averaged effectiveness, η	73
<i>Fig.7.2</i> Contours of constant effectiveness downstream of the injection hole for 90° injection with $U_j/U_\infty = 0.7$ and $\rho_j/\rho_\infty = 2.5$	75
<i>Fig.7.3</i> The effect of varying density ratio on the centreline distribution of effectiveness ...	76
<i>Fig.7.4</i> The effect of varying velocity ratio on the downstream distribution of spanwise averaged effectiveness, η	78
<i>Fig.7.5</i> The effect of varying velocity ratio on the centreline distribution of effectiveness, $\hat{\eta}$...	80
<i>Fig.7.6</i> Graph of centreline effectiveness, $\hat{\eta}$, against blowing parameter, M , for varying density and velocity ratios at $X/D = 6.53$	81
<i>Fig.7.7</i> Graph of centreline effectiveness, $\hat{\eta}$, against momentum parameter, I , for varying density and velocity ratios at $X/D = 6.53$	83
<i>Fig.7.8</i> Graph of centreline effectiveness, $\hat{\eta}$, against blowing parameter, M , for varying density and velocity ratios at $X/D = 23.78$	84
<i>Fig.7.9</i> Graph of centreline effectiveness, $\hat{\eta}$, against momentum parameter, I , for varying density and velocity ratios at $X/D = 23.78$	85
<i>Fig.7.10</i> Graph of centreline effectiveness, $\hat{\eta}$, against blowing parameter, M , for varying density and velocity ratios at $X/D = 73.72$	86
<i>Fig.7.11</i> Variation of the distribution of spanwise averaged effectiveness, η , with pressure gradient for normal injection with $S/D = 3$...	88

	<u>page</u>
<i>Fig.7.12</i> Variation of centreline effectiveness, $\hat{\eta}$, with pressure gradient for normal injection with $S/D = 3$	89
<i>Fig.7.13a</i> Contours of constant injectant concentration in the absence of a pressure gradient for normal injection with $S/D = 3$ and at $X/D = 4.25$	90
<i>Fig.7.13b</i> Contours of constant injectant concentration in the presence of a pressure gradient for normal injection with $S/D = 3$ and at $X/D = 4.25$	90
<i>Fig.7.14</i> Downstream distribution of spanwise averaged effectiveness, $\bar{\eta}$, with varying boundary layer displacement thickness, δ^*/D	93
<i>Fig.7.15a</i> Contours of constant injectant concentration at $X/D = 4.25$ and $\delta^*/D = 0.16$ for normal injection with $S/D = 3$	94
<i>Fig.7.15b</i> Contours of constant injectant concentration at $X/D = 4.25$ and $\delta^*/D = 0.24$ for normal injection with $S/D = 3$	94
<i>Fig.7.16</i> The effect of hole spacing, S/D , on the downstream distribution of spanwise averaged effectiveness	96
<i>Fig.7.17</i> Comparison with results of other experimenters, spanwise averaged effectiveness against equivalent slot widths downstream	98
<i>Fig.7.18</i> The effect of hole spacing, S/D , on the downstream distribution of spanwise averaged effectiveness, $\bar{\eta}$	100
<i>Fig.7.19</i> The effect of varying velocity ratio on the downstream distribution of spanwise averaged effectiveness, $\bar{\eta}$, for 35° injection angle	102
<i>Fig.7.20</i> Contours of constant effectiveness for a 35° injection angle (a) $M = 0.49$; (b) $M = 1.04$; (c) $M = 1.37$; (d) $M = 2.43$	103
<i>Fig.7.21a</i> Comparison with the results of Liess (7.3) and Goldstein et al (7.10)	105
<i>Fig.7.21b</i> Comparison with results of Smith (7.2)	106
<i>Fig.7.22</i> Sketch showing areas of possible heat flow in a non-adiabatic wall	107

	<u>page</u>
<i>Fig.7.23-</i> Downstream distribution of spanwise averaged effectiveness, $\bar{\eta}$, with varying boundary layer displacement thickness for 35° injection angle	109
<i>Fig.7.24</i> Comparison of variation of spanwise averaged effectiveness, $\bar{\eta}$, with boundary layer displacement thickness, δ^*/D , with results from Liess (7.3)	110
<i>Fig.7.25</i> Variation of downstream distribution of spanwise averaged effectiveness, $\bar{\eta}$, with injection angle	112
<i>Fig.7.26</i> Contours of constant injectant concentration at $X/D = 4.25$, $M = 1.4$ for: (a) 35°; (b) 55°; (c) 90° injection angle	114
<i>Fig.7.27</i> Vertical distribution on the centreline of injectant concentration, C/C_j for 35°, 55° and 90° injection angle	115
<i>Fig.7.28</i> Comparison of velocity profiles with those of Pai et al (7.8)	117

Chapter 8

<i>Fig.8.1</i> Variation of averaged effectiveness, $\bar{\eta}$, with hole spacing, S/D , and blowing parameter, M ..	120
<i>Fig.8.2</i> Variation of averaged effectiveness, $\bar{\eta}$, with blowing rate for $S/D = 2.5$	122
<i>Fig.8.3</i> Variation of averaged effectiveness, $\bar{\eta}$, with injection angle and blowing parameter, M ...	123
<i>Fig.8.4a</i> Variation of minimum effectiveness, $\check{\eta}$, with hole spacing, S/D , and blowing parameter, M ..	126
<i>Fig.8.4b</i> Variation of lateral effectiveness gradient $\frac{\hat{\eta} - \check{\eta}}{S/D}$, with hole spacing, S/D , and blowing parameter, M	126
<i>Fig.8.5a</i> Variation of minimum effectiveness, $\check{\eta}$, with injection angle, β , and blowing parameter, M	128
<i>Fig.8.5b</i> Variation of lateral effectiveness gradient, $\frac{\hat{\eta} - \check{\eta}}{S/D}$ with injection angle, β , and blowing parameter, M	128

	<u>page</u>
<i>Fig.8.6</i> Vertical distribution on the centreline of injectant concentration and velocity for normal injection at two blowing parameters: M = 1.39 and 2.44 	129
<i>Fig.8.7</i> Vertical distribution on the centreline of injectant concentration and velocity for 35° injection at two blowing parameters: M = 1.38 and 2.43 	130
 <u>Chapter 9</u>	
<i>Fig.9.1</i> Comparison of predictions from the bulk mixing model with the experimental data obtained for normal injection 	137
<i>Fig.9.2</i> Graphs of $\log_{10}(\frac{1}{\bar{\eta}} - 1)$ against $\log_{10}(X/D)$ (Smith, (9.2)). 	140
<i>Fig.9.3</i> Comparison of predictions of spanwise averaged effectiveness distribution using the point source model (9.3) (ϵ_p evaluated by two different methods), with the exper- imental data 	144
<i>Fig.9.4</i> Comparison of predictions of vertical dis- tribution of injectant concentration on the centreline from the point source model (9.3) with the experimental data 	146
<i>Fig.9.5</i> Centreline effectiveness, $\bar{\eta}$, as a function of blowing parameter divided by area ratio, M/R, from ref.9.4 	148
<i>Fig.9.6</i> (a), (b), (c): lateral distribution of effectiveness with injection through cylind- rical and shaped holes. (d): comparison of centreline effectiveness values from (a) and (c), plotted against a function of downstream distance 	149
<i>Fig.9.7</i> Graph of spanwise averaged effectiveness, $\bar{\eta}$, plotted against $(\cos^2\beta)^{-1.35} X/D$ (ref.9.5) for two injection angles: 35° and 55° 	152
<i>Fig.9.8</i> Vertical distribution of injectant concen- tration compared with theoretical distri- bution 	153

	<u>page</u>
<i>Fig. 9.9</i> Correlation of spanwise averaged effectiveness, η , for normal injection and $S/D = 3$...	156
<i>Fig. 9.10</i> Comparison of predicted and experimental values of spanwise average effectiveness distribution	157
<i>Fig. 9.11</i> Correlation of spanwise average effectiveness for normal injection	159
<i>Fig. 9.12</i> Comparisons of predicted and experimental values of spanwise averaged effectiveness, η for normal injection	161
<i>Fig. 9.13</i> Correlation applied to 35° injection angle ...	162
<i>Fig. 9.14</i> Modified correlation for angled injection with $S/D = 3$	164
<i>Fig. 9.15a</i> Correlation for angled injection applied to the results of Liess (9.8)	165
<i>Fig. 9.15b</i> Correlation for angled injection applied to the results of Goldstein et al (9.9)	166
<i>Fig. 9.16</i> Comparison of the measured with the predicted lateral distribution of effectiveness ...	168

Appendix 1

<i>Fig. A1.1</i> Velocity profiles on, and either side of, the centreline without injection	A.2
<i>Fig. A1.2</i> Contours of constant effectiveness	A.3

Appendix 2

<i>Fig. A2.1</i> Predicted and measured flow rates through two of the orifice plates	A.6
---	-----

Appendix 3

<i>Fig. A3.1</i> Graph of $\log_{10} \frac{\rho^2 C_p}{\mu k}$ against $\log_{10} V^2$ for calibration of the katharometer	A.8
---	-----

Appendix 4

Fig.A4.1 Sketch of isokinetic testing apparatus ... A.12

Fig.A4.2 Sketches showing possible effect of not
sampling isokinetically A.14

L I S T O F P L A T E S

(following) page:

<i>Plate 4.1</i>	A general view of the experimental apparatus	40
<i>Plate 4.2</i>	View of the working section showing the secondary and mainstream flow controls	... 40
<i>Plate 4.3</i>	View of the working section and instrument- ation 41
<i>Plate 4.4</i>	The normal and 55° injection plates 45
<i>Plate 4.5</i>	The adverse pressure gradient contour	... 46

L I S T O F T A B L E S

	<u>page</u>
<u>Chapter 1</u>	
TABLE 1.1 Typical parameters for a film cooled Turbine Blade 	11
<u>Chapter 2</u>	
TABLE 2.1 Table of the parameters covered by other Researchers 	13a
<u>Chapter 5</u>	
TABLE 5.1 Details of Test parameters and Run numbers ...	66
<u>Chapter 8</u>	
TABLE 8.1 Boundary Layer details at $X/D = 60.6$	132
TABLE 8.2 Summary of Injection Angle Comparisons ...	134
<u>Chapter 9</u>	
TABLE 9.1 Ranges of downstream distance over which the Models predict effectiveness to within 0.05 and 0.01 	169
<u>Appendix 5</u>	
TABLE A5.1 Details of Main Test parameters for each Series of Runs in Table A5.2 	A.16
TABLE A5.2 Tables of effectiveness and Injectant Concentration (expressed as percentages) and Velocity Ratio: for the overall condition outlined in Table 5.1 	A.17

N O M E N C L A T U R E

- A, area;
- C, mass concentration of gas;
- C_p , specific heat;
- D, diameter of cooling holes;
- h, heat transfer coefficient;
- h' , enthalpy;
- H, ratio of boundary layer displacement to momentum thickness δ^*/θ ;
- H_1 , height of water;
- I, momentum parameter $\frac{\rho_j U_j^2}{\rho_\infty U_\infty^2}$;
- K, constant ;
- k, thermal conductivity;
- M, blowing parameter or blowing rate $\frac{\rho_j U_j}{\rho_\infty U_\infty}$;
- \dot{m} , mass flow rate;
- \dot{m}_{ent} , entrained mass flow rate
- \dot{m}_e , entrained mass flow rate per unit lateral distance;
- N, number of holes in a row;
- p, pressure;
- \dot{q} , heat flow rate per unit area;
- r, radius;
- R, ratio of exit to entrance area for a shaped hole;
- R_e , Reynolds number;
- S, distance between holes in a single row;

- S_1 , equivalent slot height $\frac{\pi D^2}{4S}$;
- S_2 , equivalent slot height $\frac{\pi D^2}{4D}$;
- T , temperature;
- U , velocity;
- \hat{U} , velocity on the centreline of a jet;
- X , downstream distance;
- \bar{X} , film cooling parameter;
- \bar{X}_1 , film cooling parameter;
- X_s , slot width;
- Y , vertical distance;
- Y_o , height of source above surface in equation 9.6;
- Y_s , height of slot;
- Z , lateral distance.
- β , angle of injection;
- δ , boundary layer thickness;
- δ^* , boundary layer displacement thickness $\int_0^\infty (1 - \frac{\rho U}{\rho_\infty U_\infty}) dy$;
- ϵ_p , turbulent diffusivity;
- η , effectiveness $\frac{T_{aw} - T_\infty}{T_j - T_\infty}$;
- η' , effectiveness based on enthalpy $\frac{h'_{aw} - h'_\infty}{h'_j - h'_\infty}$;
- $\hat{\eta}$, effectiveness on centreline;
- $\check{\eta}$, minimum effectiveness;
- $\bar{\eta}$, spanwise average effectiveness $\frac{1}{s} \int_{-\frac{s}{2}}^{\frac{s}{2}} dz$;
- $\bar{\bar{\eta}}$, average effectiveness $\frac{1}{X_2 - X_1} \int_{X_1}^{X_2} \bar{\eta} dX$;

- θ , boundary layer momentum thickness $\int_0^{\infty} (1 - \frac{U}{U_{\infty}}) \frac{\rho U}{\rho_{\infty} U_{\infty}} dy$;
- μ , kinematic viscosity;
- ν , dynamic viscosity;
- ρ , density;
- ϕ , temperature difference: $T - T_{\infty}$;
- ϕ_1 , temperature difference: $T_j - T_{\infty}$;

Subscripts:

- aw, adiabatic wall;
- j, injectant;
- s, slot
- w, wall
- 1, $\left. \begin{array}{l} \} \\ \} \end{array} \right\}$ gas stream components;
- 2, $\left. \begin{array}{l} \} \\ \} \end{array} \right\}$
- δ , boundary layer;
- ∞ , mainstream.

CHAPTER 1 : INTRODUCTION

This Chapter introduces the subject of film cooling and explains the need for film cooling research. It also introduces the problems associated with such research.

=====

1.1 The Gas Turbine

An aircraft powerplant should, ideally, have a high power to weight ratio, be reliable, have a low level of mechanical vibration and be economical at high speeds. The gas turbine satisfies all these demands except, perhaps, the last one; but it offers speeds in excess of all means of propulsion other than rocket propulsion and, because of this, aircraft and gas turbines have developed rapidly in the last thirty years.

A sectional view of a gas turbine engine is shown in fig. 1.1. Air is drawn into the engine and compressed by a rotating compressor, after which it passes to a combustion chamber where fuel is added and the mixture burns with a continuous flame. The hot exhaust products pass through the turbine, driving it round, before passing out of the engine via a nozzle. The compressor is driven by the turbine via one or more shafts.

From this simplified picture, and from the graphs at the foot of fig.1.1, it will be clear that the turbine operates in

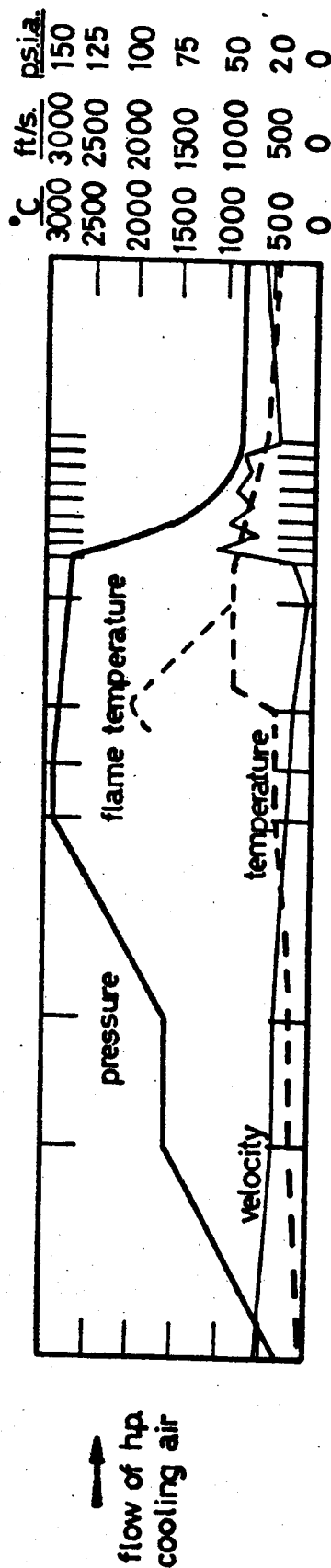
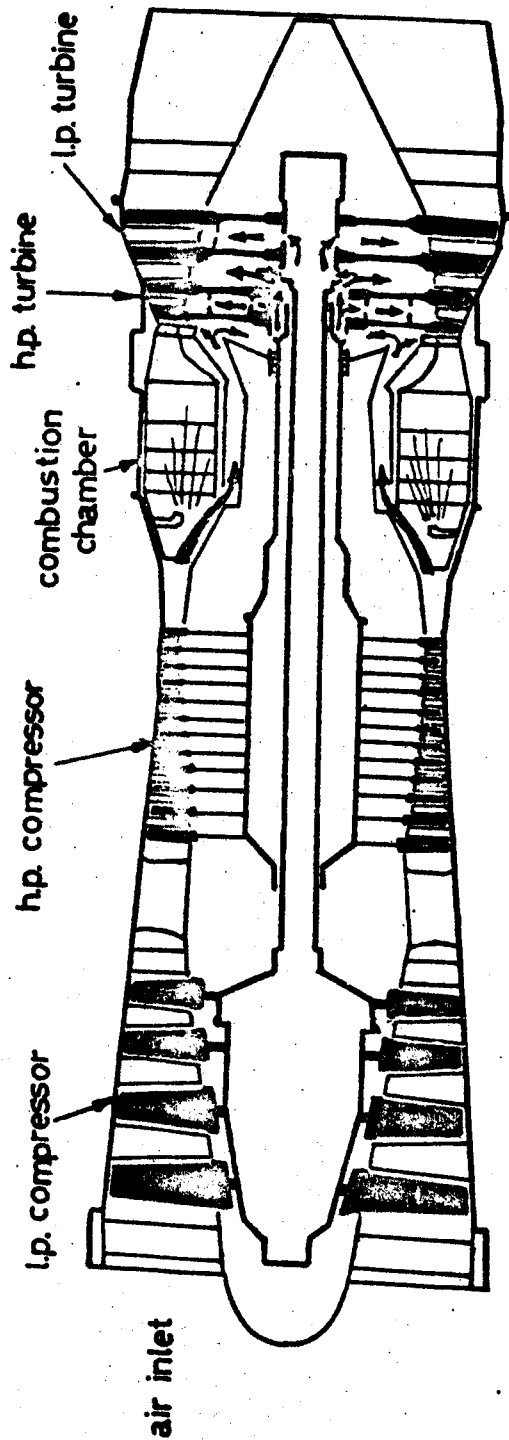


Fig. 1.1 Schematic cross-sectional view of a typical jet engine and a graph giving pressures, temperatures and velocities through the engine from reference 2.2

a hostile environment composed of combustion products at high temperatures and pressures.

To achieve the high power to weight ratio, a gas turbine has to have high component efficiencies, including a high turbine efficiency, and efforts are always being made to raise them yet higher. The isentropic efficiency of a turbine can be increased by raising the temperature drop across the turbine. This in turn can be achieved by raising the turbine entry temperature. The result of this has been a steady rise in turbine entry temperatures, as shown in fig 1.2. Initially, the rise in temperature was met by improved materials, but in the 1950's, the cooled blades came into operation and improvements in blade cooling techniques permitted a more rapid rise of turbine entry temperatures.

1.2 Turbine Blade Cooling

Three basic methods are used in current engines to cool the turbine blades and the static vanes. These are:-

- (i) convection cooling
- (ii) impingement cooling
- (iii) film cooling.

Fig 1.3 shows a cross section of an hypothetical blade. The cooling air which is taken from the high pressure end of the compressor is fed into internal passages within the blade via the blade root. The air cools the blade by convection as it passes along the passages, which are often elliptical in

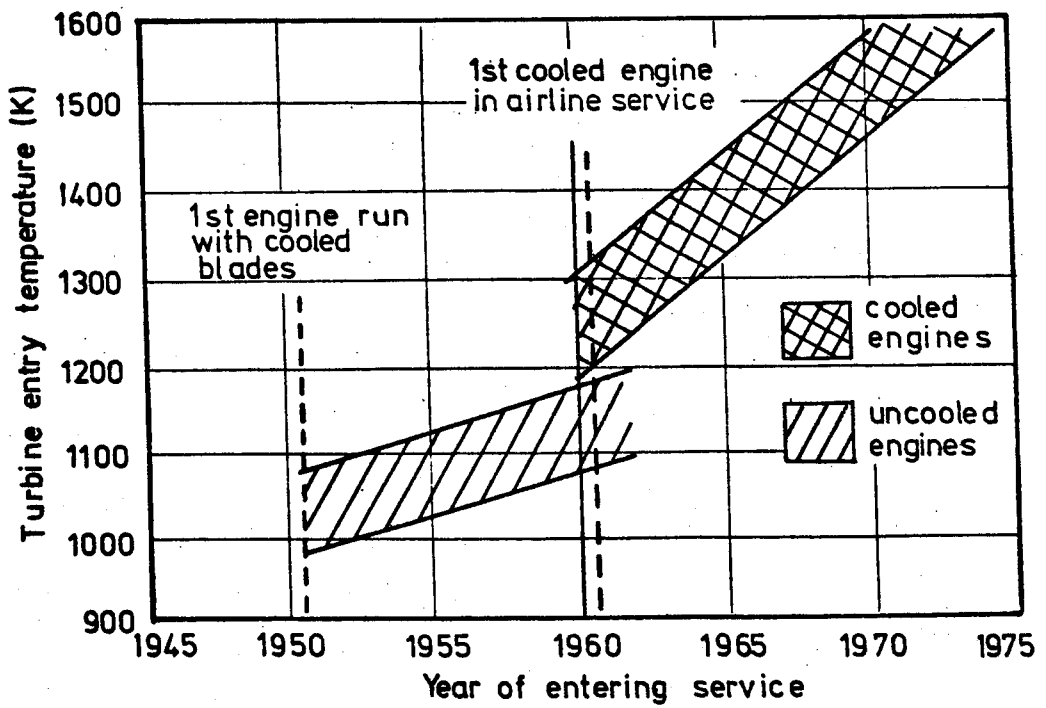


Fig.1.2 The rise in turbine entry temperature over the last 30 years

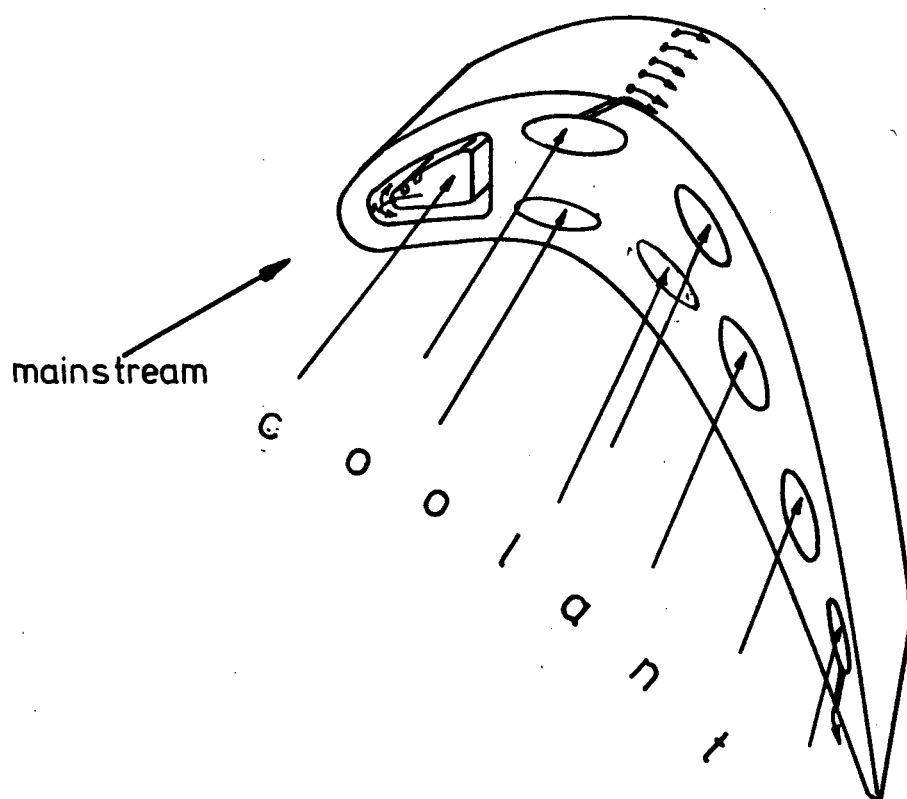


Fig. 7.3 Cross-sectional drawing of an hypothetical cooled turbine blade

shape to increase the surface area, and may have turbulence-promoting projections inside to increase the heat transfer. In some cases this passage contains an insert which has holes in it to permit jets of coolant to impinge on the inside of the blade wall, again increasing the heat transfer rate.

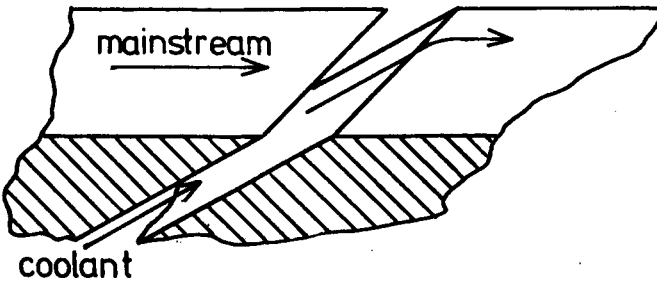
Additional use of the cooling air can be made by allowing some of the air to pass through the surface of the blade, thus forming on the outside a layer of coolant protecting the blade surface from the hot mainstream. The latter technique is called film cooling.

This work is concerned only with film cooling, although it must be stated that the optimum cooling system utilises film cooling and convection cooling, as outlined by Colladay (1.1).

1.3 Film Cooling

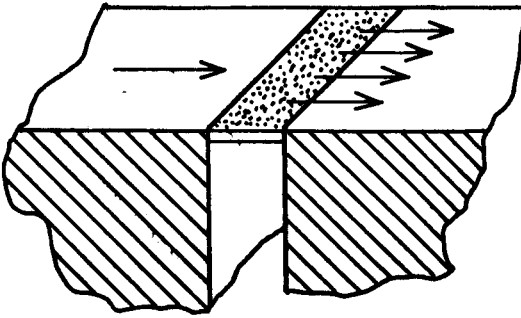
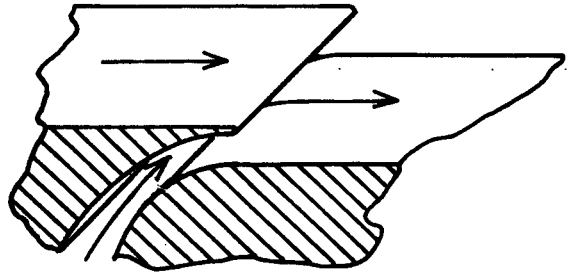
There are several ways in which the coolant can be brought to the surface of a blade for film cooling. Fig 1.4a shows a slot arrangement which is used in some applications, and fig 1.4b a similar system using a rearward facing step. Fig 1.4c shows an arrangement using a porous surface, a method known as transpiration cooling.

All three methods are at present unsatisfactory for use in turbine blades, due to the very high levels of stress produced by the high rotational speeds and the clogging of any porous surfaces with dirt. However, the transpired turbine



(a) Angled slot

(b) Rearward facing step



(c) Porous surface

(d) Discrete holes

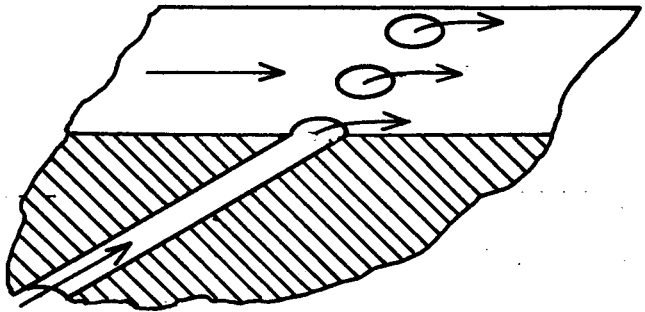


Fig.1.4 Film cooling configurations

blade does hold possibilities for the future and offers a very high degree of protection (1.2).

This leaves film cooling via discrete holes, fig 1.4d. Either single or multiple row or full coverage film cooling is possible, but this work only considers film cooling from a single row of discrete holes.

In film cooling a heat transfer coefficient, h , is usually defined such that

$$\dot{q} = h (T_w - T_{aw})$$

where T_w is the local wall temperature and T_{aw} the wall temperature if there were no conduction through, or along, the walls, that is, an adiabatic wall temperature.

With no film T_{aw} would be equal to the freestream temperature for low speed flow, or the recovery temperature in a high speed flow. As the heat transfer coefficient is not usually very different with or without film cooling (although opinions do differ as Chapter 2 shows), the determination of the adiabatic wall temperature is most important.

A dimensionless adiabatic wall temperature, η , is usually used, which is defined as

$$\eta = \frac{T_{aw} - T_{\infty}}{T_j - T_{\infty}}$$

for low speed flows and is commonly termed the "film cooling effectiveness". Thus, if η is known, the heat transfer rate

to the blade, and hence the blade metal temperatures, can be calculated.

As the fatigue and creep life of a blade falls rapidly with increasing blade temperature, the designer needs to know the bulk blade temperatures to within a few degrees. This means that he also needs to know the film cooling effectiveness with considerable accuracy, say to within 0.03.

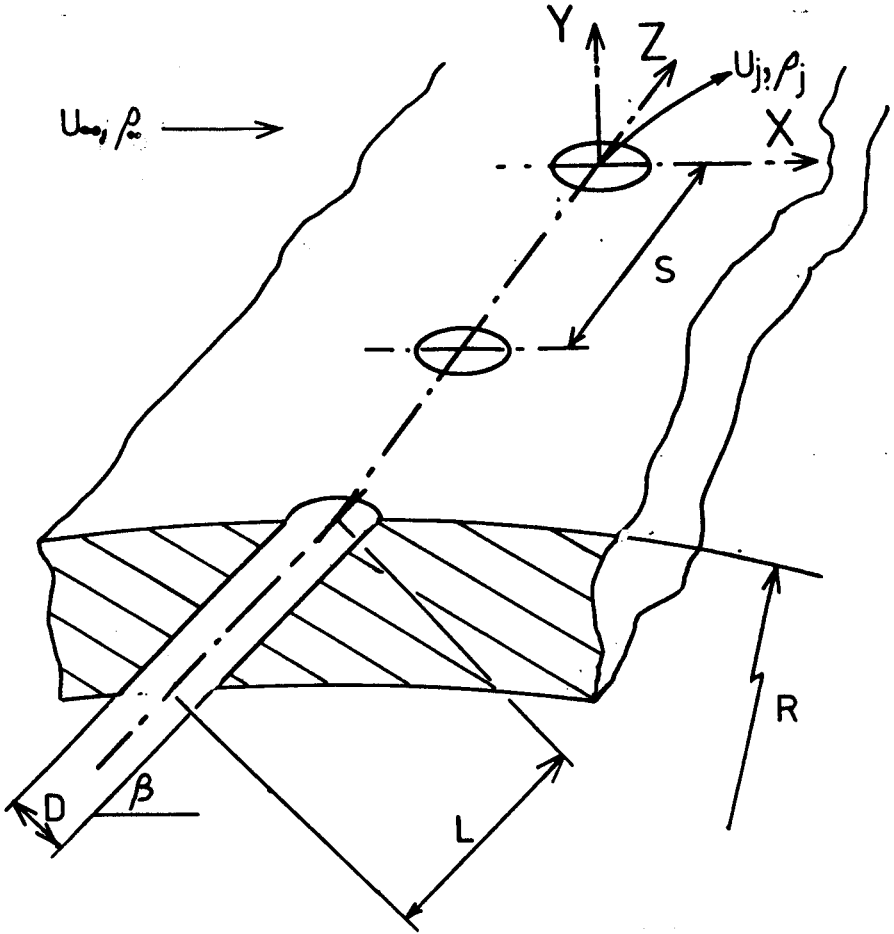
1.4 Film Cooling Parameters

Fig.1.5 lists those parameters which might be expected to have an effect on the film cooling effectiveness. They are divided into geometric parameters, which are concerned with the physical geometry of the blade and cooling holes, and flow parameters which describe the flow of both the mainstream and injectant, generally in non-dimensional terms.

In Table 1.1 are presented typical values found in gas turbines for the parameters of fig.1.5 and other parameters.

The correct modelling of all these parameters in a theoretical study, or the reproduction of the values in Table 1.1 in an experimental programme without actually using a gas turbine (which would be a slow and costly process), or the scaling of the parameters, presents a real problem for a researcher in this field.

The following chapters explain how the problem was approached in the current research, and present the results and conclusions obtained.



GEOMETRIC: Hole diameter, D
 Hole spacing, S
 Hole inclination, β
 Surface Curvature, R

FLOW: Density ratio, ρ_j/ρ_∞
 Velocity ratio, U_j/U_∞
 Pressure gradient, $\Delta p/X$
 Boundary layer, $\delta, \delta^*/D, \theta$
 Blowing parameter, $M = \rho_j U_j / \rho_\infty U_\infty$
 Turbulence intensity.

Fig.1.5 Parameters influencing the performance of a single row of holes and the co-ordinate system used in the present work.

	<u>Mainstream</u>	<u>Injectant</u>
Temperature (K)	1500	700 - 1000
Pressure (bar)	13	20
Reynolds Number	10^6	$1 \text{ to } 3 \times 10^4$
Mass flux ratio	0.1 to 2	
Density ratio	1 to 2	
Turbulence intensity	8%	
Boundary layer displacement thickness (m)	3×10^{-6} to 4×10^{-5}	
Injection hole diameter (m)	0.25×10^{-3} to 0.75×10^{-3}	
Hole spacing	2.5 diameters minimum	
Number of rows	Variable	

TABLE 1.1 Typical parameters for a film cooled Turbine Blade

CHAPTER 2 : LITERATURE SURVEY

This chapter reviews previously published works on film cooling which are relevant to the present study, and shows the need for the current work.

=====

2.1 General

A great deal of research has been done into film cooling during the last fifteen years; mostly, however, this effort has been concentrated on film cooling via slots and rearward facing steps and, to a lesser extent, on transpiration cooling. In comparison with this, there is relatively little data on film cooling with discrete hole injection, and even less in the way of a theoretical approach to the problem.

Unless it serves to illustrate a particular point, this survey ignores the large volume of work in which two-dimensional injection geometry is used, as a good survey of such work was published in 1971 by Goldstein (2.1) and a further survey by Smith (2.2) in 1974.

Table 2.1 presents a synopsis of the current survey and includes those parameters which the author feels to be of importance. The table will be referred to throughout the survey, which deals primarily with injection via a row of holes.

2.2 Experimental Techniques

Basically, two different techniques have been used to measure film cooling effectiveness: either a temperature measurement technique using a heated injectant or mainstream, or a foreign gas technique, involving the measurement of the concentration of the injectant, or some constituent of the injectant. A discussion of the relative merits of these methods is included in Chapter 3.

2.2.1 Temperature Measurement

R. J. Goldstein et al in a series of experiments (2.3, 2.4, 2.5, 2.6) have used the temperature technique to provide data on film cooling effectiveness, with a low speed wind tunnel and thermocouples to measure the adiabatic wall temperatures. Metzger et al (2.7, 2.8, 2.9) have also used a low speed wind tunnel to provide effectiveness data, which they obtain via the heat transfer coefficient. They had two wind tunnels - one, of rather small cross section, measuring 2" x 0.5"; the other, more realistically, measuring 16" x 6".

Lander and Fish (2.10) used a combustion chamber to provide a hot mainstream for a cascade of blades, where they measured the effectiveness on a blade under steady state conditions. Liess et al (2.11, 2.12) have also carried out tests to provide data at higher Mach numbers using the temperature technique.

Jones and Schultz (2.13) and Smith (2.2) employed a

ref.	slots	single hole	No. of rows	injectn angle	β_i/β_e	M	δ^*/D	$\Delta p/X$	heat transfer	η	theoretical	experimental	notes
2.1													
2.2	x		1, 2	30°, 90°	> 1					x		x	review
2.3		x		35°, 90°	< 1	0.1-2				x		x	shock tunnel
2.4			1	15°, 35°	< 1	0.5-2	0.05-0.08			x		x	35° spanwise in hole
2.5		x		35°, 90°	< 1	0.1-2				x		x	
2.6			1	35°	< 1+3.5	0.1-2.2	0.05-0.31			x		x	shaped and cylindrical holes
2.7	x				< 1				x	x		x	transient coding technique
2.8	x		1	20°, 60°	< 1	0.1-0.75			x	x		x	" "
2.9	x		1	20°, 60°	< 1	0.25-0.75			x	x		x	results deduced from heat transfer
2.10			2	32°, 45°	> 1	0.3-1.05			x	x		x	cascade+combustion can
2.11			1	35°	< 1	0.65-1.1				x		x	S/D = 2.22, 3.33, 4
2.12			1	35°	> 1	0.1-2	0.05-0.62	-	x	x		x	
2.13			1, 2	30°, 90°	> 1	0.1-1.9				x		x	shock tunnel
2.14	x		1	30°	2.07	1-2		+0.0-		x		x	
2.15		x	1	35°	< 1	0.2-1.95	0.05-0.15		x	x		x	
2.16			1	0°	1, 2.1	0.4-2				x		x	holes in rearward step
2.17			multiple	45°, 90°	1, 4.23	0.2-1				x		x	holes at 2, 8 D pitch
2.18			"	45°	115.42			-		x		x	turbulence intensity varied
2.19		x									x		slots at 45°, 80°, 90°
2.20	x		2, 4	90°	< 1			-		x		x	
2.21	x				< 1			+		x		x	mach 6 mainflow
2.22	x						0-0.61			x		x	recirculation studies
2.23			1	90°	1	3-2.65				x		x	
2.24			multiple	90°	< 1				x	x		x	study of deflected jet
2.25		x		35°, 90°	< 1	0.1-2							
2.26											x		
2.27			1							x			
2.28		x		90°							x		

TABLE 2.1 Table of the Parameters covered by other Researchers

shock tunnel to provide the high speed, high pressure and temperature mainstream to approximate to the conditions in a gas turbine. Here, of course, the flow was of short duration and they used thin film heat transfer gauges to measure the heat transfer rates from which the film cooling effectiveness was deduced.

Finally, the temperature method was used by Nicolas and Le Meur (2.14), but they also did some concentration measurements to compare with their 'temperature' results and found good agreement between the two methods.

Most of these experimenters have also measured the ratio of the heat transfer coefficients with and without secondary flow. All, except Goldstein et al who used a steady state system, used a method which relied upon the measuring of the transient heating or cooling response of a test surface, from which the heat transfer coefficient could be calculated.

2.2.2 Concentration Measurement

Fewer experimenters have used the foreign gas technique. Rastogi and Whitelaw (2.16) used air, with helium as a tracer gas, as the injectant and also mixtures of Freon 12 and air in a series of wind tunnel tests in 1972.

Freon 12 and air with a helium tracer were also injected into a wind tunnel mainstream by Le Brocq et al (2.17) and by Launder et al (2.18), the latter using carbon dioxide as a

third injectant. The density of Freon 12 is 4.26 times the density of air, while carbon dioxide density is 1.54 times that of air.

2.3 Injectant to Mainstream Density Ratio

Table 2.1 shows that the effect of the density ratio has received little attention, although several workers have studied a small number of differing density ratios. Rastogi and Whitelaw (2.16) used a rearward facing step with circular holes in it, through which they injected foreign gases. They found that the effect of the density and velocity ratio was complex, although their results showed similarities with previous work involving two-dimensional injection geometries.

Le Brocq, Launder and Priddin (2.17) found a significant improvement in the film cooling effectiveness with multiple row cooling when Freon 12 was injected, compared with the results obtained using air at the same blowing parameter. They noted that the jets of Freon 12 tended to remain closer to the surface and not become detached as did the air jets. They suggested that this was due to the lower injection velocities with the Freon 12 at the same blowing rates.

Launder and York (2.18) continued this work by injecting carbon dioxide as well as the air and Freon 12 of the previous experimenters. They found that the carbon dioxide results lay between the other two, as might be expected. They suggested that the maximum concentration of coolant for the three injectants occurred at the same velocity ratio and, therefore, that

the density ratio had little effect. In fact, this was true for the results presented for eight diameters behind the 6th row of holes, but not behind the first row. Furthermore, there is no evidence that it would be true, either closer to the hole or further downstream, or for a different injection angle.

The increase in effectiveness due to using dense Freon 12 was also noticed by Goldstein et al (2.6), who compared results obtained with heated Freon 12 and those with heated air at the same blowing parameter. They found an improvement in the collapse of their data if they plotted effectiveness against the momentum parameter, rather than the blowing parameter, for a downstream distance of 6.7 diameters. Again there is no information for other distances downstream from the injection point.

Table 2.1 shows that many experimenters (including Goldstein et al, Metzger et al, and Liess et al) have worked with density ratios of less than unity; these are not typical of a gas turbine blade cooling situation. They have then generally used the blowing parameter as the basis of comparison for their results. As the trajectory of a jet in a cross flow is more likely to be a function of the jet's momentum, (as is suggested by Abramovich, 2.19), the momentum parameter would seem to be a better correlating parameter - as Goldstein et al (2.6) suggest. However, as a perfect collapse of the data is not achieved, the true relationship between effectiveness, velocity and density ratios must be more complex.

The correct order of density ratio was used by S.S. Pappell (2.20), one of the earliest researchers into discrete hole film cooling. He considered only two or four rows of holes, which he found to be inferior in their film cooling performance to the slots which he tested.

Jones and Schultz (2.13), who presented data for one and two rows of holes, also used a representative density ratio. They noted the effect of "lift-off" as the jets - especially in the single row tests - became detached from the test surface as the blowing rate was increased.

Smith (2.2), also using the shock tunnel, found that his results - like those of Goldstein et al - correlated better against the momentum parameter than the blowing parameter. However, there is a great deal of scatter around the mean lines drawn through Smith's data, and the mean lines show no tendency to predict the fall in effectiveness with "lift off" close to the injection holes for 90° injection.

2.4 The Boundary Layer Displacement Thickness

As can be seen from Table 2.1, only two workers have considered the effect of the boundary layer thickness: Goldstein et al (2.4, 2.15) and Liess (2.12). In general, they found that an increase in the boundary layer displacement thickness tended to reduce the effectiveness, this being most marked close to the injection holes, and at low blowing parameters.

The effect is explained by suggesting that, with a thinner boundary layer, the jets traverse a shorter distance of low

momentum flow before being deflected. Liess' results show a much greater variation in effectiveness with boundary layer displacement thickness, than do those of Goldstein et al; also they show the effect to extend over a distance of 50 diameters downstream. Goldstein et al show the effect to have almost disappeared on the centreline within 30 diameters.

Fig.2.1a shows the results from fig.19 of ref (2.12).

If the curve for the blowing rate of 0.33 is extrapolated from $X/D = 13$ to $X/D = 10$, a value of effectiveness is obtained of 0.19. Plotting this on Liess' curve of effectiveness vs boundary layer displacement thickness, fig.2.1b, one finds that this point lies well above the mean line. Also, Liess shows a sharp decrease in effectiveness between $\delta^*/D = 0.2$ and 0.3 of nearly 30%.

These discrepancies highlight the fact that both Goldstein et al and Liess vary the ratio of the boundary layer displacement thickness to hole diameter, by using different hole sizes, and by varying the mainstream velocity - the latter having the effect of altering both the boundary layer thickness and the Reynolds number.

In one case Goldstein et al varied the boundary layer thickness directly, by moving the boundary layer trip wire. However, the overall result is that it is impossible to determine the extent of the effectiveness variation, which is due to the change in boundary layer thickness alone.

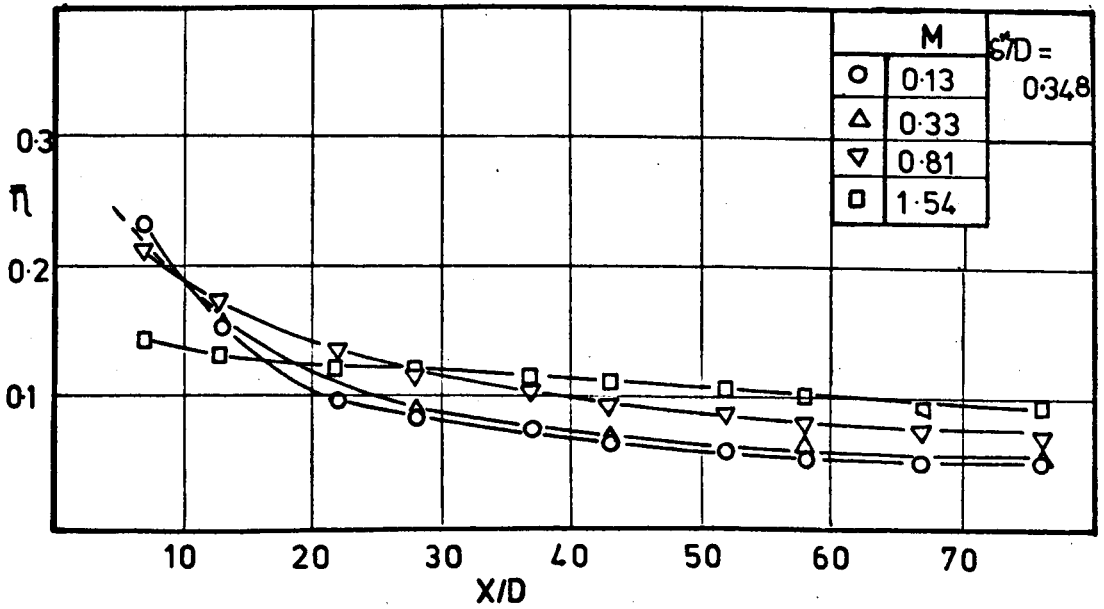


Fig. 2.1a Spanwise averaged effectiveness, $\bar{\eta}$, plotted against dimensionless distance downstream X/D , from Liess (2.12 fig.19)

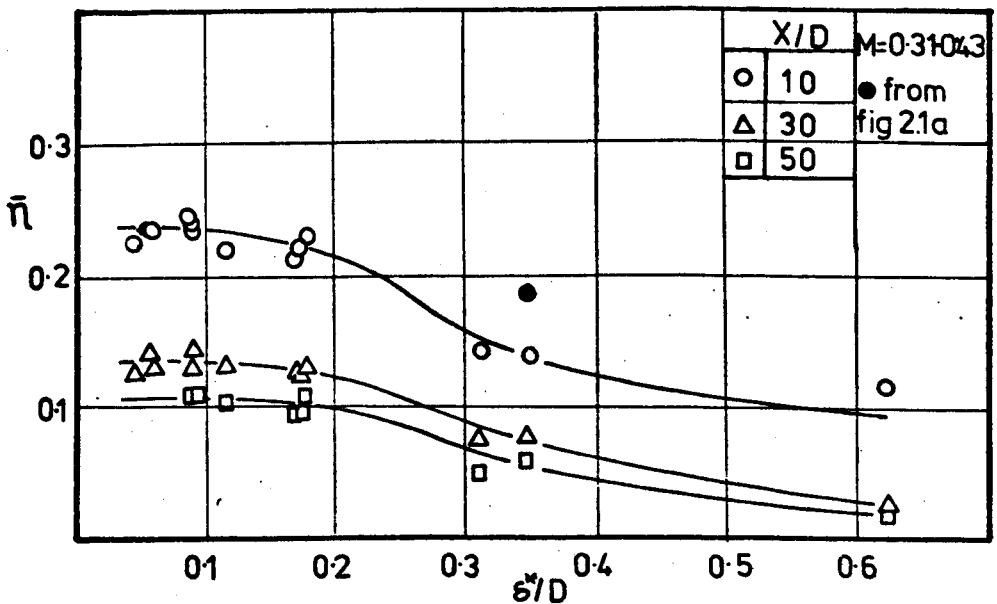


Fig. 2.1b Variation of spanwise averaged effectiveness, $\bar{\eta}$, with boundary layer displacement thickness, δ^*/D , from Liess (2.12 fig.25)

2.5 The Pressure Gradient

As Table 2.1 shows, Liess (2.12) is also one of the three researchers to consider the effect of pressure gradients on film cooling; the others are Nicolas and Le Meur (2.14) and Launder and York (2.18). Lander and Fish (2.10) have measured the film cooling effectiveness in the presence of pressure gradients, but have no results without the pressure gradients to compare these with.

Liess found that a contour placed in the roof of the working section of his wind tunnel, giving a favourable pressure gradient, produced a fall in effectiveness far downstream of the injection holes. Liess suggests that this was probably due to increased mixing, but it is difficult to make any quantitative statement, as the pressure gradients only extended between 0 and 15 and 0 and 25 diameters downstream.

These results are at variance with those of Launder and York, who used a flat, angled plate in the roof of their working section which, they found, improved the effectiveness behind the first row of holes in their multiple row injection plate by 25%. The experimenters point out that the blowing rate will vary down the injection plate, due to the change in static pressure along it. This had been partly eliminated by increasing the pressure drop through the delivery system, but any variation would result in lower blowing rates from the first row and, thus, a higher effectiveness.

The angled plate employed by the experimenters stretched from some considerable distance upstream of the injection holes

to over 40 diameters downstream. This must therefore have produced varying boundary layer thicknesses over the first row of holes, depending upon the level of mainstream acceleration which would, in turn, have produced variations in effectiveness - regardless of the pressure gradient.

Nicolas and Le Meur (2.14) conducted a series of experiments in which they used both curved and straight ducts, with and without contours, to produce the pressure gradients. They found that a negative pressure gradient on a flat plate tended to maintain the cooling film further downstream, and that cooling via holes with the pressure gradient was as good as cooling via a slot.

When comparing a concave surface with a constant pressure flat plate, the authors found an improvement of up to 60% at a blowing rate of unity. Improvements over the flat plate situation were also noticed on the convex side of the working section, but they were not so marked. No values for the boundary layer thicknesses were given, so again it is difficult to ascribe the variations to any particular effect.

Hartnett et al (2.21), in tests on a slot arrangement, found little difference between the levels of effectiveness produced by favourable pressure gradients starting at the point of injection, and those produced without a pressure gradient. There, the boundary layer displacement thickness was similar for all cases considered. Zakkay et al (2.22) suggested that an adverse pressure gradient should improve the film cooling

effectiveness at high Mach numbers with sonic tangential injection.

2.6 Injection Geometry

A glance at Table 2.1 shows that remarkably few researchers have considered injection from a row of holes normal to the mainstream; also, that where comparisons between different angles of injection have been made, they usually include no more than two angles. In general, the lower the angle of injection, the higher the effectiveness (2.2).

The results of Rastogi and Whitelaw (2.16), obtained using a three-dimensional wall jet, may almost be regarded as the limiting case as the angle of injection decreases to zero. They also scaled the dimensions of one configuration by a factor of 6.25, repeated the test, and found that the results were sensibly the same.

Goldstein et al (2.6) considered angled injection - both through long injection tubes, giving fully developed velocity profiles, and short injection holes about three diameters long. Very little difference was found between the two arrangements.

Further tests were conducted using a row of shaped holes which were circular in cross section at inlet, but widened out at an angle of 10° near the exit. The effect of these holes was to increase the effectiveness by a factor of three, at a distance of 2.5 diameters from the injection holes and at a blowing rate of 2. Flow visualisation tests showed that the

jets from the shaped holes tended to remain closer to the surface than those from the cylindrical holes, giving this huge rise in effectiveness. Higher values of lateral effectiveness were also noted when the shaped holes were used.

The results from this research are discussed more fully in Chapter 9 of the current work, but it is noticeable that the results shown spanning three holes are considerably different for each hole: e.g. for the cylindrical holes, the peak value for one hole is 0.69 at a distance of 2.7 diameters downstream, while for the neighbouring hole the equivalent figure is 0.53. Even at large distances from the injection position, the results are not two-dimensional, nor do the peaks correspond to the hole centrelines.

The results presented by Goldstein et al on the shaped holes have been largely confirmed by Smith (2.2).

In an early paper (2.4), Goldstein et al also considered holes at 35° and 15° to the surface, injecting normally to the flow - that is, in a lateral direction. This, they found, had the effect of giving greater lateral protection, but lower peak values of effectiveness for low blowing rates. As the blowing rate was increased, the laterally injected jet did not tend to become detached from the surface, thus giving a higher peak effectiveness than a hole at 35° with the flow.

Hole spacing has been investigated by only two groups of researchers in the film cooling field: Liess and Carnel (2.11), and Metzger et al (2.8, 2.9). The latter considered hole

spacings of 1.55 and 1.71, both of which are far too small to be used in turbine blades, but are used later to compare with data from the current work.

Liess, on the other hand, considered three spacings - 2.22, 3.33 and 4 diameters. Surprisingly, although the smallest hole spacing was found to give the highest effectiveness close to the holes ($X/D = 0.5$), from 3 diameters to 25 diameters the 3.33 spacing was superior on the centreline, suggesting some interaction between the jets, perhaps.

Unfortunately, there is no other data with which this can be compared, except the statement by Le Brocq et al (2.17), that a hole and row spacing of two diameters with multiple row cooling gave values of effectiveness close to those obtained using a sintered injection plate. They then tested a spacing of 8 diameters and recommended a maximum of 5; this was later reduced to three diameters by Launder and York (2.18) "if hot spots were to be avoided".

Sterland & Hollingsworth (2.23) varied the hole spacing from 0 to 6 diameters at high blowing rates ($M > 4.5$). They found that at close hole spacings there were regions of recirculating flow behind the holes, which disappeared when the hole spacing increased to 4 diameters.

2.7 Heat Transfer Coefficients

The measurement of the heat transfer coefficient is outside the scope of the current work, but a study of the

results of those experimenters who have taken such measurements does show certain discrepancies, which may reflect on the effectiveness measurements taken by the same researchers. Table 2.1 therefore includes heat transfer coefficient measurements.

Quite simply, the transient temperature techniques used by Metzger et al (2.7, 2.8, 2.9, 2.24), Liess (2.12) and Lander and Fish (2.10), produced ratios of heat transfer, with and without cooling, that were always greater than unity, rising in some instances to 1.6. Meanwhile, the steady state technique of Eriksen et al (2.15) gave results which were often below unity.

Eriksen et al throw doubt on the results obtained by Metzger et al with the 2" x 0.5" cross section wind tunnel, although the latter claim to achieve similar results with a larger apparatus. The results of Metzger et al do suffer from being averaged in the streamwise as well as the spanwise direction. Lander and Fish's results had the remarkable feature that, as the blowing rate was increased, the ratio of heat transfer coefficients decreased, this being the opposite to the observation of all the other experimenters.

2.8 Theoretical Models and Correlations

At the present, there is a great need for a full theoretical approach to the discrete hole film cooling problem, but there has been very little published on the subject. There have been several studies on jet deflection by a mainstream,

and Ramsey et al (2.25) give a good review of these works. These studies tend, if they use integral methods, to consider average values. For discrete hole cooling, the few experimental results presented above the surface do not indicate that the trajectory methods are likely to succeed. The future must lie with the numerical computational techniques of finite elements and finite difference, and progress is being made in this direction by Spalding and Patankar (2.26).

Several researchers on slot cooling proposed a boundary layer type, bulk mixing model. This was used by Jones and Schultz (2.13) and Smith (2.2), when they used the parameter \bar{X} and an equivalent slot height S_1

where

$$\bar{X} = \frac{X}{MS_1} \left(\text{Re}_j \frac{\mu_j}{\mu_\infty} \right)^{-0.25}$$

and

$$S_1 = \frac{\pi D^2}{4S}$$

The agreement was not good except for multiple rows of holes, low angles of injection and shaped holes. Obviously, the model cannot deal with the "lift off" situation, and tends to over-predict the effectiveness close to the holes.

However, the model is designed for two-dimensional flows, and the fact that there is any agreement is perhaps surprising. Smith also attempted a correlation on his two dimensional data using an entrainment principle, and found that this worked well for slots, but again it failed to cope with the fully three-dimensional effect of hole injection.

Kelly (2.27) has recently proposed a modification to the bulk mixing type model, where he uses an equivalent slot height S_2 , where:

$$S_2 = \pi D^2 / 4D$$

He then used the two-dimensional model to give a streamwise distribution and averaged the results in a spanwise direction. This he called the zero spanwise mixing model. The predictions of effectiveness were better than those from the earlier method, as the effectiveness at the edge of the injection holes was now less than unity; but there is no more physical justification for this model than for the equivalent slot model, and the improvement it offers is possibly due to good fortune.

Finally, a three-dimensional model has been suggested by Eriksen et al (2.28), who used two models based on heat sinks - or sources if a heated jet is used. One method used a point source positioned above each hole and the other a line source. The success of the models depended upon the choice of the height of the sources above the test surface, and the empirical evaluation of a turbulent diffusivity from experimental data.

They found that the point source gave good agreement on the centreline up to a blowing rate of 0.5, but was rather poor for the lateral values. This was largely because the turbulent diffusivity was not constant over the surface and the use of an average value gave the wrong distribution of effectiveness.

The line source, however, overcame the difficulty of the lateral distribution to a certain extent, although once again, as the blowing rate increased above 0.5, the predicted curves were of a different shape from the experimental ones.

Eriksen et al recommended that the method be used for interpolating between sets of data, from which the turbulent diffusivity can be deduced.

2.9 Conclusion

The above survey outlines the gaps and contradictions in the published work concerning discrete hole film cooling. The lack of success with simple models and the relative newness of the three-dimensional flow models explain why an experimental approach is generally chosen to help solve the problem of discrete hole film cooling.

CHAPTER 3 : OBJECTIVES AND METHODS

Chapter 3 outlines the objectives of the present work, explains why an experimental approach was chosen and considers the implications of the methods used.

=====

Consideration of previous work plus the needs of the turbine designer led to the programme at Nottingham having both a long and a short term objective.

The long term objective is to provide a mathematical model for the gas turbine designer. This model should allow him to compare different film cooling configurations, predict the local film cooling effectiveness and, ultimately, the heat transfer rate at any point downstream of a row - or combination of rows - of holes. This is in comparison with the present design techniques which, in general, give spanwise averaged values of effectiveness only.

The short term objective is to provide for the designer data, and perhaps correlations, which he can apply to obtain the spanwise averaged effectiveness and the aerodynamic penalties for a given film cooling configuration. The data should also indicate to him the relative importance of the various film cooling parameters.

To meet the long term objective, a great amount of data is required against which the model may be tested and validated. This data must cover a wide range both of conditions and parameters. Any model which is produced to meet the long term objective should obviously be as simple as possible - consistent with providing the required accuracy over the operating conditions. This simplicity would mean generally that the model would be easier to use and less costly in terms of computing time.

To this end, data are also required to determine which are the important parameters and must be included, and which are less important and may safely be disregarded. Furthermore, as the rate of heat transfer is closely related to the flow conditions, a model is most likely to be successful if it models the flow correctly. Therefore, data are also required on the flow field downstream of a row of cooling holes.

The data requirements of the two objectives are substantially the same and have been partially met in a piecemeal fashion (as outlined in the Literature Survey) by contributions from many authors using differing apparatus and techniques. The result of this diversity of technique is that it is difficult to compare with much confidence parameters investigated by different experimenters. In addition to this, several parameters have hardly been considered at all, as Table 2.1 demonstrated.

Little work has been done on the case of normal injection from a row of holes, an aspect encountered near the leading edge of a turbine blade. The effect of the boundary layer thickness has been considered (reference 3.1,3.2), but it is difficult to determine how much of the measured effect was due to the variation in the boundary layer, and how much to the change in mainstream Reynolds number. The effect a pressure gradient has on the film cooling effectiveness has not been systematically studied, and very little work has been done with adverse pressure gradients.

Many experimenters have been forced by the nature of their experiment to measure only the spanwise averaged effectiveness which, although meeting the short term requirement, will be of only limited value in providing a basis for a model to predict the local effectiveness at any point. Finally, as the literature survey showed, much of the early experimental data was obtained using a density ratio of injectant to mainstream that was not representative of gas turbine conditions.

Clearly the long term objective - obtaining the data and producing a full mathematical model - is beyond the scope of a three year research project; so an experimental programme was decided upon to provide data for both the long and short term objectives.

The objectives of this current work may be summarised as follows:-

- (i) To provide data covering a range of practical density ratios, giving the lateral distribution of effectiveness as well as the streamwise distribution.
- (ii) To investigate the effect of various parameters on the film cooling effectiveness, by using the same apparatus and techniques for all measurements.
- (iii) To investigate the nature of the flow downstream of a row of injection holes.
- (iv) To produce a correlation for preliminary design investigations.
- (v) To examine existing simple models with a view to their possible modification and improvement.

These objectives determined the nature of the experiment to be carried out and the type of experimental rig to be built.

The film cooling holes in a turbine blade are typically 0.25 to 0.75mm in diameter. It was therefore considered desirable to scale up the hole size and use a low speed mainstream to facilitate the studying of the three-dimensional nature of the jets, and the lateral distribution of effectiveness. However, the increased hole size implies an increased secondary and mainstream flow rate. To achieve the desired density ratio of around 2, by heating to a high temperature, a large mass of mainstream air would have been extremely expensive. The current research is being carried out on a

limited budget and therefore this method had to be ruled out.

Having eliminated the use of a heated mainstream, two possibilities were left: firstly using a cooled injectant, secondly injecting a foreign gas at ambient temperature and making use of the heat/mass transfer analogy. The former had the advantage that heat transfer measurements could be taken, but the disadvantage that there would be problems with condensation and icing. Furthermore, both the heated mainstream and chilled injectant methods require the measurement of an adiabatic wall temperature from which the film cooling effectiveness is obtained. Such a wall is difficult to build and develop, and is unlikely to be truly adiabatic.

The foreign gas technique has the advantages of simplicity and low cost; there are no temperature measurements, and no requirement for an adiabatic wall or expensive heating equipment. Against this it must be stated that one has to have analysing equipment to measure the concentration of the foreign gas and hence the concentration of the coolant. Also measurements of the heat transfer coefficient are not possible. In view of the extreme difficulty of measuring heat transfer accurately - as witnessed by the differences between the results from different sources, which were highlighted in the previous chapter - perhaps this is no real disadvantage, though reliable heat transfer coefficient data would be invaluable.

However, a foreign gas technique does permit a more detailed study of the mixing processes, as there can be no

conduction from the surface to the jet due to imperfect adiabatic walls. Furthermore, a foreign gas technique opens the way to having a large range of injectant to mainstream density ratios.

Clearly the use of a foreign gas was admirably suited to the objectives, budget and time available, and would give an interesting comparison with other work using the alternative techniques.

At this stage it might be helpful to consider some of the implications of a foreign gas technique which involves the use of the mass transfer analogy. The use of the analogy is discussed by Goldstein (3.3) and by Spalding (3.4). Goldstein states that the turbulent Lewis number should be unity, but Spalding says simply that the Lewis number should be unity or that the flow should be turbulent, and quotes Forstall and Shapiro (3.5). He points out that if this is the case, we have only to interchange $(C - C_2) / (C_1 - C_2)$ and $(T - T_2) / (T_1 - T_2)$, where C is the fractional mass concentration of one gas component and 1 and 2 refer to the two gas streams.

Both Spalding and Forstall et al were considering coaxial jet streams, but Nicolas and Le Meur (3.6) have shown that the mass transfer analogy may safely be applied to discrete hole film cooling. Finally, the analogy requires an impermeable wall, which is the equivalent of the adiabatic wall in the heat transfer case, but is obviously much easier to construct.

In the same work (3.3) Goldstein notes that there is some question as to the proper concentration to use to determine the effectiveness, but that the mass fraction is the most widely used.

Burns and Stollery (3.7) suggest that for foreign gas cooling:

$$\eta' = \frac{h'_{aw} - h'_{\infty}}{h'_j - h'_{\infty}} = \frac{C_w - C_{\infty}}{C_j - C_{\infty}}$$

and that

$$\eta = \frac{T_{aw} - T_{\infty}}{T_j - T_{\infty}} = \frac{\frac{Cp_j}{Cp_w}}{\left(\frac{Cp_j}{Cp_w} - 1\right) + \frac{1}{\eta'}}$$

In the case of a real blade the values of Cp for the coolant and mainstream will be approximately equal; so if the heat/mass transfer analogy is true, then:

$$\eta = \eta' = \frac{C_w - C_{\infty}}{C_j - C_{\infty}}$$

If the injected fluid contains a single constituent not contained in the mainstream $C_{\infty} = 0$, $C_j = 1$ and we have

$$\eta = C_w.$$

It was decided to use as a foreign gas the refrigerant gas dichlorodifluoromethane, CCl_2F_2 , known by the more familiar name 'Freon 12'. This gas had been used in preliminary

studies carried out at Nottingham (3.8, 3.9) with some success from 1970 on. It is 4.26 times as dense as air and it was decided to mix it with air in different proportions to give a range of injectant to mainstream density ratios. Therefore the effectiveness is defined as

$$\eta = \frac{C_w}{C_j}$$

Turning to the parameters it was hoped to include in the experimental programme, the first priority was to consider the hitherto largely neglected density ratio and, at the same time, the velocity ratio, so that the usefulness of the blowing parameter, M , could be assessed.

Following this, the boundary layer displacement thickness at the injection position was to be changed independently of the other variables. The pressure gradient over the point of injection was also to be varied systematically. Rather than consider a linear acceleration, or simply a pressure gradient over the injection position alone, it was planned to study a series of linear pressure gradients, of both a favourable and adverse nature, extending far downstream.

The other flow parameter which might be expected to affect the effectiveness of a film - namely the free stream turbulence intensity - could not be altered. Unfortunately, the blower it was planned to use would not permit the placing of turbulence-promoting grids in the flow if a high mainstream Reynolds number was to be attained. The freestream turbulence was therefore kept to a low level. It is worth noting

that the experiments of Launder and York (3.10) suggest that the turbulence intensity is not a major parameter.

It was intended to vary the injection geometry and consider different angles of injection and hole spacings. Neither of these parameters had previously been considered in great detail. Although the angle of injection had been varied by a number of workers, no-one had considered more than two angles, and normal injection had been almost totally ignored to date in spite of its use near the leading edge of a blade.

Single row geometries only were to be considered, with sufficiently long injection holes to ensure the injected flow would be fully developed. This would eliminate one variable, the coefficient of discharge of the hole, which can be considered separately. The row of holes was to be in a flat plate so that all curvature effects would be eliminated - these being, it was felt, beyond the scope of this study.

The flat injection surface meant that the pressure gradients would have to be produced by using a contoured surface opposite the injection surface. Flat surfaces at differing heights from the injection point would be used to vary the boundary layer thickness by accelerating the flow upstream of the injection position to the same nominal mainstream velocity, thus not altering the Reynolds number, based on the hole diameter, at the injection point.

The parameters studied may be summarised as follows:-

1. INJECTANT AND MAINSTREAM FLOW PARAMETERS

- (i) Injectant to mainstream density ratio, ρ_j / ρ_∞
- (ii) Injectant to mainstream velocity ratio, U_j / U_∞

hence

- (iii) Blowing parameter, $M = \rho_j U_j / \rho_\infty U_\infty$

$$\text{Momentum parameter } I = \rho_j U_j^2 / \rho_\infty U_\infty^2$$

- (iv) Boundary layer displacement thickness, δ^* and momentum thickness, θ

- (v) Pressure gradient, $\Delta p / X$

2. FILM COOLING CONFIGURATION PARAMETERS

- (i) Angle of injection, β
- (ii) Hole spacing, S/D .

The range of values of the above parameters are listed in Table 5.1 in Chapter 5 which deals with the experimental programme.

It was hoped that these experimental techniques and the apparatus described in the next chapter would provide data to meet the objectives outlined earlier and provide the basis for a correlation of film cooling effectiveness.

CHAPTER 4 : THE EXPERIMENTAL APPARATUS

Here the experimental apparatus and its method of construction are described with reference to the objectives stated in the previous chapter.

=====

The experimental apparatus was designed and built on a relatively small budget and to this end was kept as simple as possible consistent with obtaining reliable results. No form of automatic data collection was used, and a simple katharometer was built to measure the concentration of Freon 12 in samples drawn from the test section.

4.1 The Wind Tunnel

An existing, centrifugal blower type, open return tunnel was used to provide the mainstream; and some of the original ducting was retained. The old arrangement had the blower feeding a working section via a diffuser, gauze and a 3:1 contraction. Provision was made for speed adjustment over a very small range close to the maximum flow rate.

The system was modified to include an additional gauze and honeycomb flow straighteners before and after the diffuser. A flexible joint was also incorporated to limit the transmission of vibration from the blower to the working section. Finally, to permit a continuous variation of speed up to the maximum, the blower was connected to a Ward-Leonard

type speed controller. Plates 4.1 and 4.2 show most of these features.

4.2 The Working Section

An entirely new working section was built for the tunnel specifically for these studies. The basic construction consisted of four longitudinal aluminium angles to which were stuck the perspex side walls. The floor of the tunnel was bolted to these angles, as were portions of the roof. The entire working section was hung from a steel frame. Fig.4.1 shows a drawing of the working section which is also in view in plates 4.1 and 4.3.

The working section can conveniently be considered in four separate parts:-

4.2.1 The Upstream Section

This section had a fixed wooden floor and roof and bolted straight on to the contraction. It measured 381 x 152.4mm in cross-section.

4.2.2 The Boundary Layer Bleed (Fig 4.2)

This was manufactured from wood with a circular arc leading edge. To permit accurate location of the stagnation point, three pressure tapings made from hypodermic tubing, one on the leading edge and the other two straddling it, were positioned at two spanwise locations. A hinged aluminium flap was used to control the flow through the bleed, and this was opened or closed to bring the

diffuser

contraction

small
traverse gear

diffuser

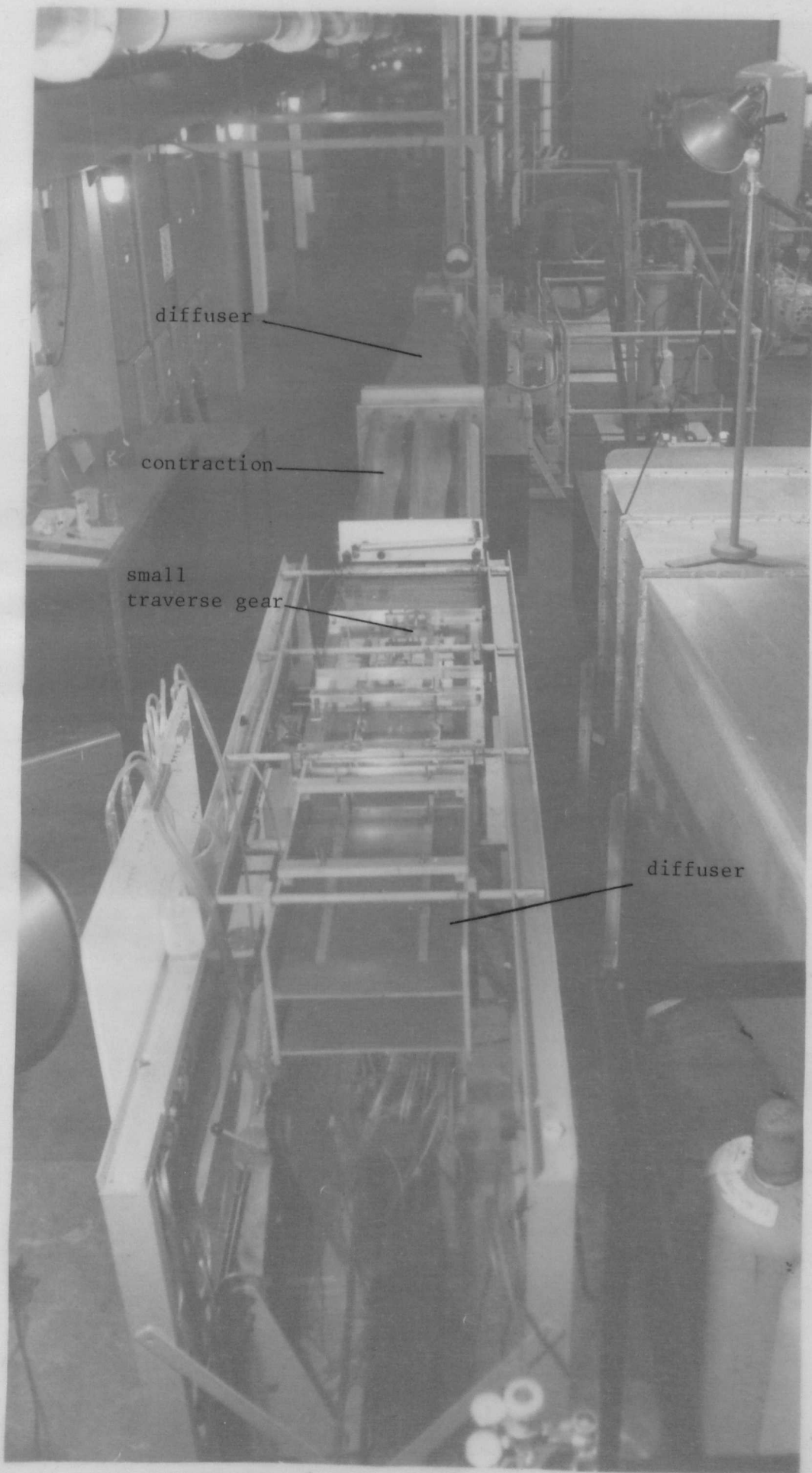
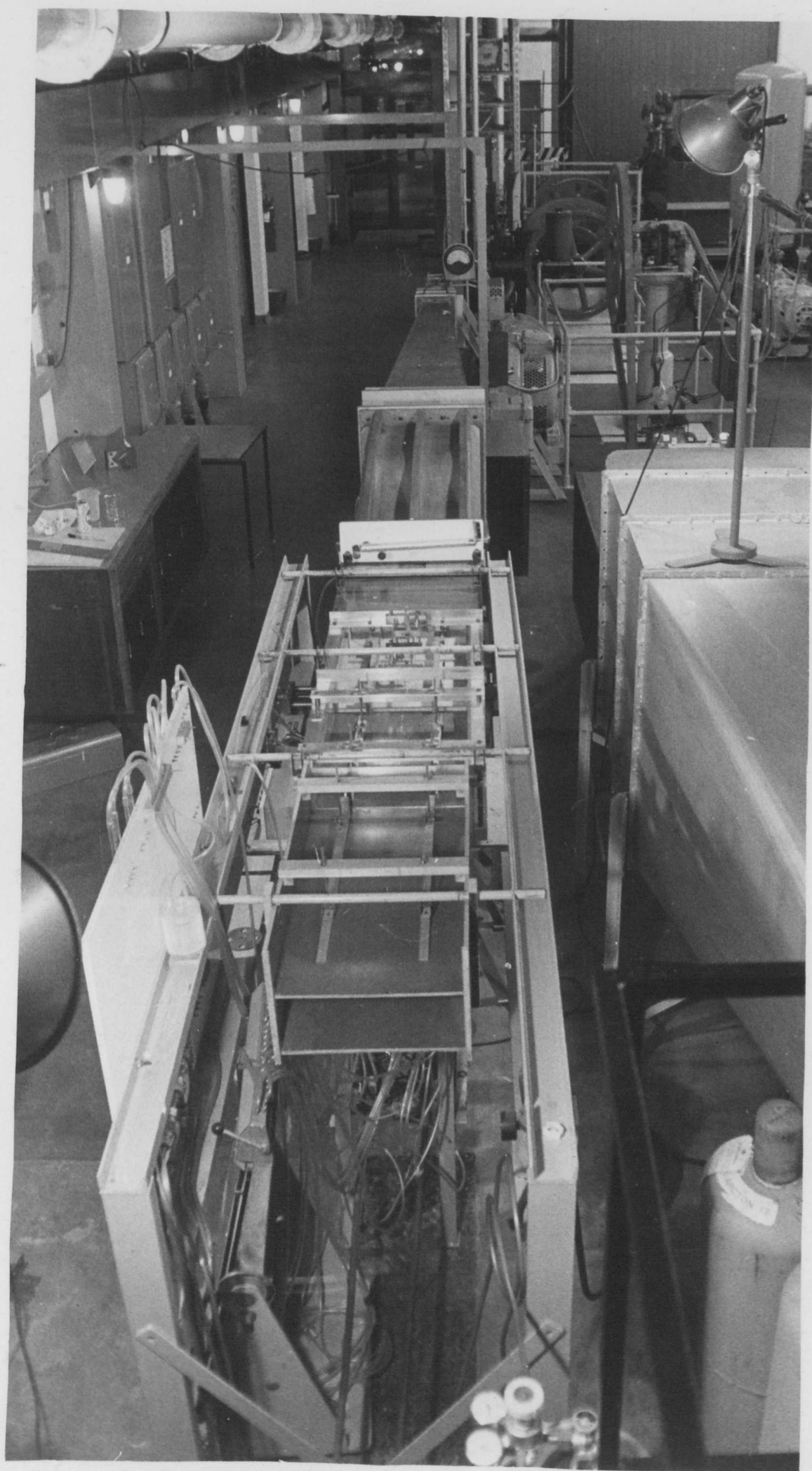


PLATE 4.1 A General View of the Experimental Apparatus



Air flow
controls

Freon 12
flow controls

Mainstream
flow control

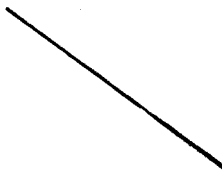
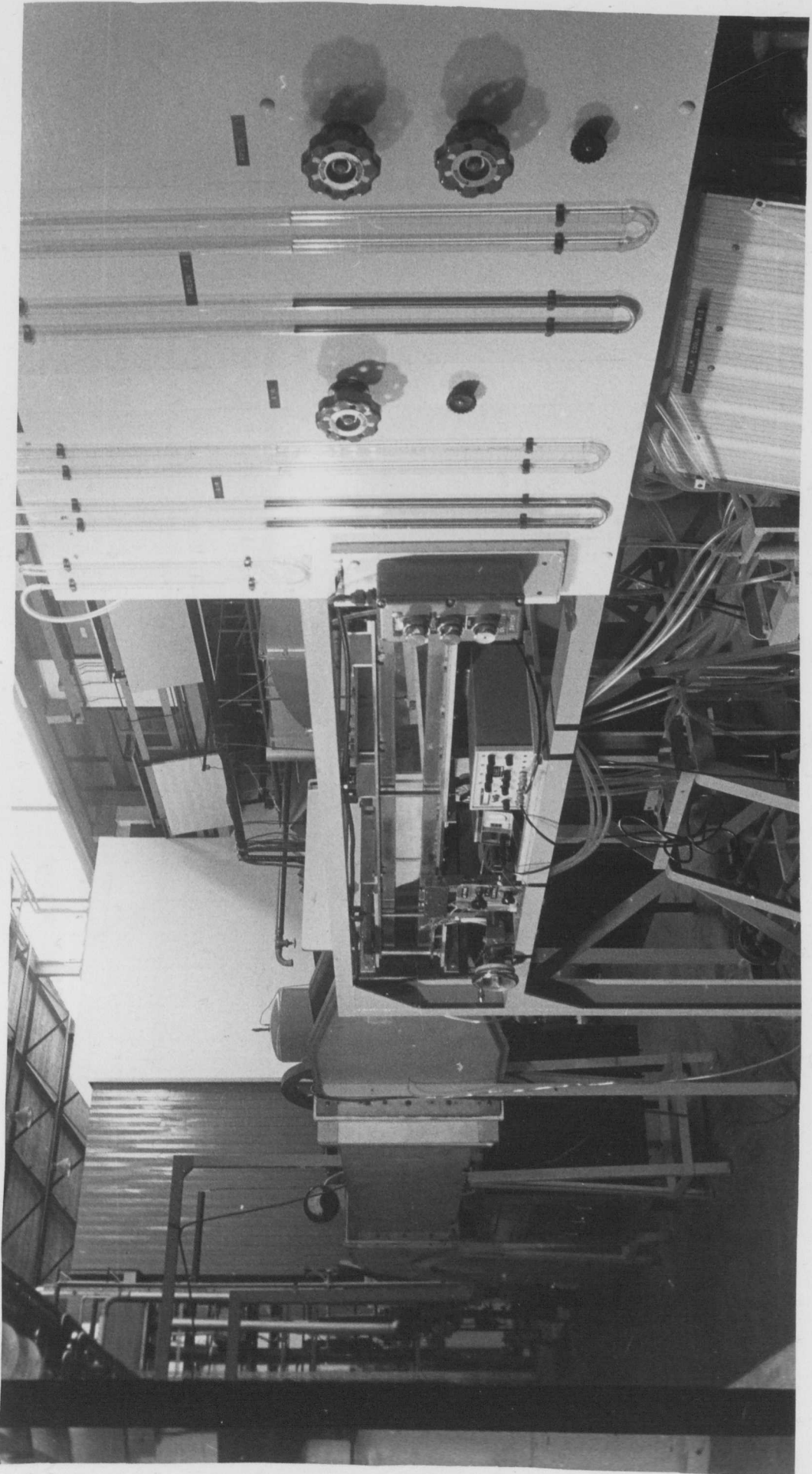


PLATE 4.2 View of the Working Section showing the Secondary and Mainstream Flow Controls



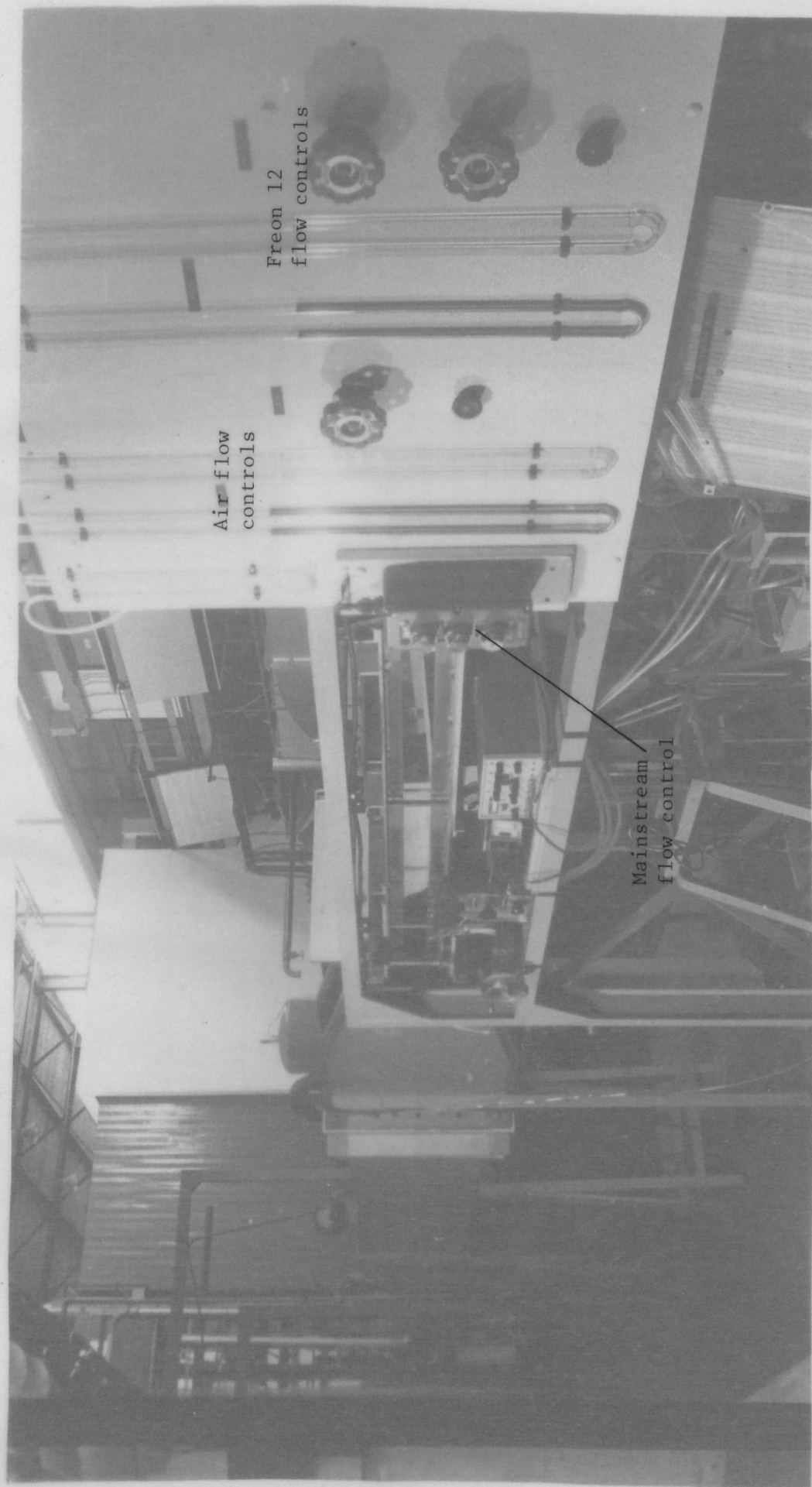


PLATE 4.2 View of the Working Section showing the Secondary and Mainstream Flow Controls

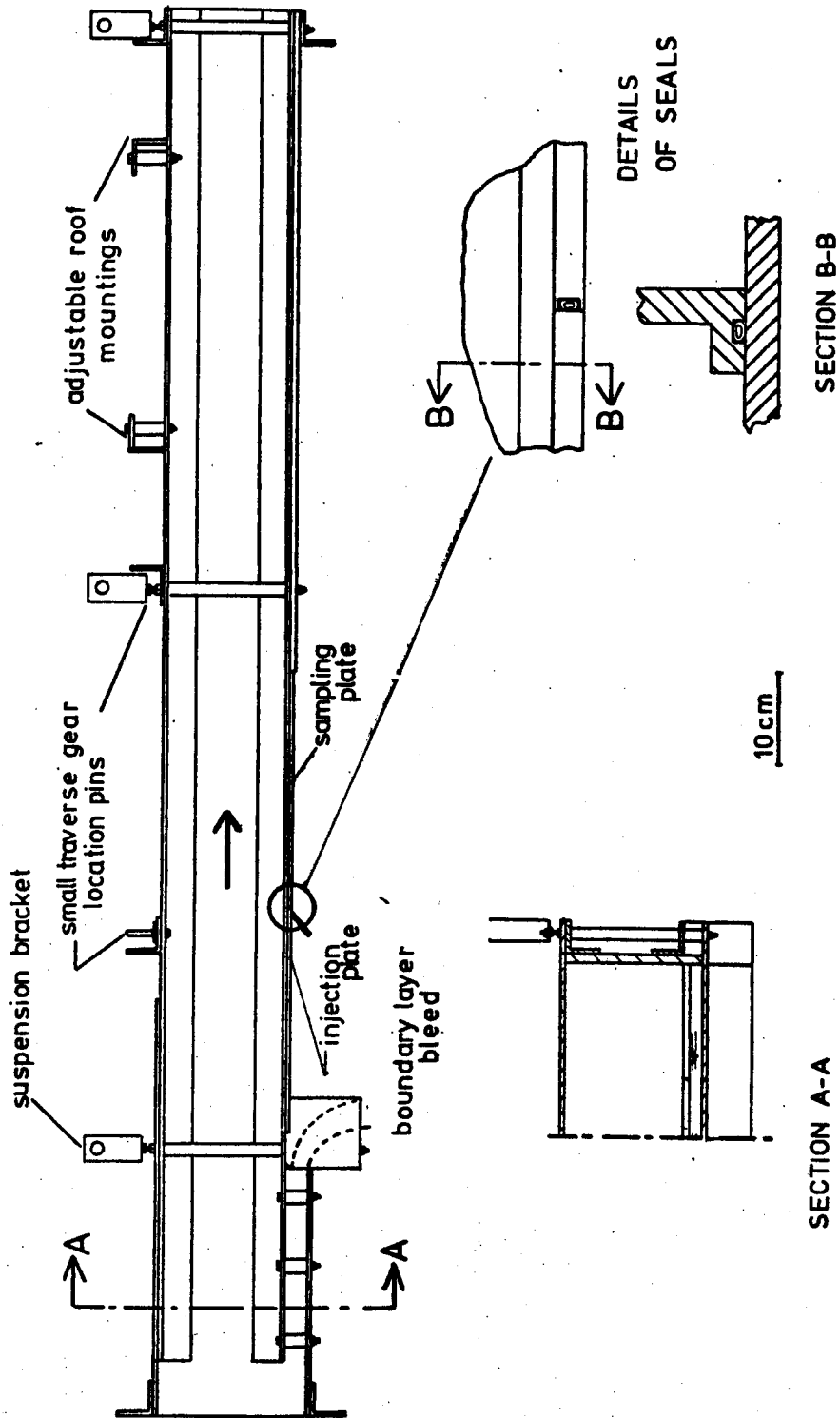


Fig. 4.1 The Working Section

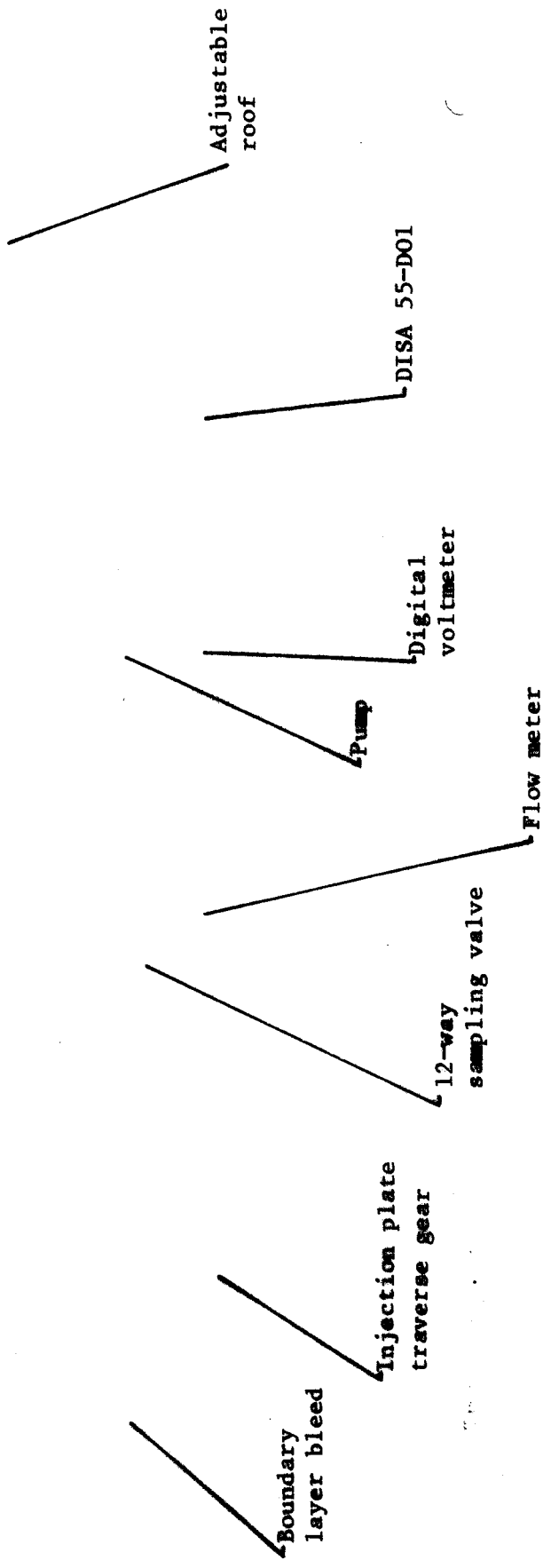


PLATE 4.3 View of the Working Section and Instrumentation

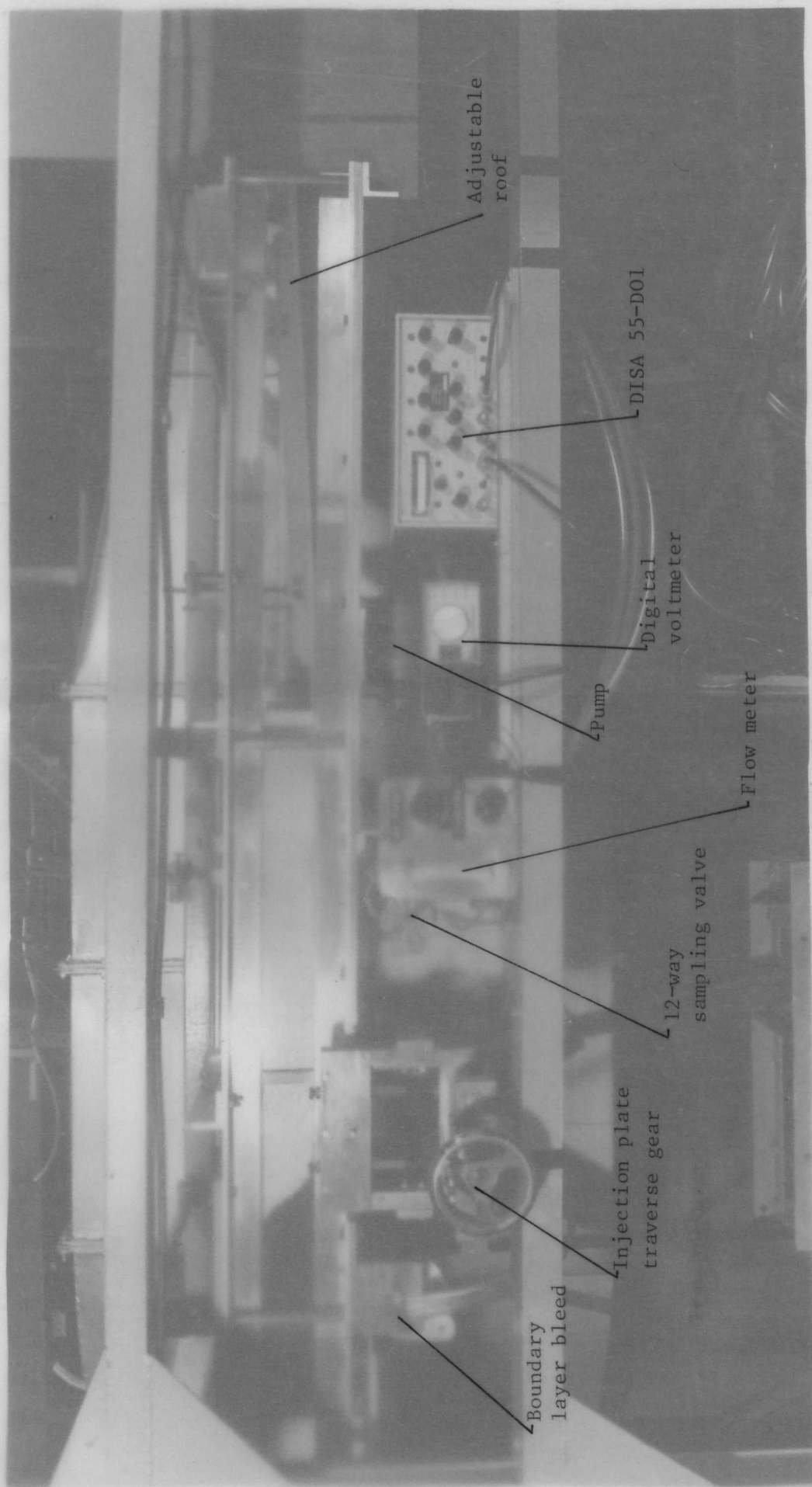
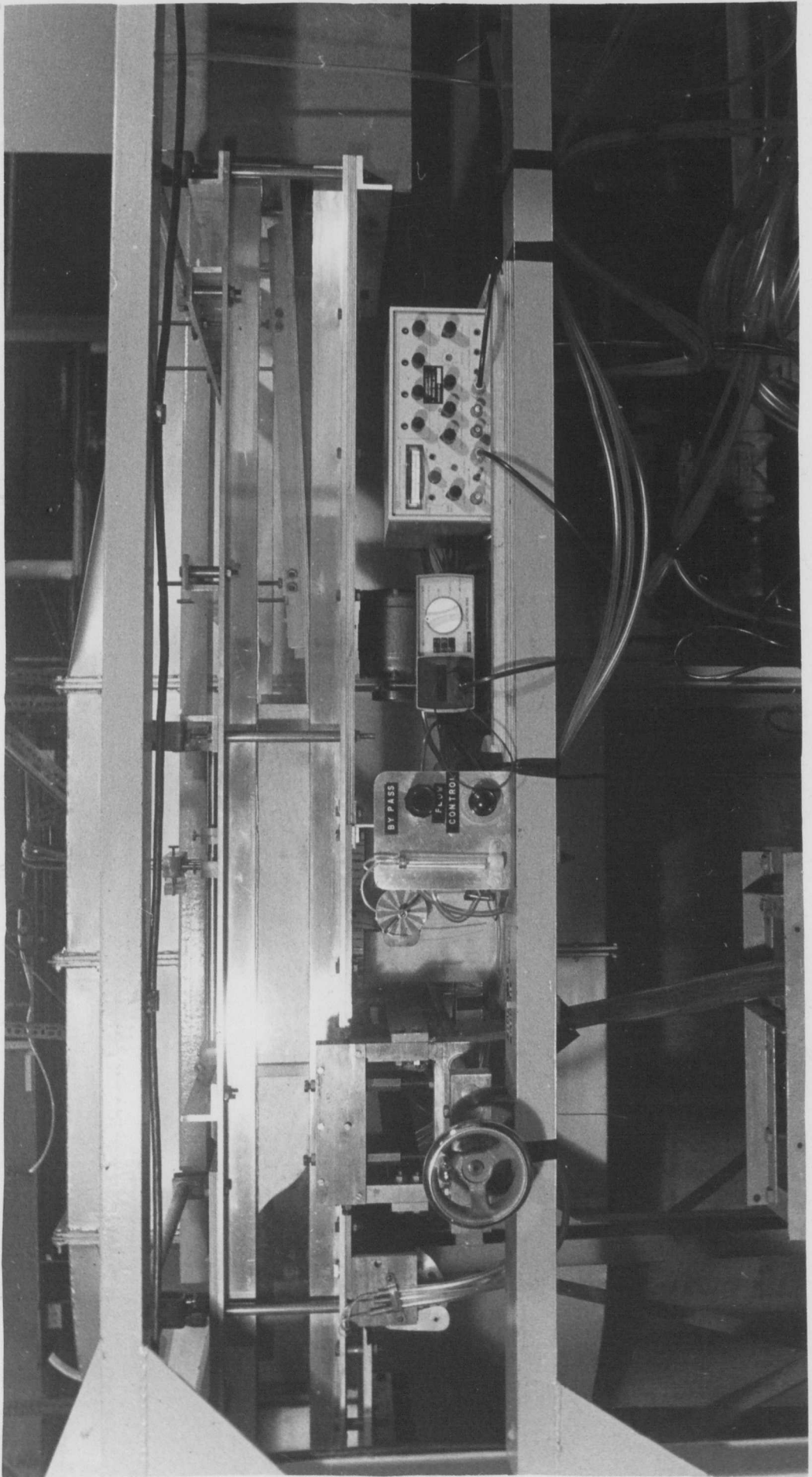


PLATE 4.3 View of the Working Section and Instrumentation



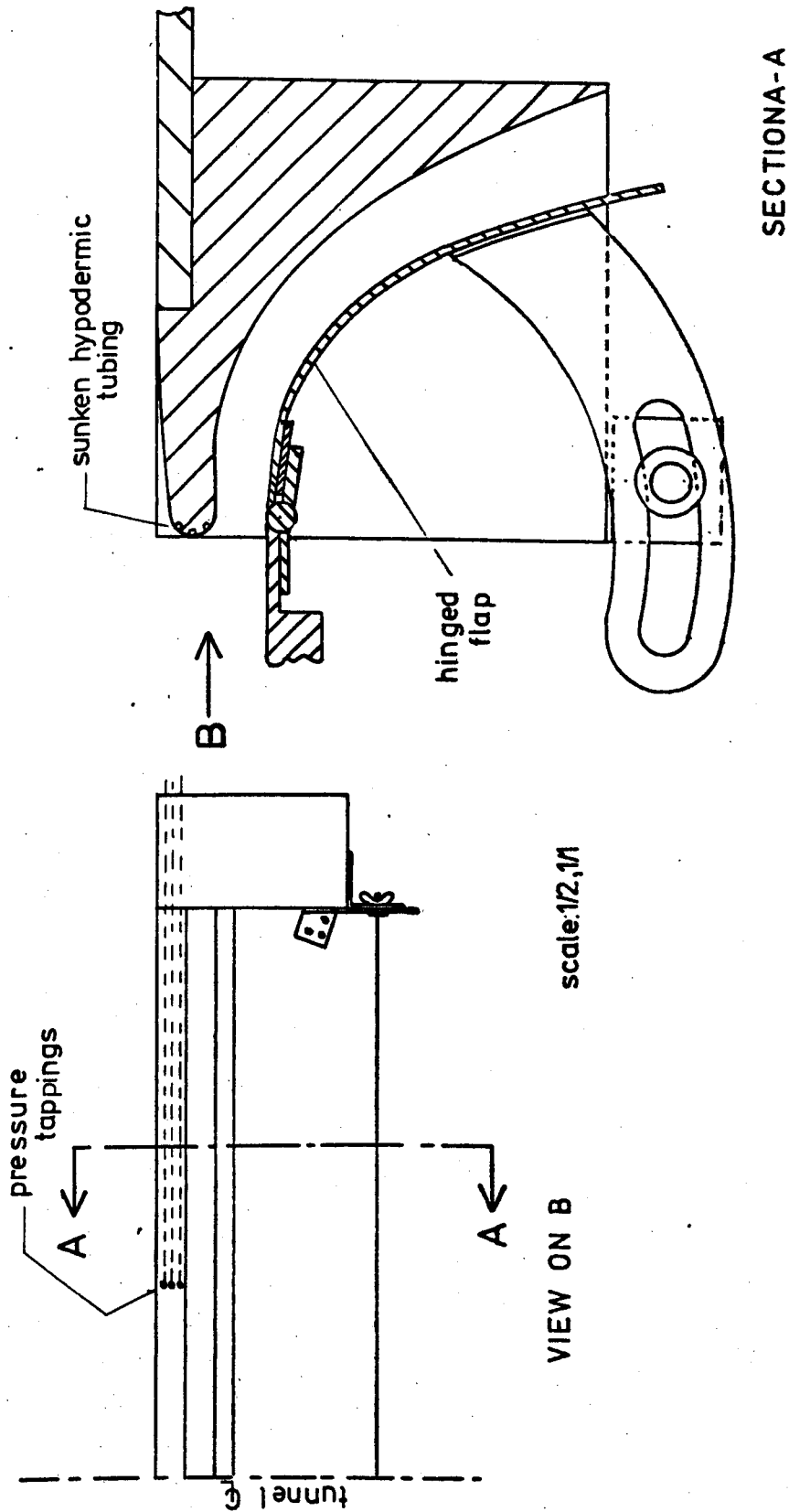


Fig. 4.2 The Boundary Layer Bleed

stagnation point (as measured by the pressure tappings) on to the leading edge.

The bleed was positioned 152mm from the entry to the working section, and reduced its height to 133mm. A boundary layer trip wire of 0.75mm dia. was used to ensure a turbulent boundary layer over the injection holes. It was positioned 42mm downstream from the leading edge of the bleed.

The wire diameter was chosen after evaluating the inequality quoted by Pankhurst & Holder (4.1):

$$\frac{U_{\infty} DX}{\nu} > 600$$

where here D is the wire diameter and X the distance from the leading edge.

4.2.3 Injection and Test Section

There were three possible methods of obtaining the measurements of effectiveness in both the spanwise and streamwise directions:-

- (i) traversing the injection holes past a line of sampling positions on the centre line of the working section;
- (ii) traversing the sampling positions past the injection holes;
- (iii) covering the area downstream of the injection holes with sampling locations.

The third method with its proliferation of holes might have led to the flow being disturbed and also, to ease the problem of changing the injection configuration, separate plates incorporating the injection and sampling holes were required anyway.

The first method was therefore chosen, as this did not require the large traverse gear demanded by the second method if large values of downstream distance were to be considered.

The result was that this part of the working section consisted of three ground steel plates, giving a smooth flat floor of uniform surface finish. Sliding seals made of polythene tubing, lubricated with a silicone based oil, were used to prevent any leakage between the plates (see detail on fig.4.1).

Subsequent tests in which measurements were taken (both with and without the joints being covered with adhesive tape) showed no variation in effectiveness - indicating that the seals were effective.

One large plate downstream of the injection holes incorporated a row of sampling holes of 0.67mm bore along the centreline. These were made by letting in to the plate lengths of hypodermic tubing of the required internal diameter. They were then joined by plastic flexible tubing to a multi-way sampling valve. Some of the sampling holes were duplicated in a parallel row, 12.5 mm from the centreline,

to permit the two dimensionality of the flow in certain instances to be checked. These sampling holes were also used to measure the local static pressures.

Upstream of the sampling plate, the injection plate containing the injection holes was mounted in a traverse gear. The injection holes were also made by drilling the ground plate and inserting lengths of hypodermic tubing of 2.29mm bore, which were then filed and finally "stoned", to give a perfectly flat surface (plate 4.4). Also visible in the photograph are some additional sampling positions which were placed in the injection plate downstream of the injection holes, to give data very close to the injection point.

The third plate was placed just downstream of the boundary layer bleed, again to give a smooth and aerodynamically flat surface and also to provide a bearing surface for the traversing plate.

This portion of the working section had no fixed roof, so that a variety of differently contoured roofs could be fitted to give the different pressure gradients and boundary layer thicknesses.

4.2.4 Downstream Sections

The final section included a wooden floor and adjustable wooden roof. The latter could be raised or lowered to match the height of any contour that was being used and could also be put at a slight angle to give some diffusion.

PLATE 4.4 The Normal and 55° Injection Plates

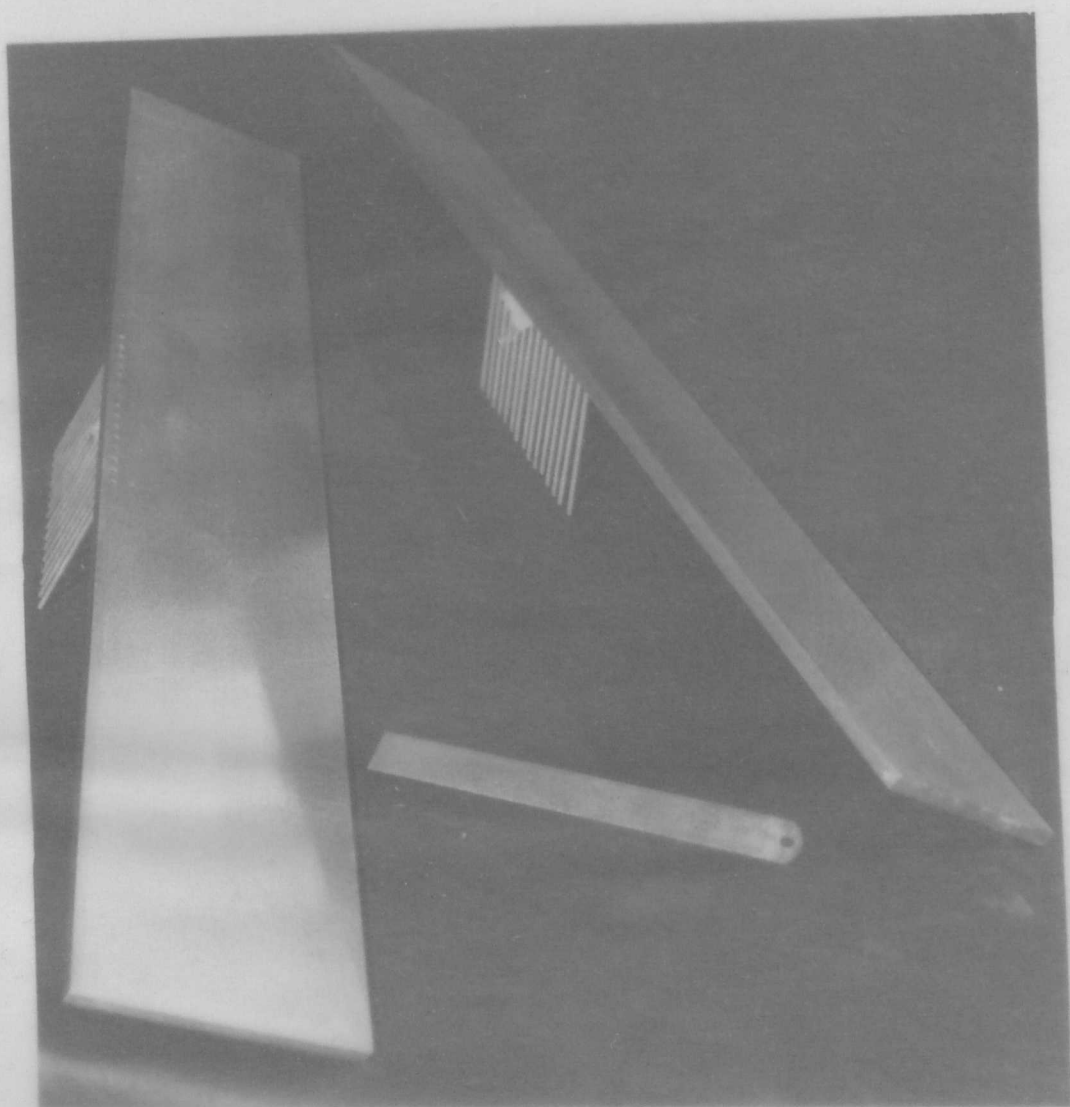
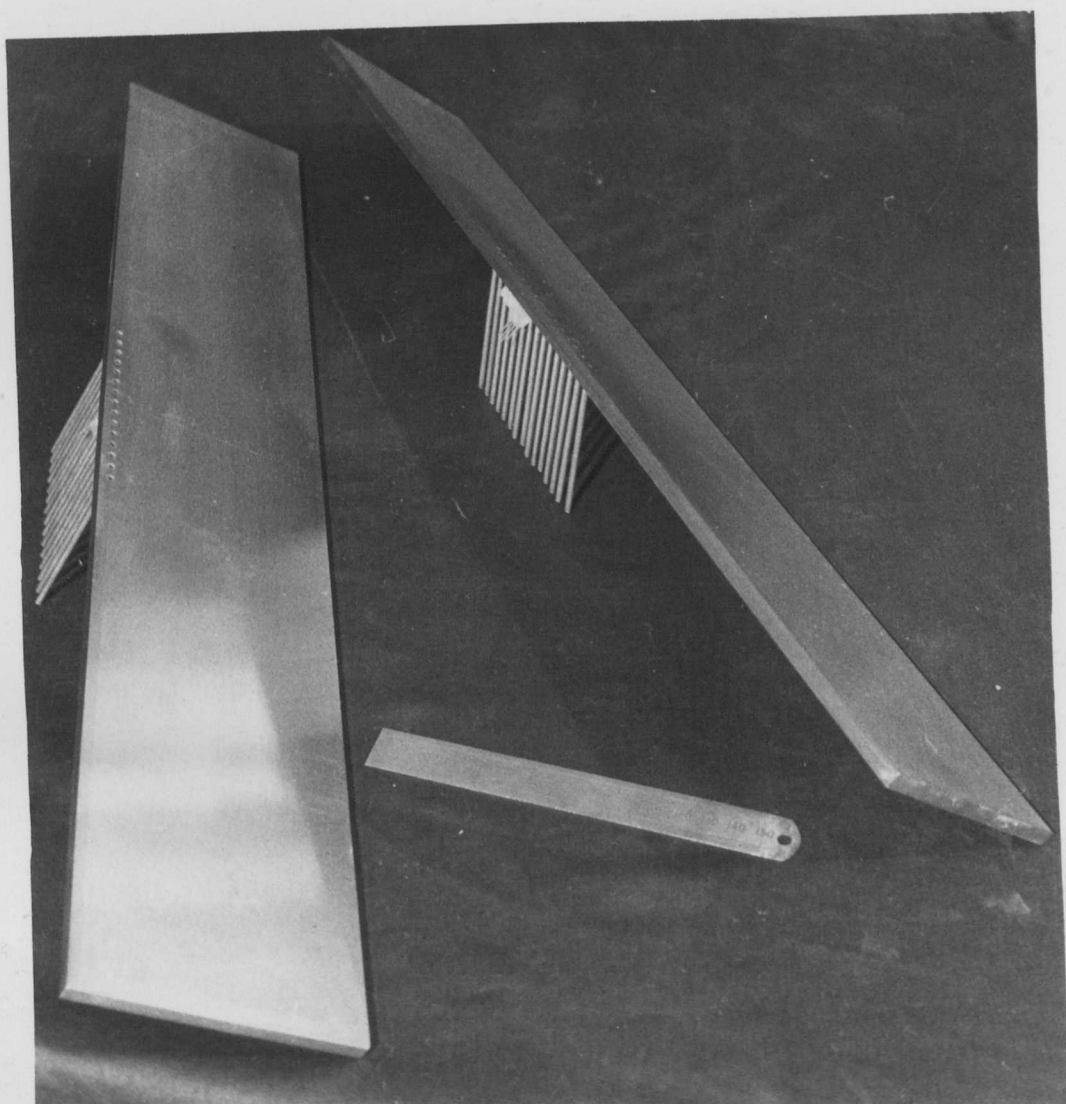


PLATE 4.4 *The Normal and 55° Injection Plates*



An additional diffuser, again with a top surface fully adjustable for height and angle, was used in certain series of tests when required to give some pressure recovery and lower the loading on the fan (plate 4.1).

4.3 The Contours

The contours, one of which is shown in plate 4.5, were constructed from wood with a strong frame and skinned with 1mm plywood. Each contour was provided with a row of holes on the centreline, through which a probe could be passed for sampling purposes, and total pressure measurements. These holes were taped over or plugged when not in use.

Fig.4.3 shows the profiles of the different contours in the tunnel. The non-accelerating contour (fig.4.3a) could be raised or lowered to tailor the boundary layer thickness to the desired value, the cantilevered flexible leading edge taking up any variation in height. The angle of the pressure gradient contours could be altered slightly to change the shape of the pressure distribution produced.

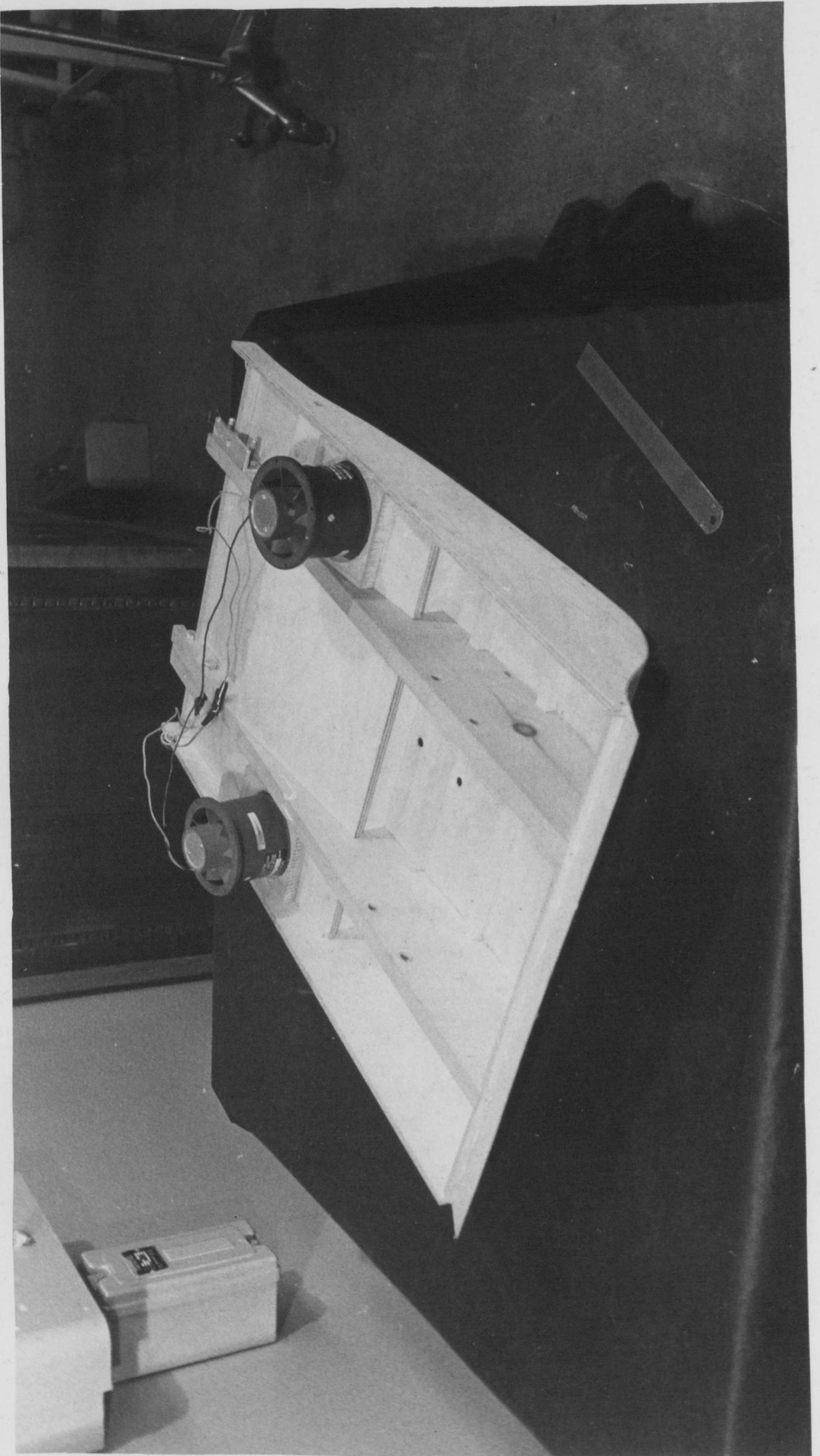
The adverse pressure gradient contour (plate 4.5) had two small ducted fans evacuating two compartments over spanwise slots. These removed some of the boundary layer and delayed separation from the contour until the end of the test section.

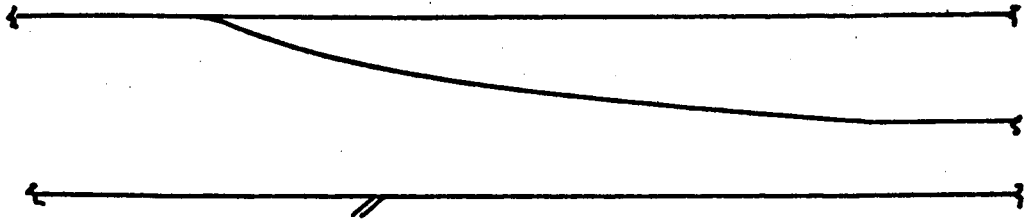
4.4 The Traverse Gear (Fig.4.4)

The traverse gear was mounted on the frame which supported the wind tunnel working section, plate 4.3, and was designed so

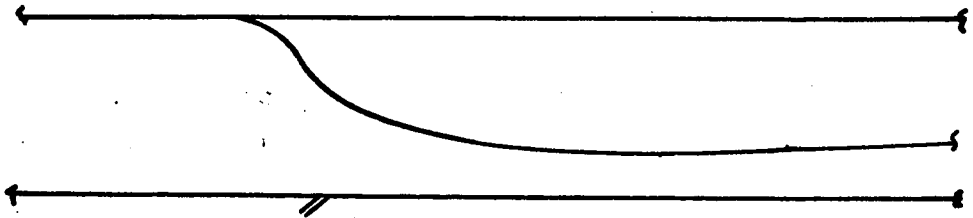


PLATE 4.5 The Adverse Pressure Gradient Contour

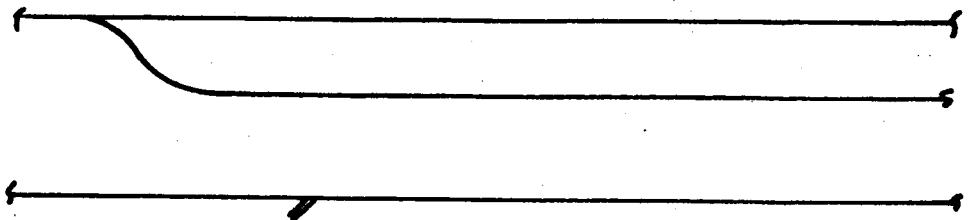




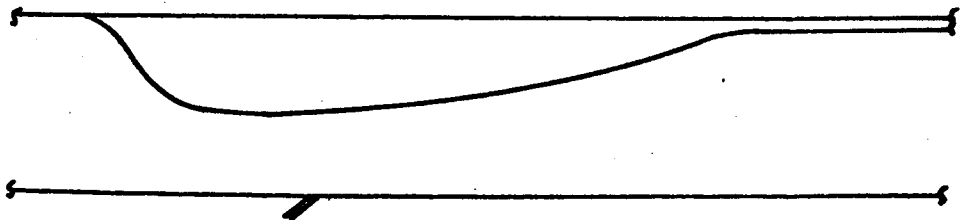
(i) mildly accelerating



(ii) strongly accelerating



(iii) nonaccelerating - thinner boundary layer



(iv) deaccelerating

scale 1/6

Fig.4.3 Profiles of contours in the working section

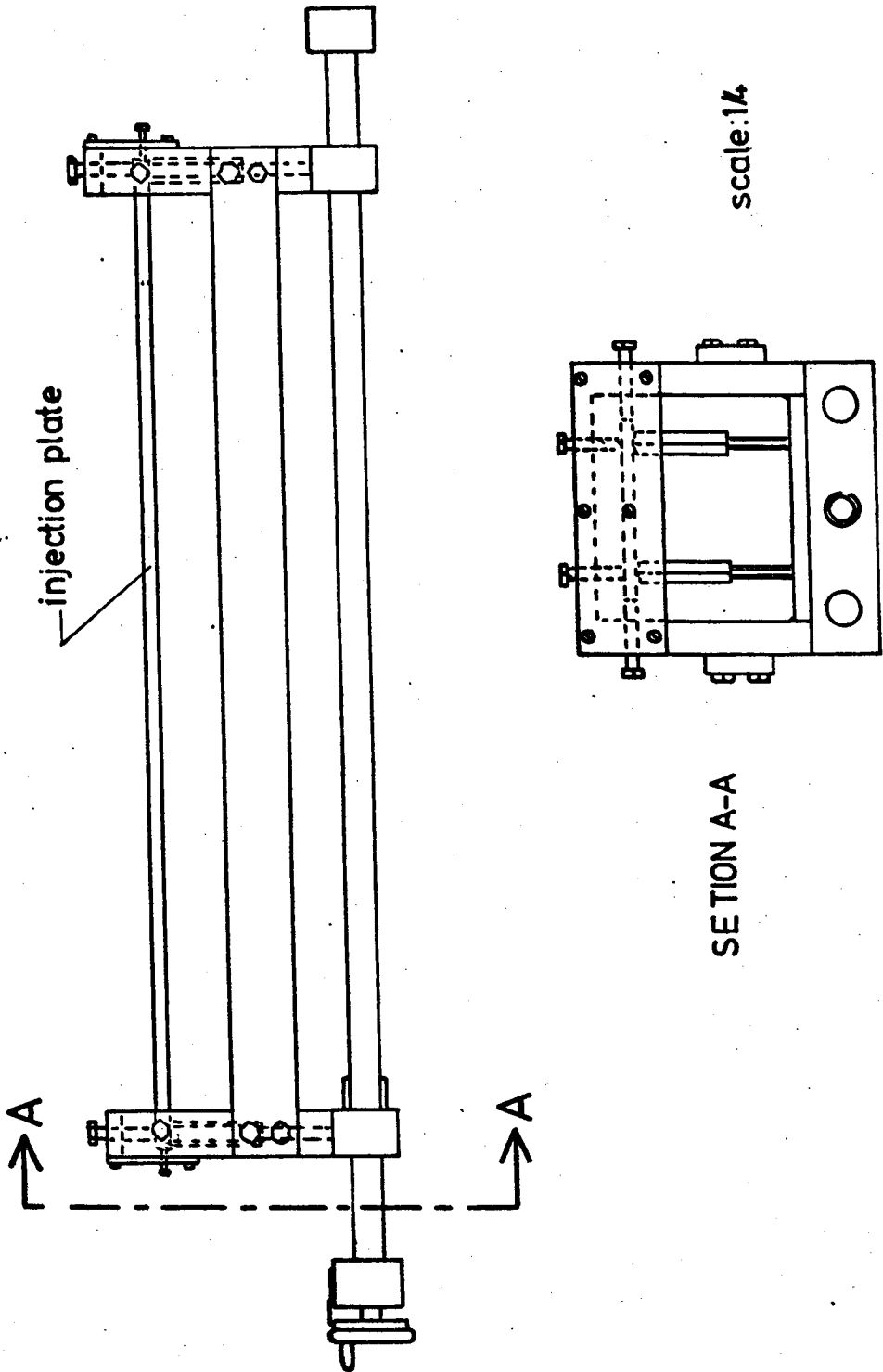


Fig. 4.4 The Injection plate traverse gear

that once it was set parallel with the floor of the tunnel at 90° to the flow direction, all further adjustments could be made with the adjusting screws which clamped the injection plate to the traverse gear. The entire construction was from mild steel and, when finally installed, it worked well, permitting sampling plates to be changed quickly. Changing a plate and adjusting it so that it was flush with the tunnel floor took less than 15 minutes.

4.5 The Probe Traverse Gear (Fig.4.5)

A small traverse gear was designed and built to carry the boundary layer probes and sampling probes. It was located on pins set in two of the cross-members over the top of the working section and was composed of two bars, parallel to the centreline of the tunnel, on which slid two carriages. These were connected by a screw so that, by locking one carriage, the other could be moved to a precise streamwise location by rotating the screw.

Vertical motion was achieved by mounting the probe-carrier on vertical shafts and using a micrometer head to give precise control.

This traverse gear was used for all boundary layer measurements and above plate sampling.

4.6 The Secondary Flow Injection System (Fig.4.6)

The injection system utilised air from the laboratory compressed air system, which was filtered and regulated to

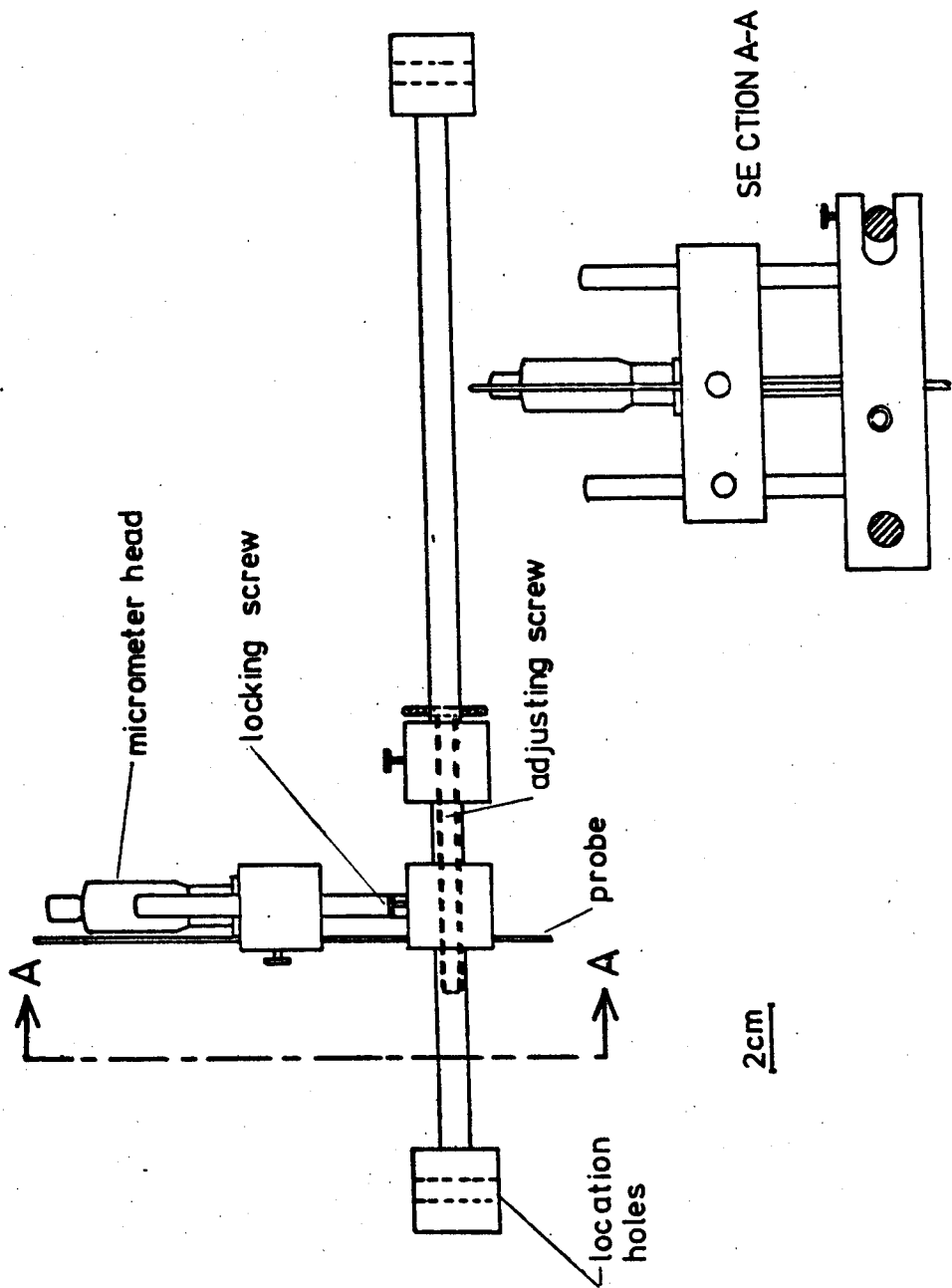


Fig. 4.5 The Probe Traverse Gear

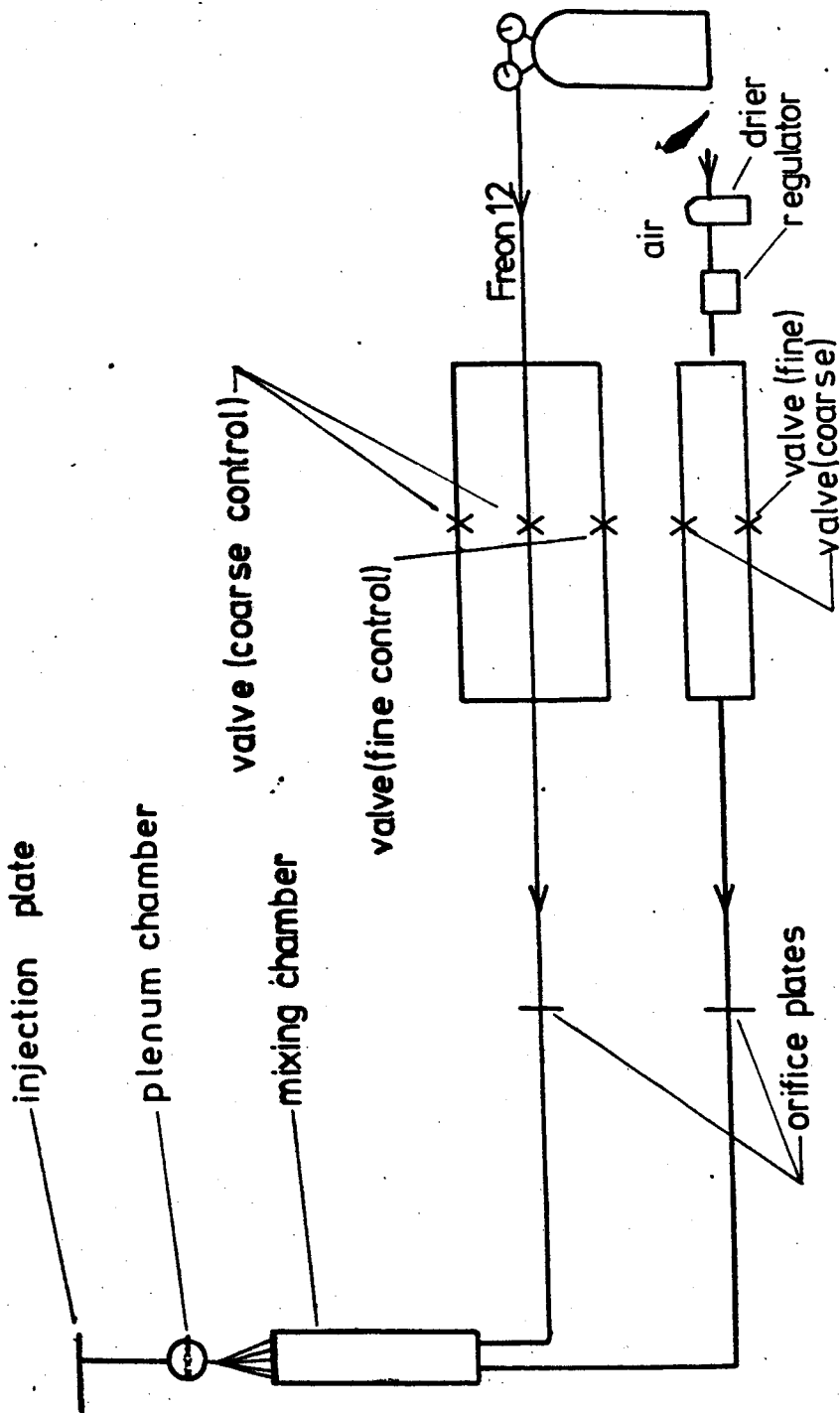


Fig. 4.6 The Secondary Flow System

$1.38 \times 10^5 \text{ N/m}^2$ gauge. It was then passed to two control valves, connected in parallel, and then to an orifice meter. The Freon 12 supply was from bottles of liquid Freon 12 under pressure. The vapour was regulated and then passed through copper pipes to another set of control valves and an orifice meter. The copper tubing helped to ensure that the vapour was at approximately ambient temperature before being mixed with the air.

4.6.1 Freon/Air Mixing Chamber (Fig.4.7)

Some difficulty was experienced with the mixing of the air and Freon 12 and several arrangements of baffles and gauzes were tried before deciding that the mixing cylinder was too short at 150mm. The length was increased to 406mm, and baffles, consisting of a disc of metal which almost sealed the cylinder and with a small hole on the periphery, were found to give the best results. The final arrangement was as in fig.4.7. This arrangement gave, within the sensitivity of the measuring instruments, the same concentration of Freon 12 from each injection hole for a given Freon 12/air mixture.

4.6.2 Plenum Chamber

Further difficulties were encountered when the total head from each injection tube was measured. It was found that the curvature of the flexible tubing (from the top of the mixing cylinder to the injection tubes) produced considerable variations in the velocities at the exit of individual holes. To overcome this, a plenum chamber with an internal gauze was

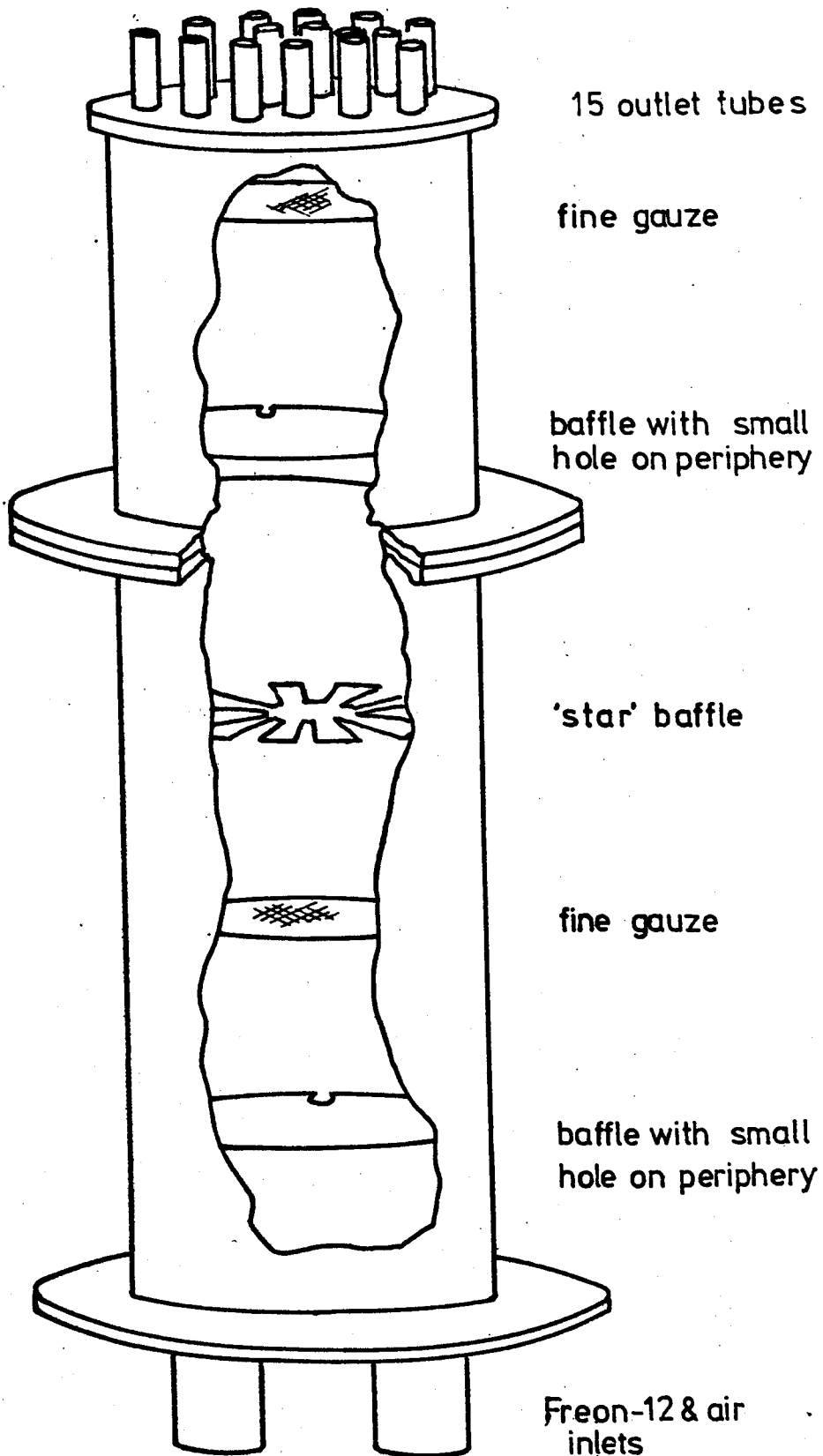


Fig.4.7 Sketch of the Freon 12/air mixing chamber

inserted between the mixing cylinder and injection tubes, fig.4.6. The exit tubes from the manifold were at the same spacing as the injection plate, so that although flexible tubing was again used, it was quite straight. Further measurements of the total heads at the injection position showed that the addition of this plenum chamber had overcome the problem.

The total length of the injection tube from the plenum chamber to the exit in the working section was over 80 diameters and the flow should have been almost fully developed. The injected flow was tested using a hot wire probe and the DISA 55-DO1 equipment, and was found to be turbulent.

4.6.3 Hole-Spacing Injection Plate (Fig.4.8)

A special injection plate was constructed to evaluate the variation of effectiveness with hole spacing. The plate had holes at 1.25 diameters pitch, combinations of which could be used to provide different hole spacings of 1.25, 2.5, 3.75 and 5 diameters. The unwanted tubes were blocked at inlet and filled flush to the surface with a soft malleable material.

These injection tubes were only 60mm in length and were fed from a manifold into which they were sealed. For simplicity, this manifold was fed from the plenum chamber described in 4.6.2.

4.7 Gas Sampling and Analysis

Fig.4.9 shows a schematic diagram of the analysing system, much of which is also visible in plate 4.3. A small pump was

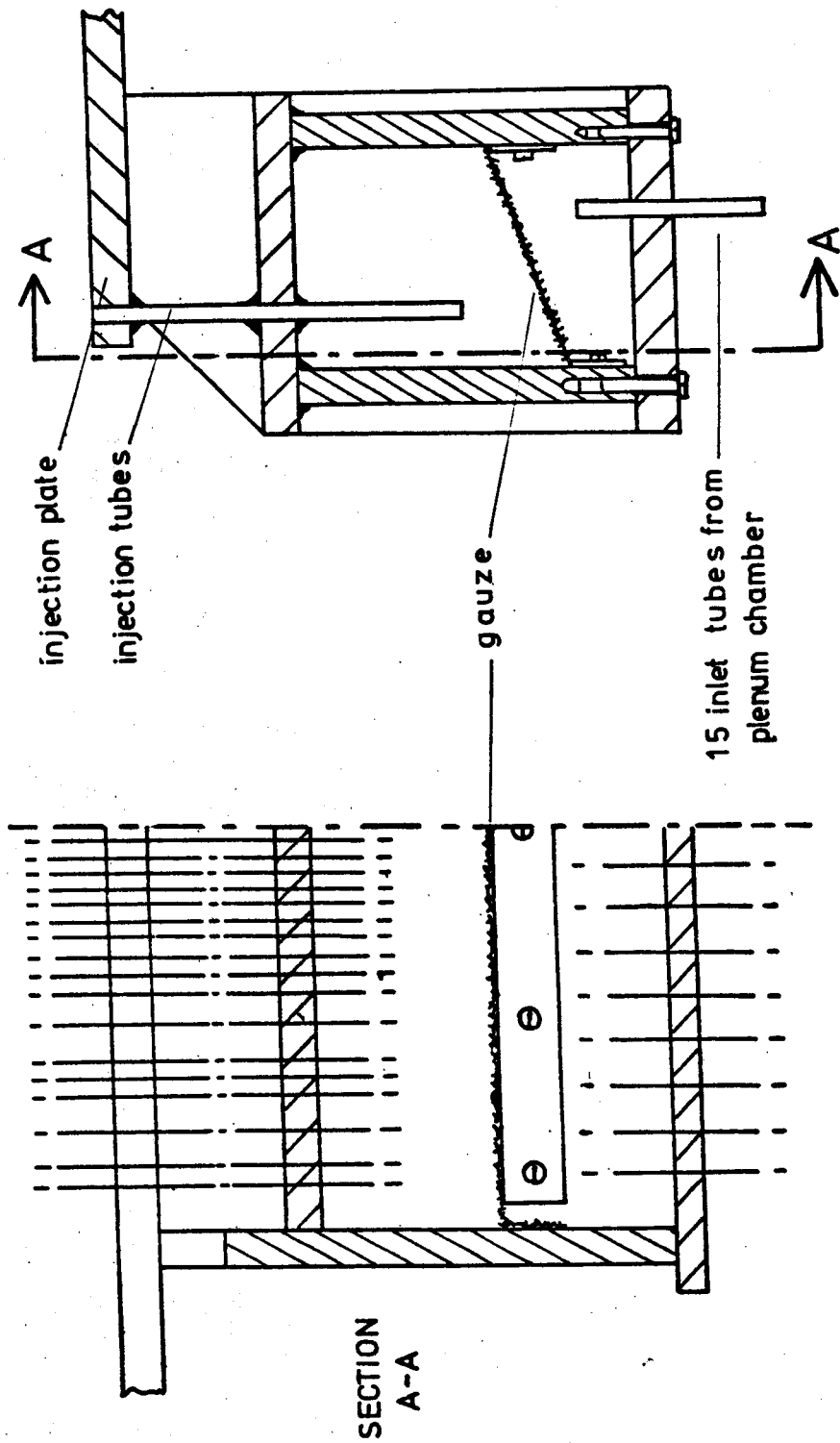


Fig. 4.8 Variable hole spacing injection plate

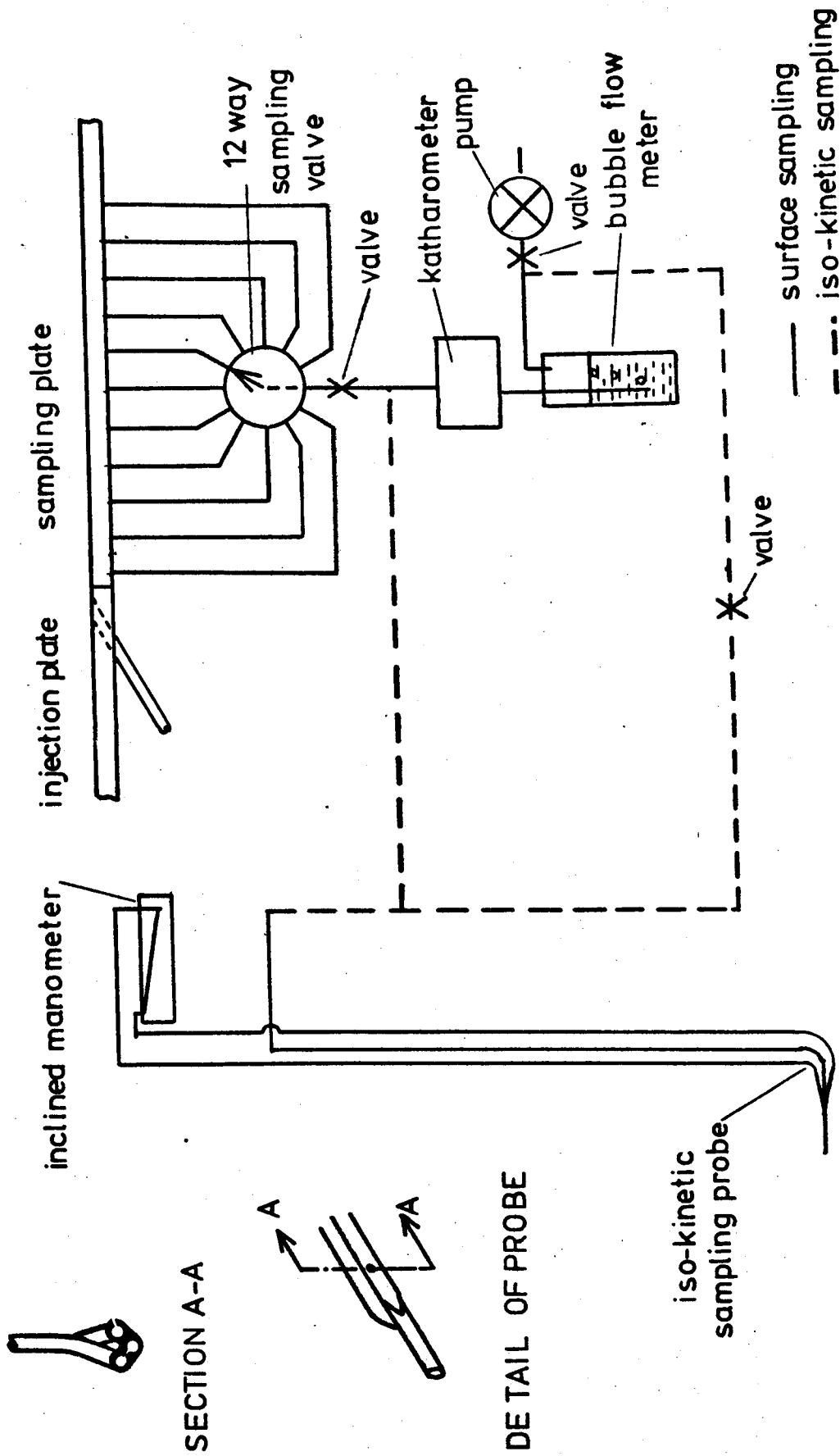


Fig.4.9 The Gas Sampling System

used to draw samples through the holes in the sampling plate via a twelve way valve to the katharometer and a simple flow meter.

The volume that had to be purged each time a sample was taken was kept as small as possible and, to this end, the katharometer was placed as close as could be managed to the sampling holes.

For samples drawn in through the sampling probe, an isokinetic sampling technique had to be used and, in order to keep the flow through the katharometer constant, most of the flow had to by-pass it, as in fig.4.9.

It was found that, providing it was small, the flow rate through the katharometer had no effect on the readings. This permitted the use of a very simple flow meter in which the flow from the katharometer bubbled through water; an estimation of the number of bubbles per second was sufficient to maintain the flow at a suitably low level. The flow rate through the katharometer was estimated as $14\text{mm}^3/\text{sec}$.

4.7.1 The Katharometer

The katharometer was manufactured entirely at the university and proved to be reliable and robust. The problem of analysing a binary mixture of gases is a simple one: there is no need to use a fractioning column and, if one is willing to calibrate regularly, only one wire is necessary.

Fig.4.10 shows a sectional view of the katharometer. The brass body ensured a slow response to variations in the ambient conditions, but this also meant that the cell had to be left for nearly 3 hours to warm up until equilibrium conditions had been reached. Platinum wire of 0.05mm diameter was used, held under slight tension, on stainless steel prongs set in P.T.F.E. plugs. It was hoped that the tension would prevent the wire from sagging when hot, which would have given rise to a different pattern of convection from the wire and greater tendency to drift.

A DISA 55-D01 constant temperature anemometer bridge was used to heat the wire to approximately 150°C. Frequent calibration was carried out, generally before and after each run, using the technique described in Appendix 3. The resolution was better than 1% by mass of Freon 12, which generally permitted the effectiveness to be measured to $\pm 0.5\%$ in absolute terms.

4.7.2 The Iso-kinetic Sampling Probe

The detail in fig.4.9 shows a sketch of the probe used in the sampling carried out above the plate. It comprised three tubes - two to measure pressures, the third being the sampling tube. The latter had a 0.55mm diameter hole drilled in the side 10mm from the end. This was connected via a similar hole in the side of one of the pressure tubes. The other pressure tube had a hole on the outside to measure the local static pressure. The sucking on the sampling tube was varied so that the pressures in both tubes were the same. The iso-kinetic sampling is discussed further in Appendix 4.

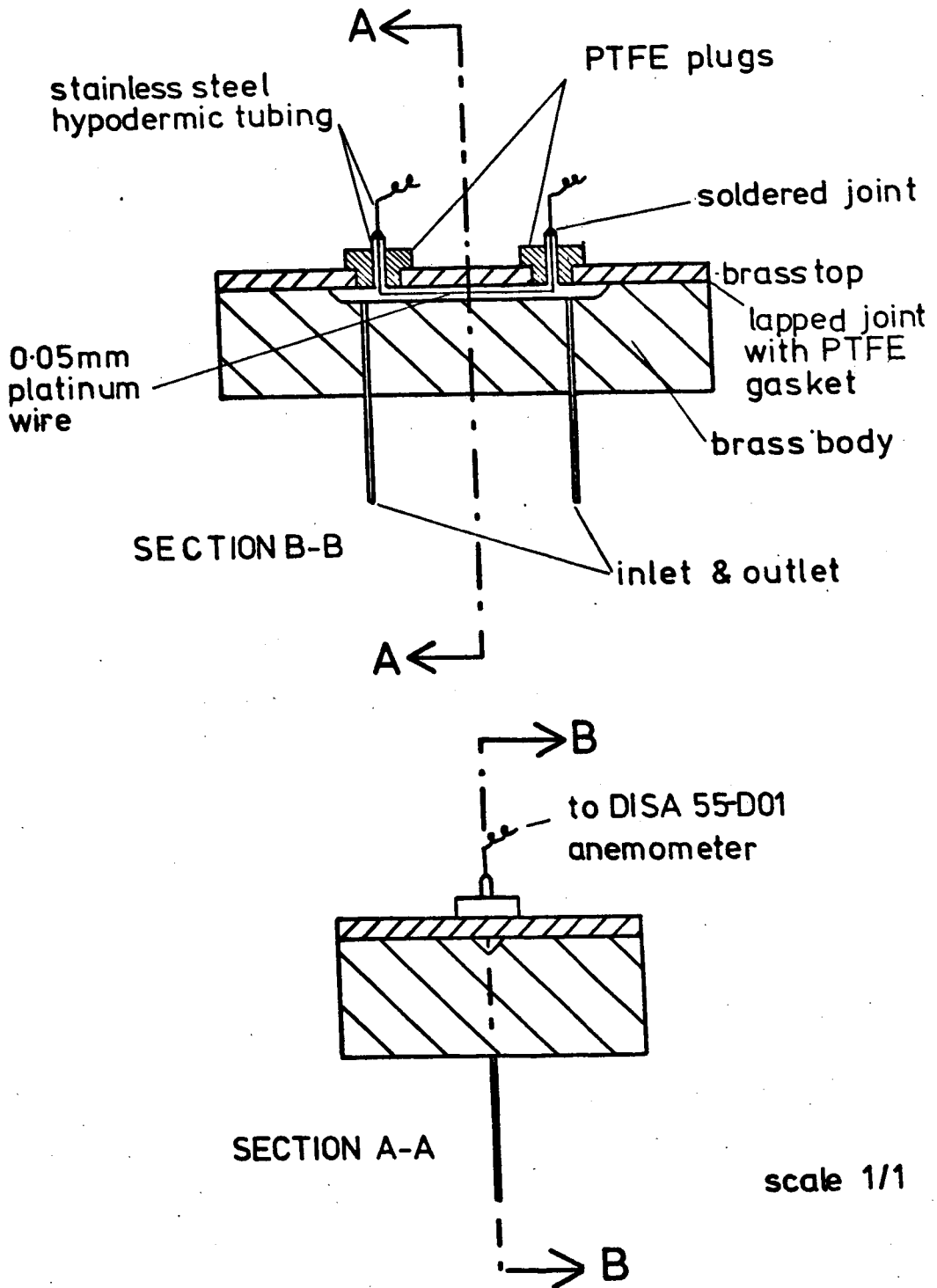


Fig. 4.10 The Katharometer

4.8 Boundary Layer Measurement

Two probes were used to measure the boundary layer thicknesses over the injection holes. For the thicker boundary layers, a flattened total head probe was manufactured, but in most cases a modified DISA boundary layer probe was used in conjunction with a DISA 55-D01 anemometer bridge. Both probes were mounted on the small traverse gear.

4.9 Conclusion

The apparatus described above, although constructed on simple lines and within a strict budget, proved to serve its purpose reliably.

CHAPTER 5 : THE EXPERIMENTAL PROGRAMME

This chapter describes the experimental programme with particular reference to the objectives of the current research and states the ranges of the parameters covered.

=====

The majority of the published data on film cooling via a row of holes has been based on a hole spacing of three diameters and in practice a spacing of between 2.5 and 5 diameters is generally used. (Below 2.5 diameters there is the danger of the blade failing due to cracks propagating between the holes.) It was therefore decided initially to consider a hole spacing of three diameters which would enable a comparison to be made with the other published work.

Injection normal to the mainstream was chosen as a standard with which to compare the other angles, so the majority of tests were conducted at this angle.

The effect of varying density ratio was studied first. Obviously, as the concentration of Freon 12 in the injectant is decreased, the sensitivity of the katharometer becomes more important. Because of this, it was decided that the minimum density ratio to be used would be 1.5, whilst the maximum would be 4.26 (i.e. with a pure Freon 12 injectant). Although the higher value is almost twice as great as the density ratios presently experienced in a real blade cooling situation, it was

felt that this was a logical extension to the work and might find application in some other field of film cooling.

In nearly all the tests measurements were taken to give a full surface distribution as far downstream as 108.6 diameters. The closeness of the readings to the hole varied, generally being 1.5 diameters downstream on the centreline of the hole, and 4.25 diameters away from the centreline.

The density ratio tests were conducted with several different flow conditions. Initially, to evaluate the working of the whole system, a favourable pressure gradient was employed of $-2.47 \times 10^3 \text{ N/m}^2/\text{m}$. The density ratio was varied for a constant velocity ratio of 0.7; then the velocity ratio was varied between 0.25 and 1.48 for a nominal density ratio of 2.0.

The next series of tests included a nominal zero pressure gradient, but tested the idea of accelerating the upstream flow to vary the boundary layer thickness. A boundary layer displacement thickness similar to that for the previous tests was obtained and the density ratio and velocity ratio variations were repeated.

The boundary layer thickness was next increased to its maximum, simply by using a flat roof over the full length of the working section. The density and velocity variations were repeated. Measurements were also taken above the test surface. At this stage it was decided to take some additional results on the centreline only, to give values of effectiveness for the range of density ratios 1.5 to 4.26 over the velocity ratios of 0.25 to 1.24.

The following series of tests again covered the range of density ratios 1.5 to 4.26 for an injectant velocity ratio of 0.7, and velocity ratios of 0.25 to 1.48 for a density ratio of 2. For this series the greatest favourable pressure gradient that could be accommodated in the working section was used, but the throttling effect of the contour meant that the mainstream velocity over the holes had to be reduced to 25.9m/sec from 30.5m/sec and the lower value was used thereafter. The pressure gradient was measured as $-9.84 \times 10^3 \text{ N/m}^2/\text{m}$ and the boundary layer displacement thickness, at the point of injection, as 0.132 relative to the hole diameter.

The acceleration parameter, $\frac{\nu}{U_\infty^2} \frac{dU_\infty}{dX}$, was calculated as 8.5×10^{-6} , which is within the range experienced on a turbine blade. Measurements of concentration were also taken above the surface.

At this point it was decided that sufficient information had been gained on the density ratio effect; consequently, all the following tests were carried out using a nominal density ratio of 2. A flat roof, giving a similar boundary layer displacement thickness to the above accelerating contour, was then used. The actual value of δ^*/D was 0.156 and the velocity ratio was varied as before. Once again measurements were taken above the surface.

The contoured roof was then changed for one giving an adverse pressure gradient of $8.47 \times 10^2 \text{ N/m}^2/\text{m}$ and a boundary layer displacement thickness of 0.27 hole diameters; the velocity variation was carried out once more.

Results were then taken with a nominal zero pressure gradient and boundary layer displacement thickness of 0.26 diameters to compare with the above.

The effect of angled injection was investigated at two angles other than 90° , namely 35° and 55° . For each angle the results were taken at a nominal zero pressure gradient and at two values of boundary layer displacement thickness (0.26 and 0.16 diameters) to enable direct comparison with the 90° case. The tests were limited to the nominal density ratio of 2 and to velocity ratios of 0.25, 0.53, 0.7 and 1.24, as it was anticipated that the general trends would be the same as for the 90° injection. In each case results were taken above the surface of the plate.

The final series of tests involved the variation of the hole spacing. The hole spacings chosen for study were 1.25, 2.5, 3.75 and 5 diameters. These were chosen so that a row of holes of 1.25 diameter pitch could be manufactured, then combinations of holes blocked to give the required spacing - thus requiring only one injection plate. It was anticipated that the 1.25 hole spacing might behave like a slot. These results were taken for the same range of parameters as the angled injection.

The 1.25 diameter spacing was repeated, with side walls at the ends of the row of holes stretching the full length of the injection and sampling plates. This was to ensure that there was a two-dimensional flow situation, since the tests without these walls at this small hole spacing were found not

to be two-dimensional far downstream (Appendix 1).

Table 5.1 indicates clearly the parameters covered and the number of tests conducted.

RUN Nos.	δ^*/D	H	β Deg.	S/D	$\Delta p/X$ N/m ² /m	U_∞ m/sec	U_j/U_∞	ρ_j/ρ_∞	Above Plate
1-19	0.32	1.24	90	3	-2.47×10^3	30.5	0.25 - 1.48	1.5 - 4.26	
40-56	0.33	1.26	90	3	-3.24×10^1	30.5	0.25 - 1.48	1.5 - 4.26	
60-99	0.63	1.32	90	3	-9.96×10^1	30.5	0.25 - 1.48	1.5 - 4.26	
100-109	0.24	1.25	90	3	-4.13×10^1	30.5	0.25 - 1.24	2.0 - 3.0	✓
120-132	0.13	1.35	90	3	-9.84×10^3	25.9	0.25 - 1.48	1.5 - 4.26	
140-146	0.13	1.35	90	3	-9.84×10^3	25.9	0.20 - 1.24	2.0, 3.0	✓
160-167	0.16	2.43	90	3	-4.73×10^1	25.9	0.25 - 1.48	2.0	
180-184	0.16	2.43	90	3	-4.73×10^1	25.9	0.25 - 1.24	2.0	✓
200-207	0.27	1.58	90	3	$+8.47 \times 10^2$	25.9	0.25 - 1.48	2.0	
220-221	0.27	1.58	90	3	$+8.47 \times 10^2$	25.9	0.7, 1.24	2.0	✓
240-247	0.26	1.62	90	3	-3.71×10^1	25.9	0.25 - 1.48	2.0	
260-261	0.26	1.62	90	3	-3.71×10^1	25.9	0.7, 1.24	2.0	✓
280-283	0.26	1.62	35	3	-3.71×10^1	25.9	0.25 - 1.24	2.0	
300-301	0.26	1.62	35	3	-3.71×10^1	25.9	0.7, 1.24	2.0	✓
320-323	0.26	1.62	55	3	-3.71×10^1	25.9	0.25 - 1.24	2.0	
340-341	0.26	1.62	55	3	-3.71×10^1	25.9	0.7, 1.24	2.0	✓
360-363	0.16	2.40	55	3	-4.27×10^1	25.9	0.25 - 1.24	2.0	
380-381	0.16	2.40	55	3	-4.27×10^1	25.9	0.7, 1.24	2.0	✓
400-403	0.16	2.40	35	3	-4.27×10^1	25.9	0.25 - 1.24	2.0	
420-421	0.16	2.40	35	3	-4.27×10^1	25.9	0.7, 1.24	2.0	✓
440-443	0.16	2.40	90	1.25	-4.27×10^1	25.9	0.25 - 1.24	2.0	
460-463	0.16	2.40	90	2.50	-4.27×10^1	25.9	0.25 - 1.24	2.0	
480-483	0.16	2.40	90	3.75	-4.27×10^1	25.9	0.25 - 1.24	2.0	
500-503	0.16	2.40	90	5.00	-4.27×10^1	25.9	0.25 - 1.24	2.0	
520-523	0.16	2.40	90	1.25	-4.27×10^1	25.9	0.25 - 1.24	2.0	

Notes: (i) $H = \frac{\text{BOUNDARY LAYER DISPLACEMENT THICKNESS } (\delta^*)}{\text{BOUNDARY LAYER MOMENTUM THICKNESS } (\theta)}$

(ii) In the final column, a ✓ indicates that measurements were taken via the probe above the test surface.

TABLE 5.1 Details of Test Parameters and Run Numbers

CHAPTER 6 : THE EXPERIMENTAL PROCEDURE

Chapter 6 outlines briefly the procedure that was followed to make ready the apparatus for a series of tests and the manner in which the tests were conducted.

=====

6.1 Apparatus Checks

Before each series of tests the injection plate was checked to ensure that it was flush with the two plates on either side and not presenting a step to the flow; also, that it was free from dust and grit. The diffuser and contours were mounted and their positions measured, so that the exact conditions could be reproduced later, if necessary.

6.2 Preliminary Adjustments

The mainflow was turned on at this stage and the correct flow velocity set up using a pitot tube. The boundary layer bleed was adjusted to balance the pressures on either side of its leading edge and the mainstream velocity was checked. The contraction was then calibrated and used subsequently for metering the mainstream velocity.

6.2.1 Boundary Layer Measurements

The boundary layer thickness was measured using two different techniques: initially, for the larger thicknesses

a flattened pitot probe was employed in conjunction with an inclined manometer; but when the thickness fell to under 2.5mm, a hot wire DISA boundary layer probe was used to give adequate spacial resolution.

The pitot probe was connected to the small traverse gear over the working section and passed through the contour. It was positioned on the test surface and lifted off the surface in small steps using the micrometer adjustment. The hot wire probe was mounted in the same manner, but was lowered towards the surface until the velocity measured was 20% of the mainstream value, or until the wire touched the surface and broke. In the first case the direction was reversed and a further set of readings obtained. The data were processed on a small computer.

The velocity close to the surface was found to vary in an approximately linear fashion with height and by extrapolating back to zero velocity a value could be obtained for the actual height of the probe above the surface. This was then allowed for in the boundary layer thickness calculations.

6.2.2 Pressure Gradient Measurements

The sampling holes in the test surface were also used as static pressure tappings and connected to a multi-tube manometer for this purpose. When the readings had been taken, the tappings were disconnected ready for the sampling measurements.

6.3 Test Procedure

6.3.1 Preliminaries

The katharometer required about 3 hours to warm up and stabilise and was accordingly switched on with the pump that drew the samples through it first thing every morning, the flow rate being adjusted to the correct level.

A computer programme containing all the data from the orifice plate calibrations was used to give the approximate settings for the manometers from inputs of injection velocity and density. A value was also given of the product of pressure and pressure drop across the orifice, $p\Delta H_1$, as in $\dot{m} \propto \sqrt{p\Delta H_1}$.

This value was then iterated towards, when the secondary flow was set up. In fact one iteration step was always sufficient, the density ratios of the resulting mixtures usually being within 2% of the desired values. The injection plate was then traversed to the correct starting position and all was ready for the tests proper.

6.3.2 Tests

When the tests were actually to be conducted, the mainstream velocity was adjusted using the pressure drop across the contraction, and the secondary velocity as outlined above.

The multiway valve was rotated to scan the different sampling holes in turn progressing downstream, and the digital voltmeter reading was noted. At the end of the

streamwise set of results a reading for air was taken to determine whether the katharometer had drifted or not. The flow rates were checked and the injection plate was traversed across to the next station where the procedure was repeated.

At the end of the tests a tube was connected directly to the katharometer and the other end was inserted into the mouth of one of the injection holes to take a sample of the injectant. This gave the concentration of Freon 12 in the injectant, and hence the injectant density and the film cooling effectiveness.

Finally, the katharometer was calibrated using a medical syringe at volume ratios of 0, 10, 30 and 100% Freon 12. The calibration was repeated several times and the results were usually the same: if not, the calibration was repeated.

6.3.3 Traversing Steps

To save gas and time, the injection plate was traversed in seven 1mm steps, starting 1mm before the centreline of the centre hole. With a hole spacing of 6.81mm, this covered the region from one side of one hole to the far side of the centreline between holes, fig.6.1.

Assuming the flow to be symmetrical about these centre-lines, this was sufficient to give a full picture of the surface distribution of effectiveness. The contour plots of surface effectiveness and those depicting the concentration

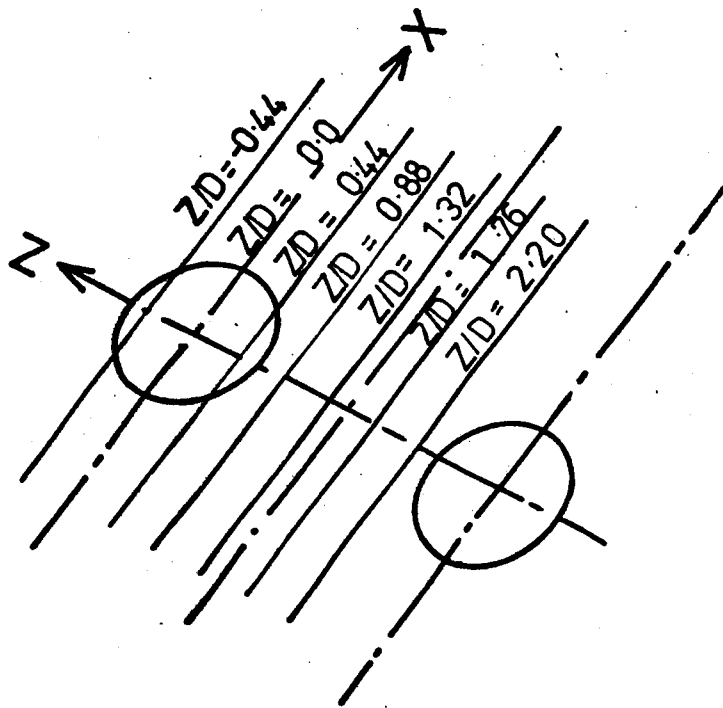


Fig.6.1 Lateral positions of downstream traverses

ratios normal to two jet centrelines indicate this to be a reasonable assumption, fig.7.15, 7.18, Appendix 1.

6.4 Tests above the Surface

The procedure for the tests conducted above the surface was the same as outlined above, except that the katharometer was not connected to the multi-way valve but to the sampling probe as described in Chapter 4. The flow rate through the probe was adjusted to give the same static pressure inside the tube as the outside static pressure, to give iso-kinetic sampling. The flow through the katharometer was then adjusted to keep it constant by opening or closing the by-pass valve, and a reading was taken. The pitot was then raised and the procedure repeated.

6.5 Processing of Results

The raw data was processed using the departmental PDP1105 computer as outlined in Appendix 3. The results obtained by the methods given above are discussed in the next chapter.

CHAPTER 7 : DISCUSSION OF RESULTS

Within this chapter the results obtained during the experimental programme are discussed and compared with the work of other experimenters. Selected results are presented which illustrate points being made. The work is considered in two parts: normal injection and angled injection.

=====

The data will generally be presented in the form of a spanwise average, $\bar{\eta}$, which was calculated from the spanwise readings using a Simpson's rule numerical integration technique. This value of effectiveness gives an indication of the overall level of effectiveness when plotted against the dimensionless downstream distance X/D . The centreline effectiveness, $\hat{\eta}$, will also be referred to.

7.1 Injection at 90° to the Mainstream

This section has been sub-divided so that effects of various other parameters (such as the density ratio, boundary layer displacement thickness, etc.) can be considered individually.

7.1.1 The Effect of the Density Ratio

A set of results in which the density ratio was systematically varied is presented in fig.7.1. The velocity ratio was maintained constant at 0.7 and the density

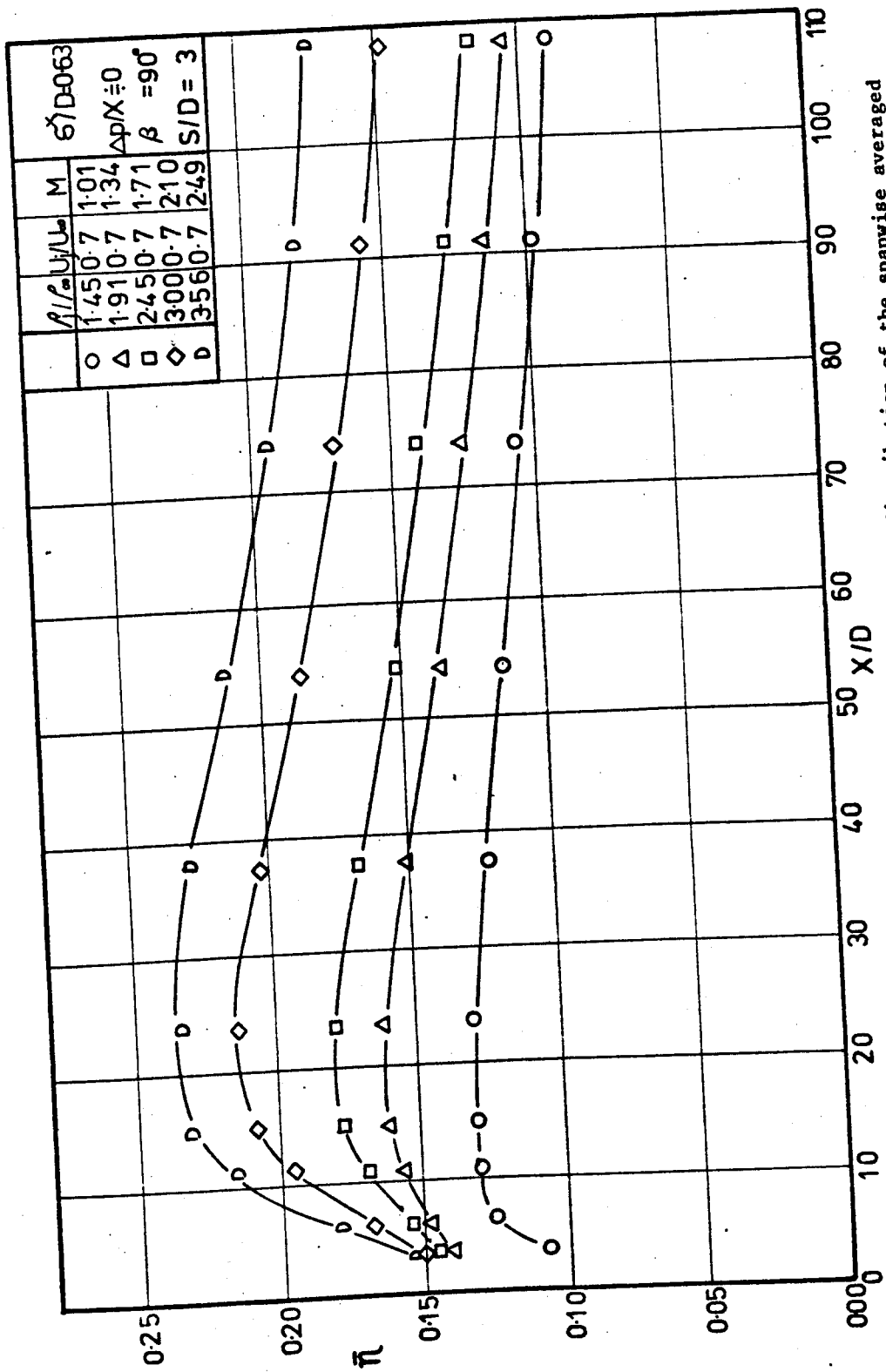


Fig. 7.1 The effect of varying density ratio on the downstream distribution of the spanwise averaged effectiveness, η

ratio varied between 1.5 and 3.6. It can be seen that, with the exception of the lowest density ratio, the spanwise averaged effectiveness is almost independent of the density ratio close to the injection point, i.e. within 5 diameters. However, further downstream the picture changes, and the effectiveness increases with increasing density ratio, or increasing blowing rate.

For the majority of the density ratios, the effectiveness reaches a maximum at about 20 diameters from the injection holes. This is partly due to the low levels of effectiveness between the holes at small X/D . Further downstream, the effectiveness rises as the jets spread laterally, until at $X/D = 25$ the results are fully two dimensional and from then on, the effectiveness slowly falls as the mainstream air is entrained from above. Fig.7.2 shows concentration contours downstream of a jet of density ratio 2.5, showing the low effectiveness between the holes and the lateral spreading of the jets.

Fig.7.3 shows the results taken on the centreline for the same series of tests. Once again, the effectiveness is independent of the density ratio close to the hole, but further downstream than 7 diameters, an increase in density ratio brings an increase in effectiveness. However, notice that here the results at low blowing rates do not achieve a maximum effectiveness, but instead, the effectiveness steadily falls as the freestream is entrained and the injectant concentration falls. At the higher blowing rates the effectiveness

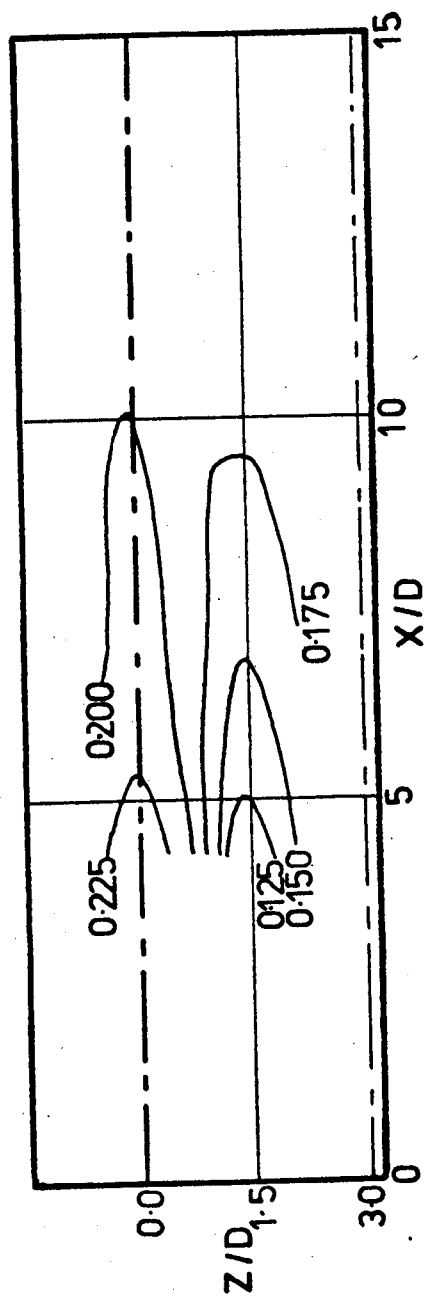


Fig. 7.2 Contours of constant effectiveness downstream of the injection hole for 90° injection with $U_j/U_\infty = 0.7$ and $\rho_j/\rho_\infty = 2.5$

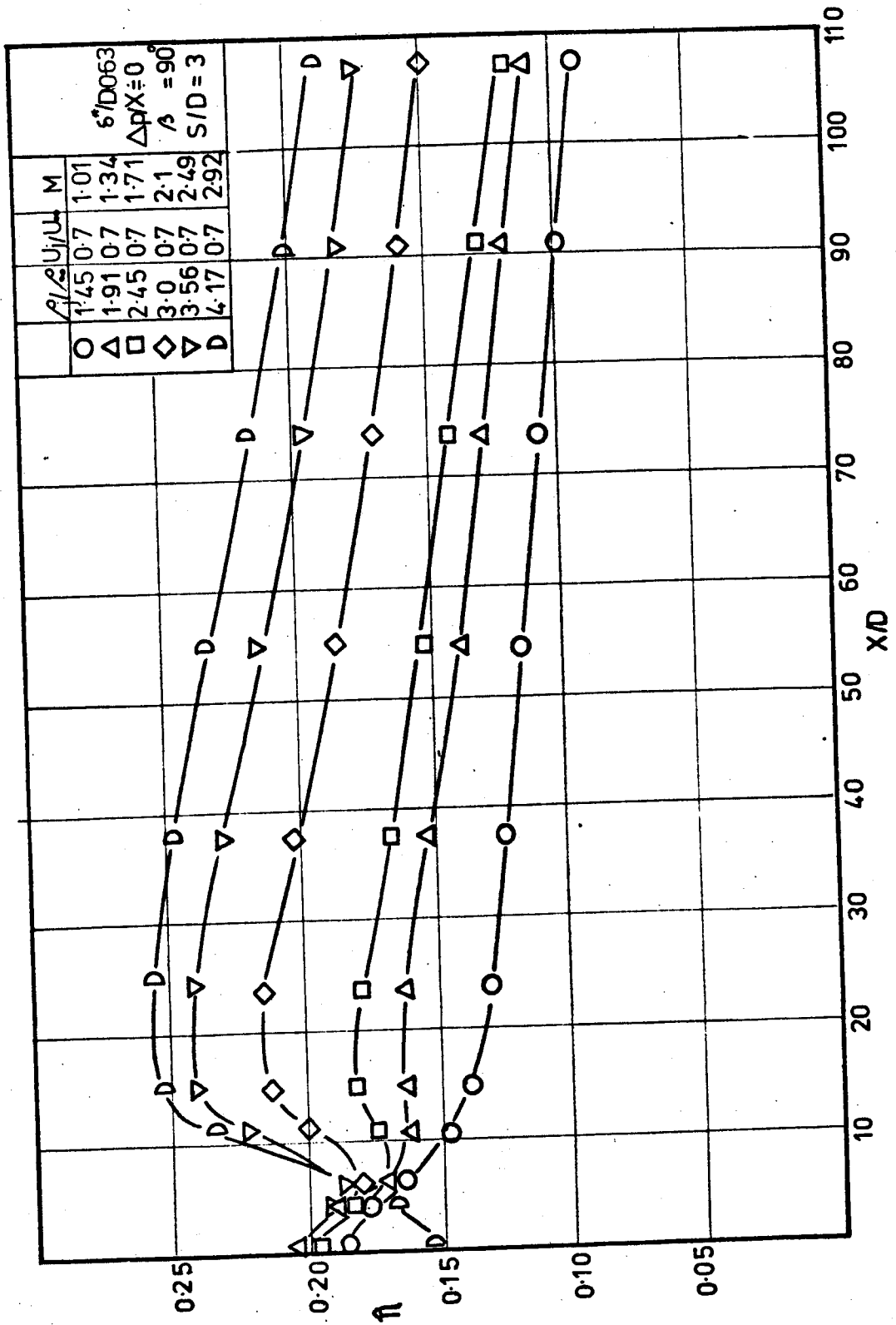


Fig. 7.3 The effect of varying density ratio on the centreline distribution of effectiveness

risers to a maximum - as it did for the spanwise averaged values, again at $X/D = 20$ - then decreases. The initial rise is assumed to be the result of the jets spreading back to the surface having initially become detached from it. For the largest blowing rate, $M = 2.92$ (not included in fig.7.1) this 'lift-off' tendency is most marked, with the effectiveness being significantly lower close to the injection holes than is the case for the other density ratios.

Curves of similar shape were obtained for the favourable pressure gradients and differing boundary layer thicknesses.

7.1.2 The Effect of Velocity Ratio

Variations of spanwise averaged effectiveness with velocity ratio at a nominally constant density ratio of 2 are shown in fig.7.4. Here a completely different pattern is produced compared with the previous figures. As the blowing rate is increased, so the effectiveness for values of X/D less than 10 falls dramatically, due to the jets becoming detached from the surface.

The effect is much more pronounced here than with the density variations, and it is clear that the velocity ratio is the more important factor in jet lift off. Moving downstream a position is reached at $X/D = 15$, where the effectiveness is almost independent of velocity ratio. Further downstream the effectiveness rises as the

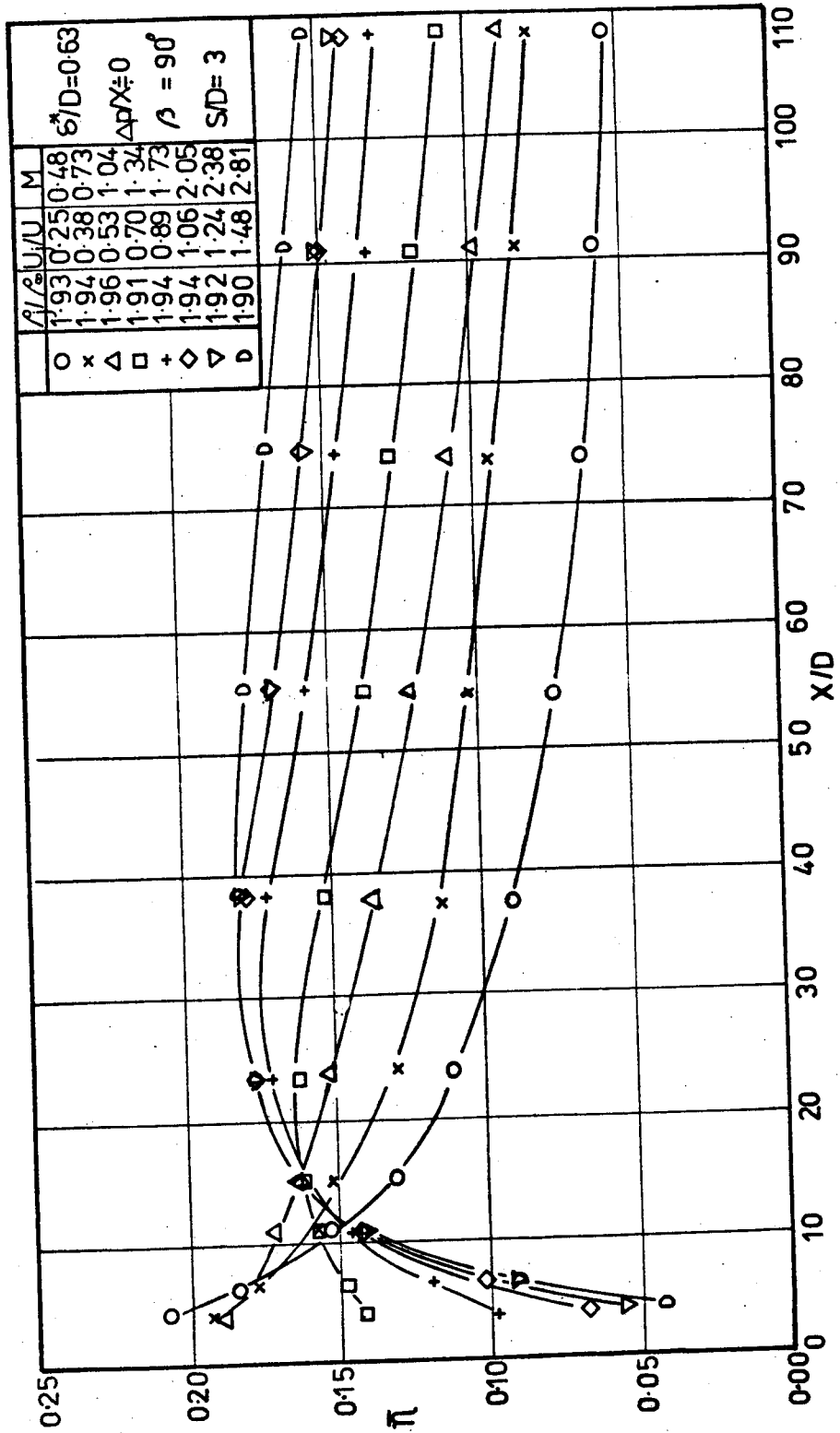


Fig. 7.4 The effect of varying velocity ratio on the downstream distribution of spanwise averaged effectiveness, $\bar{\eta}$

amount of injectant is increased, that is, as the blowing rate is increased.

The picture for the centreline values, fig.7.5, is substantially the same, with lower levels of effectiveness close to the injection position. The same pattern was observed for differing boundary layer thickness and pressure gradients.

These results are in rough agreement with those of Goldstein et al (7.1), but their results do not show the increase in effectiveness on the centreline with increasing blowing rate as they considered only a single injection hole.

Comparing also with Smith's results (7.2) at the same momentum parameter, fair agreement is found, although the present results show an effectiveness of 0.14 at 80 diameters, compared with 0.055 for Smith's results. Note that the mean line given in Smith's results was used in the comparison, with its limitations as discussed in Chapter 2.

7.1.3 The Blowing and Momentum Parameters

The preceding sections give an indication of the complex nature of the relationships between the effectiveness and the density and velocity ratios. To date, it has been the practice to compare results on the basis of the blowing parameter or blowing rate or, alternatively, the momentum parameter. Fig.7.6 shows a carpet plot of

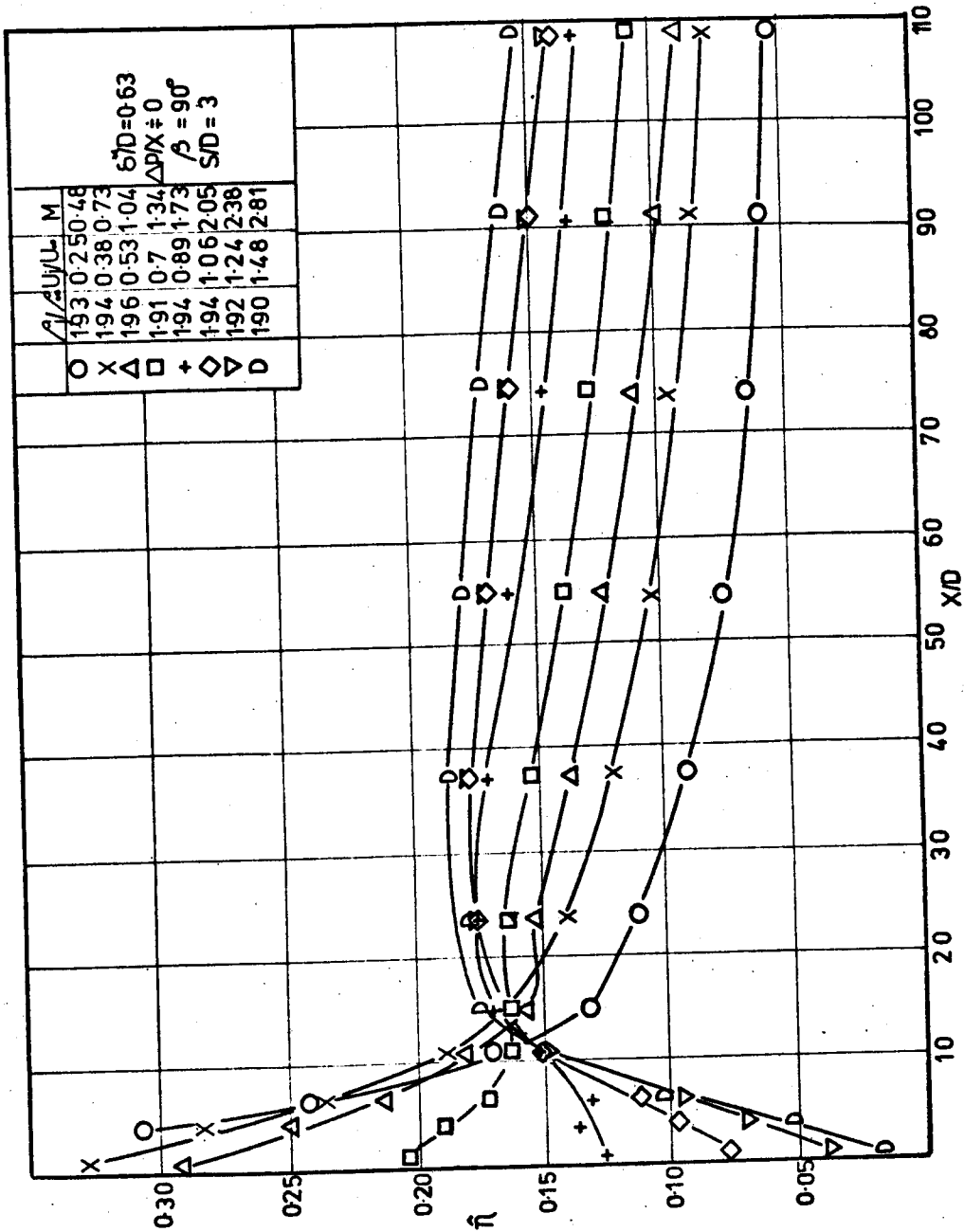


Fig. 7.5 The effect of varying velocity ratio on the centreline distribution of effectiveness, η

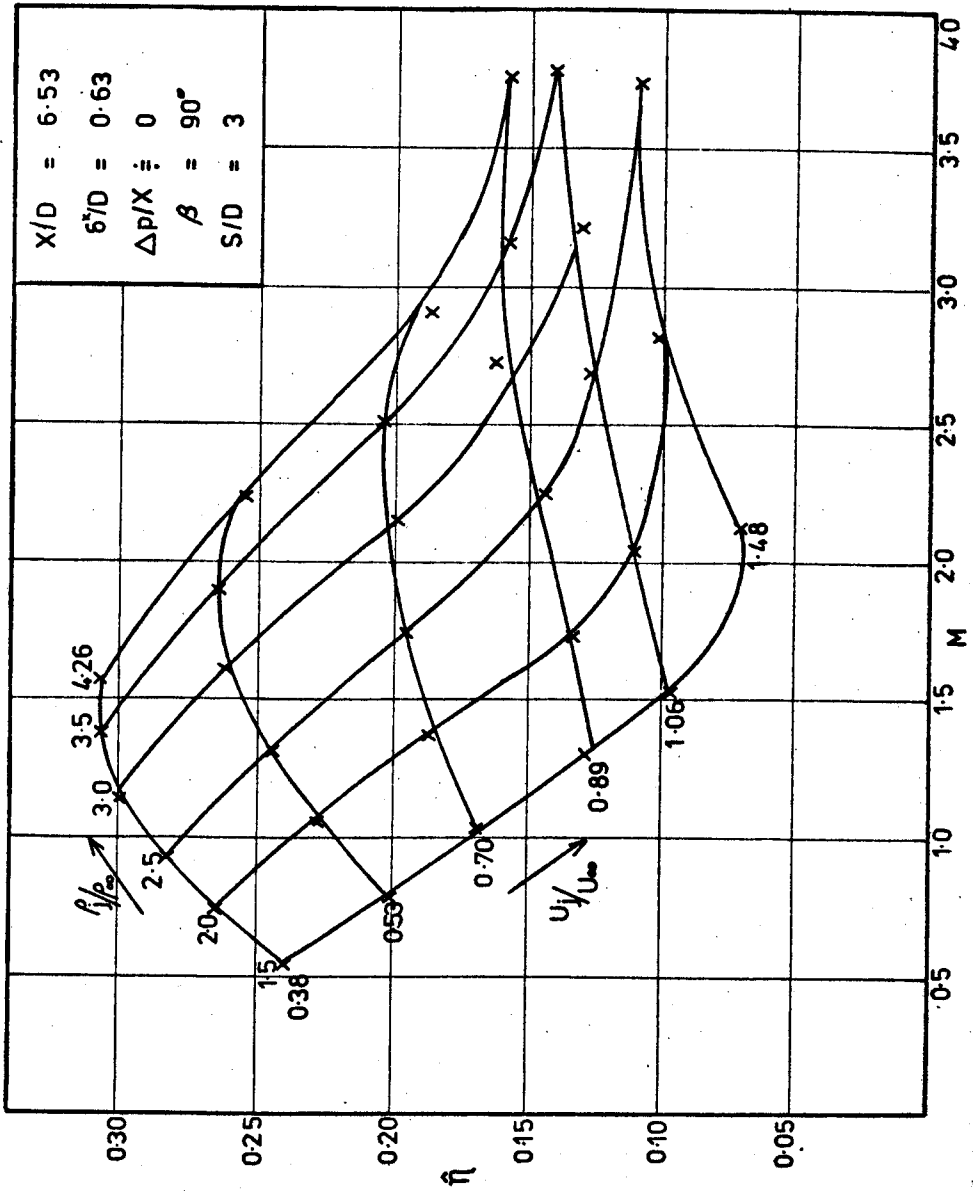


Fig. 7.6 Graph of centreline effectiveness, η , against blowing parameter, M , for varying density and velocity ratios at $X/D = 6.53$

centreline effectiveness vs. blowing parameter for varying density and velocity ratios at $X/D = 6.5$. It can be seen that the density ratio does affect the effectiveness, but not as strongly as the velocity ratio.

Considering a value of blowing parameter of 1, the effectiveness varies from 0.17 at a density ratio of 1.5 to 0.27 at a density ratio of 2.5. Clearly, the blowing parameter cannot be used to correlate results taken at differing density ratios as has been done - at least, not at this downstream distance.

Plotting the same results against the momentum parameter, fig.7.7, does improve the collapse but taking a momentum parameter of unity gives effectiveness values of 0.13 and 0.22 at density ratios of 1.5 and 2.5 - showing that the momentum parameter is only marginally better as a correlating parameter than the blowing rate.

Fig.7.8 shows that at a downstream distance of 23.8 diameters, the dependence of the effectiveness on the density ratio has increased, especially at low values of blowing rate. Comparing this with the momentum parameter for the same station, fig.7.9, one now finds that the former gives the better collapse of the results. This is because, as stated earlier, the effectiveness is almost independent of velocity ratio at a value of $X/D = 15$.

Progressing further downstream to 74 diameters, fig. 7.10, the blowing rate has become a correlating parameter for

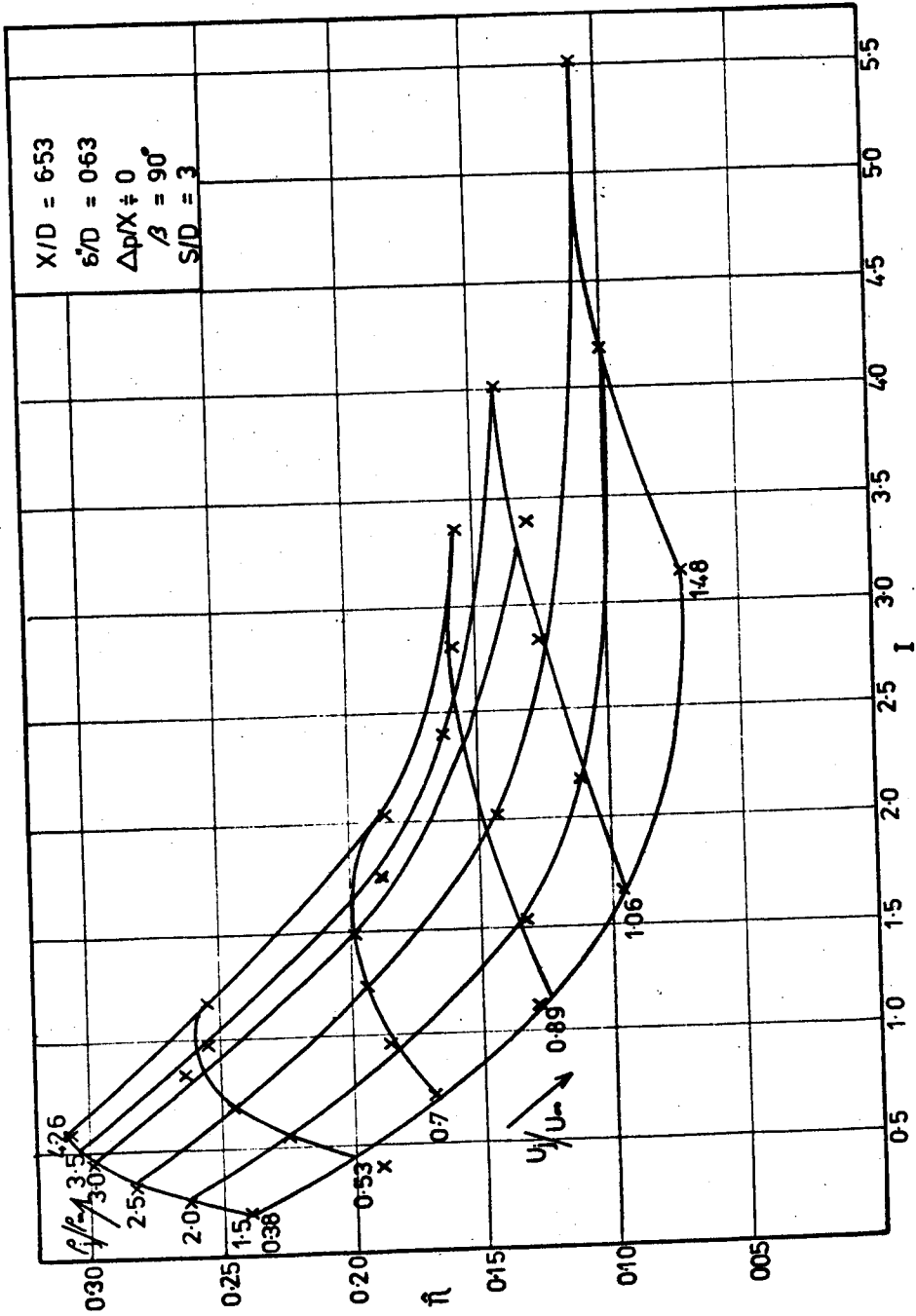


Fig. 7.7 Graph of centreline effectiveness, η , against momentum parameter, I , for varying density and velocity ratios at $X/D = 6.53$

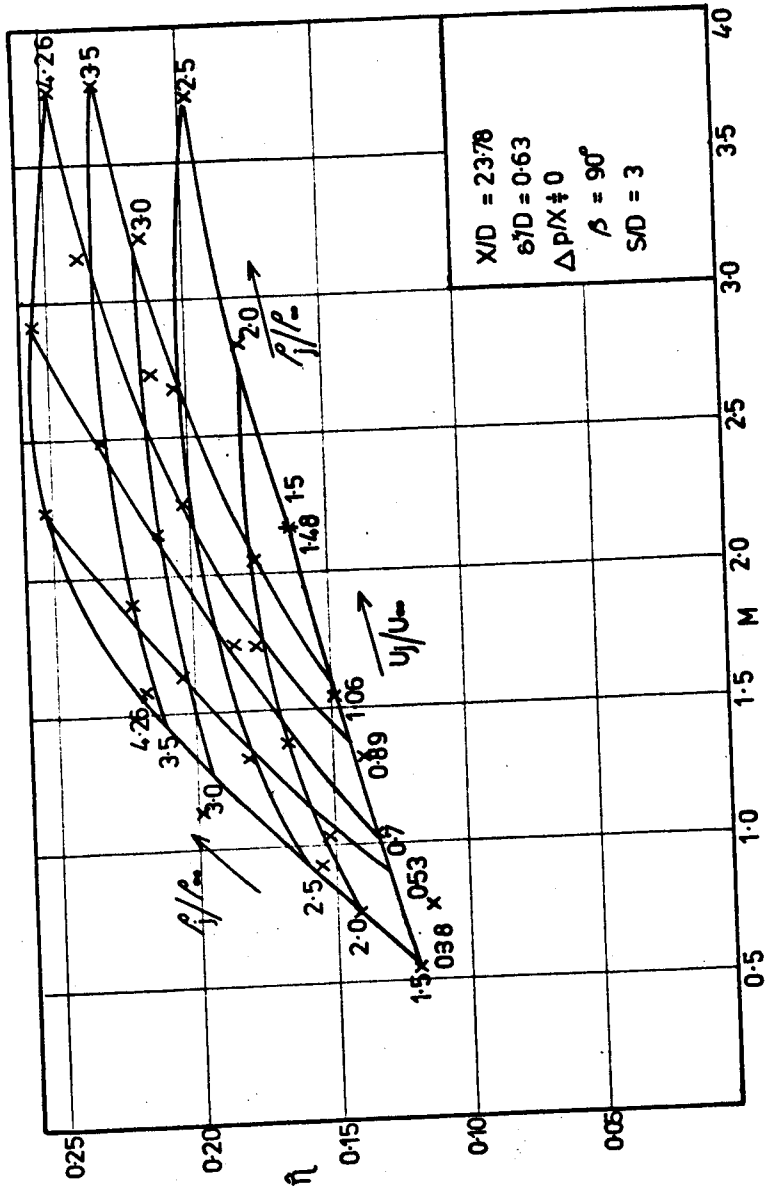


Fig. 7.8 Graph of centreline effectiveness, η , against blowing parameter, M , for varying density and velocity ratios at $X/D = 23.78$

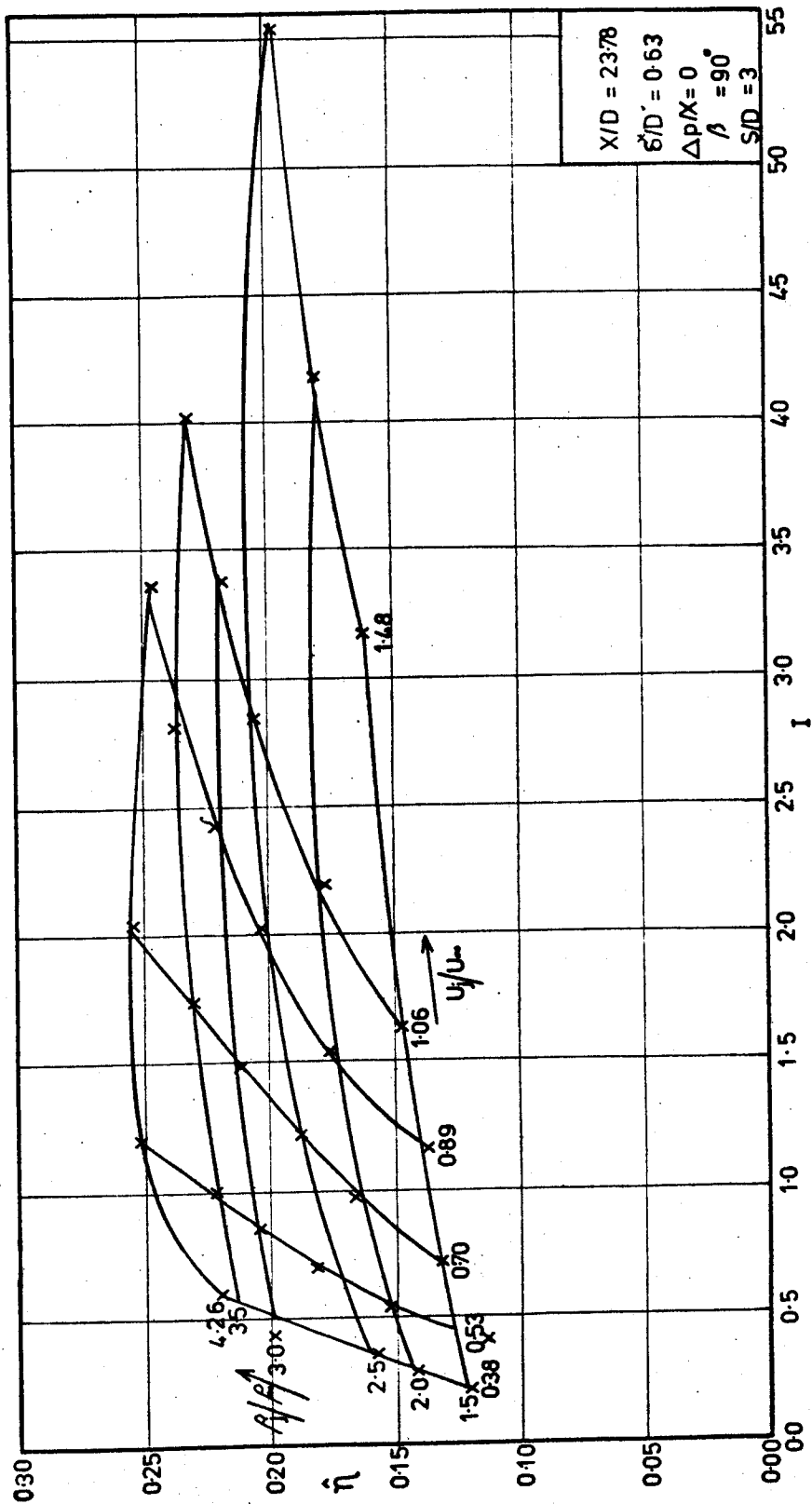


Fig. 7.9 Graph of centreline effectiveness, η , against momentum parameter, I , for varying density and velocity ratios at

$X/D = 23.78$

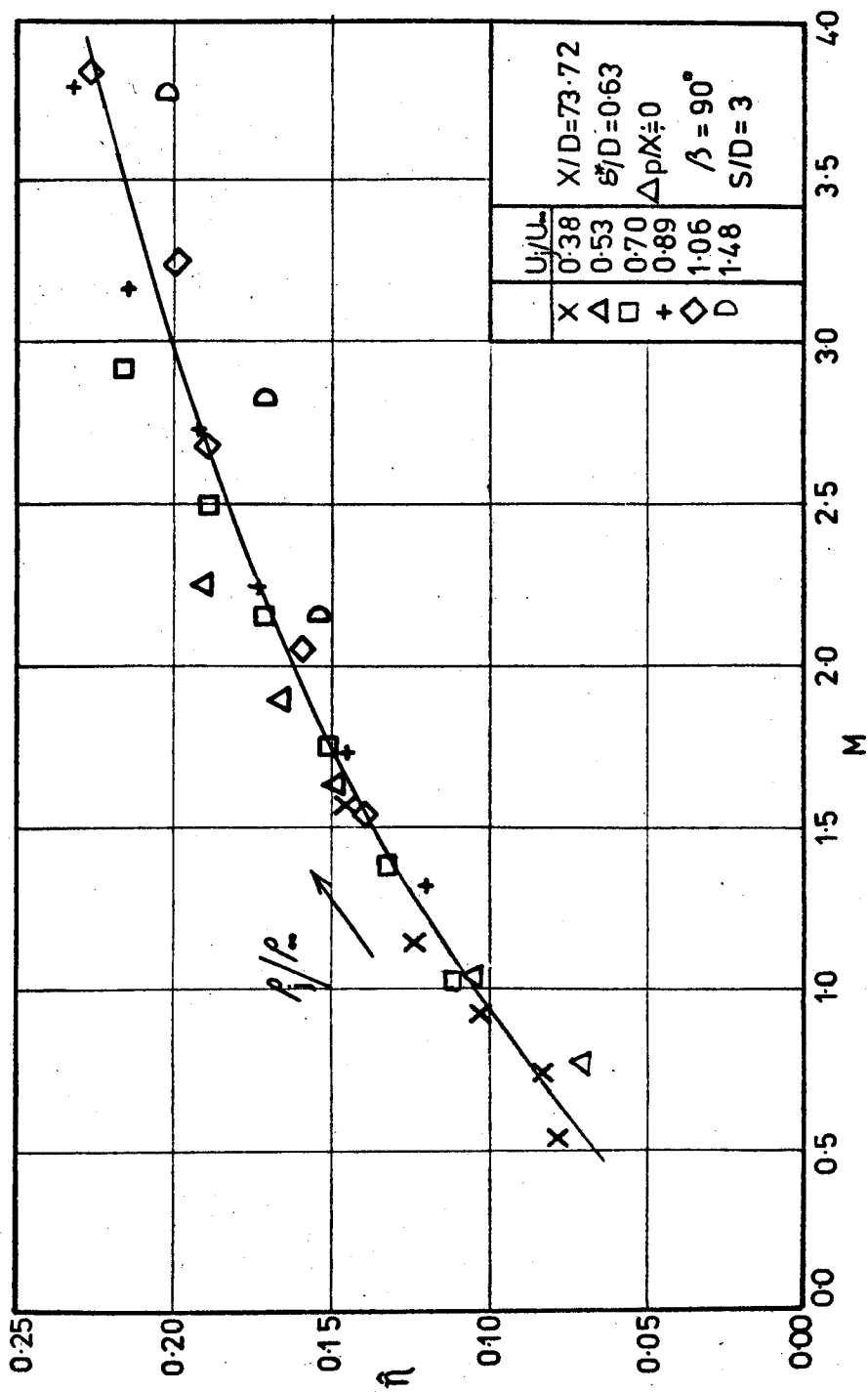


Fig. 7.10 Graph of centreline effectiveness, η , against blowing parameter, M , for varying density and velocity ratios at $X/D = 73.78$

film cooling via normal holes, an increase in coolant flow rate giving an increase in effectiveness.

7.1.4 The Effect of Pressure Gradient

Two favourable pressure gradients were studied, namely $-2.47 \times 10^3 \text{N/m}^2/\text{m}$ and $-9.84 \times 10^4 \text{N/m}^2/\text{m}$. The former produced no reliable difference in the levels of effectiveness when compared with results obtained at a similar boundary layer thickness and will not be discussed further.

The second pressure gradient had the effect of lowering the spanwise average effectiveness downstream, fig.7.11, especially at the higher blowing rates. This is in general agreement with the results of Liess (7.3).

For the larger blowing rates the loss of effectiveness with the favourable pressure gradient extends as close as 5 diameters from the injection holes, but for low blowing rates there does appear to be a tendency for the effect to be reversed between 10 and 30 diameters, with the pressure gradient increasing the effectiveness.

Turning to the centreline effectiveness, fig.7.12 shows that close to the hole - even at large blowing rates - the favourable pressure gradient gives an improvement over the zero pressure gradient. This would seem to imply that a favourable pressure gradient hinders the lateral spreading of the injectant. This is verified by the traverses done above the plate fig.7.13, where the jets in

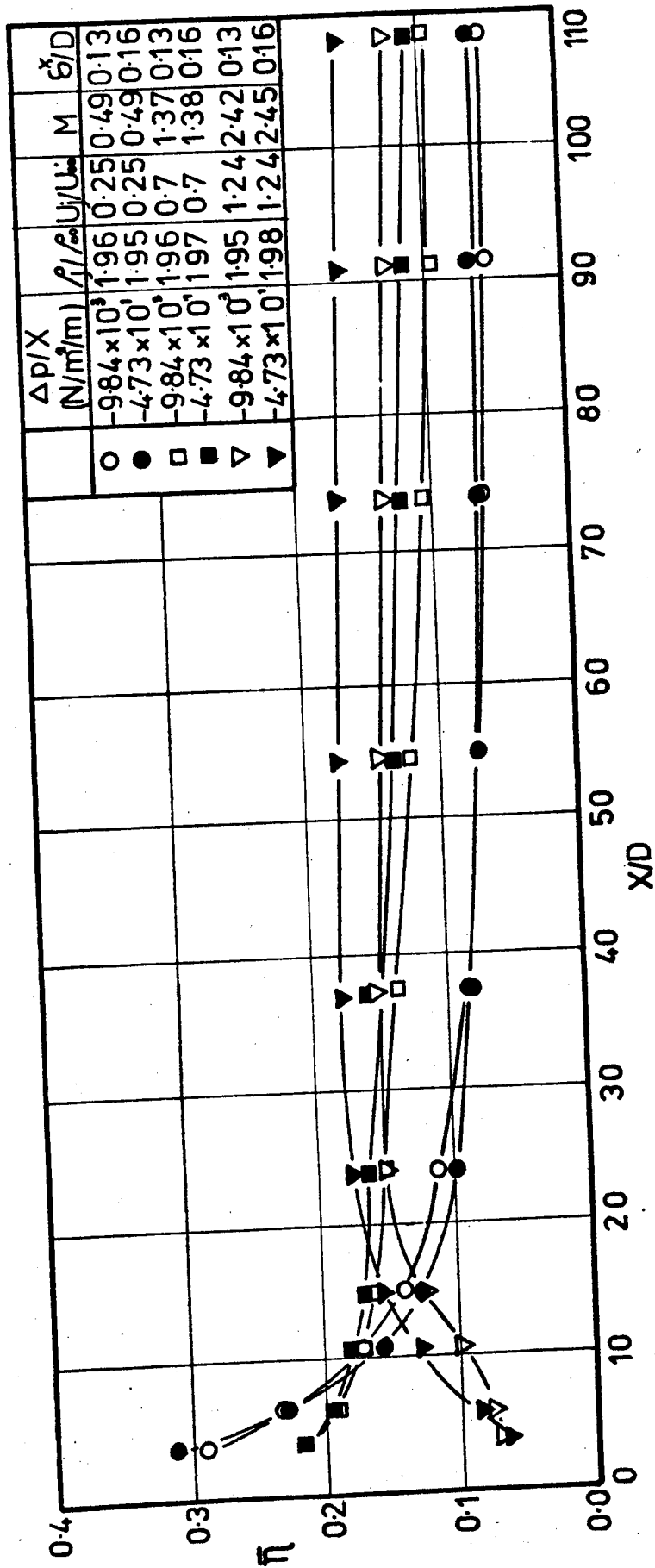


Fig.7.11 Variation of the distribution of spanwise averaged effectiveness, $\bar{\eta}$, with pressure gradient for normal injection with $S/D = 3$

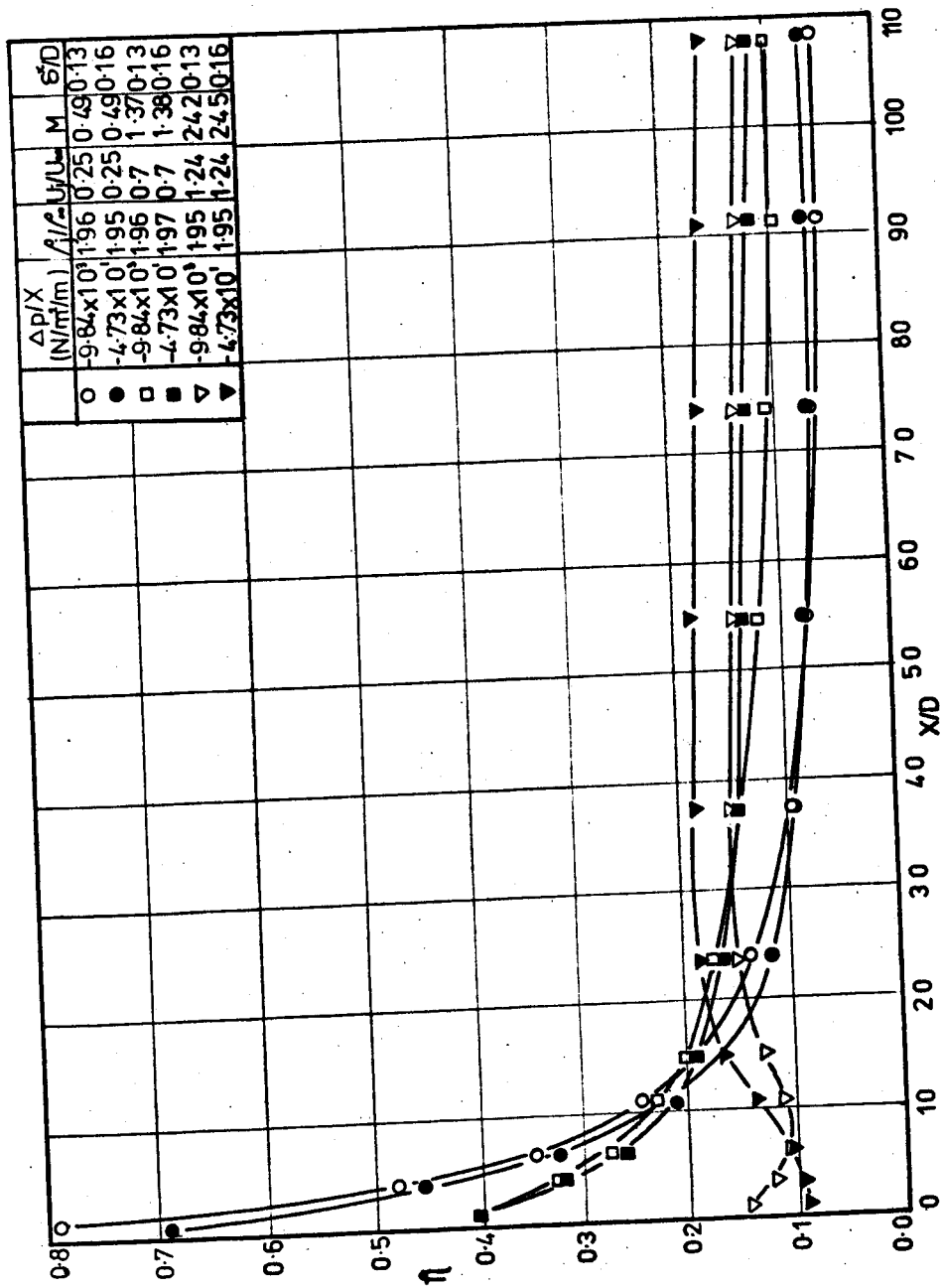


Fig. 7.12 Variation of centreline effectiveness, η , with pressure gradient for normal injection with

$S/D = 3$

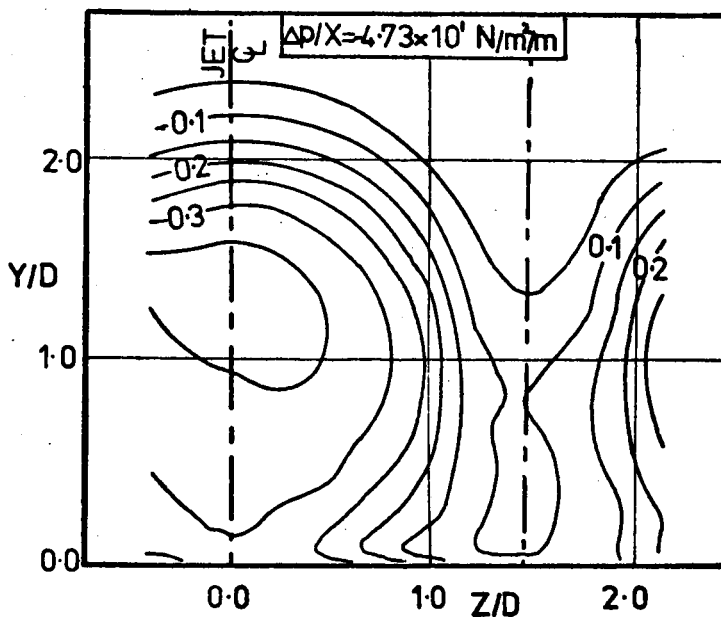


Fig. 7.13a Contours of constant injectant concentration in the absence of a pressure gradient for normal injection with $S/D = 3$ and at $X/D = 4.25$

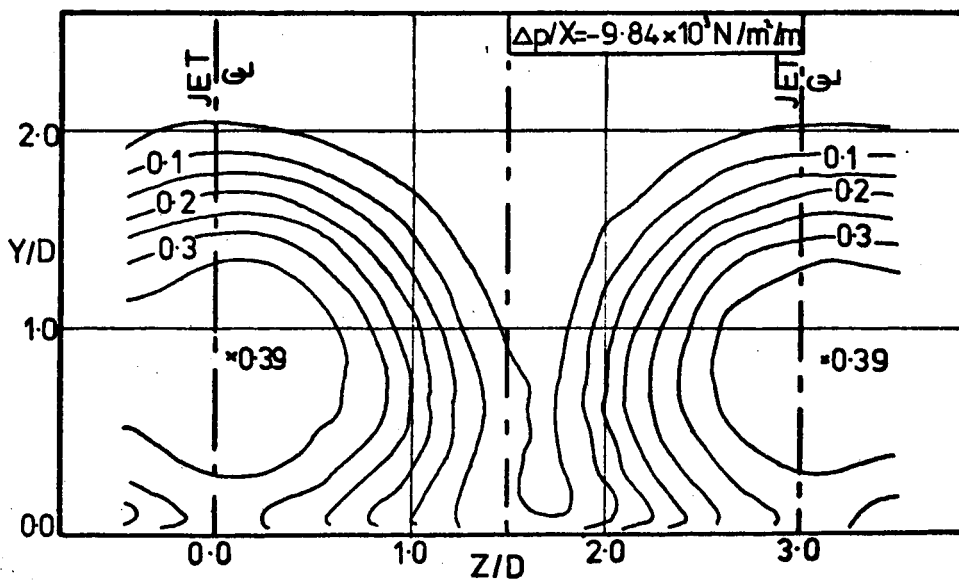


Fig. 7.13b Contours of constant injectant concentration in the presence of a pressure gradient for normal injection with $S/D = 3$ and at $X/D = 4.25$

the presence of the pressure gradient are not only more compact, but also closer to the surface.

This may be due to the fact that as the velocity ratio is the same in both cases, the rate of entrainment of the mainstream into the jet will also be approximately the same. However, due to the rapidly accelerating flow with the pressure gradient, a particle in a jet would take less time to reach a given station downstream, resulting in less entrainment and a more compact jet. The lower effectiveness laterally at low X/D balances the higher centreline value in most cases, to give little change in the spanwise averaged effectiveness.

The effect of the favourable pressure gradient will also be to retard the growth of the boundary layer, which will have been completely remodelled by the injected flow. The result of having this thinner layer of injectant may well be to ensure that any air entrained from the freestream reaches the surface more rapidly, thus lowering the effectiveness downstream. The traverses normal to the plate and far downstream show the thickness of the coolant layer with the favourable pressure gradient to be approximately 70% of the thickness without the pressure gradient.

The tests on the adverse pressure gradients showed the same general trends, this time with the pressure gradient producing an improvement downstream. Unfortunately, the differences in measured effectiveness, like the adverse pressure gradient itself, were small and it is difficult to draw any firm conclusions.

7.1.5 The Effect of the Boundary Layer Thickness

Three different ratios of boundary layer displacement thickness to hole diameter will be considered here, namely 0.63, 0.32 and 0.16. (This variation was achieved independently of the other main parameters, unlike most of the boundary layer thickness variations produced by Liess (7.3) and Goldstein et al (7.4).)

Fig.7.14 shows the variation in the spanwise averaged effectiveness produced by these different boundary layers with a velocity ratio of 0.7 and a nominal density ratio of 2. As can be seen, a decrease in the displacement thickness produces a rise in effectiveness, as noted by Liess (7.3); the effect only extends from close to the injection holes to 20 diameters downstream. Further downstream, the variations in boundary layer thickness have no effect.

The increase in effectiveness is generally accepted as being due to the decreased depth of low momentum flow forming the boundary layer, resulting in the jets being deflected more rapidly - an opinion shared by Goldstein et al (7.4). However, the traverses normal to the jets and close to the holes for displacement thicknesses of 0.16 and 0.24 diameters, do not show any significant difference in the height of the jets, fig.7.15.

The variation in the displacement thickness may not have been sufficient to show any real difference in jet height, although the momentum thicknesses, which might be

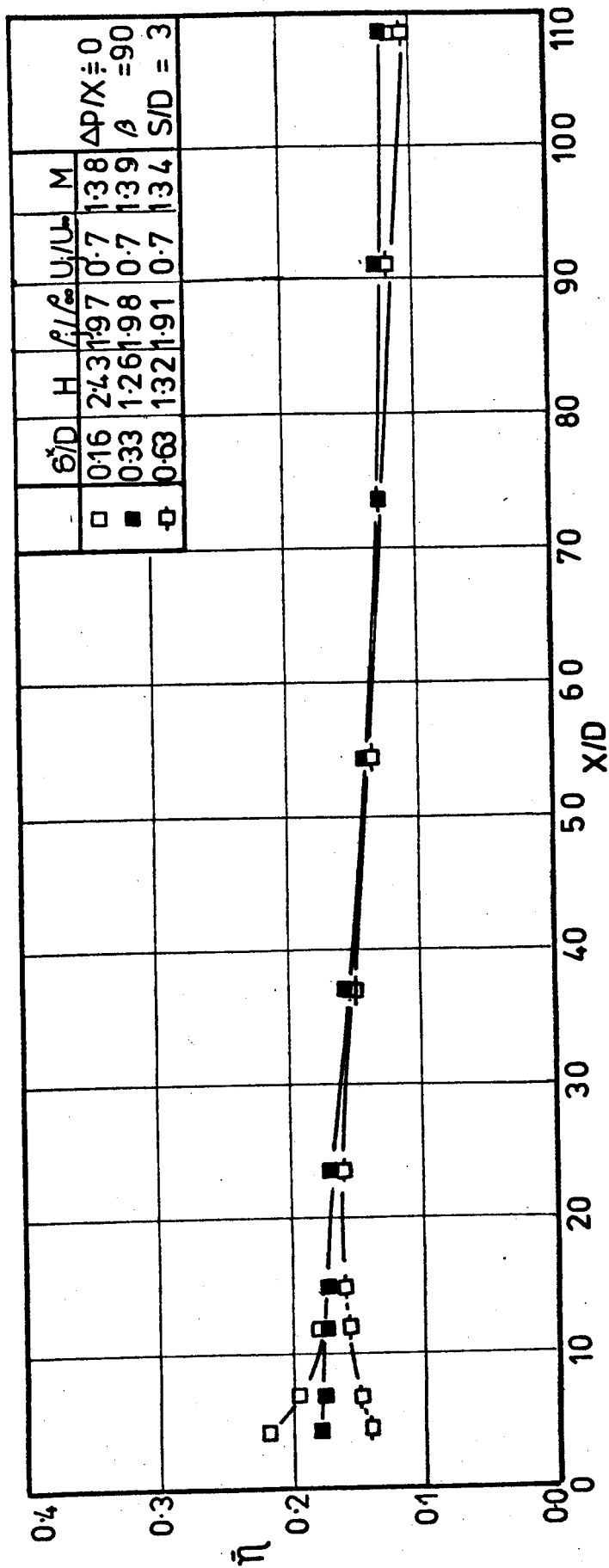


Fig. 7.14 Downstream distribution of spanwise averaged effectiveness, $\bar{\eta}$, with varying boundary layer displacement thickness, δ^*/D

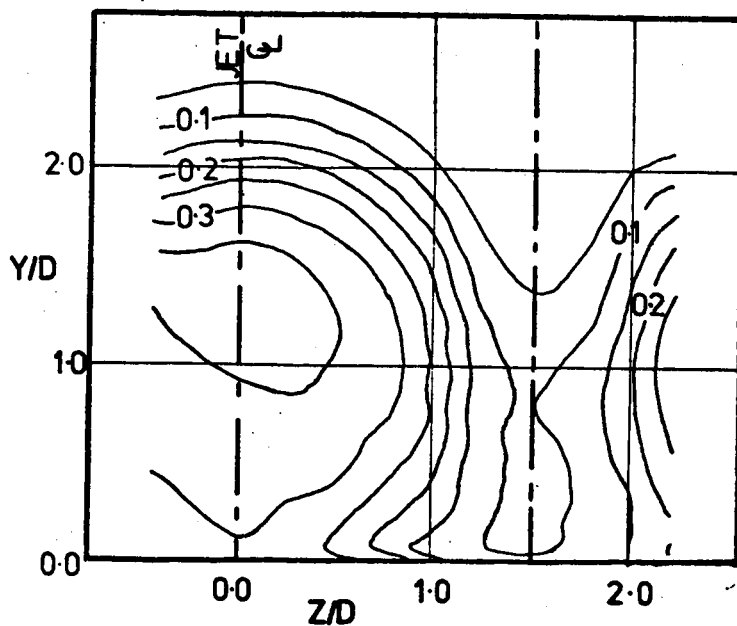


Fig.7.15a Contours of constant injectant concentration at $X/D = 4.25$ and $\delta^*/D = 0.16$ for normal injection with $S/D = 3$

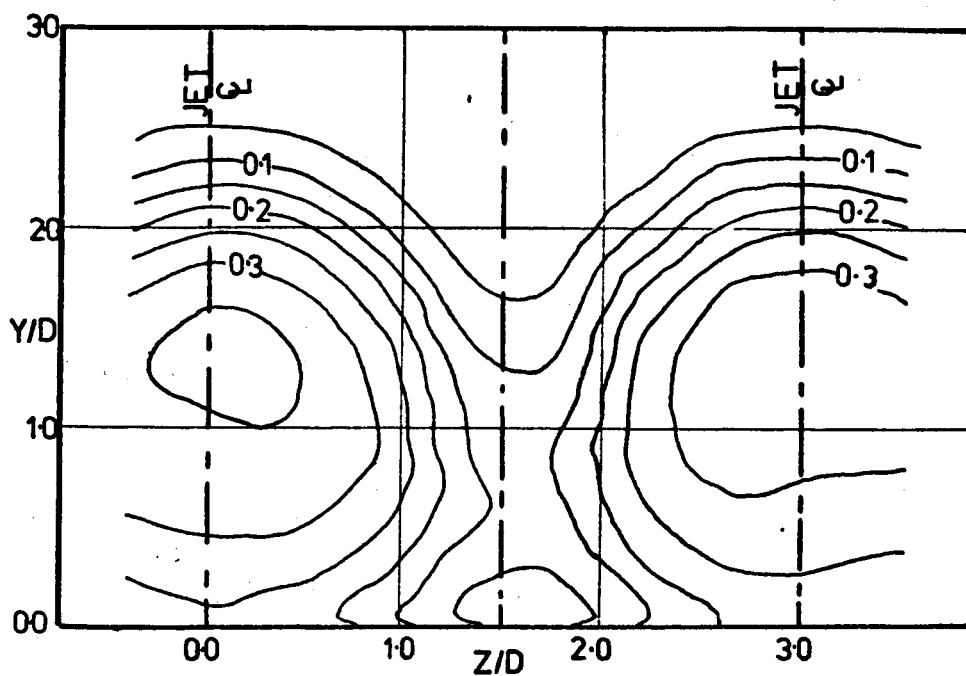


Fig.7.15b Contours of constant injectant concentration at $X/D = 4.25$ and $\delta^*/D = 0.24$ for normal injection with $S/D = 3$

expected to have a greater influence on the jet trajectories, were 0.066 and 0.176 diameters. This considerable difference and the lack of jet height variation would suggest that the generally accepted explanation for increased effectiveness with decreased boundary layer thickness is not correct.

Fig.7.15 does show that there is a higher concentration of injectant below the central core of the jet in the case of the thinner boundary layer and also there appears to be slightly less lateral diffusion.

One explanation for this is that the edges of the jets would experience greater shear with the thinner boundary layer due to the increased velocities close to the surface. This would tend to remove the edges of the jets, bringing them forward and under the main body of the jets. This tendency of the mainstream to curl around and under a jet was noticed by Ramsey et al (7.5) - also, earlier, by Abramovich (7.6).

At $X/D = 60.6$ the effectiveness profiles on the centre-line for the boundary displacement thicknesses of 0.24 and 0.16 diameters are almost identical as the levels of effectiveness would suggest.

7.1.6 The Effect of Hole Spacing

The variation of the spanwise averaged effectiveness with hole spacing is presented in fig.7.16 for a velocity ratio of 0.7 and a density ratio of nominally 2. The curves all have the same basic shape and the effectiveness increases as the hole

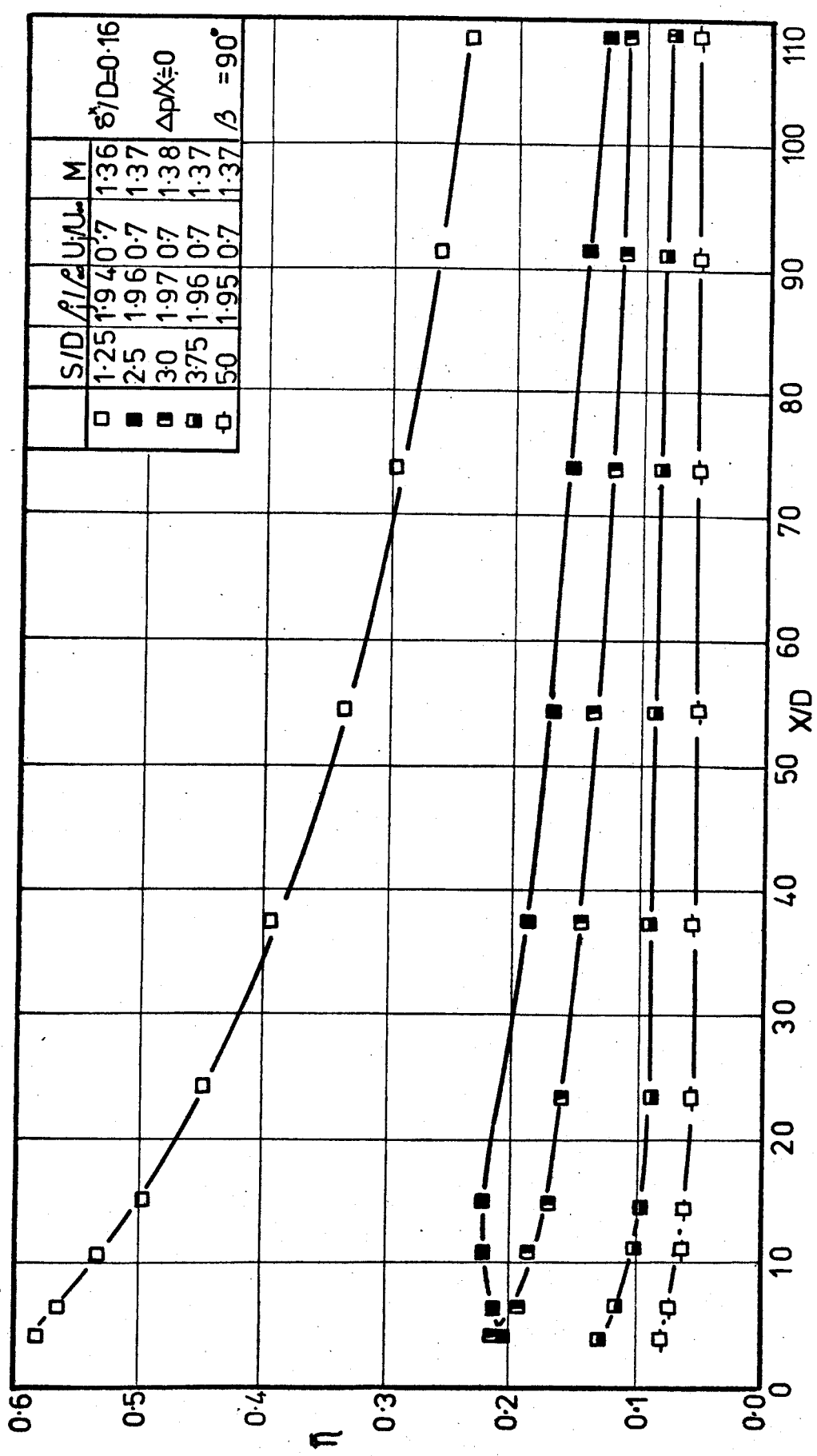


Fig. 7.20 The effect of hole spacing, S/D , on the downstream distribution of spanwise averaged effectiveness

spacing is decreased. There is an enormous improvement when the hole spacing is reduced to 1.25 diameters from 2.5 diameters (the minimum value used in practice). In fact, the 1.25 diameter spacing gave results which were two dimensional by 4.25 diameters downstream and it is interesting to compare the results with those obtained using slot geometries (fig.7.17) on the basis of an equivalent slot width where $S_1 = \frac{\pi D^2}{4S}$.

Included in the figure are results obtained by Foster (7.7) with a slot injecting at an angle normal to the mainflow. He found that there was a long separation region downstream of the slot which was ventilated via the ends of the jet, and this seems to produce low levels of effectiveness. With a closely spaced row of holes, the freestream is still able to pass between the jets - thus destroying their structure and giving higher values of effectiveness than the slot.

Data due to Pai & Whitelaw (7.8) are also included. These data were obtained using a rearward facing step and, as might be expected, the level of effectiveness is much higher than for the hole data; however, far downstream the situation is reversed and the holes give a slightly higher effectiveness, probably due to the higher blowing rate.

The data of Metzger and Fletcher (7.9) are also presented in fig.7.17. The hole spacings were small at 1.55 and 1.71 diameters and the angle of injection was 20° . These results are surprisingly lower than those obtained in the current research and no explanation can be offered (although it

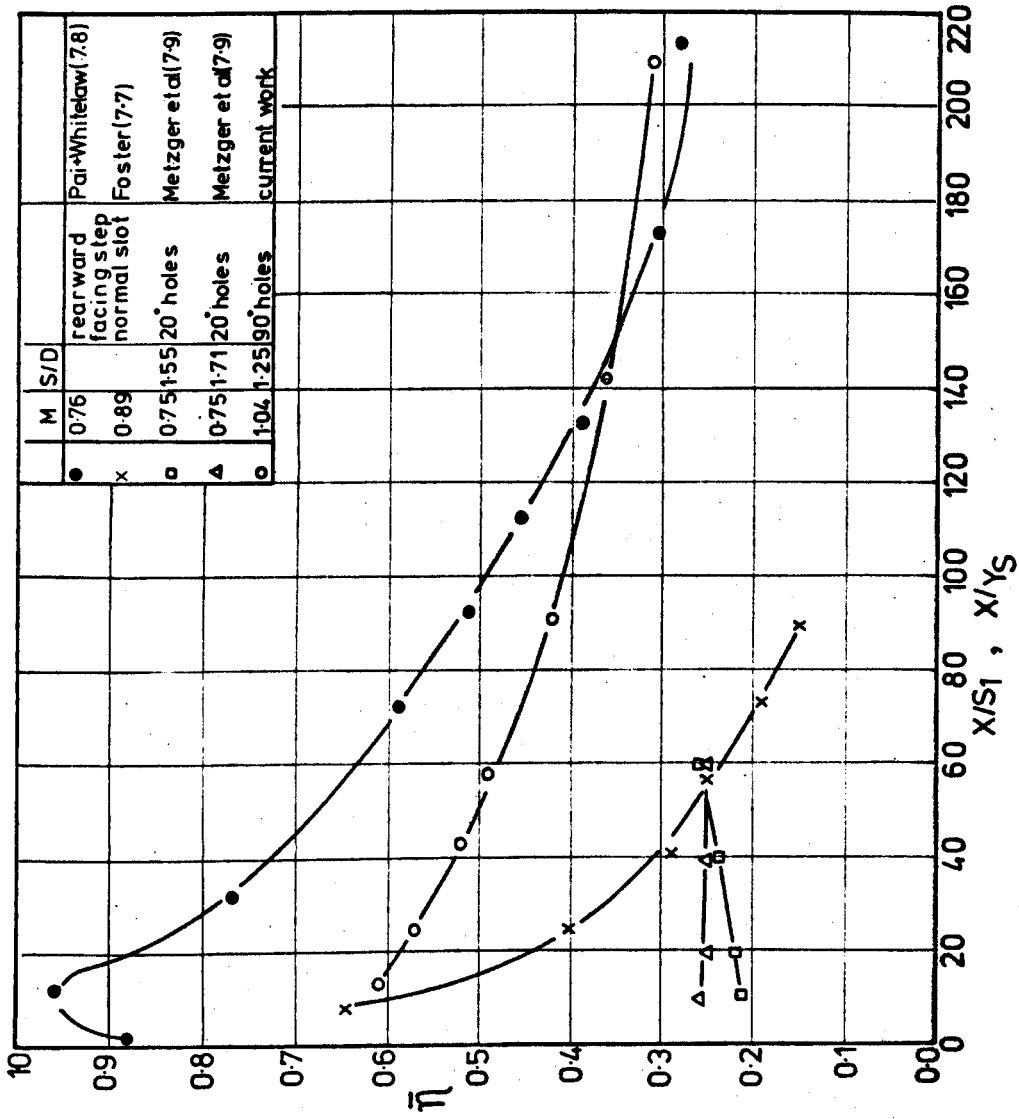


Fig. 7.17 Comparison with results of other experimenters: spanwise averaged effectiveness against equivalent slot widths downstream

is interesting to note that the larger hole spacing gives the higher effectiveness for up to 50 equivalent slot widths from the holes).

Fig.7.18 shows the results obtained at a velocity ratio of 1.24. Here the largest hole spacing results in an extremely low effectiveness, possibly because at this spacing the holes are acting like single holes rather than a row. Goldstein et al (7.10) noticed that for holes at 35° and at large blowing rates, a single hole gave much lower levels of effectiveness than a row at 3 diameter spacing. This they attributed to the interaction of jets in a row.

Obviously the wider hole spacings give poor coverage between the holes for a distance downstream, which increases with the hole spacing; the results for the largest hole spacing become two dimensional only after 70 diameters.

The centreline values reflect the trends in the averaged results, except that (excluding the 1.25 spacing) the centreline effectiveness close to the holes does not vary a great deal with spacing, as one might expect.

It is interesting to note that results for the 3 diameter spacing were taken at a different time from those of the other hole spacings. The fact that they fit so well into the general pattern indicates the high level of repeatability of the results.

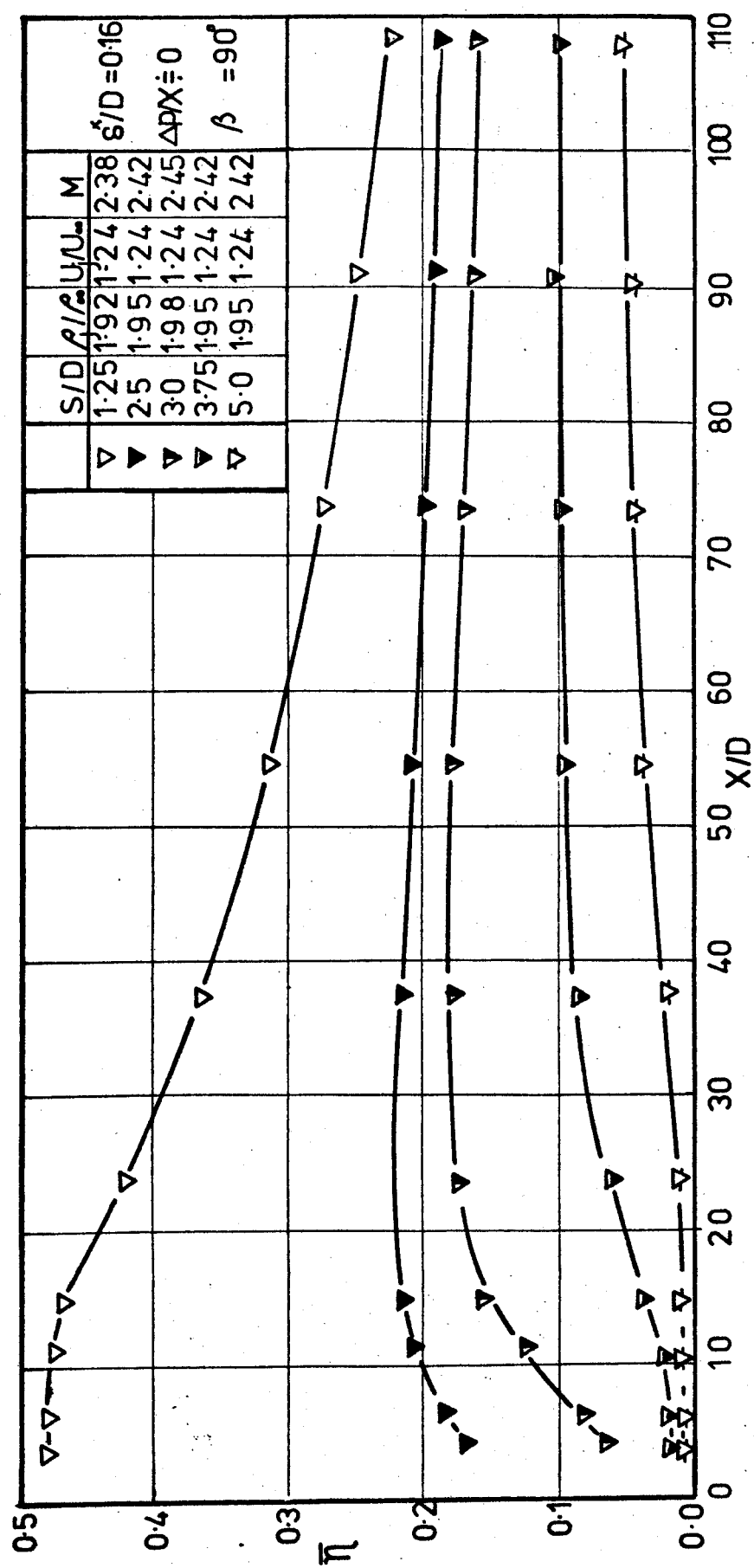


Fig. 7.28 The effect of hole spacing, S/D , on the downstream distribution of spanwise averaged effectiveness, $\bar{\eta}$

7.2 Angled Injection

This section, covering the two angled injection geometries of 35° and 55° , is sub-divided in the same manner as for the normal injection.

7.2.1 The Effect of Velocity Ratio

The feature of jet 'lift-off' noticed for the 90° injection is again apparent with the angled injection. In fig.7.19 the effectiveness falls very rapidly close to the injection position, with rising velocity ratio for an injection angle of 35° .

However, for the 90° case, the high velocity ratios give the highest effectiveness by about 20 diameters downstream. In comparison, the maximum effectiveness at a distance of 100 diameters downstream is produced by a medium blowing rate for the 35° injection. It is as if the jet never mixes fully with the mainstream, although the surface measurements generally show a two-dimensional picture by 70 diameters.

The 55° injection geometry shows a situation between the 35° and 90° cases, with the maximum blowing rate giving the maximum effectiveness at 35 diameters downstream.

The centreline effectiveness followed the same pattern but the values were much higher than the spanwise averaged values, implying low levels of effectiveness between the holes. This was indeed the case, as can be seen in fig.7.20 where a series of surface contours are presented for 35°

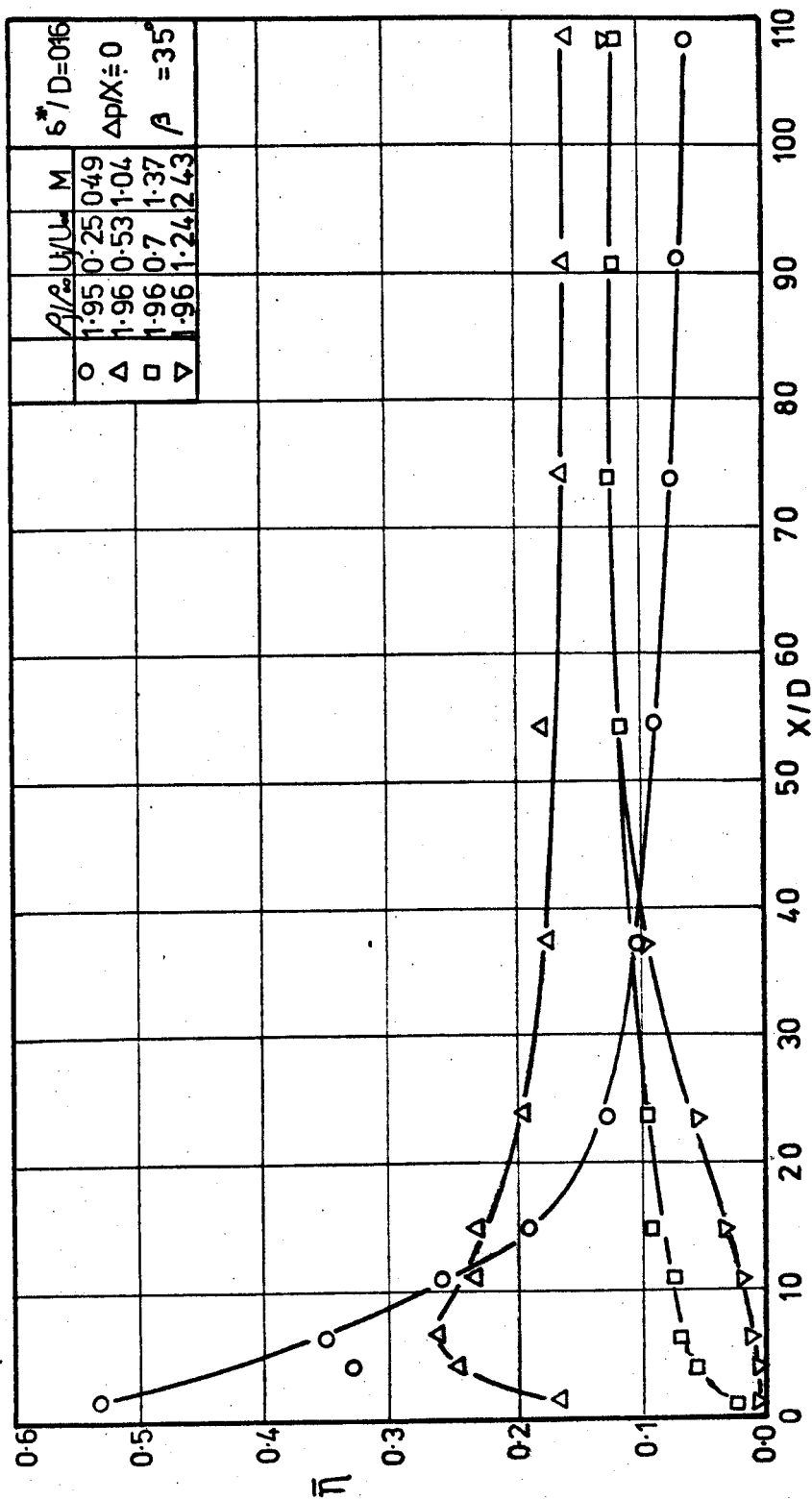


Fig. 7.19 The effect of varying velocity ratio on the downstream distribution of spanwise averaged effectiveness, $\bar{\eta}$, for 35° injection angle

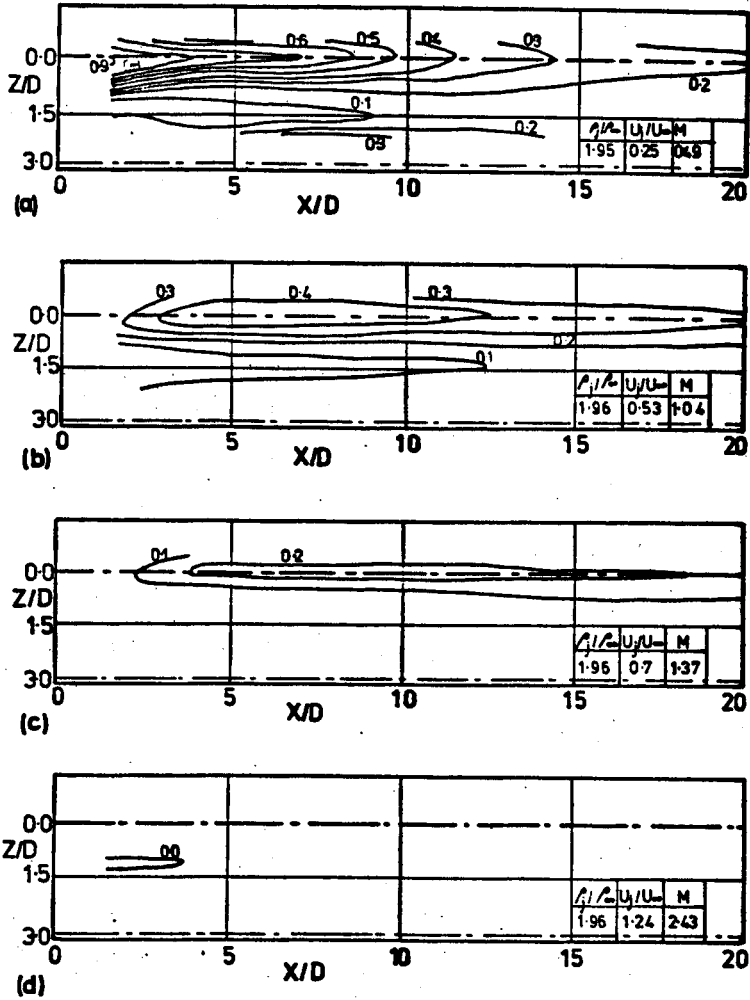


Fig.7.20 Contours of constant effectiveness for a 35° injection angle (a) $M = 0.49$; (b) $M = 1.04$; (c) $M = 1.37$; (d) $M = 2.43$.

injection. They show clearly the large gradients of effectiveness between the holes and, moving from top to bottom with increasing velocity ratio, they show the low effectiveness area caused by the 'lift off' moving downstream.

It is possible to compare the 35° angled results with those of Goldstein et al (7.10), Liess (7.3) and Smith (7.2) - fig.7.21. The agreement with Goldstein et al's results is fair with the curves being of roughly the same shape - excepting the one for unity blowing rate, which strangely gives Goldstein et al their lowest effectiveness downstream. The present results tend to give higher levels of effectiveness (except at large blowing rates close to the hole), but of course they were taken at a higher density ratio and the comparison is not really valid, as previously stated.

Comparison with Liess' results shows better agreement in terms of the shape of the curves, but again his results are lower for a given value of blowing parameter. Comparing with Smith at a similar momentum parameter, one finds a great variation due in the main to the using of the mean line, as described before.

The apparently low values of effectiveness measured at large values of blowing rate close to the holes may be the result of the other results being too high due to an imperfectly adiabatic wall. Fig.7.22a shows how for inclined tubes there is a large temperature gradient across

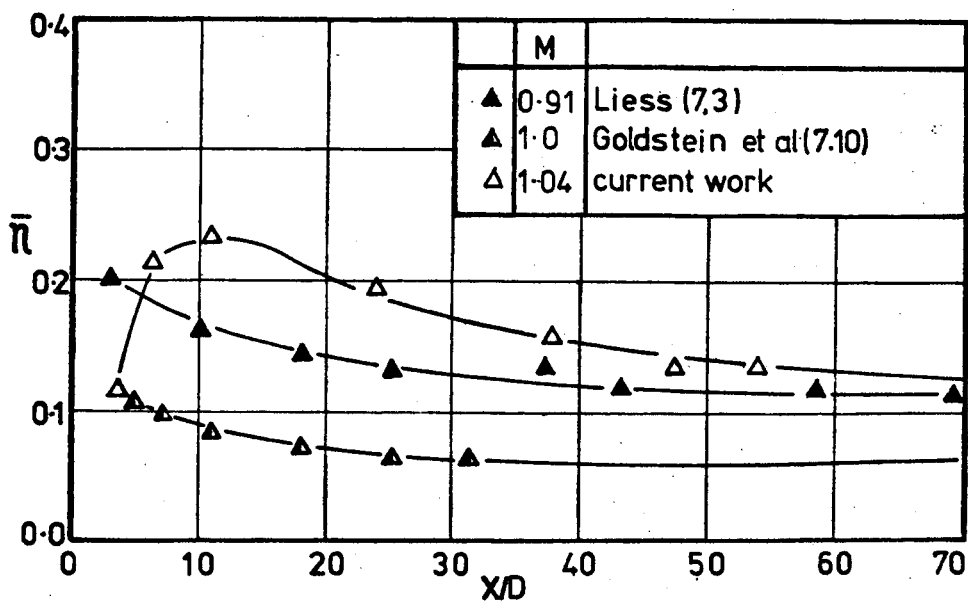
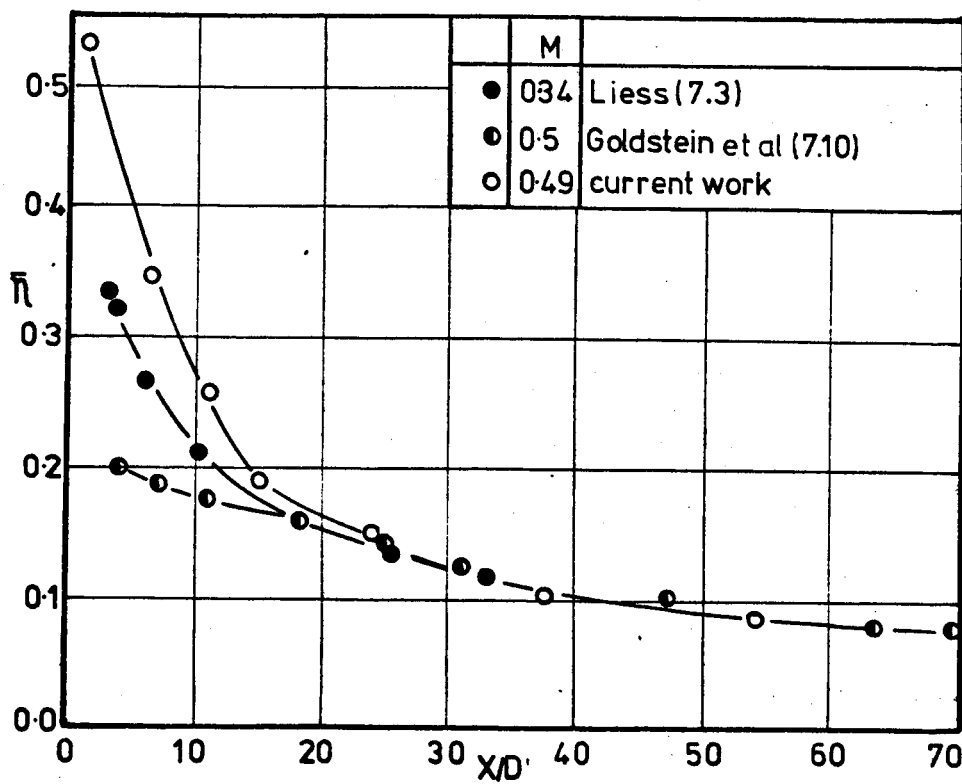


Fig. 7.21a Comparison with the results of Liess (7.3) and Goldstein et al (7.10)

continued ...

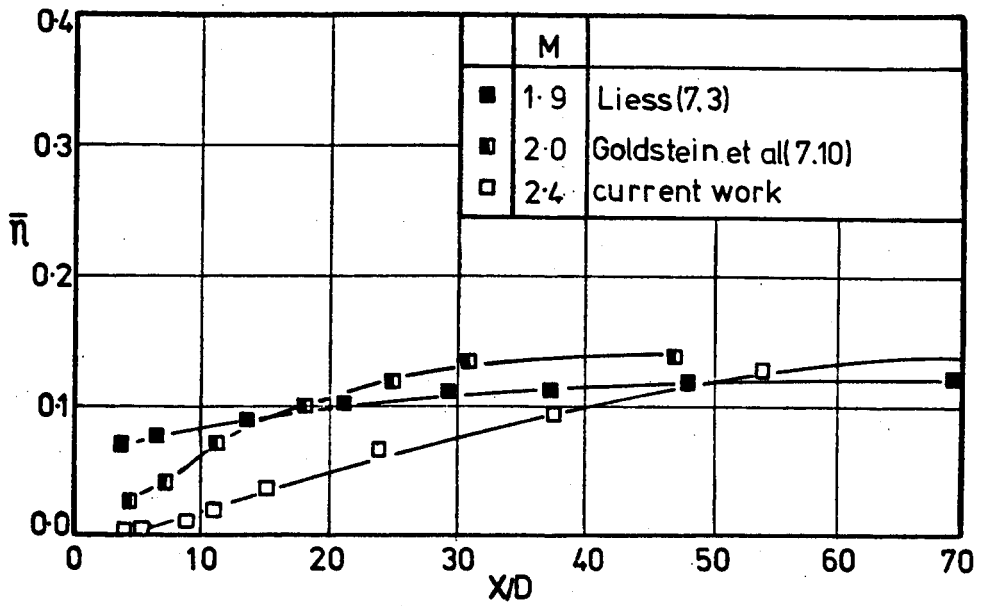


Fig.7.21a continued ...

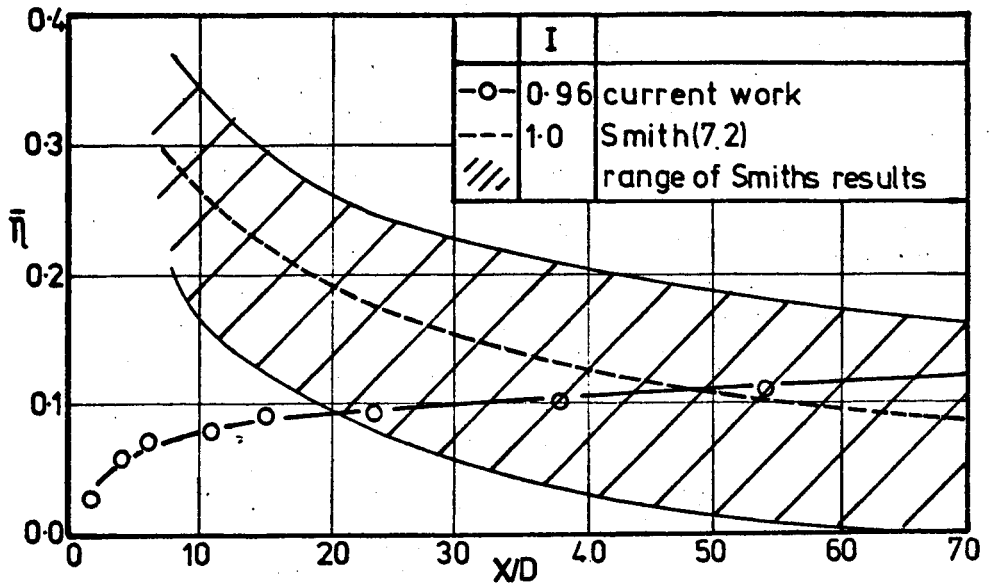


Fig.7.21b Comparison with results of Smith (7.2)

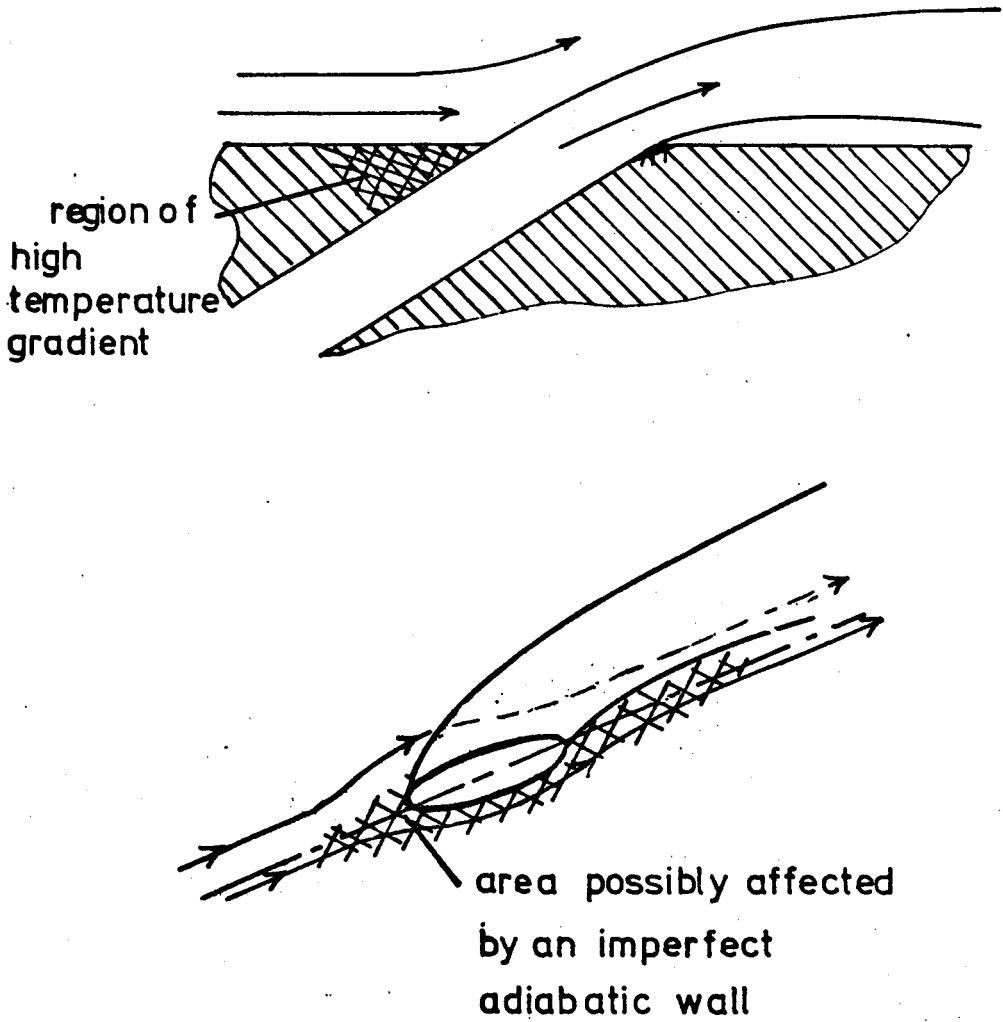


Fig. 7.22 Sketch showing areas of possible heat flow in a non-adiabatic wall

the thin wedge of material between the cooling hole and the top surface. The result may be that the surface is not at the mainstream temperature and is cooling (or heating) the boundary layer sub-layer.

The same may apply to the edges of the hole. As the blowing rate is increased and the jet lifts off from the surface, fig.7.22b, and the mainstream flows round and beneath the jet, the cooled sub-layer will produce a lower temperature on the surface over which it passes. This would give rise to an effectiveness which is higher than it should be. There is no way of testing this hypothesis, but it does provide an explanation for this apparent anomaly.

7.2.2 The Effect of Boundary Layer Thickness

The improvements in the level of effectiveness noted with the 90° injection, as the boundary layer displacement thickness was reduced, were observed again with the angled injection, Fig.7.23 --although in two places the trend was reversed. The variation in the 55° injection case was always an increase in effectiveness with a decrease in boundary layer thickness.

In both cases the improvement decreased as the blowing rate increased and was noticeable over the first 20 or so diameters. Plotting the available points on Liess' (7.3) figure - fig.7.24 - shows the variation of effectiveness with boundary layer displacement thickness at $X/D = 10$ to

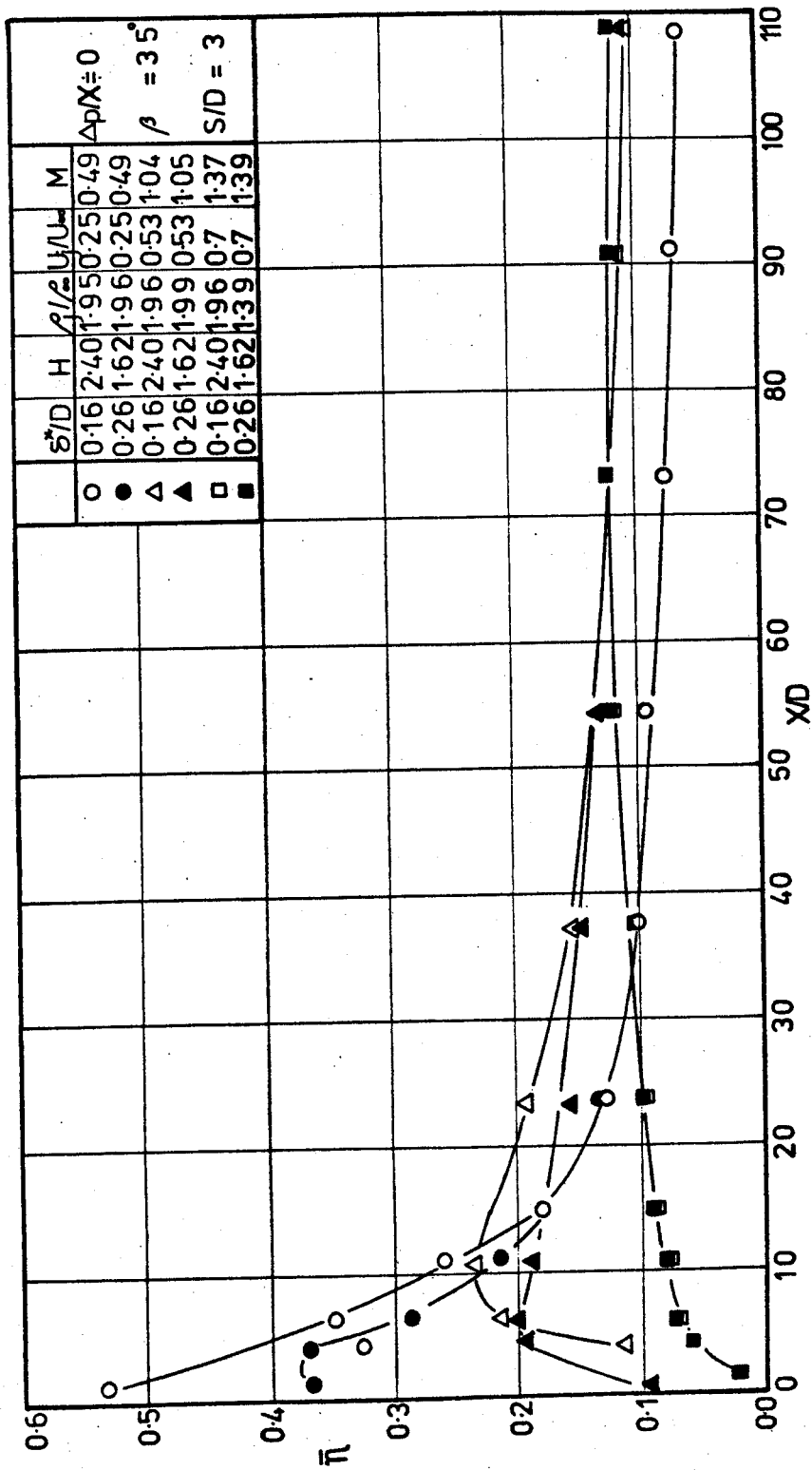


Fig. 7.23 Downstream distribution of spanwise averaged effectiveness, $\bar{\eta}$, with varying boundary layer displacement thickness for 35° injection angle

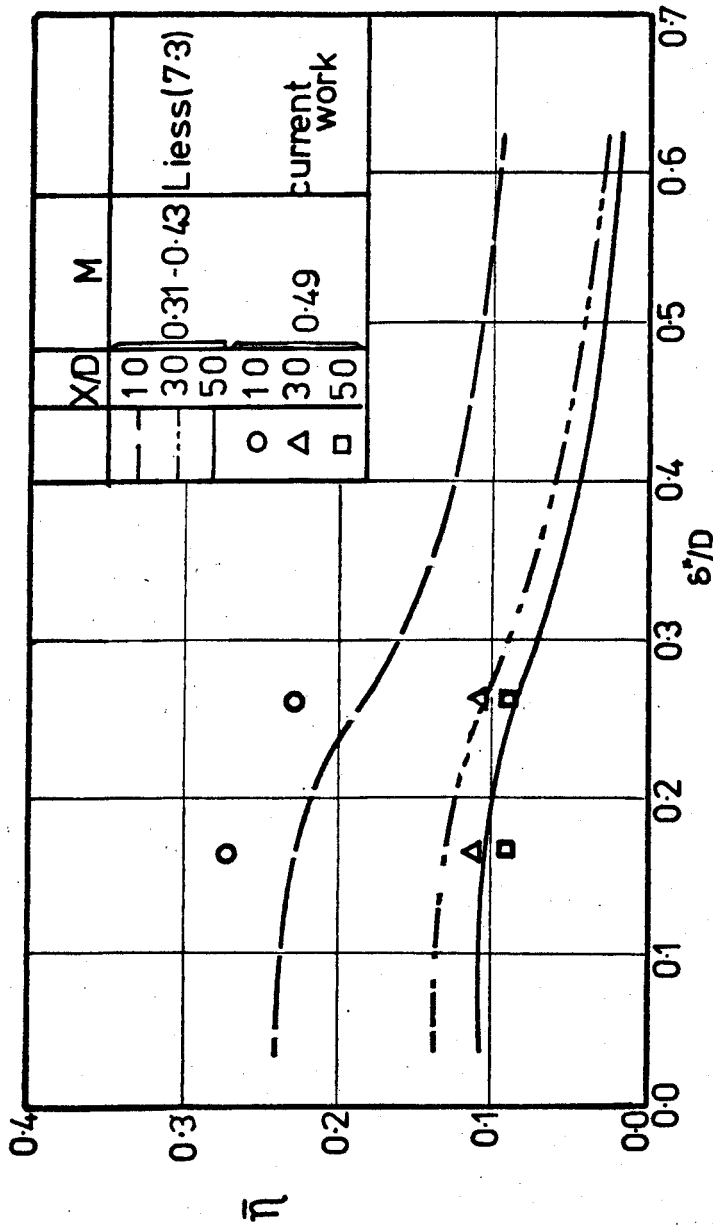


Fig. 7.24 Comparison of variation of spanwise averaged effectiveness, $\bar{\eta}$, with a boundary layer displacement thickness, δ^*/D , with results from Liess (7.3)

be the same, although with a higher level of effectiveness than Liess' data. However, at the other downstream stations there is poor agreement, as in the current work the effect was not noticeable beyond 20 diameters downstream.

7.2.3 Effect of Injection Angle

Fig.7.25 shows the effect that the injection angle has on the spanwise averaged effectiveness. For the lowest blowing rate, the 35° injection gives the highest effectiveness for the first 50 diameters downstream, after which the three angles give the same results. For the next blowing rate, the 90° injection is initially the best, but is surpassed by the others at $X/D = 7$, the results again being approximately the same after 50 diameters.

Once the blowing rate reaches 1.4 the 90° injection is clearly the best, due to the exaggerated "lift off" effect with the shallower angles. This is even more marked at the maximum blowing rate where the 35° injection never approaches the levels of effectiveness of the other two angles.

Included in fig.7.25 are data produced by Rastogi & Whitelaw (7.11) with a row of holes in a rearward facing step. The density ratio and blowing rate are comparable, but the hole spacing was only two diameters. However their case, which might be regarded as a 0° injection angle with discrete holes, gives significantly higher effectiveness over the distances considered.

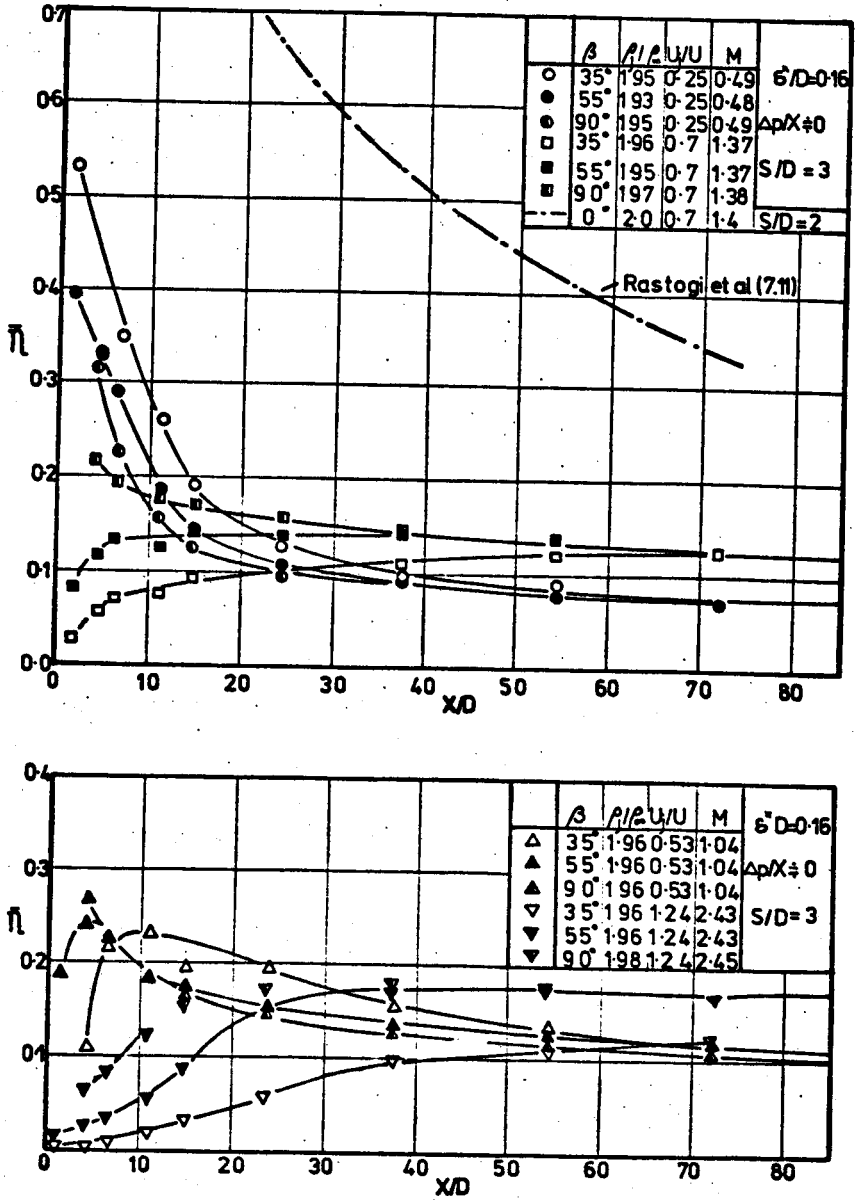


Fig.7.25 Variation of downstream distribution of spanwise averaged effectiveness, $\bar{\eta}$, with injection angle

Fig.7.26 demonstrates the "lift off" of the angled injection. The figure represents again a vertical plane 4.25 diameters downstream of the point of injection for the three angles. The 35° injection has the highest peak concentration of coolant at the lowest height above the surface. The 90° has the lowest concentration at the greatest height.

The next figure, 7.27, shows results for a vertical traverse on the centreline 23.8 diameters downstream. Here, the 35° injection still gives a definite maximum concentration now at a height of 2.5 diameters. The 55° jet gives a maximum at 2 diameters and the 90° jet a barely noticeable maximum at 1 diameter above the surface.

This indicates that the shallow angled jet is still very much a jet, but the 90° jet has been virtually destroyed as it was deflected parallel to the mainstream. This might be expected, as the shear forces on a normal jet would obviously be much greater than for the shallow angled case.

The improvement in effectiveness noticed, far downstream with the 90° jets, with an increase in blowing parameter will only occur once the flow has become two-dimensional and the mainstream is being entrained solely from above. This does not occur for the angled jets until much further downstream.

Fig.7.26 also demonstrates that an angled jet does not spread as rapidly in the lateral direction for reasons already outlined. The effect of this is to reduce the cooling between the holes. So, although at low blowing rates a shallow angle

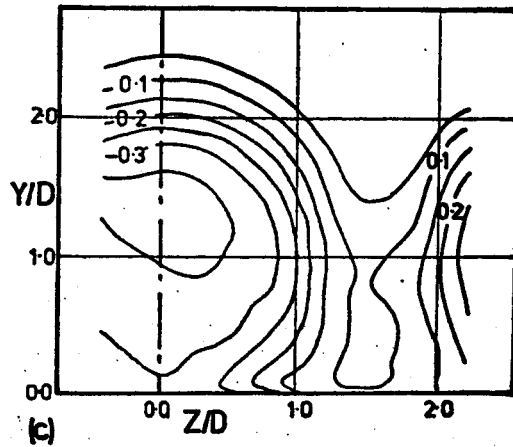
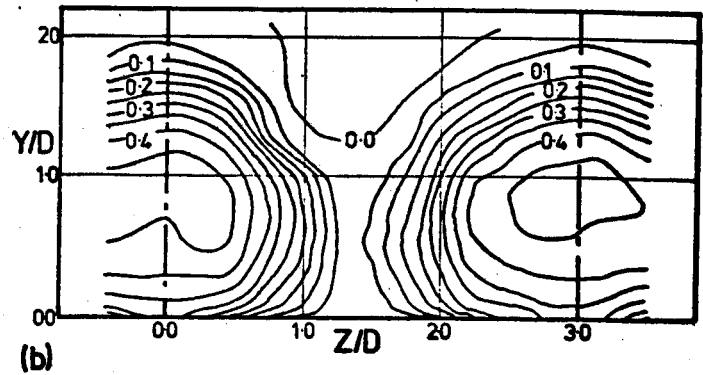
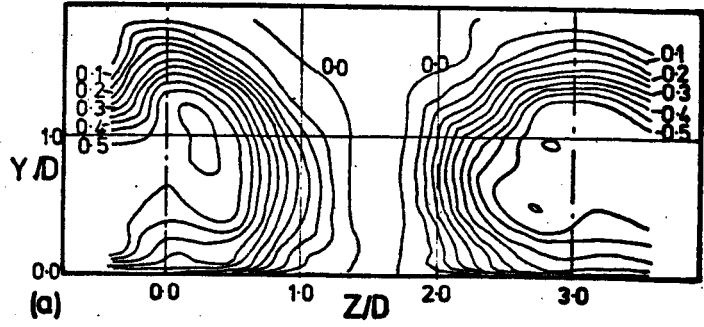


Fig. 7.26 Contours of constant injectant concentration at $X/D = 4.25$, $M = 1.4$ for: (a) 35° ; (b) 55° ; (c) 90° injection angle

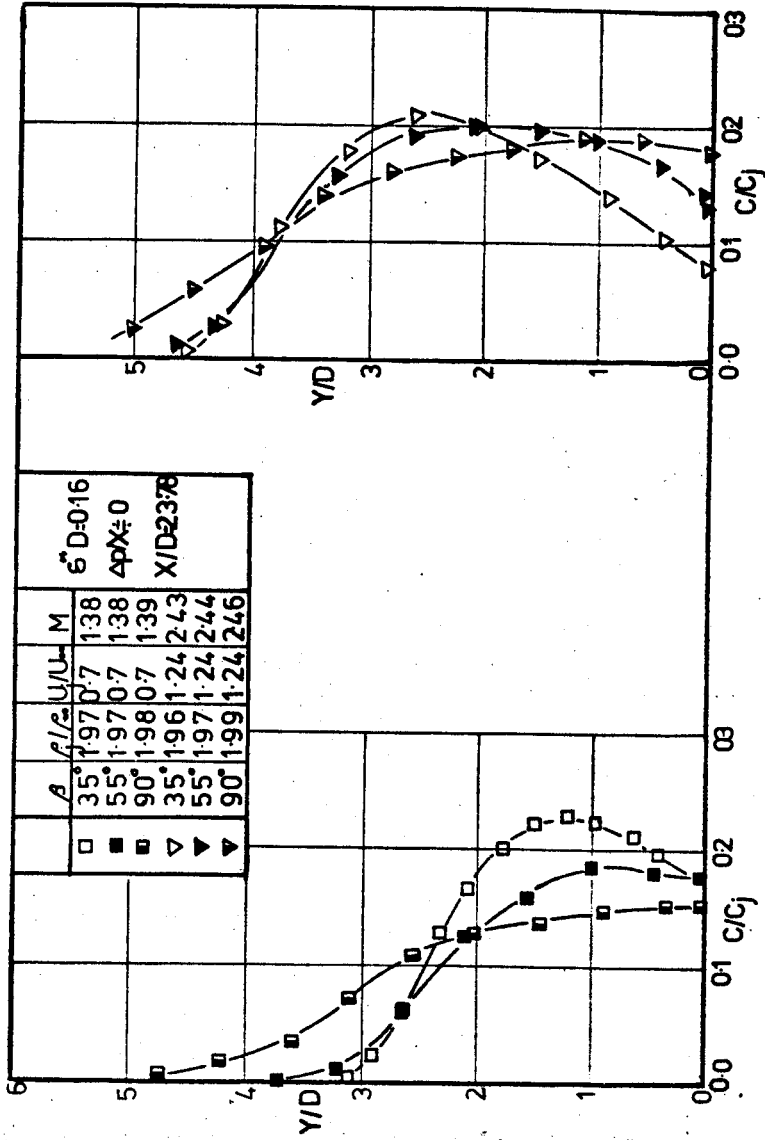


Fig. 7.27 Vertical distribution on the centreline of injectant concentration, C/C_j , for 35°, 55° and 90° injection angle

gives higher spanwise averaged effectiveness than a 90° jet, it does so by raising the centreline value considerably and reducing the value between the holes - giving rise to hot and cold streaks, coinciding with the spaces and holes respectively, and continuing some distance downstream. This effect can actually be noticed in the patterns of discolouration downstream of a row of angled holes on a turbine blade.

Obviously at high blowing rates, the cooling between the holes is even worse for an angled jet, but the gradients of effectiveness are not so steep.

Fig.7.28 shows the velocity profiles, measured 60.6 diameters downstream of the injection holes, for the three injection angles. They are plotted on the basis of an equivalent slot height and compared with the rearward step data of Pai and Whitelaw (7.8). The 35° and 55° curves are very similar, but fall between the 90° injection and step data as might be expected. The aerodynamic penalties incurred with the different injection angles are discussed in the next chapter.

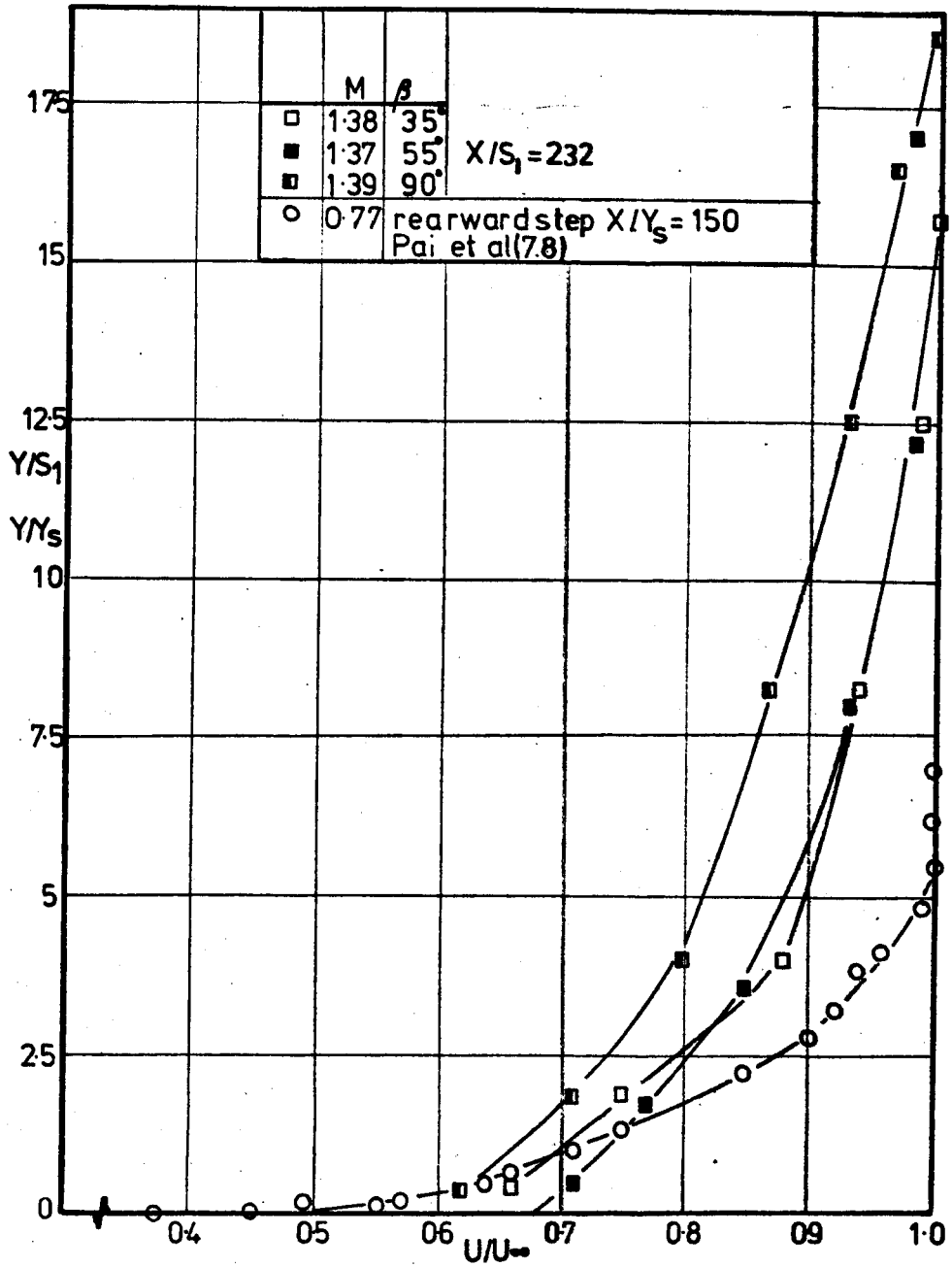


Fig.7.28 Comparison of velocity profiles with those of Pai et al (7.8)

CHAPTER 8 : FURTHER DISCUSSION OF RESULTS

The aim of this chapter is to consider the basic injection geometry variations, namely hole spacing and injection angle, from the point of view of a turbine blade designer.

=====

8.1 General

Three simple and practical criteria for film cooling via holes are considered: firstly the overall effectiveness in a streamwise, as well as a spanwise direction; secondly, the spanwise distribution of effectiveness; thirdly, the aerodynamic penalties incurred by injecting into - and thus modifying - the boundary layer.

8.2 Overall Effectiveness

A new effectiveness, calculated from the spanwise averaged values, is used to evaluate the average effectiveness over a surface. This is denoted by $\bar{\eta}$ and is defined as:

$$\bar{\eta} = \frac{1}{x_2 - x_1} \int_{x_1}^{x_2} \bar{\eta} dx$$

This effectiveness was evaluated for varying hole spacing and injection angle, for values of X/D of 1 to 25, 1 to 50 , 1 to 75 and 1 to 100.

8.2.1 The Effect of Hole Spacing

The variation of the overall effectiveness with blowing rate for differing hole spacings is presented in Fig.8.1. The hole spacing of 1.25 diameters, of course, gives values much higher than the other hole spacings. Excepting this smallest spacing, the large values of blowing rates (say, greater than 1.5) tend to give the highest levels of effectiveness over the 1 - 100 diameters range, while the lower blowing rates give the highest values over the 1 - 25 diameter range.

Considering a single row of holes and assuming the designer knows the mass flow rate of coolant, \dot{m} , where

$$\dot{m} = \rho_j U_j A$$

where

$$A = \frac{\pi D^2 N}{4}$$

and N is the number of holes in the single row for a fixed blade length, L_j , so that

$$N = L/S$$

then,

$$\dot{m} = M p_\infty U_\infty \frac{\pi D^2}{4} \frac{L}{S}$$

If the pressure ratio across the cooling holes is known, and assuming that the coefficient of discharge for the holes is constant, then $\rho_j U_j^2 / \rho_\infty U_\infty^2$ can be calculated. This leaves S and D as the variables

and,
$$D^2/S = \text{const.}$$

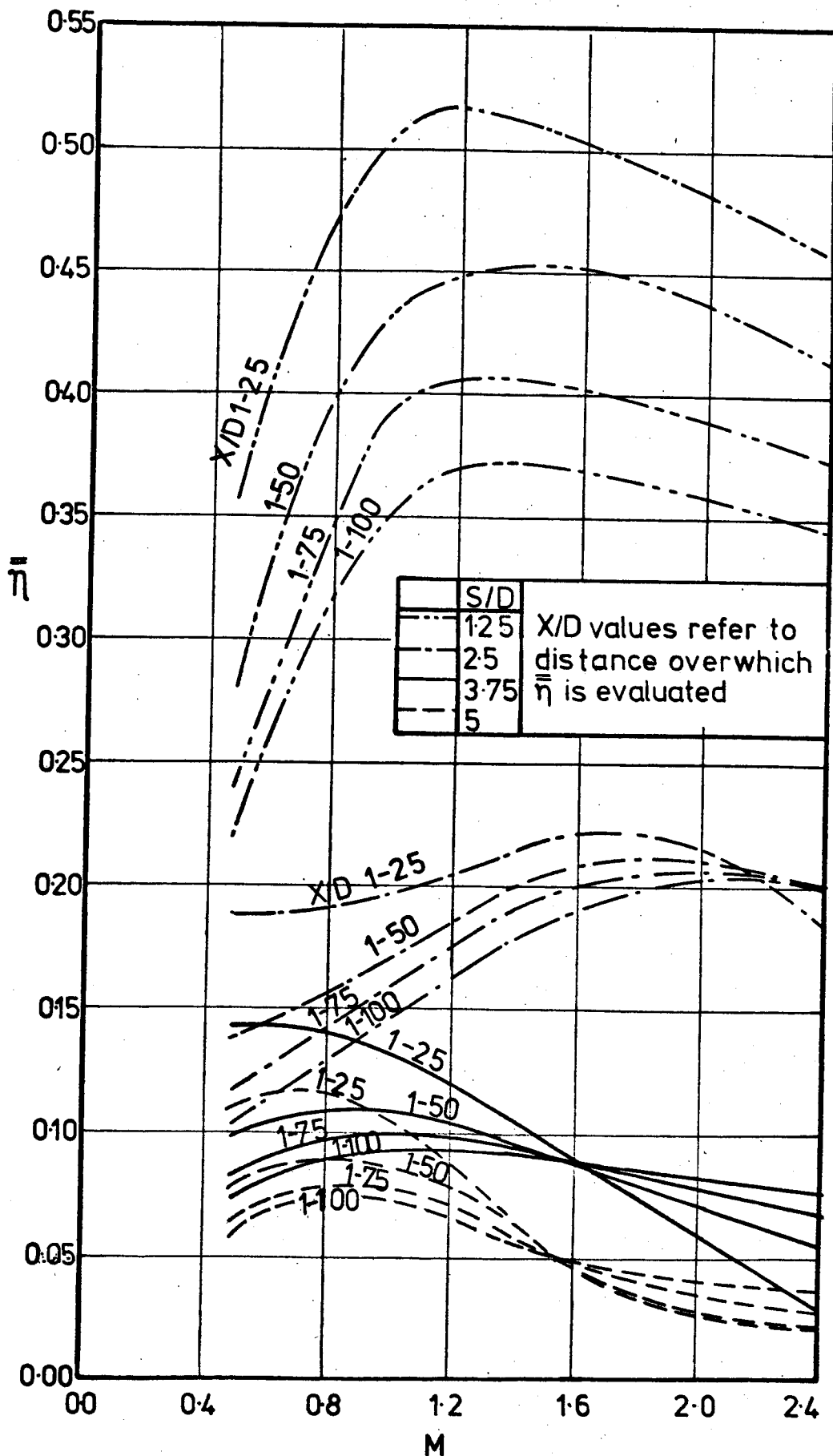


Fig.8.1 Variation of averaged effectiveness, $\bar{\eta}$, with hole spacing, S/D , and blowing parameter, M

Obviously, this is a grossly oversimplified picture; however, using it to consider a crude example with a chosen hole diameter of 2mm, a hole spacing of 5 diameters and a distance downstream which the designer wishes to be cooled of 50mm (or, here, 25 diameters), fig.8.1 shows $\bar{\eta} = 0.11$. Now, considering a hole diameter of 1mm and, therefore, a hole spacing of 2.5 and a distance downstream of 50 diameters, the level of effectiveness is 0.155. In both cases $M = 1.0$

In other words, reducing the hole spacing and using smaller holes has given a higher effectiveness. A study of fig.8.1 indicates that this is always the case. However, in the limit as the hole spacing is reduced, a slot will be formed which - as the work of Foster (8.1) shows - need not give the optimum film cooling performance.

In practice there will be a minimum limit on hole size and hole spacing, and a figure such as fig.8.1 would be of value in determining the average levels of effectiveness that could be achieved with a given configuration. This would be especially true if fig.8.1 were used with plots such as fig.8.2, which shows the results for the 2.5 diameter spacing, where distances downstream (other than the four used here) could be easily read off.

8.2.2 The Effect of the Angle of Injection

The effect of the injection angle on the streamwise averaged effectiveness is shown in Fig.8.3. Here it can be seen that for low values of blowing rate, less than 0.9, the

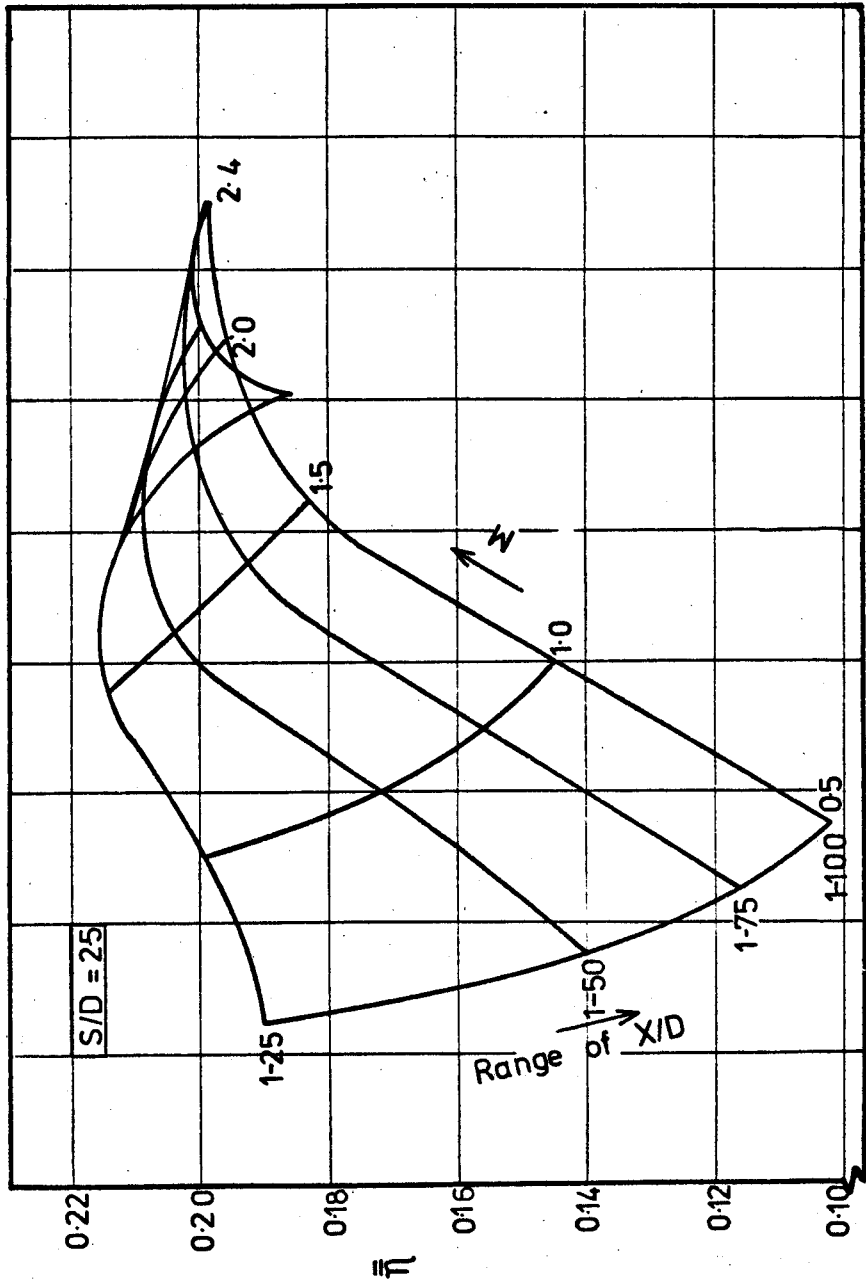


Fig. 8.2 Variation of averaged effectiveness, $\bar{\eta}$, with blowing rate for $S/D = 2.5$

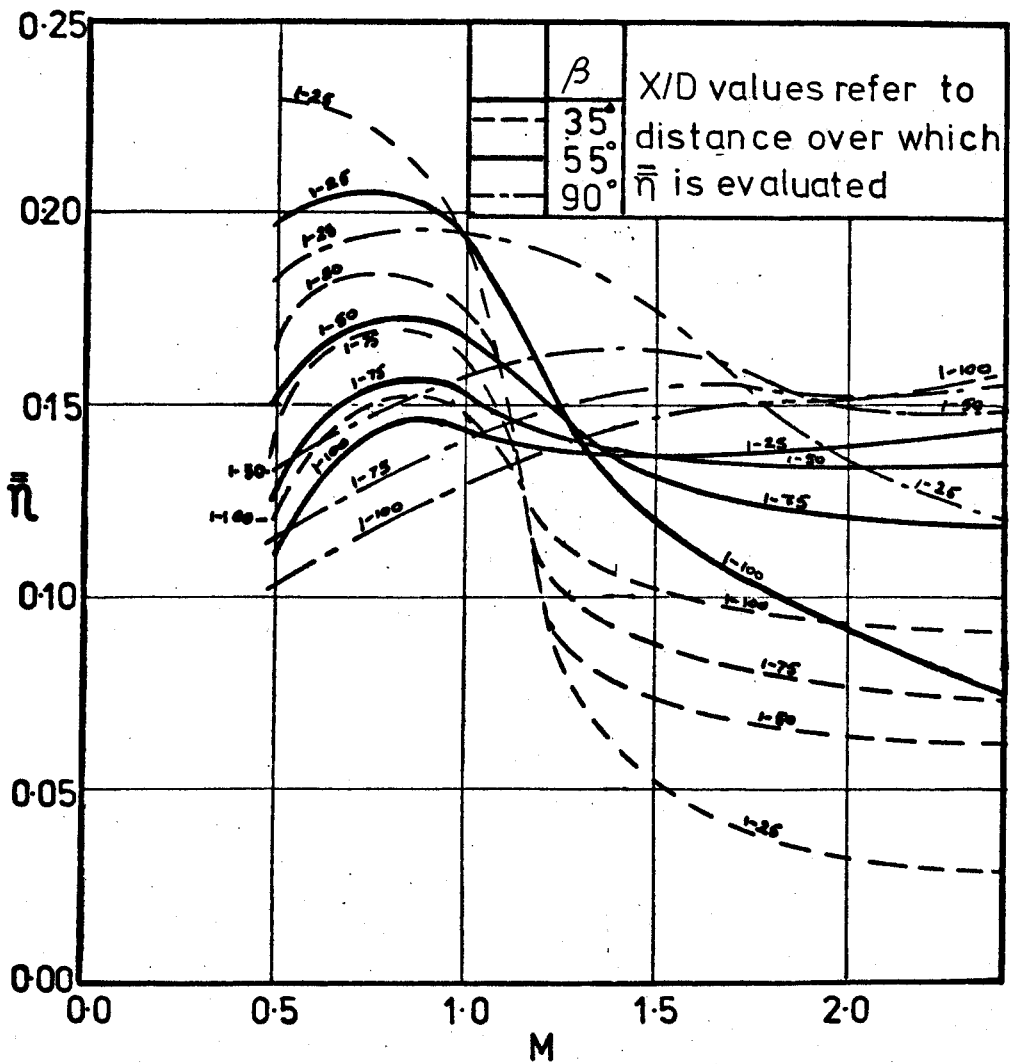


Fig.8.3 Variation of averaged effectiveness, $\bar{\eta}$, with injection angle and blowing parameter, M .

35° injection angle gives the highest level of effectiveness for every downstream case. However, as the blowing rate increases to, say, 1.0, although the 90° injection is best over the 1 - 25 diameter range, closely followed by the 55° injection, the 35° injection is still the best over the other distances.

At even higher values of blowing rate, the normal injection is much superior to the other angles. So, the 35° injection offers a considerable gain in effectiveness over the other two angles at low blowing rates and in the range of 1 - 25 diameters. Further downstream the advantage is relatively small and may be outweighed by other factors such as the effectiveness distribution. However, at large values of blowing rate, normal injection is the best.

8.3 Distribution of Effectiveness

There is some difficulty here, as to what criteria one should consider to give a picture of the distribution of the effectiveness in a spanwise direction.

The designer is going to be interested in the minimum effectiveness which occurs between the holes in a row, so that local metal temperatures can be maintained at levels suitable for the particular materials. Also, he is going to be interested in the gradients of effectiveness, so that large temperature gradients leading to thermal fatigue and cracking can be eliminated.

To this end two criteria were chosen: firstly the minimum effectiveness at $X/D = 4.25$, which generally occurred

between the holes; and secondly, the ratio of the maximum difference between a centreline value and minimum value at the same X/D to the hole spacing,

$$\text{i.e. } \frac{\hat{\eta} - \check{\eta}}{S/D},$$

which generally occurred at $X/D = 4.25$.

8.3.1 The Effect of Hole Spacing

Fig.8.4a shows the minimum effectiveness plotted against the blowing rate as the hole spacing is increased. The minimum effectiveness obviously falls as the hole spacing increases. A hole spacing of larger than 3.75 diameters is going to give a minimum effectiveness of little more than 0.1 for a blowing rate as low as 0.5, making a larger spacing than, say, 3.5 undesirable. This is the largest spacing to give an effectiveness of 0.1 at a blowing rate of 1.

Considering the effectiveness gradient between the holes, fig.8.4b shows that the 1.25 spacing is again the best arrangement and that the values increase as the hole spacing increases. For the widest hole spacing, however, there does seem to be a slight improvement, but this is due to the lower level of centreline effectiveness and the fact that the minimum values reach zero effectiveness at low blowing rates, thus not allowing any further deterioration.

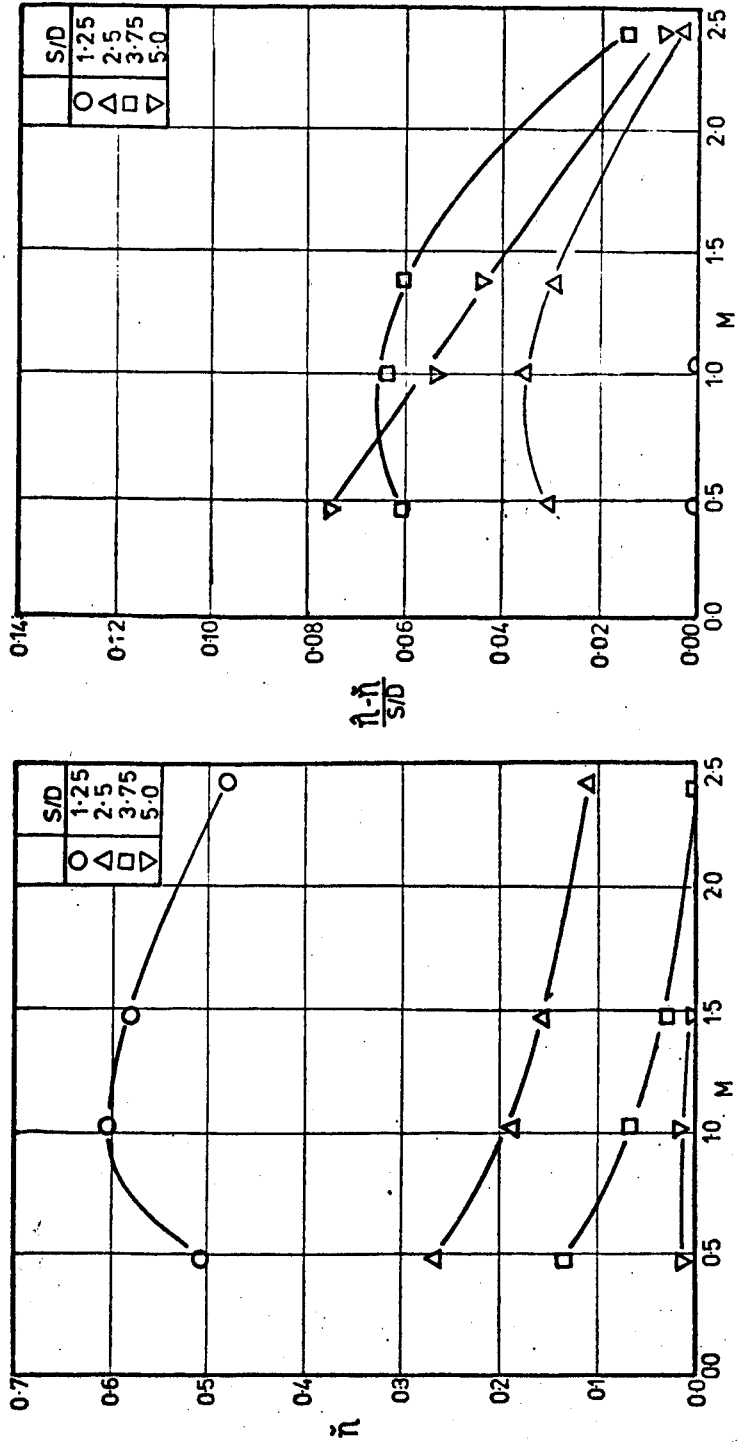


Fig. 8.4a Variation of minimum effectiveness, η , with hole spacing, S/D , and blowing parameter, M

Fig. 8.4b Variation of lateral effectiveness gradient, $\frac{\eta - \bar{\eta}}{S/D}$, with hole spacing, S/D and blowing parameter, M

8.3.2 The Effect of Angled Injection

Considering the same parameters as in the previous section, Fig.8.5a shows that 90° injection is a considerable improvement over both angled cases for the minimum effectiveness criterion. For a blowing rate of 1.0, the 90° injection gives a minimum effectiveness of 0.17 compared with 0.03 for 55° and 0.01 for 35° injection.

The effectiveness gradients plotted in fig.8.5b again show the superiority of 90° injection, where the effectiveness gradient is half the value for 35° injection at a blowing rate of unity.

For both criteria, the 55° injection shows little improvement over the 35° case.

8.4 The Aerodynamic Penalties

The increase in the boundary layer thickness which might be expected from injecting fluid, usually at low velocity ratios, into the boundary layer is of interest to the designer. Too large a boundary layer will impair the performance of the blade by assisting flow separation and modifying the velocity of the mainflow through the passages between the blades. Only the variation of the injection angle is considered here, as this was expected to have a major effect on the boundary layer thickness resulting after injection.

8.4.1 The Effect of Injectant Angle

Figs.8.6 and 8.7 show the complex way in which a jet

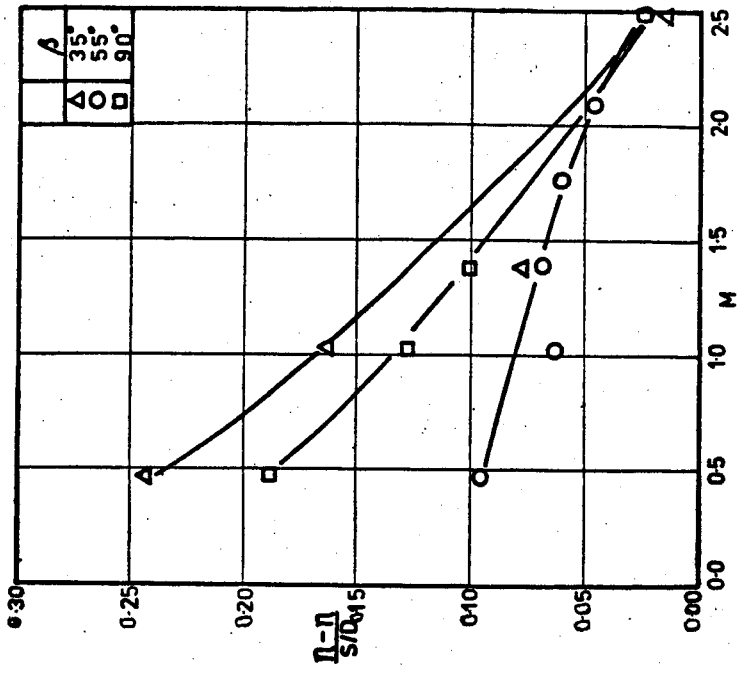


Fig. 8.5a Variation of minimum effectiveness, η , with injection angle, β , and blowing parameter, M

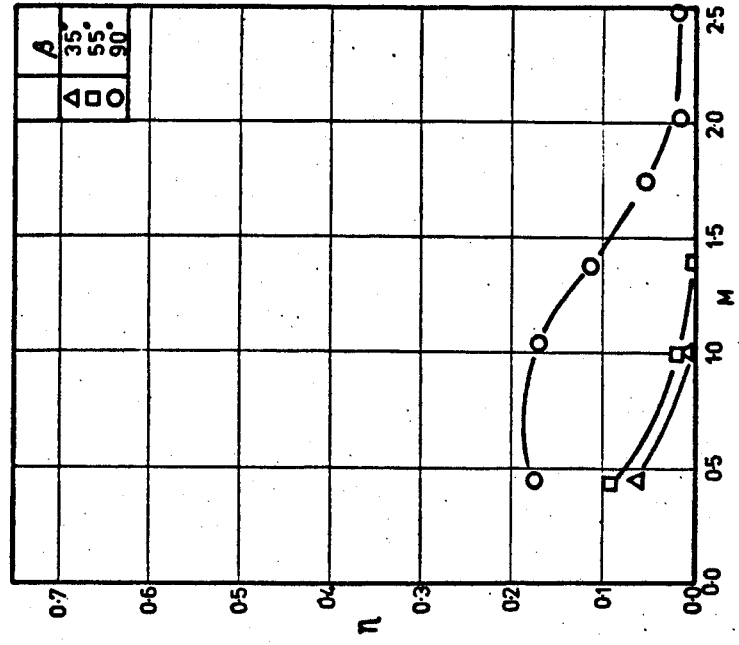


Fig. 8.5b Variation of lateral effectiveness gradient, $\frac{\eta - \tilde{\eta}}{S/D}$, with injection angle, β , and blowing parameter, M .

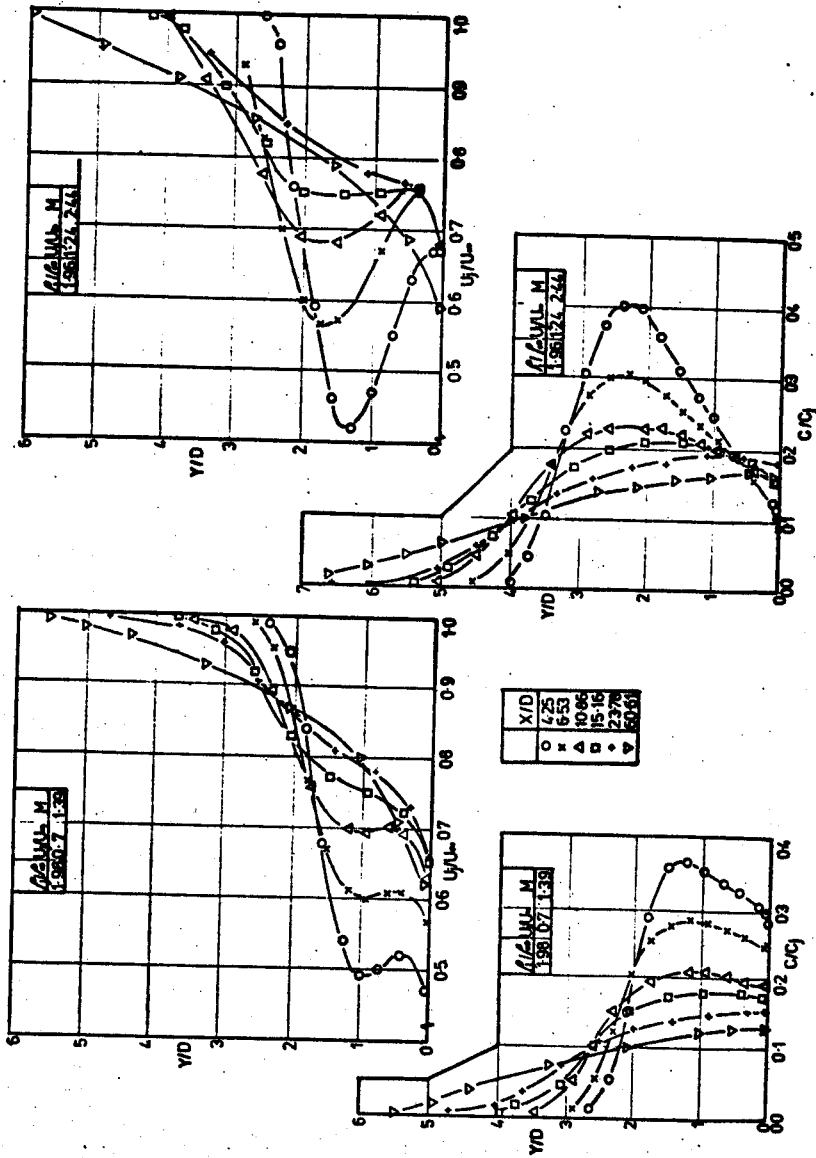


Fig. 8.6 Vertical distribution on the centreline of injectant concentration and velocity for normal injection at two blowing parameters: $M=1.39$ and 2.44

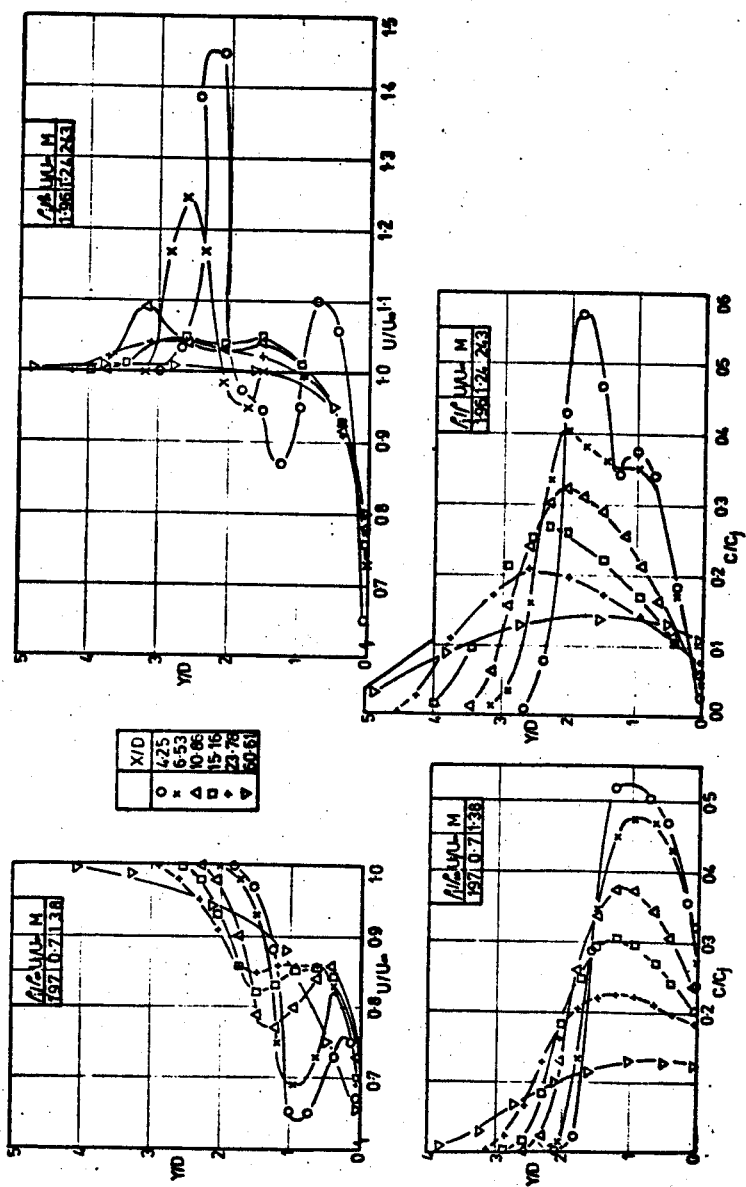


Fig. 8.7 Vertical distribution on the centreline of injectant concentration and velocity for 35° injection at two blowing parameters: $M = 1.38$ and 2.43 .

modifies the boundary layer, and how the levels of injectant concentration above the surface do not reflect the velocity distribution.

For a distance downstream of 4.25 diameters, the minimum velocity away from the surface occurs for the 90° injection at a velocity ratio of 1.24 rather than 0.7. For the angled cases the increase in velocity ratio gives rise to a peak velocity above the mean velocity ratio, due to the velocity distribution within the injection tubes. The figures show that by 60.6 diameters downstream, a roughly uniform boundary layer profile has been produced, and values of boundary layer displacement and momentum thickness have been calculated at this downstream position.

The surface concentrations for these velocity ratios show the flow to be very nearly two-dimensional in nature at this distance downstream.

The calculated values are shown in Table 8.1. The boundary layer displacement thickness at the holes but without injection was 0.16 diameters. Assuming that δ^*/δ remains constant and that $\delta \propto X^{4/5}$, a displacement thickness at $X/D = 60.6$ of 0.19 diameters could be expected in the absence of injection.

Considering a blowing rate of 1.4 or velocity ratio of 0.7, the table shows that the 90° injection is the worst, giving a displacement thickness of 0.47 diameters compared with 0.23 for the 35° case and 0.26 for the 55° case. All three

<i>Angle</i> β	<i>Blowing</i> <i>Rate M</i>	δ^*/D	θ/D	H
90	1.4	0.47	0.55	0.85
90	2.48	0.53	0.77	0.69
55	1.4	0.26	0.35	0.74
55	2.48	0.02	0.31	0.06
35	1.4	0.23	0.31	0.73
35	2.48	-0.23	0.07	-3.3

TABLE 8.1 Boundary Layer Details at $X/D = 60.6$

produce an increase in the displacement thickness compared with the calculated result without blowing.

However, as the blowing rate increases to 2.48, with a velocity ratio of 1.24, the situation for the 90° injection worsens, with the boundary layer displacement thickness increasing to 0.53 diameters; whilst for the 35° injection it drops to -0.23 diameters - which means that the injectant is increasing the momentum of the boundary layer above that of the mainstream and actually reducing the displacement thickness. The momentum thicknesses show the same trends.

The strange results, with the shape factor 'H' being less than unity and the displacement thickness being negative in one instance, are largely due to the considerable density gradients present, especially with the shallow injection angle.

No results were taken for low blowing rates, but from the results presented it would appear that at low blowing rates the 90° injectant might not be any worse than, if as bad as, the angled cases.

8.5 Summary

The Table 8.2 attempts to simplify the complex picture which has emerged during the chapter with regard to the angle of injection.

The numbers are in order of preference, i.e. 1 is the best. No attempt was made to weight the rankings to give a genuine optimisation as in different circumstances the varying

CRITERION	35°		55°		90°	
	$M < \mathcal{L}$	$M > \mathcal{L}$	$M < \mathcal{L}$	$M > \mathcal{L}$	$M < \mathcal{L}$	$M > \mathcal{L}$
$\bar{\eta}$ 1 - 25	1	3	2	2	3	1
$\bar{\eta}$ 1 - 50	1	3	2	2	3	1
$\bar{\eta}$ 1 - 75	1	3	2	2	3	1
$\bar{\eta}$ 1 - 100	1	3	2	2	3	1
$\bar{\eta}$	3	3	2	2	1	1
$\frac{\hat{\eta} - \bar{\eta}}{s}$	3	3	2	2	1	1
Aerod.	1	1	2	2	3	3
TOTAL	11	19	14	14	17	9

TABLE 8.2 Summary of Injection Angle Comparisons

criteria will assume differing degrees of importance - although totals are included out of interest.

CHAPTER 9 : MODELS & CORRELATIONS

In this chapter some of the film cooling correlations which have been proposed are tested against the data obtained during this study, and a new correlation is suggested.

=====

9.1 The Bulk Mixing Models

The basic form of this model, as proposed by Stollery and El-Ehwany (9.1), will not be considered here as it has the serious limitation that the effectiveness close to the injection hole must be unity. However, it is interesting to compare the experimental results with Kelly's modification to the two dimensional model which was discussed in Chapter 2.

9.1.1 Kelly's Model

Smith (9.2) shows that for Kelly's modification to the bulk mixing model:

$$\bar{\eta} = 3.09 \left(\frac{D}{S}\right) (\bar{X}_1 + 4.1)^{-0.8}$$

$$\text{where } \bar{X}_1 = \frac{X}{MS_2} \left(\frac{P_j U_j S_2}{\mu_\infty} \right)^{-0.25}$$

$$\text{and } S_2 = \frac{\pi D^2}{4D}.$$

Fig.9.1 shows results for two blowing rates, 0.48 and 1.4.

According to Kelly's model, the results from different hole

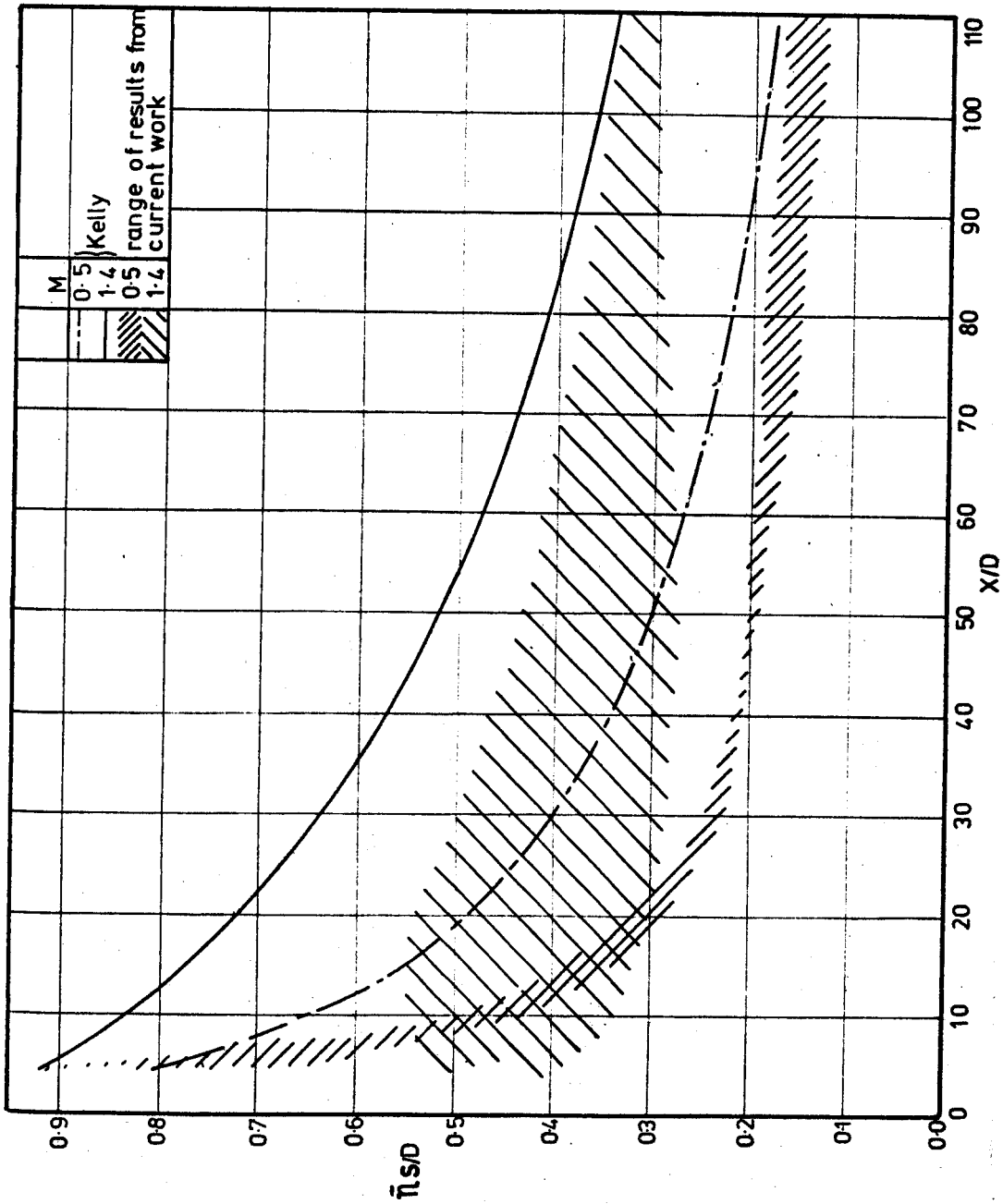


Fig. 9.1 Comparison of predictions from the bulk mixing model with the experimental data obtained for normal injection

spacings should collapse onto the same line for constant values of blowing rate. However, this is only true for the low blowing rate, and the data does not coincide with the prediction.

The figure also shows the inability of this sort of model to cope with the "lift off" phenomenon and it predicts an increase in effectiveness close to the injection position as the blowing rate increases.

9.1.2 Smith's Model

In ref (9.2), Smith presents a correlation for slot data which is based on the bulk mixing model. He derives the entrained mass flow rate, \dot{m}_{ent} to be

$$\dot{m}_{ent} = \dot{m}_j \left(\frac{1}{\bar{\eta}} - 1 \right) \quad \dots\dots (9.1)$$

Defining an entrained mass flow rate per unit lateral distance, \dot{m}_e

$$\dot{m}_e = \frac{\dot{m}_{ent}}{S} \quad \dots\dots (9.2)$$

and $\dot{m}_j = \rho_j U_j \pi D^2 / 4$.

Substituting into 9.1 and using $M = \frac{\rho_j U_j}{\rho_\infty U_\infty}$

$$\frac{\dot{m}_e}{\rho_\infty U_\infty} = \frac{\pi D}{4} \left(M \frac{D}{S} \left\{ \frac{1}{\bar{\eta}} - 1 \right\} \right)$$

$$\frac{\dot{m}_e^4}{\rho_\infty^4 U_\infty^4 \pi D} = M \frac{D}{S} \left\{ \frac{1}{\bar{\eta}} - 1 \right\} \quad \dots\dots (9.3)$$

For the current work, where ρ_∞ , U_∞ and D are constant,

$$\dot{m}_e \propto M \frac{D}{S} \left\{ \frac{1}{\bar{\eta}} - 1 \right\}.$$

Fig.9.2a shows that for $M = 1$, the correlation gives good agreement for all but the smallest hole spacings. However, fig.9.2b shows that this is not true when the blowing rate is raised to 1.4. If the blowing rate is raised even further, the entrainment appears to decrease as X/D increases. This, as Smith pointed out, is because the model does not reflect the physical situation.

This can be further demonstrated by calculating the entrained mass flow rate from the traverses, normal to the surface, carried out in the present work.

If the mass flow rate in the boundary layer, \dot{m}_δ , is defined as:

$$\dot{m}_\delta = \int_0^\delta \rho U dy$$

and

$$\delta^* \rho_\infty U_\infty = \rho_\infty U_\infty \int_0^\delta \left(1 - \frac{\rho U}{\rho_\infty U_\infty} \right) dy$$

$$= \rho_\infty U_\infty \delta - \int_0^\delta \rho U dy$$

$$= \rho_\infty U_\infty \delta - \dot{m}_\delta$$

then

$$\dot{m}_\delta = \rho_\infty U_\infty (\delta - \delta^*)$$

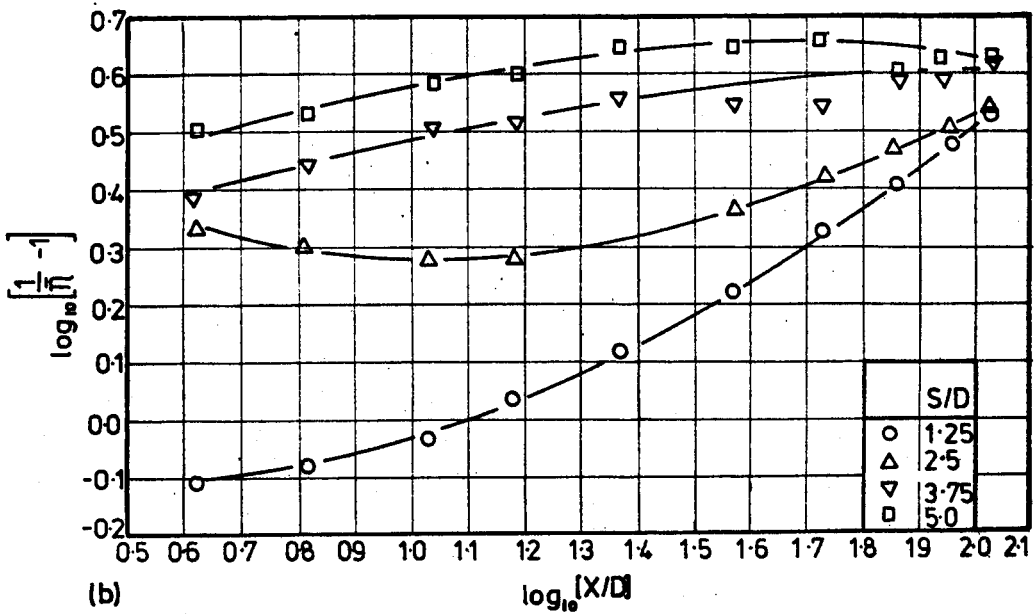
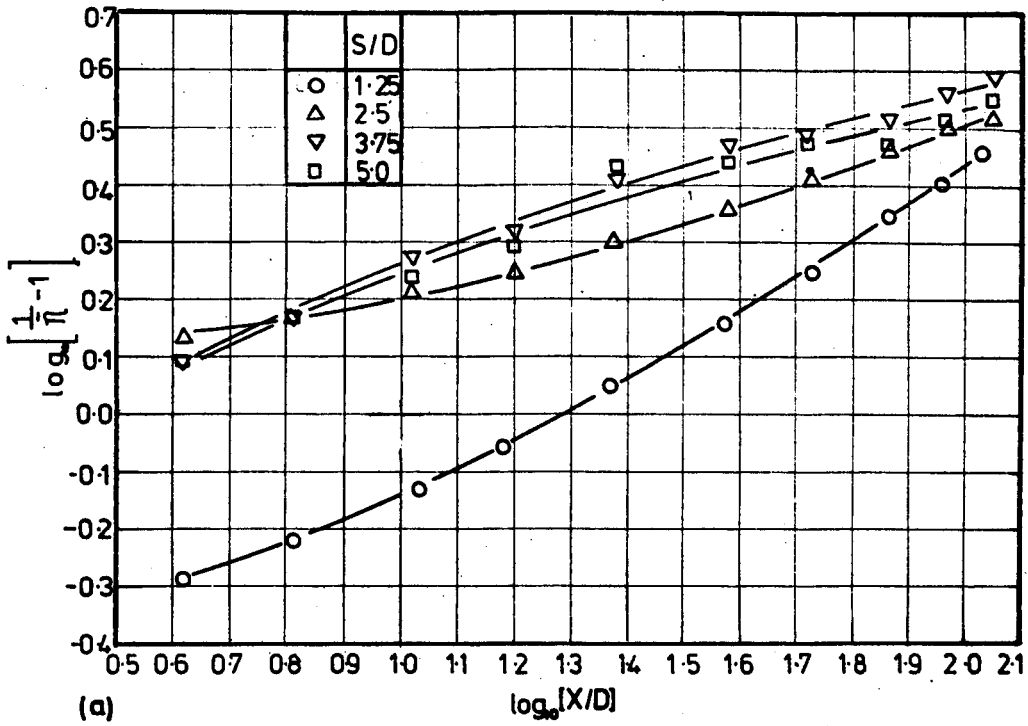


Fig. 9.2 Graphs of $\log_{10} \left(\frac{1}{\eta} - 1 \right)$ against $\log_{10} (X/D)$ (Smith, (9.2))

The entrained mass flow rate, \dot{m}_{ent} , may be written:-

$$\begin{aligned}\dot{m}_{ent} &= S\dot{m}_{\delta} - \dot{m}_j \\ &= S\rho_{\infty}U_{\infty}(\delta - \delta^*) - \dot{m}_j \\ &= S\rho_{\infty}U_{\infty}\left[(\delta - \delta^*) - M\frac{\pi D^2}{4S}\right]\end{aligned}$$

from 9.2

$$\dot{m}_e = \rho_{\infty}U_{\infty}\left[(\delta - \delta^*) - M\frac{\pi D^2}{4S}\right] \quad \dots\dots (9.4)$$

Re-arranging 9.3 and dividing into 9.4, the two different methods of calculation being differentiated by the suffices 3 and 4, we have:

$$\frac{\dot{m}_{e_4}}{\dot{m}_{e_3}} = \left(\frac{\delta - \delta^*}{\frac{M\pi D^2}{4S}} - 1\right) \left[\frac{1}{\frac{1}{\eta} - 1}\right] \quad \dots\dots (9.5)$$

For the case of 90° injection, with $M = 1.4$ at $X/D = 60.61$ and with three diameters hole spacing, $\dot{m}_{e_4}/\dot{m}_{e_3}$ was found to be 1.6. If the assumptions (on which this and the other bulk mixing models are based) were correct, the value should have been unity.

It is interesting to note that the correlation does show up any scatter in the results, especially at low values of effectiveness, and any further collapse that could be obtained using this correlation would enable effectivenesses to be

calculated with some accuracy. However, the method is still basically the same bulk mixing model and suffers from the same limitations and deficiencies.

9.2 The Heat Sink Model

The formulae given by Eriksen et al (9.3) were for single hole injection. These were altered for injection through a row of holes using the superposition technique. From Eriksen et al :-

$$\frac{\phi(X, Y, Z)}{\phi_1} = \frac{MU_{\infty} D}{16\epsilon_p \frac{X}{D}} \exp \left(\frac{-U_{\infty} D}{4\epsilon_p \frac{X}{D}} \left[\left(\frac{Y - Y_0}{D} \right)^2 + \left(\frac{Z}{D} \right)^2 \right] \right) +$$

$$\frac{MU_{\infty} D}{16\epsilon_p \frac{X}{D}} \exp \left(\frac{-U_{\infty} D}{4\epsilon_p \frac{X}{D}} \left[\left(\frac{Y + Y_0}{D} \right)^2 + \left(\frac{Z}{D} \right)^2 \right] \right) \dots (9.6)$$

where ϵ_p is a turbulent diffusivity and Y_0 the height of the sink above the surface.

If only surface values are considered $Y = 0$ and

$$\frac{\phi(X, 0, Z)}{\phi_1} = \frac{2MU_{\infty} D}{16\epsilon_p \frac{X}{D}} \exp \left(\frac{-U_{\infty} D}{4\epsilon_p \frac{X}{D}} \left[\left(\frac{Y_0}{D} \right)^2 + \left(\frac{Z}{D} \right)^2 \right] \right)$$

For a row of holes at 3 diameter spacings the effectiveness on the centreline ($Y = 0, Z = 0$) is given by superposition as:

$$\frac{\phi(X,0,0)}{\phi_1} = \frac{2MU_{\infty}D}{16\epsilon_p \frac{X}{D}} \exp \left(- \frac{U_{\infty}D}{4\epsilon_p \frac{X}{D}} \left(\frac{Y_0}{D} \right)^2 \right) + \sum_{n=1}^{\infty} \frac{4MU_{\infty}D}{16\epsilon_p \frac{X}{D}} \exp \left(- \frac{U_{\infty}D}{4\epsilon_p \frac{X}{D}} \left[\left(\frac{Y_0}{D} \right)^2 + \left(\frac{nS}{D} \right)^2 \right] \right)$$

This equation was then used to evaluate the values of ϵ_p from the measured effectiveness. Variation of Y_0 , to keep it close to the values encountered in the experiments, had little effect on the value of ϵ_p obtained. However, if too large a value were chosen, the iterative procedure necessary to calculate ϵ_p could not be made to converge. For these reasons a constant value for Y_0 of 0.5 diameters was chosen.

For low blowing rates ϵ_p was approximately constant for varying distance downstream; however, for the large blowing rate of $2.91 \epsilon_p$ varied from approximately 3000 to 60 as X/D varied from 4 to 100. This means that the method of Eriksen et al, of taking an average value for ϵ_p , gives poor results at high blowing rates - as, indeed, they noted.

The turbulent diffusivity was found to vary in a consistent manner and could be approximated by :-

$$\epsilon_p = 30M^{10}(X/D)^{-0.56}$$

The results obtained for the centreline effectiveness using this calculated value of ϵ_p are shown in Fig.9.3, with values obtained using the average turbulent diffusivity included for

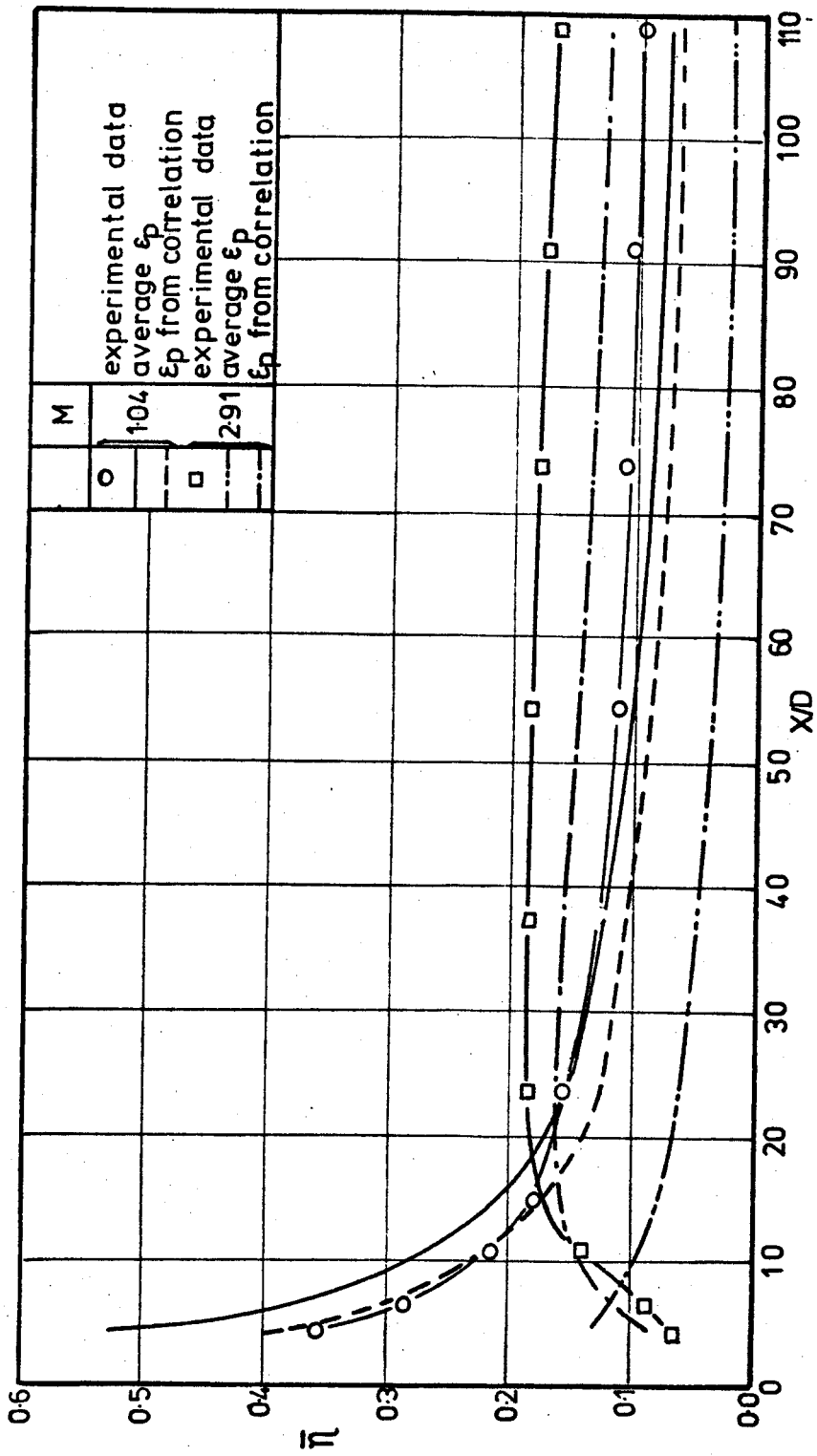


Fig. 9.3 Comparison of predictions of spanwise averaged effectiveness distribution using the point source model (9.3) (ϵ_p evaluated by two different methods), with the experimental data

comparison. Two blowing rates are considered, 1.04 and 2.91. The effectiveness given by the lower blowing rate is slightly better approximated by the average turbulent diffusivity of Eriksen et al., but at the higher blowing rate the proposed correlation gives a much improved result.

Unfortunately, the results away from the centreline were in poor agreement with the experimental results, as observed by Eriksen et al. Clearly the turbulent diffusivity is not constant across the surface in the lateral direction either. To overcome this difficulty Eriksen et al proposed a line sink model and an attempt was made to apply a similar technique to this model to obtain an empirical relationship for ϵ_p . However, this had to be abandoned due to difficulties with convergence of the iterative process.

Fig.9.4 compares the predicted temperature ratio distribution normal to the surface with the measured injectant concentration ratios. The model clearly fails to predict the vertical distribution, especially close to the holes where the situation is complex. Eriksen et al suggested that the model be used to interpolate between sets of results from which 'local' values of ϵ_p can be calculated. Clearly, it is of limited value in the absence of data.

9.3 Shaped Holes

As reported in Chapter 2, Goldstein et al (9.4) and Smith (9.2) noticed that an improvement in effectiveness can be obtained by using shaped rather than cylindrical holes.

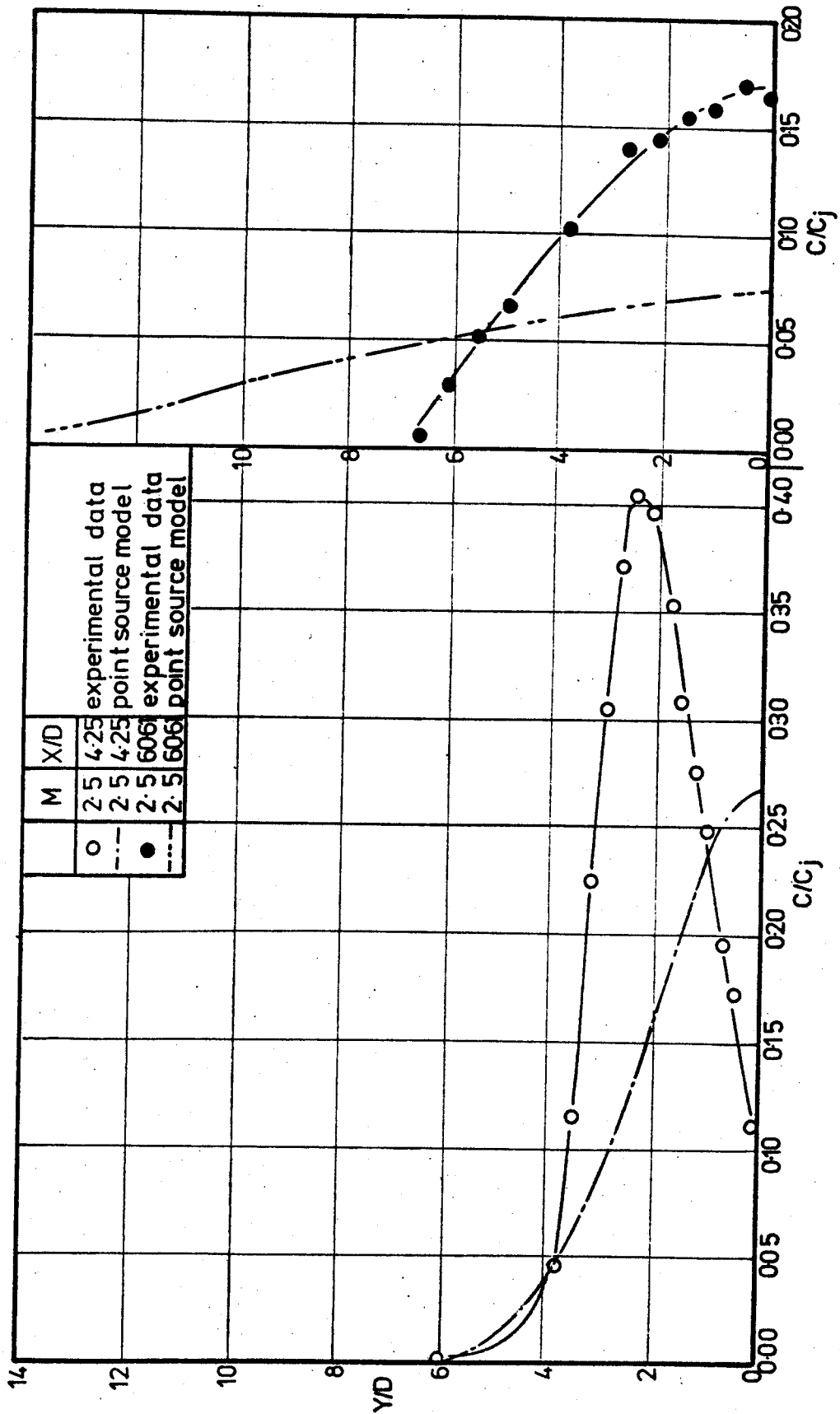


Fig.9.4 Comparison of predictions of vertical distribution of injectant concentration on the centreline from the point source model (9.3) with the experimental data

Goldstein et al found that their results with shaped holes correlated better when plotted against M/R , fig.9.5, where R is the ratio of the cross-sectional area of the hole, normal to the axis of the tube, to the internal area at the entrance to the tube. This implies, as one might expect, that the improvement is due to the fact that the velocity of the injectant is lower at the exit from a shaped hole than it is with a plain hole, therefore giving a lower value of M at exit than at entry to the tube.

This suggests that the data should, perhaps, be compared on the basis of the exit and not the entrance diameter. As the holes are not necessarily circular in cross-section, the ratio ' R ' can be used to give an equivalent exit diameter. Therefore the hole spacing might be defined as $S/(D\sqrt{R})$ and the downstream distance as $X/(D\sqrt{R})$.

Figs. 9.6a, 9.6b and 9.6c, reproduced from reference 9.4 of Goldstein et al, show the increased effectiveness with the shaped holes. Fig.9.6c shows shaped holes at 6 diameters spacing at entrance and with $S/(D\sqrt{R}) = 3.75$, which is therefore comparable with the cylindrical holes of fig.9.6a at 3 diameters spacing. The similarity of the two figures is obvious, and the difference in effectiveness between the holes between the two figures is of the same order as was noticed in the present work for these hole spacings.

The centreline values of figs.9.6a and 9.6c are reproduced in fig.9.6d, plotted against $X/(D\sqrt{R})$.

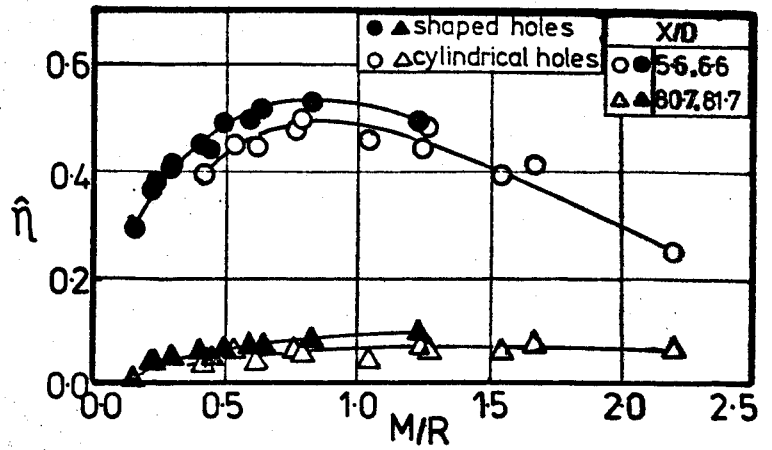


Fig.9.5 Centreline effectiveness, $\hat{\eta}$, as a function of blowing parameter divided by area ratio, M/R , from ref.9.4

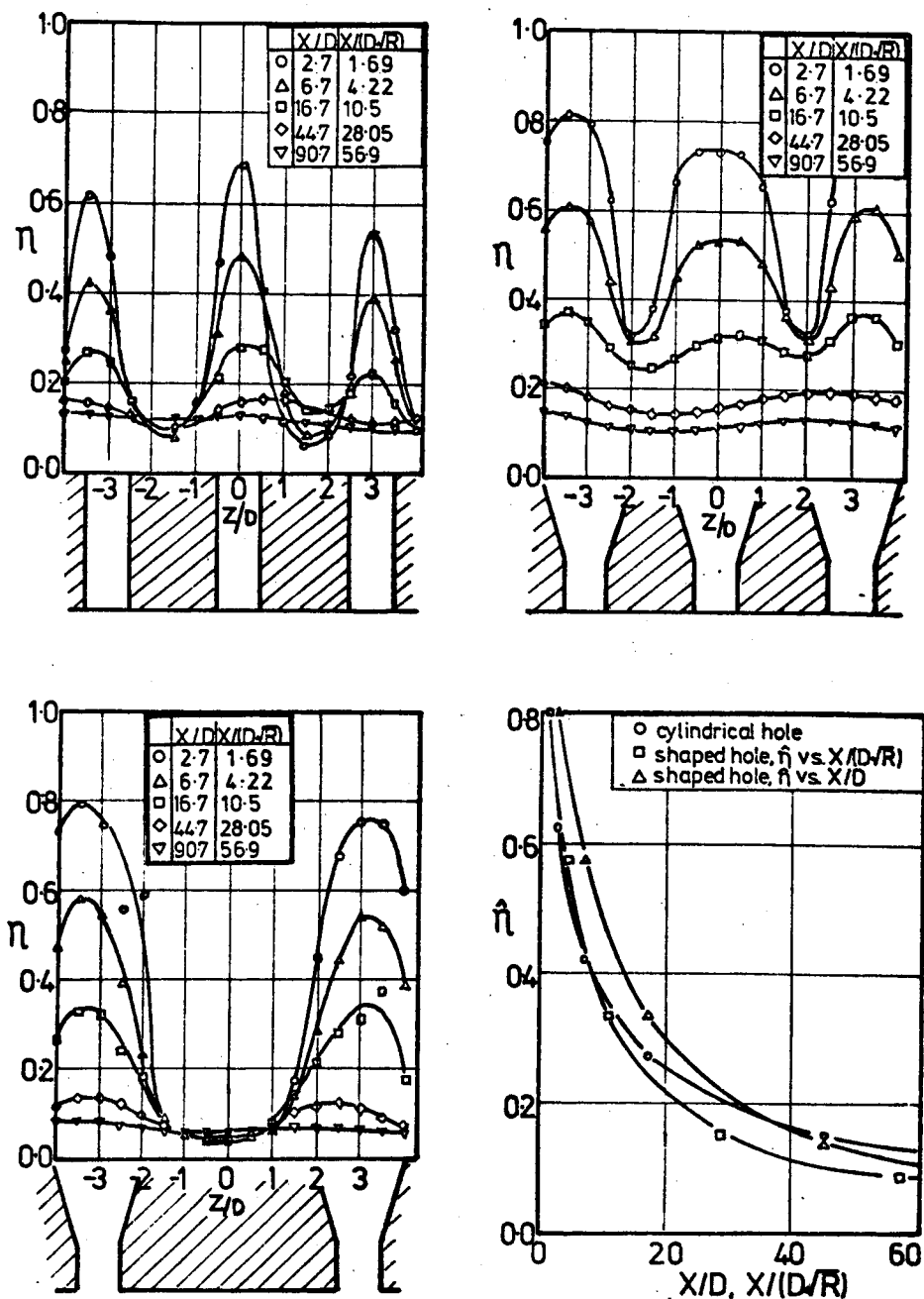


Fig.9.6 (a), (b) and (c): lateral distribution of effectiveness with injection through cylindrical and shaped holes
(d): comparison of centreline effectiveness values from (a) and (c) plotted against a function of downstream distance

The results close to the hole are approximately the same (this was noticed for the centreline values at different hole spacings), but further downstream the closer hole spacing gives a higher effectiveness as would be expected.

Unfortunately, Smith does not present sufficient information for a similar exercise to be carried out on his work. However, scaling the results using the root of the area ratio would appear to give good results with the shape of hole proposed by Goldstein et al.

9.4 The J.F. Louis Correlation

As only the abstract has been read of Louis' paper, which has yet to be printed, only brief comments are made upon it here.

Louis (9.5) plots adiabatic effectiveness against

$$\left(\frac{\rho_j U_j^2}{\rho_\infty U_\infty} \phi \cos^2 \beta \right)^{-1.35} \text{Re}^{-0.25} X/D$$

where, here, ϕ is the ratio of coolant to bulk mean temperature.

This implies initially that if the correlation results in a single line for a row of holes, then for normal injection where $\cos \beta = 0$, the effectiveness is constant and independent of the blowing parameter, distance downstream, etc.

The correlation also suggests that for the inclined

injection geometries $(\cos^2\beta)^{-1.35}$ X/D should provide some collapse of the data for the same blowing rate and mainstream conditions. Fig.9.7 shows this not to be the case, although the scatter in the figure presented in ref (9.5) covers in some instances a range of effectiveness from 0.5 to 1.0.

9.5 Simple Jet Models

The possibility of using the theoretical approach to jet entrainment developed for jets in a co-flowing stream was considered. Forstall and Shapiro (9.6) found that the velocity profiles of the jets could be approximated by

$$\frac{U - U_{\infty}}{\hat{U} - U_{\infty}} = \frac{1}{2} \left(1 + \cos \frac{\pi r}{2r_m} \right)$$

where \hat{U} is the velocity on the axis of the jet, r the distance from the axis and r_m the distance at which the velocity is the average of the peak and freestream velocities.

With a solid boundary, as in the current work, this is not possible. When applied to the concentration profiles, the result is as shown in fig.9.8. The surface exposed to the free-stream is approximated quite well by the curve. However, beneath the jet there is no comparison at all. Further downstream the concentration profiles depart even further from the curve.

This all implies that such a jet model is unlikely to work for film cooling predictions.

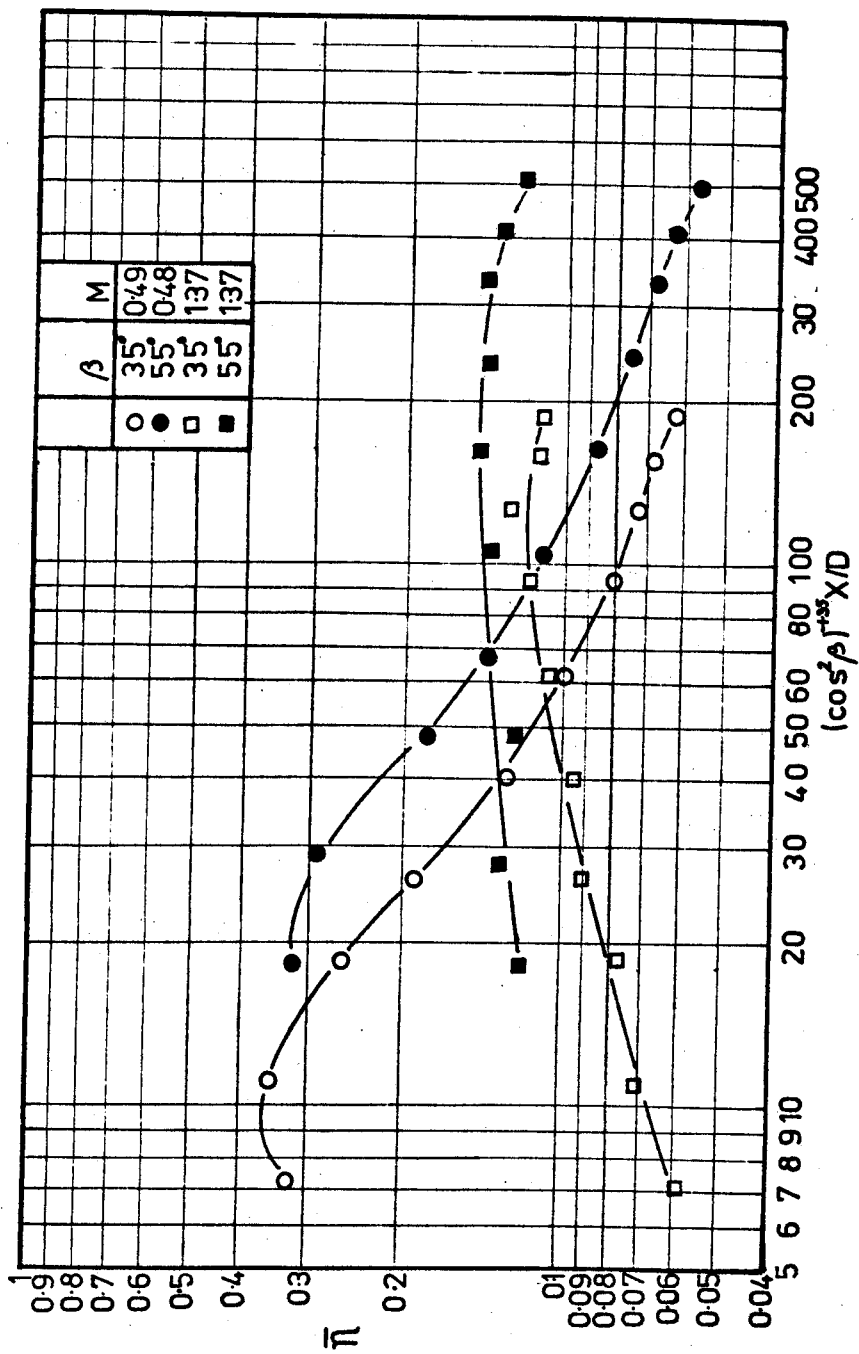


Fig.9.7 Graph of spanwise averaged effectiveness, \bar{n} , plotted against $(\cos^2 \beta)^{-1/35} X/D$ (ref.9.5) for two injection angles: 35° and 55° .

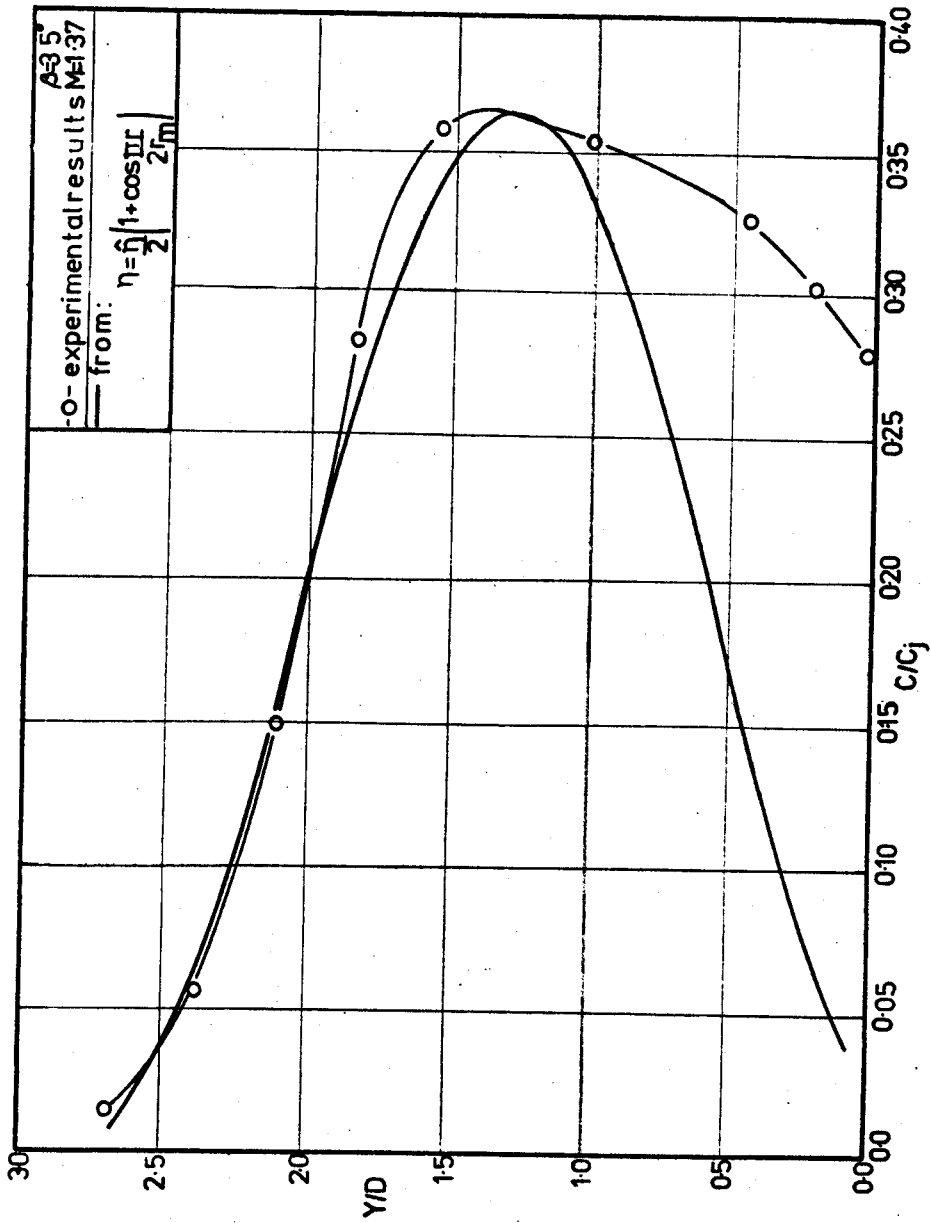


Fig. 9.8 Vertical distribution of injectant concentration compared with theoretical distribution

The results obtained in the present research show that the height above the surface of the maximum injectant concentration and maximum velocity did not co-incide - an effect also observed by Ramsey (9.7). This underlines the difficulties in an approach of the type just described.

9.6 The Nottingham Correlation

The majority of the experiments for the current work were carried out on a normal injection geometry, and for this reason the first attempts at finding a correlating parameter for the data were aimed at the 90° injection case. The correlations were arrived at empirically by consideration of the way the various parameters affected the film cooling effectiveness.

9.6.1 Normal Injection

It was clear at the outset that it was useless to plot $\bar{\eta}$ against a function of X/D ; this would not take into account the entirely different shapes of the graphs close to the injection holes, which were produced by variation of the blowing rate. This could only be done by dividing the effectiveness by some function of the blowing rate. The basic correlation for the normal injection, with a hole spacing of three diameters, requires the plotting of:

$$\log_{10} \left[\frac{(100\bar{\eta})^{0.7} \frac{X}{D}}{\frac{\rho_j}{\rho_\infty} \left(\frac{U_j}{U_\infty} \right)^{1.7}} \right] \quad \text{vs} \quad \log_{10} \left[\frac{\left(\frac{X}{D} \right)^{1.6}}{\frac{\rho_j}{\rho_\infty} \left(\frac{U_j}{U_\infty} \right)^3} \right]$$

The effectiveness is multiplied by 100 to produce a

percentage which makes the final numbers positive.

Fig.9.9 shows that this serves to collapse data at different density and velocity ratios for varying X/D with a hole spacing of three diameters.

The data can be approximated by the polynomial:

$$A = B^3 K_4 + B^2 K_3 + B K_2 + K_1$$

$$\text{where } A = \log_{10} \left[\frac{(100\bar{\eta})^{0.7} \frac{X}{D}}{\frac{\rho_j}{\rho_\infty} \left(\frac{U_j}{U_\infty} \right)^{1.7}} \right] \quad B = \log_{10} \left[\frac{\left(\frac{X}{D} \right)^{1.6}}{\frac{\rho_j}{\rho_\infty} \left(\frac{U_j}{U_\infty} \right)^3} \right]$$

$$\text{and } K_1 = 0.3209$$

$$K_2 = 1.1003$$

$$K_3 = -0.1554$$

$$K_4 = 0.0118$$

Using this polynomial, one can calculate values of effectiveness for differing density and velocity ratios at different downstream distances. Comparing values calculated in this manner with the equivalent experimental data gives a measure of the usefulness and accuracy of the correlation. This exercise was carried out and the result is presented in fig.9.10 for two values of velocity ratio and two values of density ratio. Except for the very large blowing rate, where there is a difference of 3% effectiveness, the calculated values follow quite closely the experimental curves.

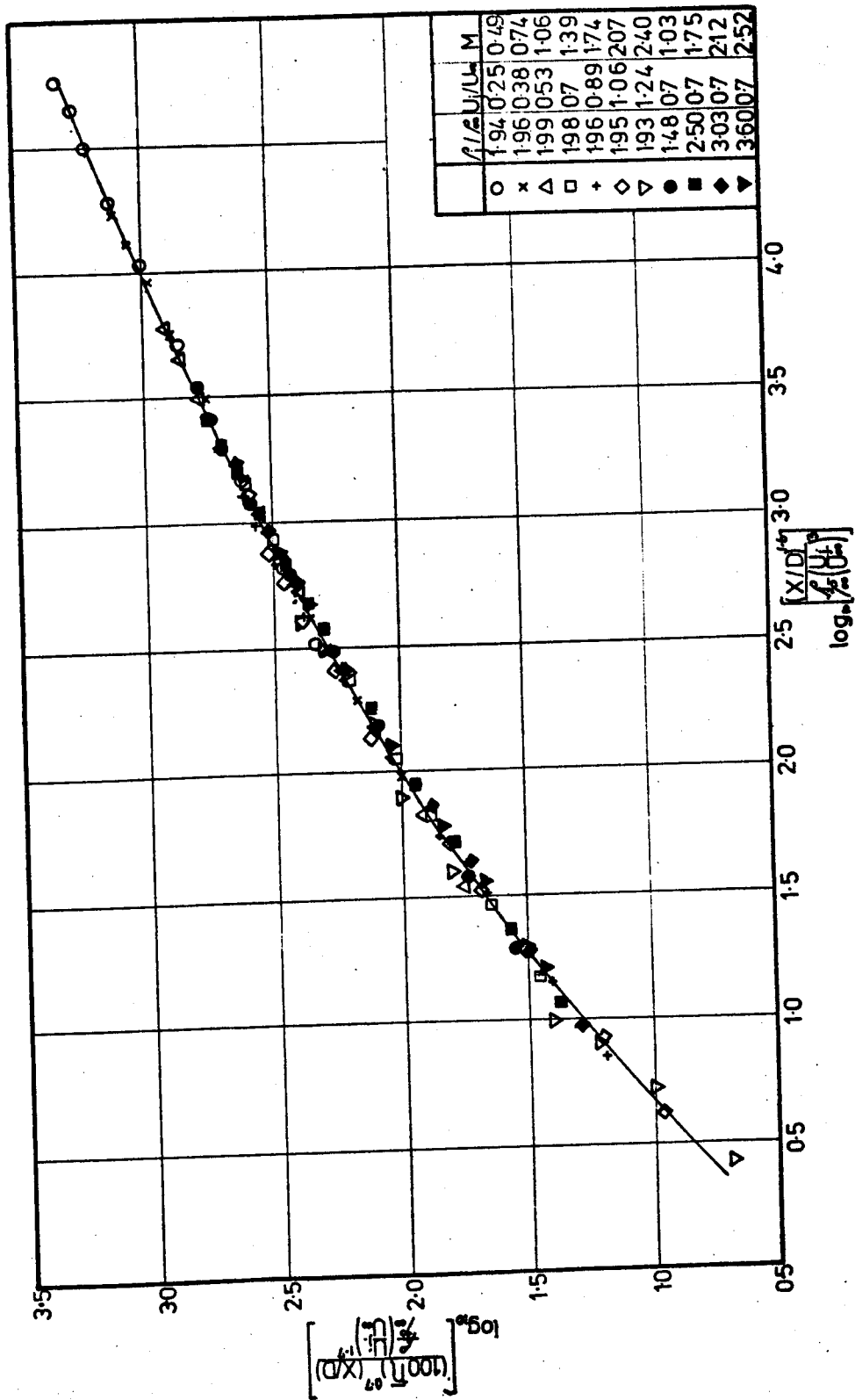


Fig. 9.9 Correlation of spanwise averaged effectiveness, \bar{n} , for normal injection and $S/D = 3$

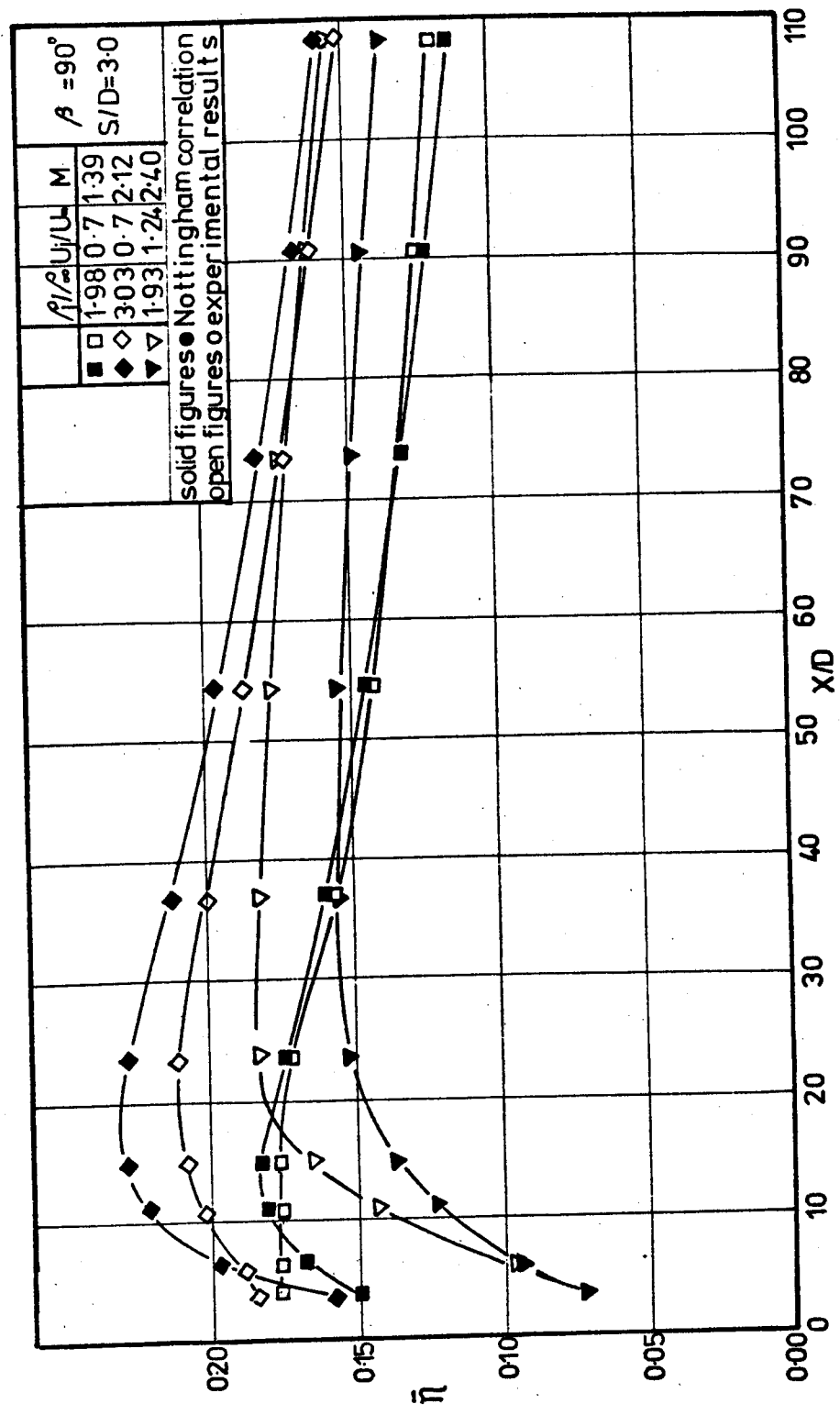


Fig.9.10 Comparison of predicted and experimental values of spanwise average effectiveness distribution

The basic correlation outlined above was found to collapse the data for any given hole spacing with normal injection onto a single line. However, the lines for each hole spacing were not congruent and the polynomial given above applies only to a hole spacing of three diameters.

9.6.2 Hole Spacing

The basic correlation was extended to incorporate the different hole spacings. Empirical methods were again used, but the curves for the various hole spacings formed a general pattern so that it was easy to collapse them onto a single line. This was achieved by plotting

$$\log_{10} \left[\frac{(100\bar{n})^{0.7} \frac{X}{D} \left(\frac{S}{D}\right)^{1.1}}{\frac{\rho_j}{\rho_\infty} \left(\frac{U_j}{U_\infty}\right)^{1.7}} \right] \text{ vs. } \log_{10} \left[\left(\frac{\left(\frac{X}{D}\right)^{1.6}}{\frac{\rho_j}{\rho_\infty} \left(\frac{U_j}{U_\infty}\right)^3} \right)^{(0.01\frac{S}{D} + 0.25)} \right]$$

The result is shown in fig.9.11. The scatter is more marked here, with the largest blowing rate tending to fall below the line at the wide hole spacings. However, the overall scatter is small and the data may be approximated by:

$$A = B^3 K_4 + B^2 K_3 + B K_2 + K_1$$

where

$$A = \log_{10} \left[\frac{(100\bar{n})^{0.7} \frac{X}{D} \left(\frac{S}{D}\right)^{1.1}}{\frac{\rho_j}{\rho_\infty} \left(\frac{U_j}{U_\infty}\right)^{1.7}} \right]$$

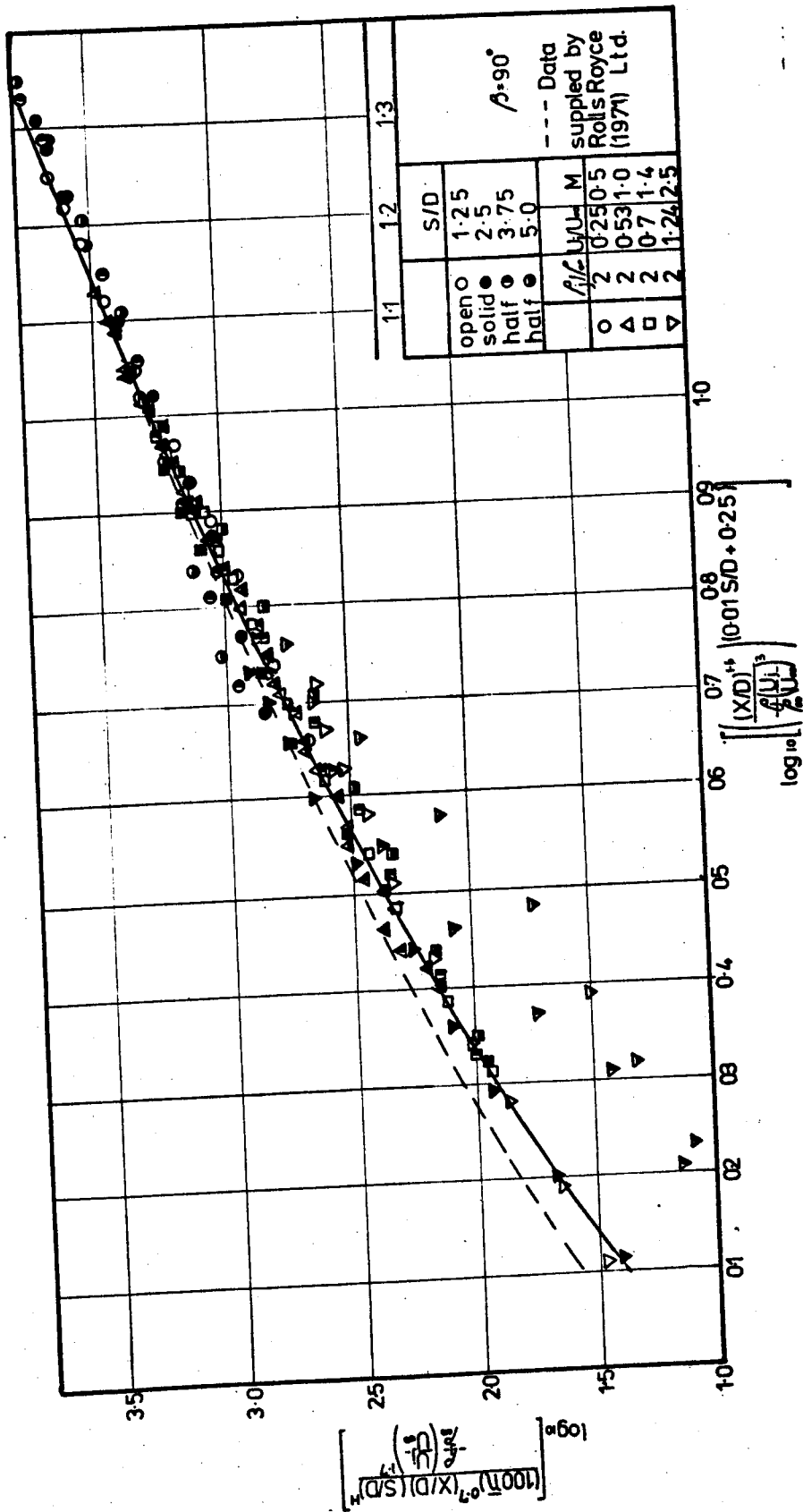


Fig. 8.11 Correlation of spanwise average effectiveness for normal injection

$$B = \log_{10} \left[\frac{(X/D)^{1.6}}{\left(\frac{\rho_j}{\rho_\infty} \left(\frac{U_j}{U_\infty} \right)^3 \right)} \left(0.01 \frac{S}{D} + 0.25 \right) \right]$$

$$\text{and } K_1 = 1.0988$$

$$K_2 = 3.0565$$

$$K_3 = -1.1561$$

$$K_4 = 0.2845$$

Values of effectiveness calculated from the equation are presented in figs.9.12a and 9.12b with the experimental data. There is the greatest discrepancy between the experimental results and the results from the correlation at the highest blowing rate, but in general the correlation results show the levels of effectiveness and the trends, especially for the ranges of values found in a turbine.

Included in fig.9.11 is a line based on data obtained by Rolls Royce. Again, a good collapse of the results was obtained and, in fact, there was less scatter than was present with the results from the current work. This is of particular importance, as the results were obtained in a totally different manner.

9.6.3 Angled Injection

When the results obtained with injection angles of 35° were plotted on the same basis as the 90° data, there was poor agreement, fig.9.13. A correction for the angled injection was

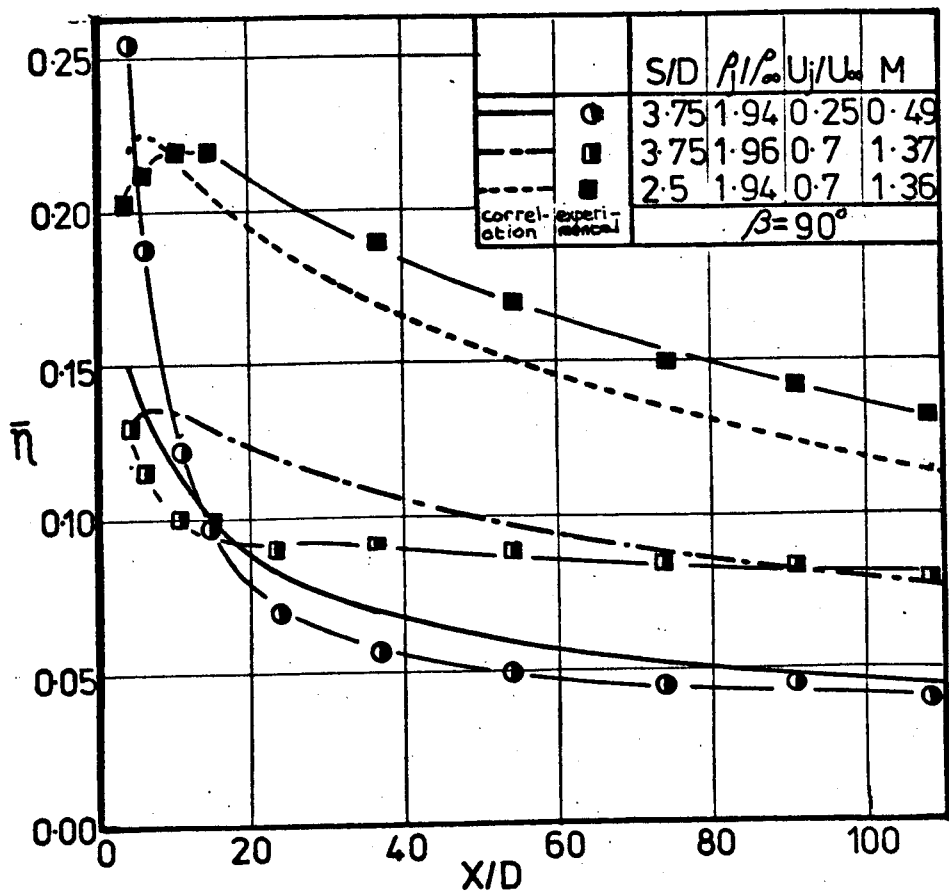
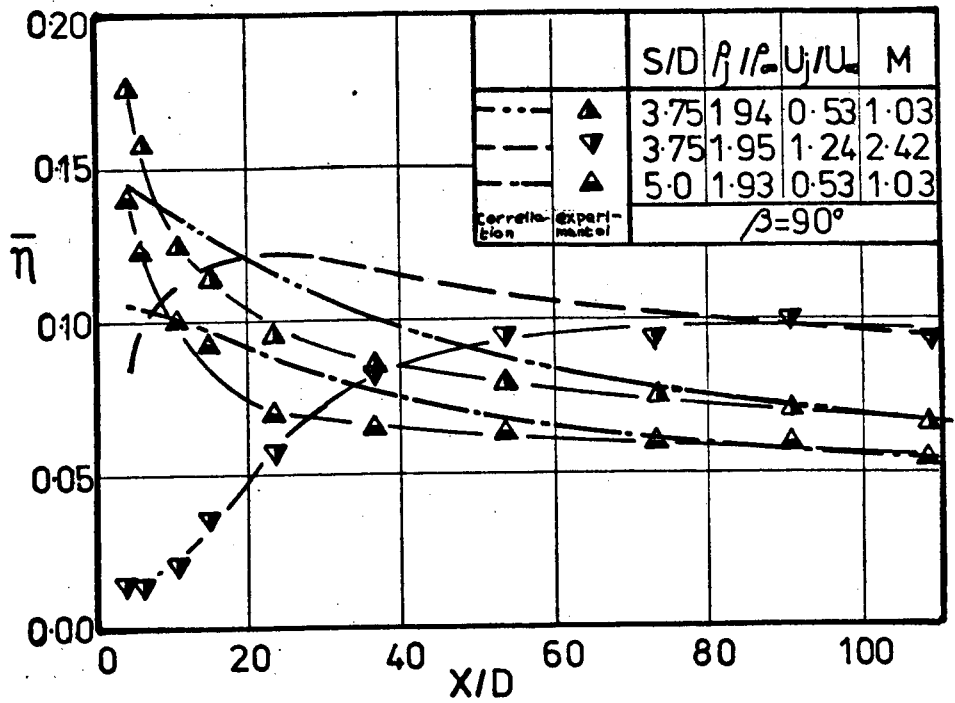


Fig.9.12 Comparisons of predicted and experimental values of spanwise averaged effectiveness, $\bar{\eta}$, for normal injection

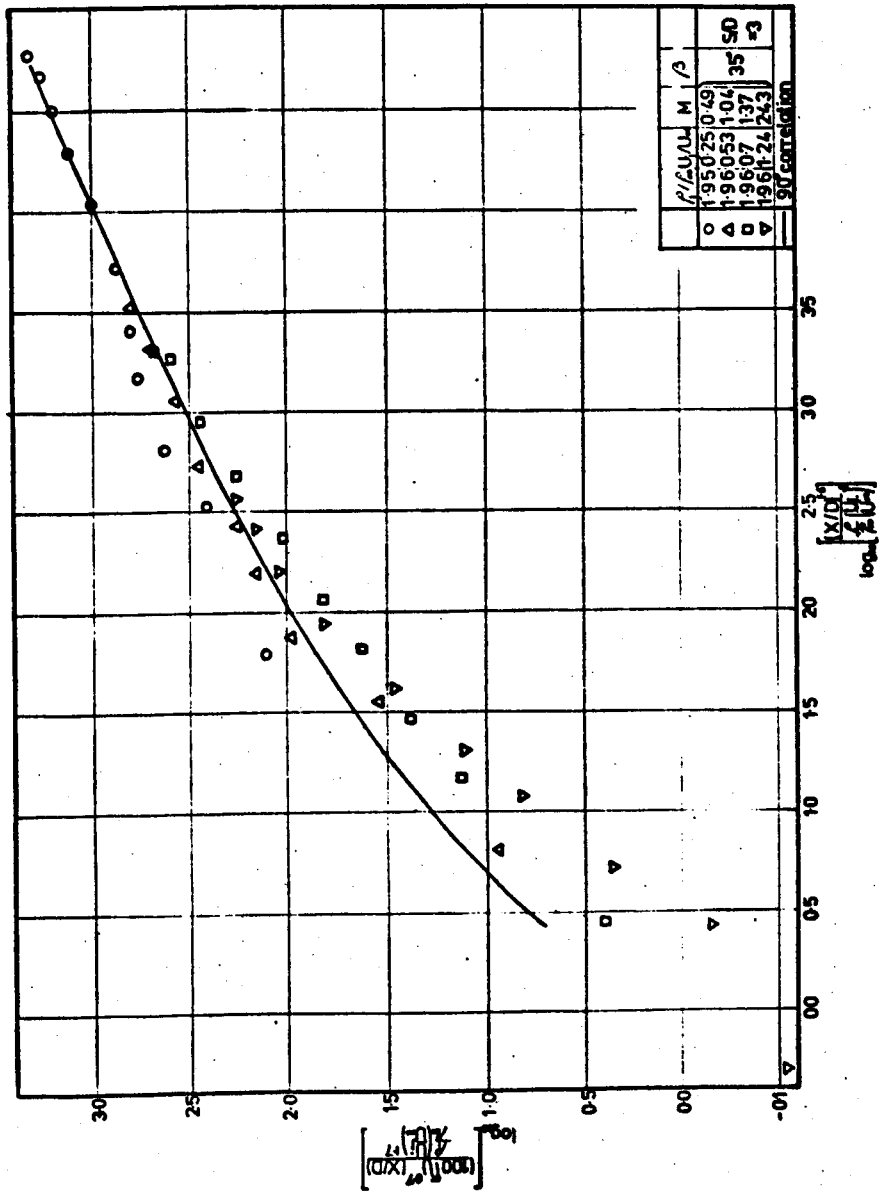


Fig. 9.13 Correlation applied to 35° injection angle

used which resulted in a correlation of the form:

$$\log_{10} \left[\frac{(100\eta)^{0.7} \frac{X}{D}}{\frac{\rho_j}{\rho_\infty} \left(\frac{U_j}{U_\infty} \right)^{1.7}} \right] + (\cos^2 \beta \exp (-0.05 X/D) 0.85 (M-0.82))$$

$$\text{vs } \log_{10} \left[\frac{\frac{X}{D}^{1.6}}{\frac{\rho_j}{\rho_\infty} \left(\frac{U_j}{U_\infty} \right)^3} \right]$$

The hole spacing terms were left out because data were only obtained for the angled injection at three diameter hole spacings, and for a nominal density ratio of 2. However, Afejuku, using the experimental apparatus and data reduction techniques developed by the author, has verified that the correlation does account for the differences in effectiveness produced by density ratio variation in angled injection cases.

Fig.9.14 shows that this correction reduced the scatter for both the 35° and 55° injection cases. However, when the results of Liess (9.8) and Goldstein et al (9.9) were compared using the correlation - figs.9.15a and 9.15b - although their results did not lie on the same mean line as the data from the present series of experiments, the correlation does still tend to collapse the data and the angle correction is of some benefit, especially for Liess's data.

The correlation clearly works better for normal injection, but can be applied with care to the angled cases.

9.6.4 Lateral Variation of Effectiveness

A cosine type formula of the form:-

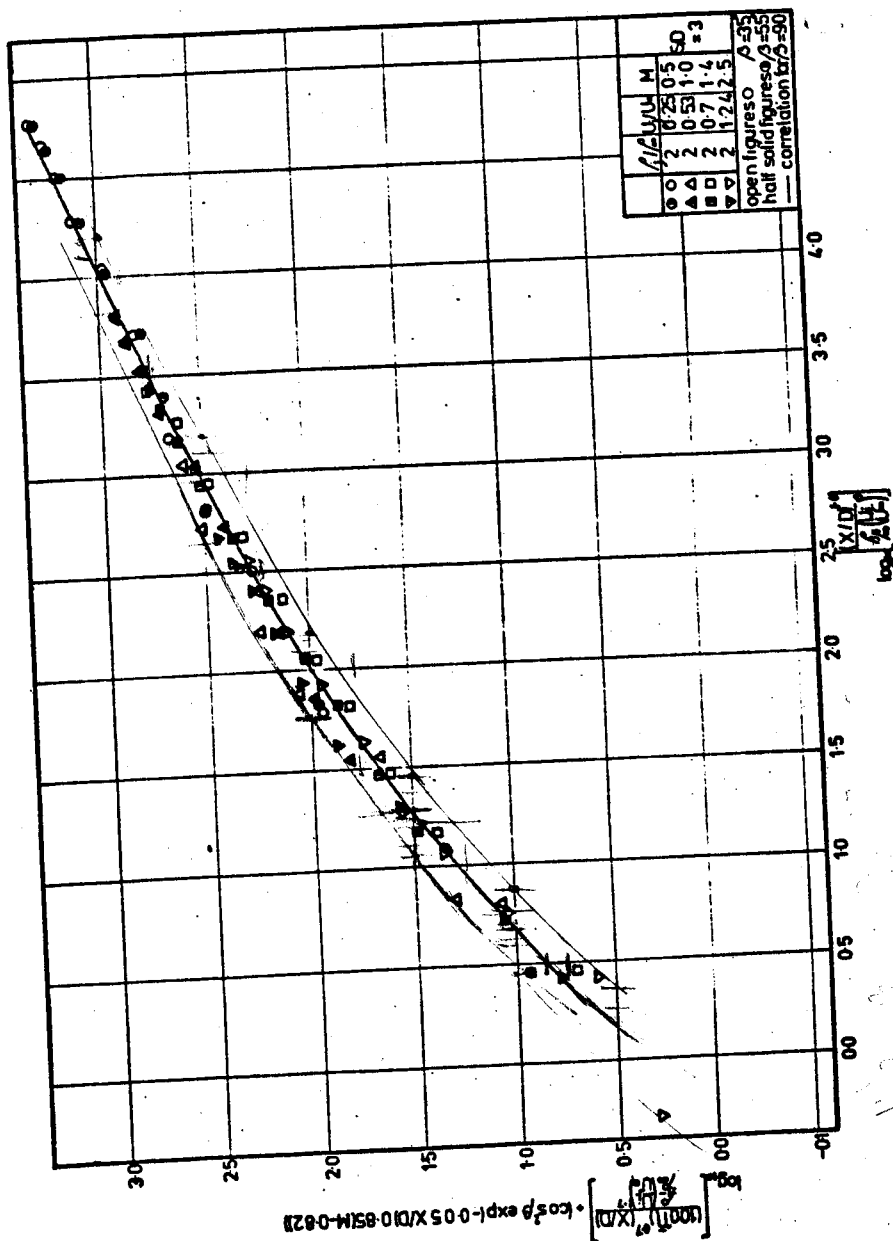


Fig. 9.14 Modified correlation for angled injection with $S/D = 3$

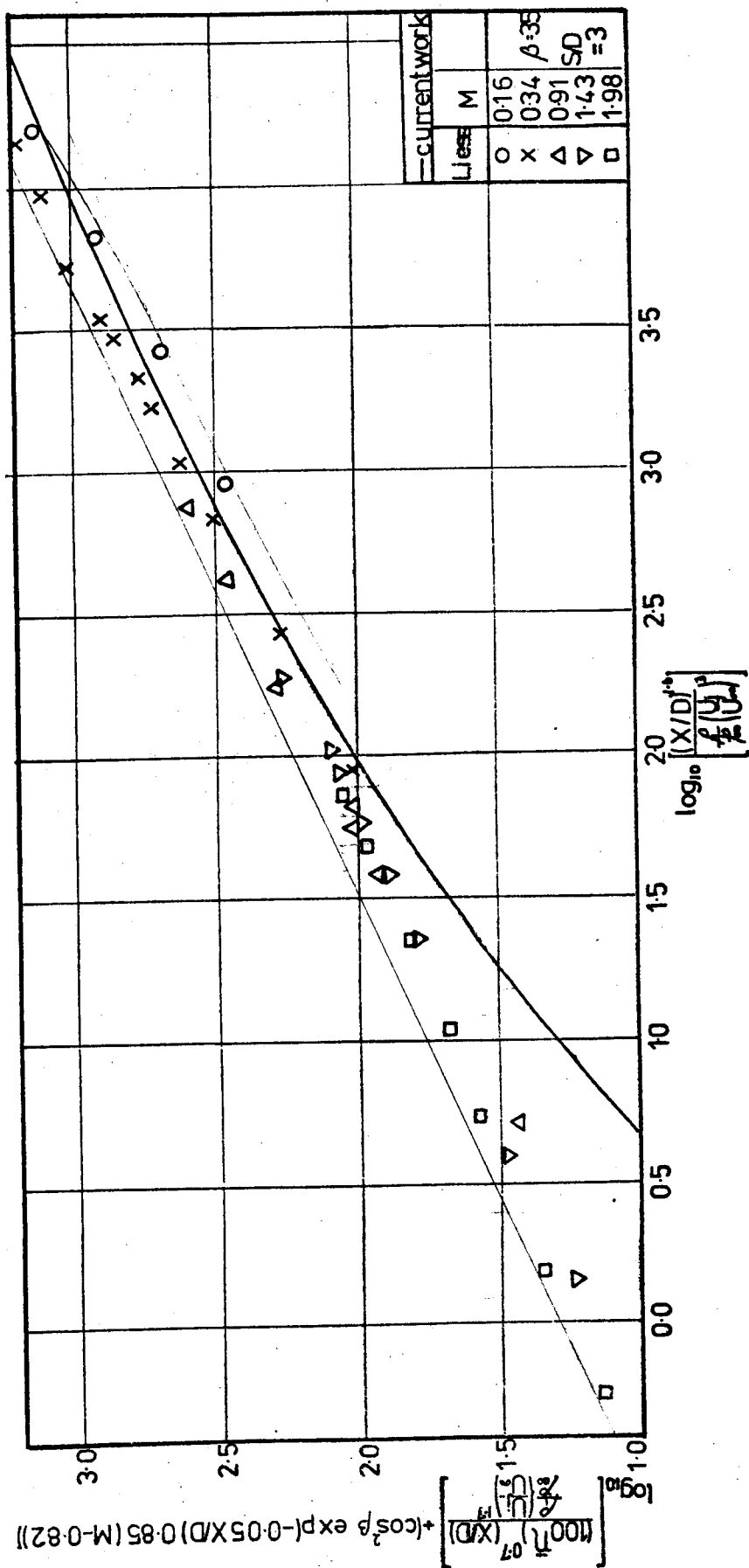


Fig. 8.16a Correlation for angled injection applied to the results of L'ess (9.8)

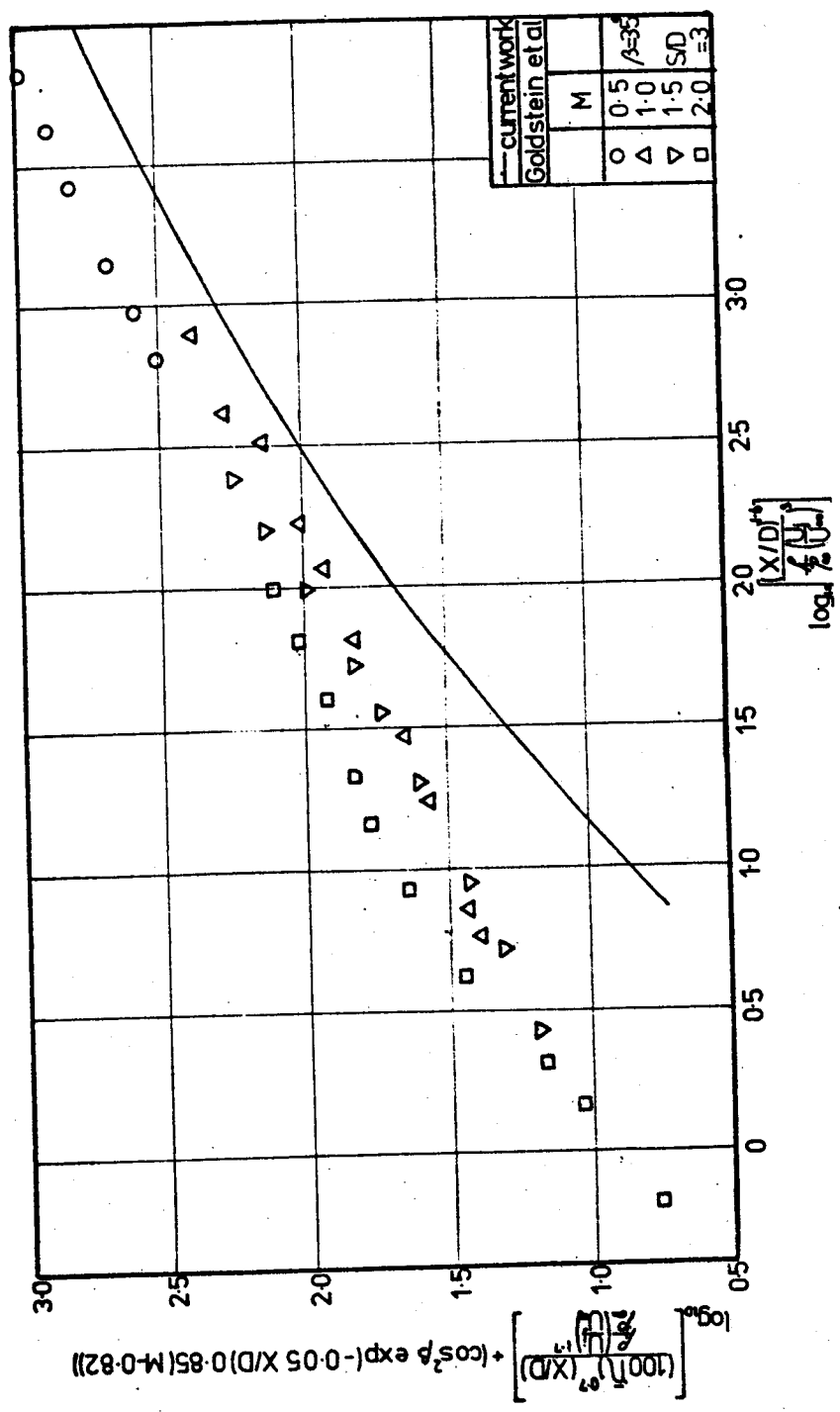


Fig. 9.15b Correlation for angled injection applied to the results of Goldstein et al (9.9)

$$\eta = \bar{\eta} + (\eta - \bar{\eta}) \left(\cos \left\{ \frac{Z}{S} \times 2\pi \right\} \right)$$

was found to approximate to the 90° injection lateral distribution of effectiveness as shown in fig.9.16a. Results are included in the figure where the difference between the minimum and the centreline effectiveness was greater than 10% of the centreline value.

The scatter is largely due to the small differences in effectiveness involved. A 0.05 error in the effectiveness gives rise to a change of up to 0.2 on the figure. When used to predict the distribution of effectiveness from centreline and span-wise averaged values, it gives a good indication of the effectiveness levels.

Fig.9.16b shows the same technique used on the 35° angled injection. In general, the results are not as good, but again a fair idea of the effectiveness levels can be obtained.

9.7 Limitations of the Models

In order to compare the basic models and correlations considered here, namely Kelly's modification to the bulk mixing model, Eriksen's model (9.3) and the correlation proposed here, it is useful to compare the ranges of parameters over which the different methods will predict the effectiveness to within 0.1 and 0.05 absolute effectiveness of the experimental results.

This is done in Table 9.1 which shows the new correlation to be an improvement on the bulk mixing model, in that it holds good for a greater range of hole spacings and blowing parameters, and also takes into account angles of injection. It is an improvement on Eriksen's method as it gives average values across a row of holes

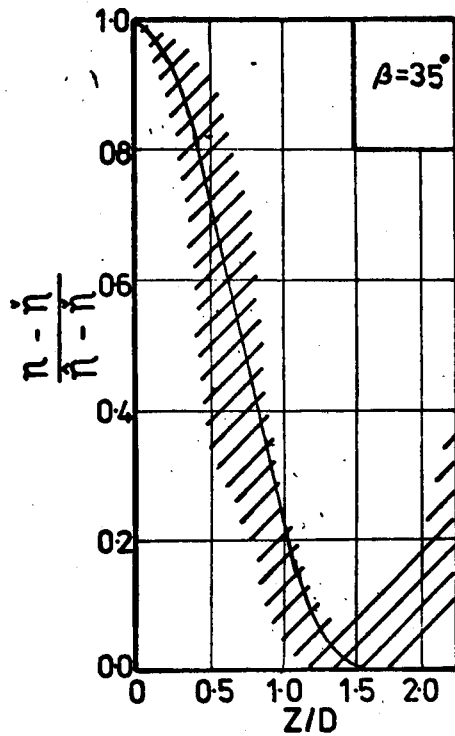
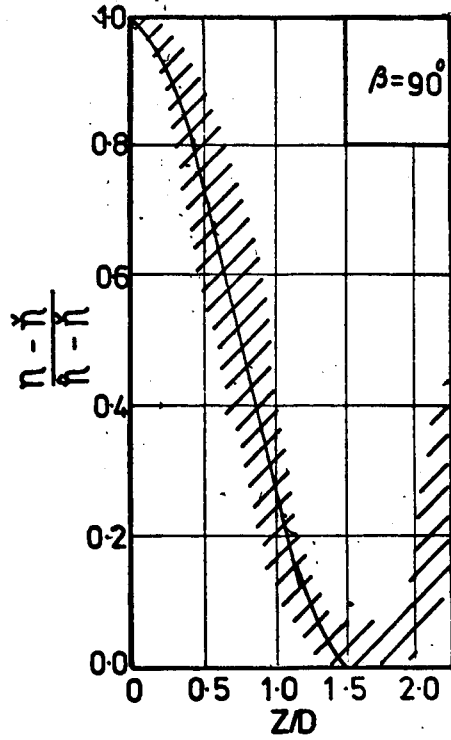


Fig.9.16 Comparison of the measured with the predicted lateral distribution of effectiveness

		<u>BULK MIXING MODEL</u>	<u>NOTTINGHAM</u>
<u>S/D</u>	<u>M</u>	<u>Range of X/D</u>	<u>Range of X/D</u>
1.25	0.5	45 < X/D < 110 (25 < X/D < 110)	5 < X/D < 110 (5 < X/D < 110)
	1.0	40 < X/D < 110 (10 < X/D < 110)	5 < X/D < 110 (5 < X/D < 110)
	1.4	75 < X/D < 110 (25 < X/D < 110)	5 < X/D < 110 (5 < X/D < 110)
	2.4	- -	5 < X/D < 30 (5 < X/D < 45)
2.5	0.5	50 < X/D < 110 (5 < X/D < 110)	5 < X/D < 110 (5 < X/D < 110)
	1.0	50 < X/D < 110 (20 < X/D < 110)	5 < X/D < 110 (5 < X/D < 110)
	1.4	30 < X/D < 110 (10 < X/D < 110)	5 < X/D < 110 (5 < X/D < 110)
	2.4	50 < X/D < 110 (25 < X/D < 110)	5 < X/D < 110 (5 < X/D < 110)
3.75	0.5	5 < X/D < 110 (5 < X/D < 110)	10 < X/D < 110 (5 < X/D < 110)
	1.0	5 < X/D < 110 (5 < X/D < 110)	5 < X/D < 110 (5 < X/D < 110)
	1.4	50 < X/D < 110 (20 < X/D < 110)	5 < X/D < 110 (5 < X/D < 110)
	2.4	80 < X/D < 110 (40 < X/D < 110)	30 < X/D < 110 (5 < X/D < 110)
5.0	0.5	5 < X/D < 110 (5 < X/D < 110)	10 < X/D < 110 (5 < X/D < 110)
	1.0	5 < X/D < 110 (5 < X/D < 110)	5 < X/D < 110 (5 < X/D < 110)
	1.4	50 < X/D < 110 (5 < X/D < 110)	5 < X/D < 110 (5 < X/D < 110)
	2.4	100 < X/D < 110 (40 < X/D < 110)	70 < X/D < 110 (40 < X/D < 110)

Note: 5 < X/D < 110 are the limits of the experimental data

TABLE 9.1 Ranges of downstream distance over which the models predict effectiveness to within 0.05 and 0.1 of the experimental results. (The 0.1 accuracy values are given in brackets)

<u>POINT SOURCE MODEL</u> (ref.9.3)		
<u>S/D</u>	<u>M</u>	<u>Range of X/D</u>
3	0.5	10 < X/D < 110 (5 < X/D < 110)
	1.0	16 < X/D < 110 (10 < X/D < 110)
	1.4	10 < X/D < 110 (10 < X/D < 110)
	2.4	10 < X/D < 20 (7 < X/D < 60)

Note: 5 < X/D < 110 are the limits of the
experimental data

TABLE 9.1 continued ...

and not just the centreline values; and, again, it can be used over a wider range of parameters.

It must be pointed out, though, that the bulk mixing model is a genuine, if imperfect, model - whereas the model of Eriksen et al and the present correlation either had input from the data or were based upon it. One might expect, therefore, the better agreement from these two methods. However, the table does show that the new correlation includes the change in shape of the curves as the blowing rate varies.

The real value of the new correlation is that if it can be shown to work on a wide range of data, then a set of data at engine conditions could be condensed on to a series of lines for different angles, or a single line if the angle correction were found to hold good. This would simplify the preliminary design of a turbine blade film cooling system, allowing the rapid comparison of different systems to be evaluated.

CHAPTER 10 : CONCLUSIONS

In this Chapter conclusions are drawn from the discussion of the previous chapters.

=====

10.1 Injectant to Mainstream Density Ratio

The density ratio is an important parameter, largely ignored to date, which must be reproduced in experimental tests unless a correlating parameter is used which fully takes it into account. Neither the blowing nor the momentum parameters were satisfactory in this respect over the full range of downstream distances (10.1).

10.2 Boundary Layer Displacement Thickness

A reduction in the boundary layer displacement thickness was found to increase the effectiveness downstream of a row of holes for approximately 20 diameters, but not due to a lowering of the jet centreline height; rather to a rise in the concentration of the injectant below the jet. The improvement was noticed for all geometries.

10.3 Pressure Gradients

The favourable pressure gradients which were produced over the injection holes were generally found to improve film cooling performance close to the holes, but they had a detrimental effect further downstream than about 20 diameters.

The jets were found to remain tighter in structure in the presence of a favourable pressure gradient, with less spreading in the lateral direction.

10.4 Hole Spacing

The conclusions drawn were that the best hole spacing configuration resulted from the smallest practical holes being placed as close as possible to one another. This not only gave the best overall coverage over the full range of downstream distances, but also prevented the occurrence of very low values of effectiveness between the holes, and high effectiveness gradients in a lateral direction.

10.5 Angle of Injection

Most of the preceding four conclusions were based on data obtained from a row of holes normal to the mainstream, but it would seem reasonable to assume that the same basic conclusions will apply to angled injection as well.

The effect of the angle of injection itself was found to be complex. In most situations the 35° case gave the best results providing the blowing rate was less than unity. If the blowing rate rose above this value, the normal injection was superior to the angled geometries. The normal injection was also judged the best geometry when the minimum effectiveness and lateral effectiveness gradients were considered.

Injection at any angle tended to increase the boundary layer displacement thickness far downstream of the injection

position at low blowing rates. The shallow angled geometries tended to decrease the boundary layer displacement thickness, whilst the 90° injection added to it substantially at large blowing rates.

10.6 Correlations & Theories

The immediate future on the theoretical side looks rather bleak. The two-dimensional, so-called "bulk mixing" models are of very limited value in the film cooling via holes situation. The three-dimensional heat sink model proposed by Eriksen et al (10.2) may be used, as they suggested, to interpolate between known results; or the proposed relationship for ϵ_p , the turbulent diffusivity, may be used. However, the latter is only for centreline values and the model is of dubious value away from the centreline.

The study of analytical solutions and models based on the co-axial jet mixing seems unlikely to work, but a full analytical approach, using a finite element or finite difference technique which does not make use of average properties across the jets, may eventually produce useful film cooling predictions.

The current work has shown that any model must, if it is to be successful, include the injection geometry (i.e. the hole spacing and injection angle) and that if the region close to the holes is of great interest, it must also include the boundary layer thickness upstream of the injection point. The pressure gradient effects were not so marked and could probably be ignored initially.

In the meantime, a correlation has been suggested for normal injection from a single row of holes, whereby plotting

$$\log_{10} \left[\frac{(100\bar{\eta})^{0.7} \frac{X}{D} \left(\frac{S}{D} \right)^{1.1}}{\frac{\rho_j}{\rho_\infty} \left(\frac{U_j}{U_\infty} \right)^{1.7}} \right] \text{ vs. } \log_{10} \left[\frac{(X/D)^{1.6} (0.01S/D + 0.25)}{\left(\frac{\rho_j}{\rho_\infty} \left(\frac{U_j}{U_\infty} \right)^3 \right)} \right]$$

collapses data at differing density ratios, velocity ratios and hole spacing onto a single line. The implication is that if a set of results can be taken at turbine operating conditions of mainstream Reynolds number, boundary layer thickness and pressure gradient, then the correlation can be used to predict results at other values of hole spacing, density ratio and velocity ratio.

The lateral distribution of the effectiveness was found to be approximated by :

$$\eta = \bar{\eta} + (\hat{\eta} - \bar{\eta}) \left(\cos \left\{ \frac{Z}{S} \times 2\pi \right\} \right)$$

10.7 The Applicability of the Current Work

It is difficult to assess with any certainty whether the results obtained during this research programme can be used directly in turbine blade cooling calculations.

The mainstream Reynolds number, based on the hole diameter, was approximately 4.5×10^3 at the injection position which is within the range found on a turbine blade, and although the pressure gradients employed were lower than in practice, the acceleration parameters, $\frac{\nu}{U_\infty^2} \frac{dU_\infty}{dx}$, were of the

right order. The velocity and density ratios used covered the ranges used in practice.

The boundary layer displacement thicknesses were rather large, with the minimum being 0.16 diameters compared with a typical value of 0.05 diameters; however, (as was shown by the traverses downstream of the injection holes), the effect of injecting into a boundary layer is generally to increase the boundary layer displacement thickness. This means that a second or third row of holes may see boundary layers of similar thickness to those used here. A low level of free-stream turbulence was used, but Launder and York (10.3) found that this was a relatively unimportant parameter.

Turning to the injection geometry, the ranges of the main parameters (the injection angle and hole spacing) which are encountered on a blade have been well covered. The injection holes, however, were considerably longer than on a blade, but Goldstein et al (10.4) found this to have neither a beneficial nor an adverse effect on the effectiveness. Finally, a flat surface was used rather than the curved surface of a typical blade: again, one would not expect this to produce any gross variation in effectiveness.

Most of the main parameters would appear to have been within the ranges encountered on a blade and perhaps the data may be used in its present form. Should this subsequently be proved wrong (perhaps by tests on a blade in situ), then the

present work will still be of value in comparing the different parameters.

10.8 Final Conclusion

Normal injection should be considered as a serious alternative to the more usual angled injection, if blade fatigue lives are to be extended; for, although it does not give the same high levels of effectiveness on the centreline, neither does it give the extremely low levels of effectiveness between the holes that are present with angled injection. Also, the holes should be as small and as close together as is practicable.

10.9 Recommendations for Further Work

The apparatus and experimental techniques developed at Nottingham lend themselves to detailed jet studies and density variation tests. The ease with which configurations can be altered also permits the study of different injection geometries. The experimental research here is to continue by studying the effect of density ratio on angled injection to verify the observations made for the 90° injection. Following this, the effect of one row of holes on another in a two row system is to be studied by varying the spacing between the rows.

Other work beyond the scope of the Nottingham apparatus includes the effects of curvature on film cooling.

Shaped holes seem to offer improvements, provided a simple and reliable manufacturing technique can be produced, and

further data to verify or otherwise the ideas on shaped holes presented here would be interesting.

The lateral injection, initially suggested by Goldstein et al (10.5), which showed promise ought to be investigated further in the context of a row of such holes, perhaps providing the basis for a two row system.

The effect of varying the hole spacing for angled injection could be investigated, as could the effect of the pressure gradients on the same geometry. There is also a possible need for work on stronger pressure gradients, perhaps only over a short downstream distance.

Finally, this work has not shown whether the Reynolds number based on the hole diameter is of great importance: work on this - using the same techniques as used here, to maintain the ratio of boundary layer displacement thickness to hole diameter over the injection position constant, with varying mainstream velocity and hole diameter - would be of value.

Further work using the apparatus described in this work will, in conjunction with the present work, increase the knowledge about film cooling and perhaps help to produce a further rise in gas turbine inlet temperatures and a more efficient jet engine.

====oooOooo=====

R E F E R E N C E S

Chapter 1

- 1.1 R.S. COLLADAY, "Importance of Combining Convection with Film Cooling", AIAA Paper 72-8, 1972.
- 1.2 F.J. BAYLEY, "Transpiration Cooled Turbines", Heat and Fluid Flow, Vol.2, No.1, 1972.

Chapter 2

- 2.1 R.J. GOLDSTEIN, "Film Cooling", Advances in Heat Transfer, Vol.7, 1971, pp.321-379, Academic Press, New York and London.
- 2.2 M.R. SMITH, "A Study of Film Cooling Effectiveness with Discrete Holes and Slots", Ph.D. Thesis, University of Oxford.
- 2.3 R.J. GOLDSTEIN, E.R.G. ECKERT, J.W. RAMSEY, "Film Cooling with Injection through Holes: Adiabatic Wall Temperatures downstream of a Circular Hole", J. of Engng. for Power, Oct.1968, pp.384-395.
- 2.4 R.J. GOLDSTEIN, E.R.G. ECKERT, V.L. ERIKSEN, J.W. RAMSEY, "Film Cooling following Injection through Inclined Circular Tubes", Israel J. of Technology, Vol.8, No.1-2, 1970, pp.145-154.
- 2.5 R.J. GOLDSTEIN, E.R.G. ECKERT, J.W. RAMSEY, "Film Cooling with Injection through a Circular Hole", NASA CR-54604, May 1968.
- 2.6 R.J. GOLDSTEIN, E.R.G. ECKERT, "Effects of Hole Geometry and Density on Three-Dimensional Film Cooling", Int.J. Heat and Mass Transfer, Vol.17, 1974, pp.595-607.
- 2.7 D.E. METZGER, H.J. CARPER, L.R. SWANK, "Heat Transfer with Film Cooling near Nontangential Injection Slots", J.of Engng. for Power, April 1968, pp.157-163.
- 2.8 D.E. METZGER, D.D. FLETCHER, "Surface Heat Transfer Immediately Downstream of Flush, Non-Tangential Injection Holes and Slots", AIAA Paper No.69 - 523, 1969.

- 2.9 D.E. METZGER, J.R. BIDDLE, J.M. WARREN, "Evaluation of Film Cooling Performance on Gas Turbine Surfaces". High Temperature Turbines, AGARD CP-73 -71, 1971, pp.24-1 - 24-7.
- 2.10 R.D. LANDER, R.W. FISH, "The External Heat Transfer Distribution on Film Cooled Turbine Vanes" AIAA Paper No.72-9, 1972.
- 2.11 C. LIESS, J. CARNEL, "Application of Film Cooling to Gas Turbine Blades", High Temperature Turbines, AGARD CP 73-71, 1971, pp.23-1 - 23-9.
- 2.12 C. LIESS, "Film Cooling with Ejection from a Row of Inclined Circular Holes - An Experimental Study for the Application to Gas Turbine Blades", Von Karman Institute Tech.Note 97, March 1973.
- 2.13 T.V. JONES, D.L. SCHULTZ, "Film Cooling Studies in Subsonic and Supersonic Flows using a Shock Tunnel", Proc.8th Int. Shock Tube Symp., 1971, pp.13/1 - 13/11.
- 2.14 J. NICOLAS, A. Le MEUR, "Curvature Effects on a Turbine Blade Cooling Film," ASME Paper 74 - GT - 156, Gas Turbine Conference and Products Show, March 30 - April 4, 1974, Zurich.
- 2.15 V.L. ERIKSEN, R.J. GOLDSTEIN, "Heat Transfer and Film Cooling following Injection through Inclined Circular Tubes", J. of Heat Transfer, May 1974, pp.239-245.
- 2.16 A.K. RASTOGI, J.H. WHITELAW, "The Effectiveness of Three-dimensional Film Cooling Slots - I. Measurements", Int.J. Heat and Mass Transfer, Vol. 16, pp.1665-1681, 1973.
- 2.17 P.V. Le BROCCQ, B.E. LAUNDER, C.H. PRIDDIN, "Discrete Hole Injection as a Means of Transpiration Cooling; an Experimental Study", Proc. Instn. Mech.Engrs, Vol.187 17/73, 1973.
- 2.18 B.E. LAUNDER, J.YORK, "Discrete Hole Cooling in the Presence of Free Stream Turbulence and Strong Favourable Pressure Gradient", Int.J. Heat and Mass Transfer, Vol.17, Nov.1974, pp. 1403-1409.
- 2.19 G.N. ABRAMOVICH, "The Theory of Turbulent Jets", Massachusetts Inst. of Technology Press, Cambridge, Mass, USA, pp.541-556, 1963.

- 2.20 S.S. PAPELL, "Effect on Gaseous Film Cooling of Coolant Injection through Angled Slots and Normal Holes", NASA TND - 299.
- 2.21 J.P. HARTNETT, R.C. BIRKEBAK, E.R.G. ECKERT, "Velocity Distributions, Temperature Distributions, Effectiveness and Heat Transfer in Cooling of a Surface with a Pressure Gradient", Int. Developments in Heat Transfer, Part IV ASME, New York, 1961, pp.682-689.
- 2.22 V. ZAKKAY, CHI R. WANG, M. MIYAZAWA, "Effect of Adverse Pressure Gradient on Film Cooling Effectiveness", AIAA Journal, Vol.12, No.5, pp. 708-710, 1974.
- 2.23 P.R. STERLAND, M.A. HOLLINGSWORTH, "An Experimental Study of Multiple Jets Directed Normally to a Cross-Flow", J.Mech.Engng.Science, Vol.17, No.3, 1975, pp.117-124.
- 2.24 D.E. METZGER, D.I. TAKEUCHI, P.A. KUENSTLER, "Effectiveness and Heat Transfer with Full-coverage Film Cooling", J. of Engng. for Power, July 1973, pp.180-184.
- 2.25 J.W. RAMSEY, R.J. GOLDSTEIN, "Interaction of a Heated Jet with a Deflecting Stream", J. of Heat Transfer, Nov.1971, pp.365-372.
- 2.26 S.V. PATANKAR, D.B. SPALDING: Imperial College, Heat Transfer Section Report, HTS/72/4, 1972.
- 2.27 J.C. KELLY, private communications, 1973.
- 2.28 V.L. ERIKSEN, E.R.G. ECKERT, R.J. GOLDSTEIN, "A Model for Analysis of the Temperature Field Downstream of a Heated Jet Injected into an Isothermal Cross-flow at an Angle of 90° ", NASA CP - 72 990.

Chapter 3

- 3.1 C. LIESS, "Film Cooling with Ejection from a Row of Inclined Circular Holes - An Experimental Study for the Application to Gas Turbine Blades", Von Karman Inst. Tech. Note 97, March 1973.
- 3.2 R.J. GOLDSTEIN, E.R.G. ECKERT, "Effects of Hole Geometry and Density on Three-Dimensional Film Cooling". Int.J. Heat and Mass Transfer, Vol.17 1974, pp.595-607.

- 3.3 R.J. GOLDSTEIN, "Film Cooling", Advances in Heat Transfer Vol. 7, 1971, pp.321-379, Academic Press, New York and London
- 3.4 D.B. SPALDING, "Some Fundamentals of Combustion", Gas Turbine Series, Vol.2, Butterworth, London
- 3.5 W. FORSTALL, A.H. SHAPIRO, "Momentum and Mass Transfer in Coaxial Jets", J.of Applied Mechanics, Dec. 1950, pp. 399-408.
- 3.6 J. NICOLAS, A. Le MEUR, "Curvature Effects on a Turbine Blade Cooling Film", ASME Paper 74 - GT - 156 Gas Turbine Conference and Products Show, March 30 - April 4, 1974, Zurich.
- 3.7 W.K. BURNS, J.L. STOLLERY, "The Influence of Foreign Gas Injection and Slot Geometry on Film Cooling Effectiveness", Int.J. Heat and Mass Transfer Vol.12, pp.935-951, 1969.
- 3.8 N.W. FOSTER, "Film Cooling of Gas Turbine Blades" B.Sc Thesis, University of Nottingham, 1970.
- 3.9 C.J. BAUGHAN, "Some Aspects of Film Cooling of Gas Turbine Blades", B.Sc. Thesis, University of Nottingham, 1971.
- 3.10 B.E. LAUNDER, J. YORK, "Discrete Hole Cooling in the Presence of Free Stream Turbulence and Strong Favourable Pressure Gradient", Int. J. Heat and Mass Transfer, Vol.17 Nov.1974, pp.1403-1409.

Chapter 4

- 4.1 R.C. PANKHURST, D.W. HOLDER, "Wind Tunnel Technique", Pitman, London, 1952.

Chapter 7

- 7.1 R.J. GOLDSTEIN, E.R.G. ECKERT, J.W. RAMSEY, "Film Cooling with Injection through a Circular Hole, NASA CP -54604, May 1968.
- 7.2 M.R. SMITH, "A Study of Film Cooling Effectiveness with Discrete Holes and Slots", Ph.D. Thesis, University of Oxford

- 7.3 C. LIESS, "Film Cooling with Ejection from a Row of Inclined Circular Holes - An Experimental Study for the Application to Gas Turbine Blades", Von Karman Inst., Tech.Note 97, March 1973.
- 7.4 R.J. GOLDSTEIN, E.R.G. ECKERT, "Effects of Hole Geometry and Density on Three-Dimensional Film Cooling", Int. J. Heat and Mass Transfer, Vol.17 1974, pp.595-607.
- 7.5 J.W. RAMSEY, R.J. GOLDSTEIN, "Interaction of a Heated Jet with a Deflecting Stream", J. of Heat Transfer, Nov.1971, pp.365-372.
- 7.6 G.N. ABRAMOVICH, "The Theory of Turbulent Jets", Massachusetts Inst. of Technology Press. Cambridge, Mass. USA, pp.541-556, 1963.
- 7.7 R.C. FOSTER, A. HAJI-SHEIKH, "An Experimental Investigation of Boundary Layer and Heat Transfer in the Region of Separated Flow Downstream of Normal Injection Slots", J. of Heat Transfer, May 1975, p.260.
- 7.8 B.R. PAI, J.H. WHITELAW, "The Influence of Density Gradients on the Effectiveness of Film Cooling". Imperial College of Science & Technology, Report C.P. No.1013, 1967.
- 7.9 D.E. METZGER, D.D. FLETCHER, "Surface Heat Transfer Immediately Downstream of Flush Non-Tangential Injection Holes and Slots", AIAA Paper No.69 - 523, 1969.
- 7.10 R.J. GOLDSTEIN, E.R.G. ECKERT, V.L. ERIKSEN, J.W. RAMSEY, "Film Cooling following Injection through Inclined Circular Tubes", Israel J. of Technology, Vol.8, No.1-2, 1970, pp.145-154.
- 7.11 A.K. RASTOGI, J.H. WHITELAW, "The Effectiveness of Three-Dimensional Film Cooling Slots - I. Measurements", Int.J. Heat and Mass Transfer, Vol.16 pp.1665-1681, 1973.

Chapter 8

- 8.1 R.C. FOSTER, "Experimental Study of Boundary Layer and Heat Transfer in the Region of Separated Flow Downstream of Normal Injection Slots", Ph.D Thesis, University of Texas at Arlington, 1973.

Chapter 9

- 9.1 J.L. STOLLERY, A.A.M. El-EHWANY, "A Note on the Use of a Boundary Layer Model for Correlating Film Cooling Data", Int.J. Heat and Mass Transfer Vol.8, 1965, pp.55-65.
- 9.2 M.R. SMITH, "A Study of Film Cooling Effectiveness with Discrete Holes and Slots", Ph.D. Thesis, University of Oxford.
- 9.3 V.L. ERIKSEN, E.R.G. ECKERT, R.J. GOLDSTEIN, "A Model for Analysis of the Temperature Field downstream of a Heated Jet Injected into an Isothermal Crossflow at an Angle of 90° ", NASA CR -72990.
- 9.4 R.J. GOLDSTEIN, E.R.G. ECKERT, "Effects of Hole Geometry and Density on Three-Dimensional Film Cooling", Int.J. Heat and Mass Transfer, Vol.17 1974, pp.595-607.
- 9.5 J.F. LOUIS, "Shock Tunnel Studies of Heat Transfer and Film Cooling Effectiveness", 10th Int. Shock Tube Symp., July 1975, Kyoto Univeristy.
- 9.6 W. FORSTALL, A.H. SHAPIRO, "Momentum and Mass Transfer in Coaxial Jets", J. of Applied Mechanics, Dec.1950, pp.399-408.
- 9.7 J.W. RAMSEY, R.J. GOLDSTEIN, "Interaction of a Heated Jet with a Deflecting Stream", J.of Heat Transfer Nov.1971, pp.365-372.
- 9.8 C. LIESS, "Film Cooling with Ejection from a Row of Inclined Circular Holes - An Experimental Study for the Application to Gas Turbine Blades", Von Karman Institute. Tech.Note 97, March 1973.
- 9.9 R.J. GOLDSTEIN, E.R.G. ECKERT, V.L. ERIKSEN, "Film Cooling following Injection through Inclined Circular Tubes", Israel J. of Technology, Vol.8, No.1-2 1970, pp.145-154.

Chapter 10

- 10.1 N.W. FOSTER, D. LAMPARD, "Effects of Density and Velocity Ratio on Discrete Hole Film Cooling", AIAA Journal, Vol.13 No.8, Aug.1975, pp.1112-1114.

- 10.2 V.L. ERIKSEN, E.R.G. ECKERT, R.J. GOLDSTEIN, "A Model for Analysis of the Temperature Field downstream of a Heated Jet Injected into an Isothermal Crossflow at an Angle of 90° " NASA CR-72 990.
- 10.3 B.E. LAUNDER, J. YORK, "Discrete Hole Cooling on the Presence of Free Stream Turbulence and Strong Favourable Pressure Gradient", Int.J. Heat and Mass Transfer, Vol.17, Nov.1974, pp.1403-1409.
- 10.4 R.J. GOLDSTEIN, E.R.G. ECKERT, "Effects of Hole Geometry and Density on Three-Dimensional Film Cooling" Int.J. Heat and Mass Transfer, Vol.17, 1974, pp.595-607.
- 10.5 R.J. GOLDSTEIN, E.R.G. ECKERT, V.L. ERIKSEN, J.W. RAMSEY, "Film Cooling following Injection through Inclined Circular Tubes", Israel J. of Tech. Vol.8, No.1-2, 1970, pp.145-154.

Appendix 2

- A2.1 BS1042 "Methods for the Measurement of Fluid Flow in Pipes" 1964.

Appendix 3

- A3.1 F.A. HOLLAND, R.M. MOORES, F.A. WATSON, J.K. WILKINSON, "Heat Transfer", Heineman, London.
- A3.2 A.K. RASTOGI, J.H. WHITELAW, "The Effectiveness of Three-Dimensional Film Cooling Slots - I. Measurements", Int.J. Heat and Mass Transfer, Vol.16 pp.1665-1681, 1973.
- A3.3 R.J. BAKER, B.E. LAUNDER, "The Turbulent Boundary Layer with Foreign Gas Injection - I. Measurements in Zero Pressure Gradient", Int.J. Heat and Mass Transfer, Vol.17, pp.275-291, 1974.

===oooOooo===

APPENDIX 1*The Two-Dimensionality of the Flow
and Repeatability of the Results*

Velocity traverses normal to the surface were carried out on the centreline and at 115 mm on either side of the centreline, level with the injection point. The resulting velocity profiles are reproduced in fig.A1.1. The three curves are almost identical, indicating that the flow is two-dimensional in nature.

Non two-dimensional flow effects would probably have been more noticeable close to the surface, where the higher levels of shear can lead to flow separation and flow reversals. Fig.A1.2 shows typical contours of effectiveness with the contours being symmetrical about the centreline and about a line between the holes, indicating again that the flow is basically two-dimensional.

As stated in the main text, difficulties were encountered with the 1.25 diameter hole spacing, as results taken downstream of holes other than the centreline hole were found to differ from the centreline values- in some instances within 15 diameters downstream. The details of these runs are to be found in Series 440 in Appendix 5. It can clearly be seen how the mainstream was being entrained from the side, lowering the effectiveness, and how this effect moved in towards the centreline as X/D increased.

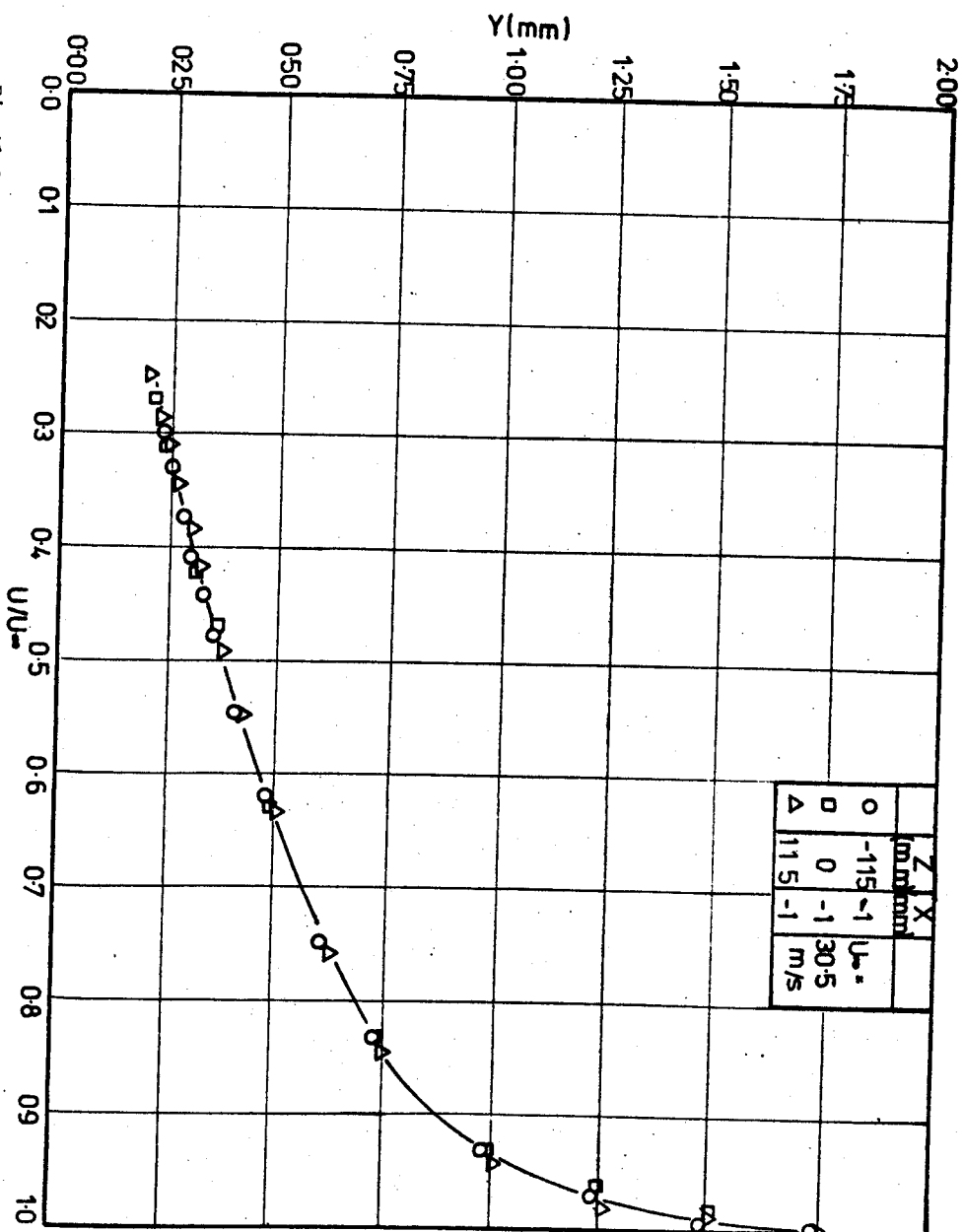


Fig. A1.1 Velocity profiles on, and either side of, the centreline without injection

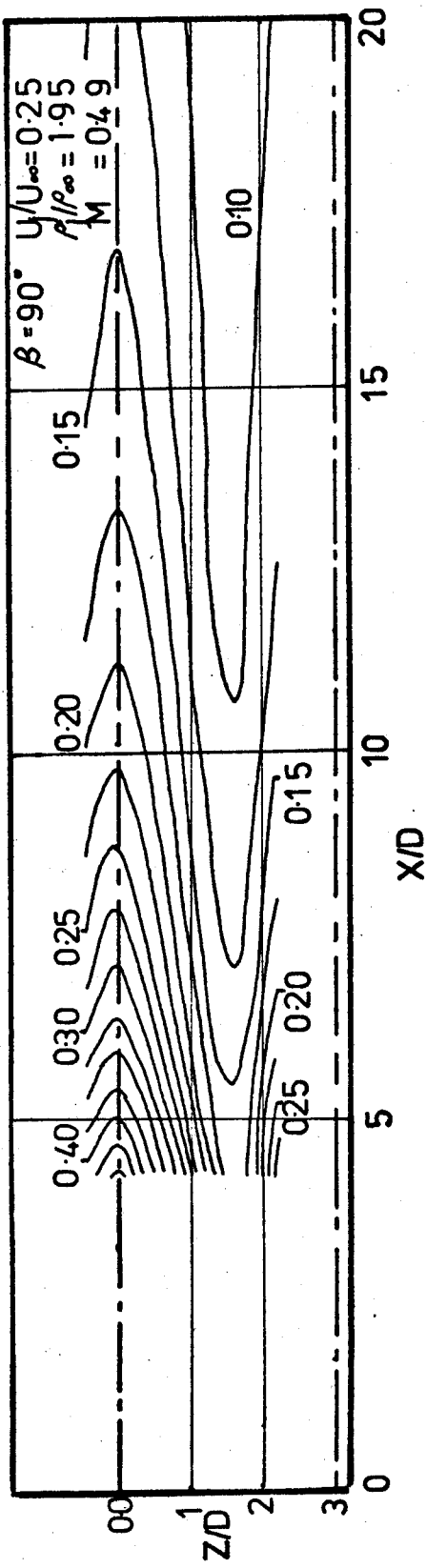


Fig.A1.2 Contours of constant effectiveness

The number of holes in the row was increased from 15 to 21 without much improvement, but when the sidewalls were included, they overcame the problem and the measurements were repeated (Series 520).

The three diameter hole spacing results were taken separately from the other hole spacings and the fact that they fit in so well to the general pattern does, as has already been stated, indicate that the results were repeatable.

The repeatability of the results was checked on several occasions, but the traverses above the surface provide the best example as they were usually taken several days after the main surface results. In general, there is good agreement between the surface measurements taken at the two different times and the effectivenesses rarely differed by more than 0.02.

There was some difference measured in effectiveness from one injection hole to another, but the same hole was always used for any particular injection plate as the centreline hole - thus eliminating this source of error, except in comparisons involving different injection plates. However, the difference in effectiveness from hole to hole was usually no more than 0.03. (See Runs 480, 483).

===ooo0ooo===

APPENDIX 2Calibration of Orifice Plates

The flow rates of Freon 12 and air were individually metered using orifice plates with corner taps. The orifice sizes were calculated using B.S.1042 (A2.1), but due to the low flow rates, it was not possible to meet the minimum recommended pipe dimensions. The pipe bore was 14mm - much less than the minimum 50mm; likewise, the orifices were smaller than the minimum of 6 mm.

As a result of this, the orifice plates had to be calibrated. This was done using a revolving drum type gas meter. The final results did not quite agree with the predicted values (fig.A2.1), the difference being about 8%.

Four orifice plates were made and calibrated, two for each line. They were changed depending upon the flow rate required.

===oooOooo===

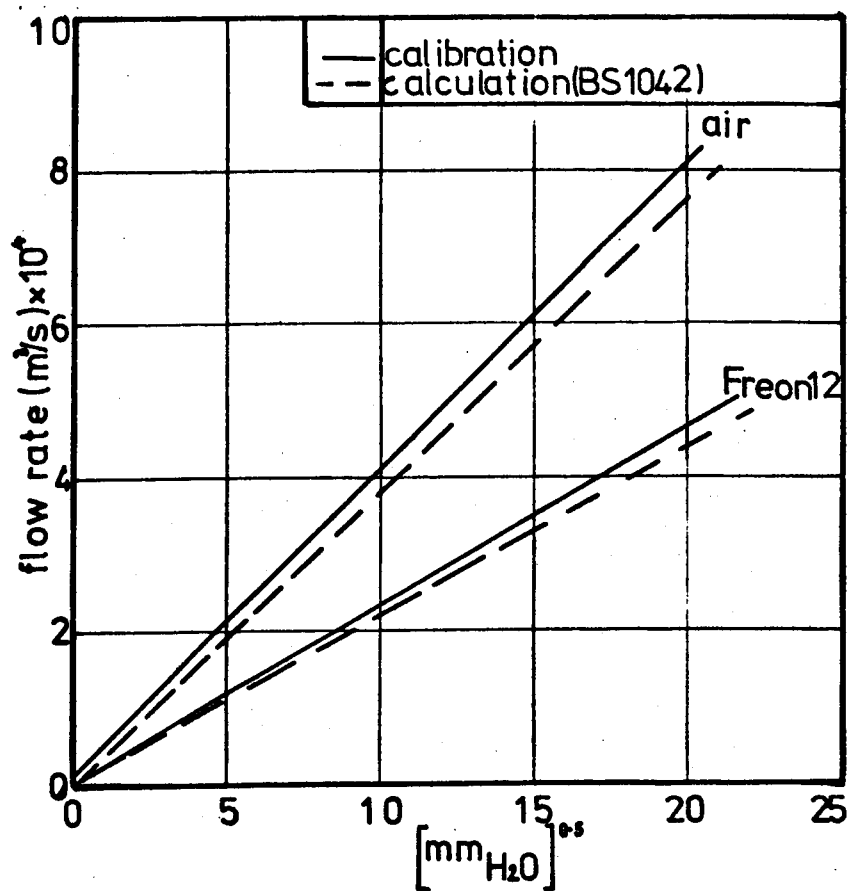


Fig.A2.1 Predicted and measured flow rates
through two of the orifice plates

APPENDIX 3

Calibration and Use of the Katharometer

The use of a single wire in the katharometer meant that it had to be calibrated every time it was used. To speed up the calibration, correlations between the indicated voltage and the properties of the mixtures (calculated as in Heat Transfer - A3.1) of the two gases were considered, assuming that the heat loss from the wire would approximate that from a horizontal cylinder.

Unfortunately this was not entirely successful, but a correlation was found whereby plotting:

$$\log_{10} \frac{\rho^2 C_p}{\mu k} \quad \text{vs} \quad \log V^2$$

gave a line with only slight curvature. Two straight lines were used to approximate to this curve, as shown in fig.A3.1. One line runs from 0% to 10% by volume of Freon 12 and the second from 10% to 100%. $\frac{\rho^2 C_p}{\mu k}$ comprises those values in a product of the Grashof and Prandtl numbers which vary with changing Freon 12 concentration.

Various methods were considered for making up the mixture of known composition to be used in the calibration, including partial pressures as used by Rastogi and Whitelaw (A3.2) and volume measurement using Orsat apparatus. However,

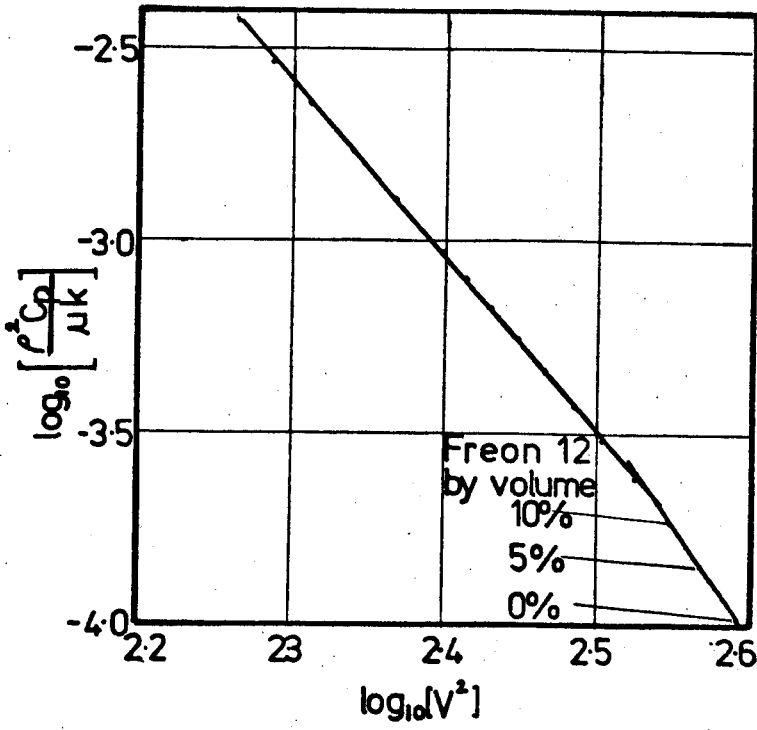


Fig.A3.1 Graph of $\log_{10} \frac{\rho^2 C_p}{\mu k}$ against $\log_{10} V^2$
for calibration of the catharometer

both methods were too slow and the Freon 12, being so dense, very rapidly started to separate out. Finally, a 50cc medical syringe was chosen. This gave the required resolution, was quick and easy to use and the small inlet ensured good turbulent mixing.

At the beginning and end of a series of tests, the syringe was used to make samples against which the katharometer was calibrated. Freon 12 concentrations of 0, 10 and 100% by volume were always used plus one other - usually 30%. From these values, the two straight lines could be calculated.

A polynomial expression was derived to relate $\log_{10} \frac{\rho^2 C_P}{\mu k}$ to the mass fraction of Freon 12, so that once the straight lines had been calculated from the calibration and values of $\log_{10} \frac{\rho^2 C_P}{\mu k}$ obtained, the mass fractions of Freon 12 and eventually the effectiveness could be calculated.

The calibration and effectiveness calculations were contained in a computer programme. The programme required inputs of the percentage by volume of Freon 12 in the calibration mixtures, the corresponding indicated voltages and the voltages measured during the tests. The output included the values of Freon 12 mass concentration and effectiveness. The voltages were measured to 0.01 volts which, in general, corresponded to 0.005 on the effectiveness with a density ratio of two.

The velocity of samples drawn through the base of the working section was very low; about 8×10^{-3} m/sec. Baker and Launder (A3.3) found that the effectiveness increased as they lowered the velocity in the sampling holes (sampling for Freon 12 in air) until the velocity in the tubes was down to approximately 1 m/s, which was 3% of the mainstream velocity. The sampling velocity in the current work was approximately 0.3% of the mainstream value and no variations in the measured values of effectiveness were observed with variation in sampling rate.

===ooo0ooo===

APPENDIX 4

Iso-Kinetic Sampling

Initially, it was hoped that samples taken above the plate could be drawn in through a probe at the correct flow rate for the katharometer, i.e. at a much lower velocity than the mainstream velocity. The assumption was that although the flow would spill around the tube, a sample would be taken from a streamline coincident with the centre of the orifice.

However, it was noticed during commissioning tests above the surface using an ordinary probe, that the value of injectant concentration varied with the rate of flow into the probe.

In an attempt to establish the reason for this, an experiment was carried out in which the tubes from the injectant supply manifold were disconnected from the injection plate and connected to a series of radial tubes leading into a pipe, fig.A4.1. The sampling probe was placed at the exit of this pipe and the concentration of Freon 12 in the flow was measured.

It was found that this measured value could not be made to change by varying the flow velocity through the probe, while keeping the flow through the katharometer constant by using the by-pass system described in Chapter 4.

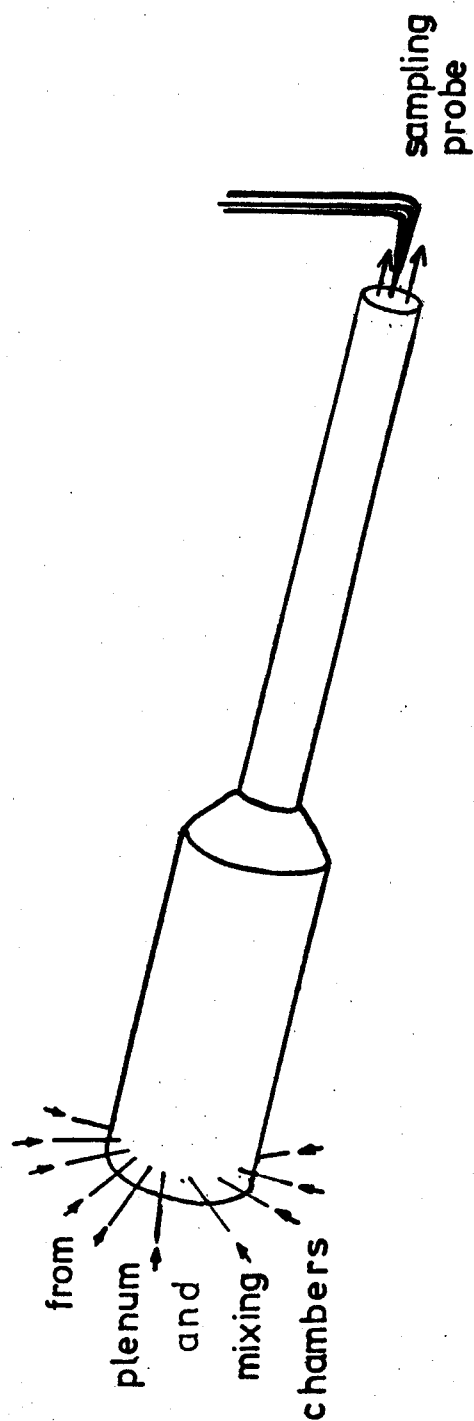


Fig.A4.1 Sketch of Iso-kinetic Testing Apparatus

The conclusion reached was that the flow out of the pipe was a homogeneous mixture, whilst the flow downstream of the row of holes would be far from homogeneous.

If the flow rate is less than iso-kinetic, then pockets of high density injectant (with higher momentum than the surrounding air) would tend to gain entrance to the probe, whilst the air is diverted around the outside. Conversely, if the flow rate is above the iso-kinetic rate, then air is drawn in from around the probe and the denser injectant carries straight on past. This is illustrated in fig.A4.2.

The hypothesis outlined above would mean that at lower flow rates a higher concentration of injectant would be found than at the higher flow rates; this was indeed the case.

Although the above could not be proved, it was decided to draw samples in at an iso-kinetic flow rate, so that the disturbance to the flow would be minimised. Description of the probe and methods used are included in Chapters 4 and 6.

===ooo0ooo===

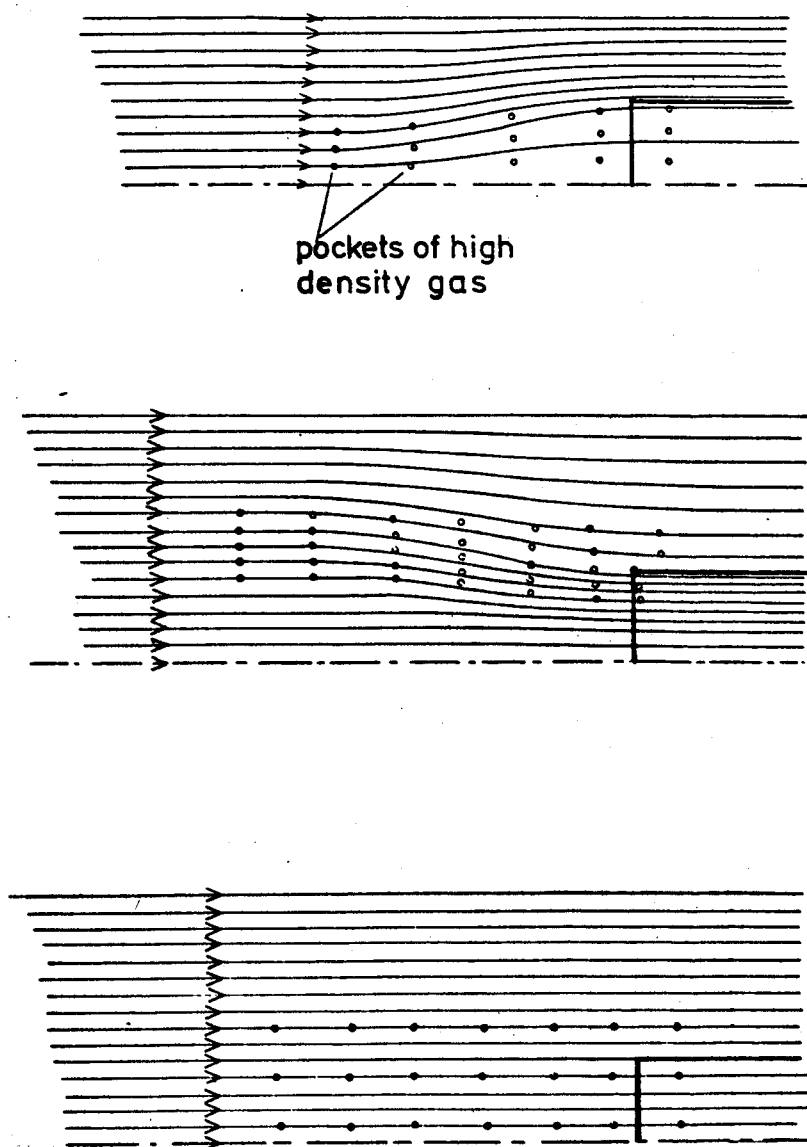


Fig.A4.2 Sketches showing possible effect of not sampling
iso-kinetically

APPENDIX 5

The Experimental Data

This Appendix contains the experimental data obtained during the experimental programme. The conditions for each series of tests are given in Table A5.1.

Table A5.2 gives the effectiveness expressed as a percentage for individual runs and the injectant concentrations for the traverses above the surface. Where velocity measurements were taken during the vertical traverses, these are also included.

The values of blowing rate, density ratio, mainstream and injectant velocities (which are in m/sec) are also given.

As experience grew in obtaining the results, some lateral positions were missed out far downstream, although for each downstream distance there are nearly always two or more values of effectiveness. This explains the blanks in some of the tables, e.g. Run 160.

===oooOooo===

RUN Nos.	δ^*/D	H	β Deg.	S/D	$\Delta p/X$ N/m ² /m	U_∞ m/sec	U_j/U_∞	ρ_j/ρ_∞	Above Plate
1-19	0.32	1.24	90	3	-2.47×10^3	30.5	0.25 - 1.48	1.5 - 4.26	
40-56	0.33	1.26	90	3	-3.24×10^1	30.5	0.25 - 1.48	1.5 - 4.26	
60-99	0.63	1.32	90	3	-9.96×10^1	30.5	0.25 - 1.48	1.5 - 4.26	
100-109	0.24	1.25	90	3	-4.13×10^1	30.5	0.25 - 1.24	2.0 - 3.0	✓
120-132	0.13	1.35	90	3	-9.84×10^3	25.9	0.25 - 1.48	1.5 - 4.26	
140-146	0.13	1.35	90	3	-9.84×10^3	25.9	0.20 - 1.24	2.0, 3.0	✓
160-167	0.16	2.43	90	3	-4.73×10^1	25.9	0.25 - 1.48	2.0	
180-184	0.16	2.43	90	3	-4.73×10^1	25.9	0.25 - 1.24	2.0	✓
200-207	0.27	1.58	90	3	$+8.47 \times 10^2$	25.9	0.25 - 1.48	2.0	
220-221	0.27	1.58	90	3	$+8.47 \times 10^2$	25.9	0.7, 1.24	2.0	✓
240-247	0.26	1.62	90	3	-3.71×10^1	25.9	0.25 - 1.48	2.0	
260-261	0.26	1.62	90	3	-3.71×10^1	25.9	0.7, 1.24	2.0	✓
280-283	0.26	1.62	35	3	-3.71×10^1	25.9	0.25 - 1.24	2.0	
300-301	0.26	1.62	35	3	-3.71×10^1	25.9	0.7, 1.24	2.0	✓
320-323	0.26	1.62	55	3	-3.71×10^1	25.9	0.25 - 1.24	2.0	
340-341	0.26	1.62	55	3	-3.71×10^1	25.9	0.7, 1.24	2.0	✓
360-363	0.16	2.40	55	3	-4.27×10^1	25.9	0.25 - 1.24	2.0	
380-381	0.16	2.40	55	3	-4.27×10^1	25.9	0.7, 1.24	2.0	✓
400-403	0.16	2.40	35	3	-4.27×10^1	25.9	0.25 - 1.24	2.0	
420-421	0.16	2.40	35	3	-4.27×10^1	25.9	0.7, 1.24	2.0	✓
440-443	0.16	2.40	90	1.25	-4.27×10^1	25.9	0.25 - 1.24	2.0	
460-463	0.16	2.40	90	2.50	-4.27×10^1	25.9	0.25 - 1.24	2.0	
480-483	0.16	2.40	90	3.75	-4.27×10^1	25.9	0.25 - 1.24	2.0	
500-503	0.16	2.40	90	5.00	-4.27×10^1	25.9	0.25 - 1.24	2.0	
520-523	0.16	2.40	90	1.25	-4.27×10^1	25.9	0.25 - 1.24	2.0	

BOUNDARY LAYER DISPLACEMENT THICKNESS (δ^*)

Notes: (i) $H = \frac{\text{BOUNDARY LAYER DISPLACEMENT THICKNESS } (\delta^*)}{\text{BOUNDARY LAYER MOMENTUM THICKNESS } (\theta)}$

(ii) In the final column, a ✓ indicates that measurements were taken via the probe above the test surface.

TABLE A5.1 Details of Main Test Parameters for each Series of Runs in Table A5.2

TABLE A5.2

Tables of effectiveness and injectant concentration (expressed as percentages) and velocity ratio: for the overall conditions outlined in Table 5.1.

RUN No.1

U_j	21.34	ρ_j/ρ_∞	1.46
U_∞	30.5	M	1.02

X/D	Z/D	-0.44	0.0	0.44	0.88	1.32	1.76	2.20
4.25		21.6	24.1	22.4	14.1			14.1
8.76		17.4	19.1	17.4	12.4	8.9	8.9	14.1
13.12		15.8	16.6	15.8	12.4	11.5	11.5	13.2
15.16		14.9	15.8	14.9	12.4	11.4	11.5	12.4
23.78		13.2	14.1	13.2	12.4	12.4	13.2	13.2
37.32		11.5	11.5	12.4	11.5	12.4	11.5	12.4
54.64		10.7	10.7	10.7	10.7	10.7	10.7	9.8
73.72		9.8	9.8	9.8	9.8	9.8	9.8	9.8
91.23		8.9	8.9	8.9	8.9	8.9	8.9	8.9
108.56		8.1	8.1	8.1	8.1	8.1	8.1	8.1

RUN No.3

U_j	16.15	ρ_j/ρ_∞	1.94
U_∞	30.5	M	1.03

X/D	Z/D	-0.44	0.0	0.44	0.88	1.32	1.76	2.20
4.25		30.1	33.3	30.1	23.0	11.9	11.9	23.5
8.76		23.0	24.9	22.5	18.5	14.5	15.0	18.5
13.12		19.5	20.5	19.1	16.5			
15.16		18.1	19.1	18.1	16.5	15.0	15.0	16.0
23.78		15.5	15.5	15.0	14.5	14.0	14.5	14.0
37.32		13.0	13.5	13.0	13.0	13.0	13.0	12.4
54.64		11.4	11.4	11.4	11.4	11.4	11.2	10.9
73.72		9.8	10.3	9.8	9.8	10.3	9.8	9.3
91.23		9.3	9.3	8.8	9.3	9.8	9.3	8.8
108.56		8.2	8.2	7.7	7.7	7.7	8.2	7.7

RUN No.2

U_j	21.34	ρ_j/ρ_∞	1.93
U_∞	30.5	M	1.35

X/D	Z/D	-0.44	0.0	0.44	0.88	1.32	1.76	2.20
4.25		23.9	25.9	23.9	18.3	8.6	8.6	17.2
8.76		19.3	21.3	18.8	15.6	12.4	12.4	16.1
13.12		17.7	18.8	17.2	16.1	15.1	14.5	16.1
15.16		17.2	18.3	16.7	16.1	15.1	15.1	16.1
23.78		15.6	16.7	15.6	15.6	15.6	15.1	15.6
37.32		14.5	14.5	14.0	14.5	14.0	14.0	14.5
54.64		12.9	12.9	12.9	13.5	12.9	12.4	12.9
73.72		11.9	11.9	11.3	11.9	11.9	11.3	11.9
91.23		11.3	10.8	10.8	11.3	10.8	10.8	11.3
108.56		9.7	9.7	9.7	9.7	9.7	9.7	10.2

RUN No.4

U_j	27.13	ρ_j/ρ_∞	1.93
U_∞	30.5	M	1.71

X/D	Z/D	-0.44	0.0	0.44	0.88	1.32	1.76	2.20
4.25		16.9	18.8	17.3	11.8			10.7
8.76		15.9	16.3	14.8	11.8	9.7	10.2	12.3
13.12		15.9	15.9	14.8	13.8	12.8	13.3	13.8
15.16		15.9	15.9	15.9	13.8	13.8	13.8	14.3
23.78		15.9	15.9	15.9	15.3	15.3	15.3	15.3
37.32		15.3	15.3	14.8	14.8	14.8	14.8	14.8
54.64		14.3	14.3	14.3	13.8	13.8	13.8	13.8
73.72		13.3	13.3	13.3	12.8	12.8	12.8	12.8
91.23		12.8	12.8	12.8	12.3	12.3	12.3	12.3
108.56		11.3	11.3	11.3	10.7	10.7	10.7	10.7

RUN · No. 5

U_j	21.34	ρ_j/ρ_∞	1.95
U_∞	36.15	M	1.15

X/D	Z/D	-0.44	0.0	0.44	0.88	1.32	1.76	2.20
4.25	27.9	30.2	27.4	19.6	9.3	11.4	21.1	
8.76	21.6	23.1	20.6	16.6	13.5	14.0	18.1	
10.86	20.6	21.1	19.1	16.1	14.0	15.1	16.1	
15.16	18.1	18.6	17.6	16.1	15.1	15.5	16.6	
23.78	15.5	15.5	15.5	15.1	15.1	15.1	15.1	
37.32	13.5	13.5	13.5	13.5	13.5	13.5	13.5	
54.64	12.0	12.0	12.0	12.0	12.0	12.0	12.0	
73.72	10.3	10.3	10.3	10.3	10.3	10.3	10.3	
91.23	9.9	9.9	9.9	9.9	9.9	9.9	9.9	
108.56	8.8	8.8	8.8	8.8	8.8	8.8	8.8	

RUN No. 6

U_j	21.34	ρ_j/ρ_∞	1.95
U_∞	24.08	M	1.72

[illegible]

RUN No. 7

U_i	21.34	ρ_i/ρ_∞	1.95
U_∞	20.12	M	2.06

[illegible]

RUN No. 8

U_j	21.34	ρ_j/ρ_∞	1.93
U_∞	17.19	M	2.39

[illegible]

RUN No.13

U_j	37.8	ρ_j/ρ_∞	1.95
U_∞	30.5	M	2.41

Z/D X/D	-0.44	0.0	0.44	0.88
4.25	9.7	10.7	9.7	7.6
8.76	13.3	12.8	11.8	11.3
10.86	14.3	13.8	13.3	13.3
15.16	16.8	16.3	15.8	15.8
23.78	17.3	17.3	16.8	16.8
37.32	17.3	16.3	16.8	16.3
54.64	16.3	16.3	15.8	16.3
73.72	15.8	15.3	15.3	15.8
91.23	14.8	14.3	14.3	15.3
108.56	12.8	12.3	13.3	12.8

RUN No.14

U_j	21.34	ρ_j/ρ_∞	2.99
U_∞	30.5	M	2.09

Z/D X/D	-0.44	0.0	0.44	0.88	1.32	1.76	2.20
4.25	23.9	26.6	25.2	20.8	12.7	10.5	15.7
8.76	21.8	22.9	21.5	20.0	17.9	17.9	18.6
10.86	21.8	22.2	21.5	20.4	19.3	19.0	21.1
15.16	21.1	21.8	21.1	21.1	20.4	20.8	20.4
23.78	20.4	20.8	20.4	20.4	20.0	20.0	20.4
37.32	19.0	19.0	18.6	19.0	18.6	19.0	19.0
54.64	17.2	17.2	16.8	16.8	16.4	17.2	17.2
73.72	15.4	15.4	15.4	15.4	15.4	15.4	15.7
91.23	14.3	14.3	14.3	14.3	14.3	14.3	14.6
108.56	12.7	12.7	12.4	12.7	12.7	12.7	12.7

RUN No.15

U_j	21.34	ρ_j/ρ_∞	3.50
U_∞	30.5	M	2.45

Z/D X/D	-0.44	0.0	0.44	0.88	1.32	1.76	2.20
4.25	22.0	24.2	22.9	18.9	12.2	10.2	15.3
8.76	21.0	22.0	20.7	19.5	18.5	17.9	18.9
10.86	21.4	21.7	20.7	20.4	19.8	19.5	20.1
15.16	21.7	21.7	21.4	21.1	20.7	20.7	20.7
23.78	21.1	21.1	21.1	21.1	20.7	20.7	21.1
37.32	19.2	19.5	19.5	19.5	19.5	19.5	19.8
54.64	17.2	17.6	17.6	17.6	17.6	17.6	17.9
73.72	15.6	15.9	15.9	15.9	16.3	16.3	16.3
91.23	14.6	14.9	14.9	14.9	15.3	15.3	15.3
108.56	12.6	12.9	12.9	13.3	13.3	13.6	13.6

RUN No.16

U_j	21.34	ρ_j/ρ_∞	4.17
U_∞	30.5	M	2.9

Z/D X/D	0.0
4.25	23.2
8.76	22.9
10.86	24.1
15.16	24.7
23.78	24.7
37.32	23.2
54.64	21.7
73.72	19.9
91.23	18.3
108.56	16.5

RUN No.17

U_j	11.43	ρ_j/ρ_∞	1.97
U_∞	30.5	M	0.74

X/D	Z/D	-0.44	0.0	0.44	0.88	1.32	1.76	2.20
4.25		36.9	39.2	34.0	25.7	10.9	15.8	27.2
8.76		25.2	23.7	12.9	14.7	15.3	19.5	
10.86		22.6	23.1	20.6	17.4	13.7	15.3	18.4
15.16		17.9	19.0	17.9	15.8	13.7	14.2	15.8
23.78		14.2	14.7	14.2	13.1	12.6	12.6	12.6
37.32		10.9	10.9	10.9	10.9	10.9	10.9	10.9
54.64		8.7	9.2	9.2	9.2	9.2	9.2	9.2
73.72		7.5	8.1	8.1	8.1	8.1	8.1	8.1
91.23		7.0	7.5	7.5	7.5	7.5	7.5	7.5
108.56		6.4	7.0	6.4	6.4	6.4	6.4	7.0

RUN No.18

U_j	7.62	ρ_j/ρ_∞	1.94
U_∞	30.5	M	0.49

X/D	Z/D	-0.44	0.0	0.44	0.88	1.32	1.76
4.25		38.1	39.5	33.4	23.5	8.67	15.2
8.76		24.6	25.5	22.0	17.3	12.5	14.6
10.86		21.5	22.0	18.9	15.2	11.9	14.1
15.16		16.8	17.3	12.5	13.6	11.4	11.4
23.78		12.5	13.0	11.9	10.9	10.3	10.3
37.32		9.7	9.2	9.2	8.6	8.1	8.1
54.64		7.5	7.5	7.0	8.1	8.1	7.0
73.72		6.4	6.4	6.4	6.4	6.4	5.8
91.23		5.8	5.8	5.8	5.8	5.8	5.2
108.56		5.2	5.2	5.2	5.2	5.2	4.8

RUN No.19

U_j	21.34	ρ_j/ρ_∞	1.97
U_∞	30.5	M	1.38

X/D	Z/D	0.0
4.25		26.4
8.76		21.2
10.86		19.7
15.16		17.8
23.78		15.8
37.32		14.2
54.64		12.8
73.72		11.2
91.23		10.7
108.56		9.7

RUN No.40

U_j	21.34	ρ_j/ρ_∞	1.98
U_∞	30.5	M	1.38

X/D	Z/D	-0.44	0.0	0.44	0.88	1.32	1.76	2.20
1.5		29.4						
4.25		22.2	24.1	22.7	16.7	9.9	9.9	16.7
6.53		19.7	21.7	20.2	17.2	13.6	13.1	15.6
10.86		18.2	19.2	18.7	16.7	16.1	16.1	17.2
15.16		17.2	17.7	17.7	17.2	17.2	17.2	17.2
23.78		16.7	17.2	16.7	16.7			16.7
37.32		15.6	15.6	15.6	15.6			15.6
54.64		14.1						14.6
73.72		13.1	13.1					13.6
91.23		12.5		12.5				13.1
108.56		12.0			12.0			12.0

RUN No.41

U_j	21.34	ρ_j/ρ_∞	2.50
U_∞	30.5	M	1.75

X/D	Z/D	-0.44	0.0	0.44	0.88	1.32	1.76	2.20
1.5		29.1						
4.25		22.3	24.2	22.3	17.6	11.4	11.8	16.7
6.53		19.9	21.5	20.3	17.6	14.7	15.1	17.2
10.86		19.6	19.9	19.6	18.4	18.4	18.4	18.7
15.16		19.9	19.6	19.2	19.2	19.2	19.2	19.2
23.78		18.7	19.2	18.7	18.7			18.7
37.32		17.6	17.6	17.6				17.6
54.64		15.9	16.3	16.3				16.7
73.72		14.7	15.1	15.1			15.1	15.5
91.23		14.3	13.9					14.3
108.56		13.5	12.7	13.5				13.9

RUN No.42

U_j	21.34	ρ_j/ρ_∞	1.99
U_∞	30.5	M	1.39

X/D	Z/D	0.0
1.5		31.2
4.25		23.9
6.53		21.0
10.86		17.4
15.16		17.4
23.78		16.9
37.32		15.9
54.64		13.2
73.72		13.2
91.23		12.7
108.56		11.7

RUN No.43

U_j	21.34	ρ_j/ρ_∞	2.54
U_∞	30.5	M	1.78

X/D	Z/D	0.0
1.5		31.3
4.25		24.0
6.53		21.3
10.86		18.4
15.16		19.7
23.78		19.3
37.32		18.0
54.64		15.5
73.72		15.5
91.23		14.7
108.56		13.4

RUN No. 44

U_j	27.13	ρ_j/ρ_∞	1.96
U_∞	30.5	M	1.74

RUN No. 45

U_j	21.34	ρ_j/ρ_∞	1.92
U_∞	30.5	M	1.37

X/D	Z/D	-0.44	0.0	0.44	0.88	1.32	1.76	2.20
1.5			20.6					
4.25		15.4	18.0	16.5	12.8	6.8	6.3	10.6
6.53		15.4	17.0	15.9	13.9	11.7	11.2	12.3
10.86		16.5	17.0	16.5	15.9	15.4	15.4	15.4
15.16		17.0	17.5	17.5	17.5	17.5	17.0	17.0
23.78		17.5	17.5	17.5	17.5		17.5	17.5
37.32		17.0	17.5	17.5			17.0	17.0
54.64		15.9	16.5	16.5	16.5			16.5
73.72			15.4			15.4		16.5
91.23			14.4	14.4			14.9	14.4
108.56			13.9					13.9

X/D.	Z/D	-0.44	0.0	0.44	0.88	1.32	1.76	2.20
1.5			30.5					
4.25		22.5	23.5	22.0	16.3	8.1	10.8	17.3
6.53		19.4	21.0	20.4	16.3	14.1	14.1	16.3
10.86		16.2	17.3	16.8	15.7	14.6	15.2	15.7
15.16		16.8	17.3	17.8	17.3	16.8	16.8	17.3
23.78		16.8	16.8	17.3	16.8	16.8	16.8	16.8
37.32		15.7	16.3	15.7	15.7	15.7	15.7	15.7
54.64		13.0	13.6		13.6			13.6
73.72		13.0	13.6					13.0
91.23		12.5	13.0					12.5
108.56		10.8	11.8					11.4

RUN No. 46

U_j	27.13	ρ_j/ρ_∞	1.96
U_∞	30.5	M	1.37

RUN No. 47

U_i	21.34	ρ_i/ρ_∞	1.48
U_∞	30.5	M	1.03

x/d	z/d	0.0
1.5		22.0
4.25		17.3
6.53		16.3
10.86		15.2
15.16		17.3
23.78		17.8
37.32		17.3
54.64		15.2
73.72		15.2
91.23		14.1
108.56		12.5

X/D	Z/D	-0.44	0.0	0.44	0.88	1.32	1.76	2.20
1.5			24.7					
4.25		19.2	21.6	20.0	14.3	7.7	8.6	15.2
6.53		17.6	20.0	18.4	14.3	10.2	10.2	13.5
10.86		15.2	16.8	16.0	13.5	12.7	12.7	14.3
15.16		14.3	15.2	15.2	14.3	14.3	13.5	14.3
23.78		13.5	13.5	14.3	14.3	14.3	14.3	13.5
37.32			12.7	13.5	12.7	13.5	13.5	12.7
54.64			11.9					11.9
73.72			11.1	11.1				11.1
91.23			10.2		11.1			11.1
108.56			9.4			10.2		10.2

RUN No. 48

RUN No.48		U_j 16.15		ρ_j/ρ_∞ 1.99				
		U_∞ 30.5		M 1.06				
X/D	Z/D	-0.44	0.0	0.44	0.88	1.32	1.76	2.20
1.5			39.6					
4.25		28.7	31.5	29.2	22.0	14.0	12.9	23.0
6.53		24.4	26.8	24.9	21.0	16.0	16.0	20.5
10.86		20.5	21.5	20.5	18.5	17.0	17.0	18.5
15.16		18.1	19.0	18.5	17.5	16.5	16.5	17.0
23.78		16.0	16.5	16.5	16.0	16.0	16.0	16.0
37.32		14.0	14.5	14.5	14.5	14.5	14.5	
54.64			12.9	12.9			12.9	
73.72			11.9		11.4		11.9	
91.23			10.9			10.9	10.9	
108.56			10.3				10.3	

RUN No. 49

RUN No.49									
		Z/D		U _j		ρ /ρ _∞		1.94	
				U _∞		M		0.49	
X/D	Z/D	-0.44	0.0	0.44	0.88	1.32	1.76	2.20	
1.5			59.3						
4.25		35.8	37.6	32.1	24.4	10.6	14.3	27.8	
6.53		27.3	29.3	25.9	19.9	13.2	14.3	21.4	
10.86		19.9	20.9	18.4	15.8	13.2	14.3	16.9	
15.16		15.8	16.9	15.5	14.3	12.7	12.1	13.7	
23.78		12.1	12.7	12.1	11.6	11.1	11.1	11.6	
37.32		10.0	10.0		9.5	9.5		9.5	
54.64			8.4	8.4				8.4	
73.72			7.3		7.3			7.3	
91.23			6.7			6.7		6.7	
108.56			6.2				6.2	6.2	

RUN No. 50

RUN No.50		U _j 11.43		F _j /ρ _∞ 1.96				
		U _∞ 30.5		M 0.73				
X/D	Z/D	-0.44	0.0	0.44	0.88	1.32	1.76	2.20
1.5			43.3					
4.25		31.3	33.6	30.0	22.2	11.5	14.1	25.1
6.53		25.6	28.0	25.1	19.2	14.6	15.6	21.2
10.86		20.2	21.1	20.7	16.6	14.6	15.6	17.7
15.16		16.6	17.7	16.6	15.1	14.1	14.1	15.6
23.78		13.5	14.6	14.1	13.5	13.1	13.1	13.5
37.32		11.5	12.0	12.0	11.5	11.5	11.5	12.0
54.64		9.9	10.4	10.4				10.4
73.72		9.3	9.3		9.3			9.3
91.23		8.8	8.8			8.8		8.8
108.56		8.3	8.3		8.3			8.3

RUN No. 51

RUN No. 51		U_j 21.34		ρ_j/ρ_∞ 3.03				
		U_∞ 30.5		M 2.12				
x/D	z/D	-0.44	0.0	0.44	0.88	1.32	1.76	2.20
1.5			28.8					
4.25		22.3	24.0	22.0	18.3	12.2	11.9	16.5
6.53		20.6	21.7	20.3	18.6	16.5	16.1	17.5
10.86		21.3	21.3	20.6	20.0	19.6	19.6	20.0
15.16		21.7	21.3	21.0	20.6	20.6	20.6	20.6
23.78		21.3	21.0	20.6	20.6		20.3	20.6
37.32		20.0	20.0					19.6
54.64		18.6	18.6	17.9				18.3
73.72		17.2			16.9			16.9
91.23		16.1				15.8		15.8
108.56		15.1				15.1		15.1

RUN No.52

U_j	21.34	ρ_j/ρ_∞	3.6
U_∞	30.5	M	2.50

X/D	Z/D	-0.44	0.0	0.44	0.88	1.32	1.76	2.20
1.5		27.3						
4.25		20.6	22.5	21.3	18.1	13.2	11.8	15.5
6.53		20.6	21.6	20.3	19.0	18.1	17.5	17.8
10.86		22.2	22.2	21.9	21.6	21.2	21.2	21.2
15.16		23.1	23.1	22.8	22.8	22.8	22.5	22.5
23.78		23.4	22.8	22.8				
37.32		21.6	21.6					
54.64		20.0	20.0	20.3				
73.72		18.7		19.0				
91.23		17.8			17.8			
108.56		16.8				16.8	16.8	

RUN No.53

U_j	21.34	ρ_j/ρ_∞	4.22
U_∞	30.5	M	2.95

X/D	Z/D	0.0
1.5		24.1
4.25		20.4
6.53		19.9
10.86		23.0
15.16		24.4
23.78		24.7
37.32		23.9
54.64		22.5
73.72		21.0
91.23		19.9
108.56		19.0

RUN No.54

U_j	32.31	ρ_j/ρ_∞	1.95
U_∞	30.5	M	2.07

X/D	Z/D	-0.44	0.0	0.44	0.88	1.32	1.76	2.20
1.5		12.6						
4.25		11.6	12.6	11.6	8.3	5.1	4.5	6.7
6.53		11.6	12.6	11.6	10.5	8.9	8.9	9.5
10.86		14.7	14.7	14.7	14.2	14.2	14.2	14.2
15.16		16.8	16.8	16.2	16.2	16.2	16.8	16.2
23.78		18.3	18.3	17.8				
37.32		18.3	18.3		17.8			
54.64		17.3	17.3			16.8		
73.72		16.8	16.8				16.2	16.2
91.23		15.7	16.2					15.2
108.56		15.2	15.2					14.7

RUN No.55

U_j	37.8	ρ_j/ρ_∞	1.93
U_∞	30.5	M	2.40

X/D	Z/D	-0.44	0.0	0.44	0.88	1.32	1.76	2.20
1.5		8.9						
4.25		7.8	8.9	8.9	6.7	4.5	3.4	5.1
6.53		9.4	9.9	9.9	9.9	9.4	8.9	8.9
10.86		14.7	14.1	14.1	14.7	14.7	14.7	14.1
15.16		15.7	16.7	16.2	16.7	16.7	16.7	16.7
23.78		18.3	18.3	18.3	17.8	17.8	17.8	17.8
37.32		18.3	18.3	18.3	18.3			
54.64		17.8	17.8	17.8				
73.72		17.3			17.3			
91.23		16.2				16.2	16.2	
108.56		15.7						15.7

RUN No.56

U_1	45.11	ρ_1/ρ_∞	1.99
U_∞	30.5	M	2.94

x/D	z/D	0.0
1.5		4.9
4.25		6.0
6.53		8.6
10.86		14.3
15.16		16.8
23.78		17.8
37.32		18.2
54.64		18.2
73.72		17.8
91.23		16.8
108.56		16.3

RUN No.60

U_j	32.31	ρ_j/ρ_∞	1.94
U_∞	30.5	M	2.05

X/D	Z/D	-0.44	0.0	0.44	0.88	1.32	1.76	2.20
1.5	7.7	7.7	7.7					
4.25	8.7	9.6	8.7	5.7	4.2	4.2	5.2	
6.53	10.6	11.1	10.1	9.6	9.2	8.7		
10.86	15.5	15.0	14.0	14.0	14.4	14.5	14.0	
15.16	17.3	17.3	16.4	15.9	16.4	16.4	15.9	
23.78	17.8	17.7	17.3	17.3	17.3			
37.32	17.3	17.7	17.3					
54.64	16.4	16.9		16.4				
73.72		15.9		15.9				
91.23		15.0			15.0			
108.56		14.0						13.5

RUN No.61

U_j	37.8	ρ_j/ρ_∞	1.92
U_∞	30.5	M	2.38

X/D	Z/D	-0.44	0.0	0.44	0.88	1.32	1.76	2.20
1.5			3.7					4.2
4.25		6.8	6.8	6.3	5.3	3.7	3.2	3.2
6.53		11.2	9.3	9.3	8.8	8.8	9.3	8.8
10.86		16.6	14.7	14.7	14.2	14.2	14.2	14.2
15.16		17.0	17.0	16.6	16.1	16.1	16.1	16.1
23.78		16.6	17.5	18.0	17.5	17.5	17.5	17.0
37.32		18.0	17.5	17.5	17.5	17.5		17.0
54.64		17.0	17.0	17.0				17.0
73.72		16.1	15.6		16.1	15.6		16.1
91.23		15.1						16.1
108.56		14.2					14.7	14.7

RUN No.62

U_j	45.11	ρ_j/ρ_∞	1.90
U_∞	30.5	M	2.81

X/D	Z/D	-0.44	0.0	0.44	0.88	1.32	1.76	2.20
1.5	1.70							1.70
4.25	5.8	5.2	4.7	4.2	3.2	3.2	2.2	
6.53	11.2	10.2	9.3	9.3	7.7	8.3	7.7	
10.86	16.1	15.6	14.7	14.2	13.7	13.2	13.2	
15.16	17.5	17.5	16.6	16.6	15.6	15.6	15.1	
23.78	18.0	18.0	18.0	17.5	16.6	16.6	16.6	
37.32	18.5	18.5	18.0	18.0	17.5	17.5	17.5	
54.64	18.0	18.0	18.0					
73.72	17.1	17.1	17.1	17.1				
91.23		16.1		15.6				
108.56		15.6					15.1	15.6

RUN No.63

U_j	21.34	ρ_j/ρ_∞	2.45
U_∞	30.5	M	1.71

X/D	Z/D	-0.44	0.0	0.44	0.88	1.32	1.76	2.20
1.5			19.7					21.1
4.25		16.3	18.2	17.4	14.1	9.8	8.6	10.9
6.53		15.9	17.1	16.7	14.8	13.7	13.3	13.7
10.86		17.1	17.4	17.1	16.7	16.7	16.3	14.8
15.16		18.2	18.2	17.8	17.4	17.4	17.1	17.8
23.78		17.8	17.8	17.8	17.4	17.4	17.4	17.4
37.32		16.3	16.7	16.7	16.7	16.7	16.7	16.7
54.64		15.2	15.2	15.2				15.6
73.72		14.1			14.1			14.1
91.23		12.9			12.9			13.3
108.56		11.7					12.5	12.1

RUN No. 64

U_j	21.34	ρ_j/ρ_∞	1.45
U_∞	30.5	M	1.01

X/D	Z/D	-0.44	0.0	0.44	0.88	1.32	1.76	2.20
1.5		18.5						
4.25		15.4	17.7	15.4	11.5	5.8	5.0	9.8
6.53		13.0	16.2	14.6	12.2	9.0	7.5	9.8
10.86		16.2	14.6	13.8	13.0	11.4	10.7	11.5
15.16		13.8	13.8	13.0	13.0	13.0	12.2	12.2
23.78		13.0	13.0	13.0	13.0	13.0	13.0	13.0
37.32		11.4	12.2	12.2				12.2
54.64			11.5	11.5				11.5
73.72			10.7	10.7	10.7		9.8	10.7
91.23			9.8					9.8
108.56			9.0				8.3	9.0

RUN No. 65

U_j	21.34	ρ_j/ρ_∞	1.91
U_∞	30.5	M	1.34

X/D	Z/D	-0.44	0.0	0.44	0.88	1.32	1.76	2.20
1.5		20.0						
4.25		16.6	18.5	17.6	14.6	7.5	5.9	
6.53		15.6	16.6	16.6	14.6	12.1	11.6	
10.86		15.6	16.1	16.1	15.6	15.1	14.6	
15.16		16.1	16.1	16.1	16.1	16.1	16.1	
23.73		16.1	16.1	16.1	16.1	16.1		
37.32		15.1	15.1	15.1	15.1	15.1	15.1	
54.64		13.6	13.6					
73.72		12.6	12.6					
91.23		11.6	11.6		11.6			
108.56		10.6				11.1		

RUN No. 65A

U_j	21.34	ρ_j/ρ_∞	1.95
U_∞	30.5	M	1.36

X/D	Z/D	-0.44	0.0	0.44	0.88	1.32	1.76	2.20
1.5		20.5						
4.25		16.7	19.1	17.7	13.3	8.9	7.3	10.9
6.53		15.8	17.2	16.7	14.3	11.9	10.9	12.3
10.86		15.8	16.3	16.3	15.8	14.8	14.8	15.3
15.16		16.3	16.3	16.3	16.3	16.3	15.8	16.3
23.78		16.3	16.3	16.3	16.3	16.3	16.3	16.3
37.32		15.3	15.3	15.3				15.8
54.64		13.8	13.8	14.3				14.3
73.72		12.8	12.8		12.8			12.8
91.23		11.9	11.9		11.9			11.9
108.56		10.9				11.4	11.4	11.4

RUN No. 66

U_j	16.15	ρ_j/ρ_∞	1.96
U_∞	30.5	M	1.04

X/D	Z/D	-0.44	0.0	0.44	0.88	1.32	1.76	2.20
1.5		29.1						
4.25		22.2	25.0	23.6	18.5	10.8	10.3	16.6
6.53		19.5	21.3	20.9	18.1	14.2	13.7	16.1
10.86		17.1	18.1	18.1	16.6	15.7	15.2	16.1
15.16		16.1	16.6	16.6	16.1	16.1	15.7	16.1
23.78		15.2	15.2	15.2	15.2	15.2	15.2	15.2
37.32		13.7	13.7	13.7				13.7
54.64		12.3	12.3		12.3			12.3
73.72		10.8	10.8		11.3			11.3
91.23		9.8	9.8			10.3		10.3
108.56		8.8						9.3

RUN No.68

U_j	27.13	ρ_j/ρ_∞	1.94
U_∞	30.5	M	1.73

X/D	Z/D	-0.44	0.0	0.44	0.88	1.32	1.76	2.20
1.5		12.6	13.6	12.1	9.1	5.4	4.9	8.0
4.25		12.6	13.6	12.1	11.6	10.6	10.0	10.0
6.53		12.1	13.1	12.6	14.1	14.6	14.6	14.6
10.86		15.6	15.1	14.6	16.1	15.1	15.1	16.1
15.16		16.6	16.6	16.6	17.1	17.1	17.1	17.6
23.78		17.6	17.6	17.6	17.1	17.1	17.1	17.6
37.32		17.1	17.1	17.1	17.1	17.1	17.1	17.1
54.64		16.1	16.1	16.1	15.1	15.1	15.1	16.1
73.72		14.6	14.6	14.6	14.1	14.1	14.1	14.1
91.23		13.6	13.6	13.6	13.1	13.1	13.1	13.1
108.56		13.1	13.1	13.1	13.1	13.1	13.1	13.1

RUN No.69

U_j	7.62	ρ_j/ρ_∞	1.93
U_∞	30.5	M	0.48

X/D	Z/D	-0.44	0.0	0.44	0.88	1.32	1.76	2.20
1.5		29.7	30.6	26.0	20.4	9.0	12.5	25.1
4.25		23.2	24.2	21.8	17.0	12.0	13.0	20.4
6.53		17.0	17.0	17.0	14.5	12.5	12.5	15.5
10.86		14.0	13.0	14.0	13.0	11.5	11.5	12.5
15.16		11.0	11.0	10.5	10.5	10.5	10.5	10.5
23.78		9.5	9.0	7.5	7.5	7.5	7.5	9.0
37.32		6.4	6.4	6.4	6.4	6.4	6.4	6.9
54.64		5.9	5.9	5.9	5.9	5.9	5.9	5.9
73.72		5.4	5.4	5.4	5.4	5.4	5.4	5.4
91.23								
108.56								

RUN No.70

U_j	11.43	ρ_j/ρ_∞	1.94
U_∞	30.5	M	0.73

X/D	Z/D	-0.44	0.0	0.44	0.88	1.32	1.76	2.20
1.5		32.7	28.2	24.5	17.9	9.5	12.0	21.2
4.25		25.4	23.6	20.8	16.4	12.5	13.9	18.4
6.53		17.4	18.8	16.9	14.9	13.5	13.9	15.4
10.86		15.4	16.4	15.4	15.4	13.9	13.5	13.9
15.16		13.5	13.9	13.0	13.0	12.5	12.5	12.5
23.78		12.0	12.0	11.5	11.5	10.9	11.5	10.9
37.32		10.4	10.4	10.0	10.0	10.0	10.0	10.0
54.64		9.5	9.5	9.0	9.0	9.0	9.0	9.0
73.72		8.5	8.5	8.5	8.5	8.5	8.5	8.5
91.23		7.9	7.9	7.9	7.9	7.9	7.9	7.9
108.56		7.4	7.4	7.4	7.4	7.4	7.4	7.4

RUN No.71

U_j	21.34	ρ_j/ρ_∞	3.00
U_∞	30.5	M	2.10

X/D	Z/D	-0.44	0.0	0.44	0.88	1.32	1.76	2.20
1.5		17.6	18.7	17.6	14.9	10.6	9.5	12.8
4.25		18.0	18.0	18.0	16.6	15.6	15.2	15.6
6.53		20.3	20.0	20.0	19.3	19.3	19.3	19.3
10.86		21.7	21.3	21.3	21.0	20.3	20.3	20.7
15.16		21.3	21.3	21.3	21.0	20.7	20.7	20.7
23.78		20.0	20.0	20.0	20.0	20.0	20.0	20.0
37.32		18.7	18.7	18.7	18.7	18.7	18.7	18.7
54.64		17.0	17.0	17.0	17.0	17.0	17.0	17.3
73.72		15.9	15.9	15.9	15.9	15.9	15.9	15.9
91.23		14.9	14.9	14.9	14.9	14.9	14.9	14.9
108.56								

RUN No.72

U_j	21.34	ρ_j/ρ_∞	3.56
U_∞	30.5	M	2.49

RUN No.73

U_j	21.34	ρ_j/ρ_∞	4.17
U_∞	30.5	M	2.92

x/D	z/D	-0.44	0.0	0.44	0.88	1.32	1.76	2.20
1.5			18.7					
4.25		18.1	19.1	17.1	14.5	12.5	10.8	12.8
6.53		19.1	18.7	18.4	17.5	17.8	17.1	17.1
10.86		22.8	22.2	21.6	21.6	21.9	21.6	21.6
15.16		24.0	24.0	23.4	22.8	22.8	22.8	22.8
23.78		24.0	24.0	23.4	23.1	23.1	22.8	22.8
37.32		22.5	22.8					22.5
54.64			21.3	20.9				21.3
73.72			19.4	19.4				19.7
91.23			18.1				18.1	18.1
108.56			17.5			17.1		17.1

x/D	z/D	0.0
1.5		15.3
4.25		16.5
6.53		18.6
10.86		23.3
15.16		25.3
23.78		25.5
37.32		24.7
54.64		23.3
73.72		21.6
91.23		20.1
108.56		18.9

RUN No.80

U_j	32.31	ρ_j/ρ_∞	2.98
U_∞	30.5	M	3.16

x/D	z/D	0.0
1.5		7.0
4.25		8.1
6.53		11.0
10.86		18.1
15.16		20.1
23.78		21.1
37.32		21.4
54.64		20.7
73.72		19.7
91.23		19.1
108.56		18.1

RUN No.81

U_j	32.31	ρ_j/ρ_∞	3.60
U_∞	30.5	M	3.78

x/D	z/D	0.0
1.5		7.8
4.25		9.5
6.53		13.5
10.86		19.8
15.16		21.3
23.78		22.8
37.32		23.1
54.64		22.8
73.72		21.9
91.23		21.0
108.56		20.1

RUN No.83

U_j	11.43	ρ_j/ρ_∞	4.20
U_∞	30.5	M	1.58

x/D	z/D	0.0
1.5		46.0
4.25		35.9
6.53		30.7
10.86		26.8
15.16		24.3
23.78		21.8
37.32		19.0
54.64		16.6
73.72		14.6
91.23		13.0
108.56		12.1

RUN No.84

U_j	45.11	ρ_j/ρ_∞	1.45
U_∞	30.5	M	2.15

x/D	z/D	0.0
1.5		2.7
4.25		4.4
6.53		7.0
10.86		12.1
15.16		15.4
23.78		16.3
37.32		16.3
54.64		16.3
73.72		15.4
91.23		14.6
108.56		13.8

RUN No.85

U_j	32.31	ρ_j/ρ_∞	1.45
U_∞	30.5	M	1.53

x/D	z/D	0.0
1.5		8.8
4.25		8.8
6.53		9.7
10.86		11.3
15.16		12.2
23.78		14.7
37.32		15.5
54.64		14.7
73.72		13.9
91.23		13.0
108.56		12.2

RUN No.86

U_j	11.43	ρ_j/ρ_∞	1.47
U_∞	30.5	M	0.55

x/D	z/D	0.0
1.5		29.2
4.25		29.2
6.53		23.8
10.86		19.1
15.16		19.1
23.78		12.6
37.32		10.2
54.64		9.4
73.72		7.7
91.23		7.7
108.56		6.9

RUN No.87

U_j	11.43	ρ_j/ρ_∞	3.03
U_∞	30.5	M	1.14

x/D	z/D	0.0
1.5		46.4
4.25		35.7
6.53		29.9
10.86		24.7
15.16		21.7
23.78		19.9
37.32		16.4
54.64		14.3
73.72		12.4
91.23		11.7
108.56		10.6

RUN No.88

U_j	11.43	ρ_j/ρ_∞	2.49
U_∞	30.5	M	0.93

x/D	z/D	0.0
1.5		47.2
4.25		34.5
6.53		28.3
10.86		22.1
15.16		19.0
23.78		15.7
37.32		13.3
54.64		11.5
73.72		10.3
91.23		9.4
108.56		8.5

RUN No.89

U_j	11.43	ρ_j/ρ_∞	3.43
U_∞	30.5	M	1.29

X/D	Z/D	0.0
1.5		30.0
4.25		24.5
6.53		21.6
10.86		19.3
15.16		18.0
23.78		16.7
37.32		15.0
54.64		13.6
73.72		12.2
91.23		11.5
108.56		10.8

RUN No.91

U_j	16.15	ρ_j/ρ_∞	2.50
U_∞	30.5	M	1.33

X/D	Z/D	0.0
1.5		33.6
4.25		27.8
6.53		24.4
10.86		21.3
15.16		19.7
23.78		18.1
37.32		16.1
54.64		14.4
73.72		13.2
91.23		12.3
108.56		11.5

RUN No.92

U_j	16.15	ρ_j/ρ_∞	3.56
U_∞	30.5	M	1.89

X/D	Z/D	0.0
1.5		35.5
4.25		27.9
6.53		25.4
10.86		24.1
15.16		23.8
23.78		22.5
37.32		20.6
54.64		18.6
73.72		16.9
91.23		15.5
108.56		14.5

RUN No.93

U_j	27.13	ρ_j/ρ_∞	1.47
U_∞	30.5	M	1.31

X/D	Z/D	0.0
1.5		13.6
4.25		12.7
6.53		13.6
10.86		13.6
15.16		13.6
23.78		15.2
37.32		15.2
54.64		13.6
73.72		12.7
91.23		12.7
108.56		11.9

RUN No.94

U_j	27.13	ρ_j/ρ_∞	2.53
U_∞	30.5	M	2.25

X/D	Z/D	0.0
1.5		13.9
4.25		13.9
6.53		14.3
10.86		18.1
15.16		19.3
23.78		20.1
37.32		19.7
54.64		18.9
73.72		17.6
91.23		16.8
108.56		16.0

RUN No.95

U_j	27.13	ρ_j/ρ_∞	3.57
U_∞	30.5	M	3.17

X/D	Z/D	0.0
1.5		12.4
4.25		12.7
6.53		15.9
10.86		20.9
15.16		22.5
23.78		23.8
37.32		23.5
54.64		22.9
73.72		21.6
91.23		20.9
108.56		19.9

RUN No.96

U_j	32.31	ρ_j/ρ_∞	2.53
U_∞	30.5	M	2.69

X/D	Z/D	0.0
1.5		9.6
4.25		10.4
6.53		12.6
10.86		17.2
15.16		19.7
23.78		20.5
37.32		20.5
54.64		19.7
73.72		18.9
91.23		18.1
108.56		16.8

RUN No.97

U_j	32.31	ρ_j/ρ_∞	3.58
U_∞	30.5	M	3.80

X/D	Z/D	0.0
1.5		5.4
4.25		10.2
6.53		14.1
10.86		19.9
15.16		21.9
23.78		23.1
37.32		23.8
54.64		23.5
73.72		22.5
91.23		21.5
108.56		21.2

RUN No. 98

U_j	45.11	ρ_j/ρ_∞	2.53
U_∞	30.5	M	3.75

x/D	z/D	0.0
1.5		4.2
4.25		9.1
6.53		10.9
10.86		16.4
15.16		18.1
23.78		19.7
37.32		28.5
73.72		20.1
91.23		19.7
108.56		18.9

RUN No. 99/1

U_j	27.13	ρ_j/ρ_∞	4.26
U_∞	30.5	M	3.79

x/D	z/D	0.0
1.5		11.1
4.25		11.7
6.53		15.6
10.86		21.7
15.16		23.5
23.78		24.6
37.32		24.6
73.72		23.2
91.23		22.6
108.56		21.7

RUN No. 99/2

U_j	27.13	ρ_j/ρ_∞	3.07
U_∞	30.5	M	2.73

x/D	z/D	0.0
1.5		14.4
4.25		15.9
6.53		16.3
10.86		19.5
15.16		21.6
23.78		22.2
37.32		21.9
73.72		20.5
91.23		19.1
108.56		18.4
		17.3

RUN No. 99/3

U_j	16.15	ρ_j/ρ_∞	4.26
U_∞	30.5	M	2.26

x/D	z/D	0.0
1.5		33.1
4.25		27.2
6.53		25.5
10.86		25.8
15.16		25.8
23.78		25.2
37.32		22.9
54.64		20.8
73.72		19.0
91.23		17.8
108.56		16.8

RUN No. 99/4

U_j	16.15	ρ_j/ρ_∞	3.07
U_∞	30.5	M	1.62

x/D	z/D	0.0
1.5		37.0
4.25		29.6
6.53		26.3
10.86		23.6
15.16		22.3
23.78		20.5
37.32		18.4
54.64		16.7
73.72		14.8
91.23		13.7
108.56		13.0

RUN No. 99/5

U_j	16.15	ρ_j/ρ_∞	1.47
U_∞	30.5	M	0.78

x/D	z/D	0.0
1.5		18.8
4.25		21.3
6.53		18.8
10.86		15.5
15.16		13.0
23.78		11.4
37.32		8.8
54.64		8.0
73.72		7.1
91.23		7.1
108.56		6.2

Run No.100		U_j		U_∞		30.5	

RUN 101		U_{∞} 30.5		U_j 7.62	
101/1		101/2		101/3	
X/D 4.25		X/D 10.86		X/D 60.61	
ρ_j/ρ_{∞} 1.96		ρ_j/ρ_{∞} 2.05		ρ_j/ρ_{∞} 1.96	
M 0.49		M 0.51		M 0.49	
Y/D 0.0		Z/D 0.0		Y/D 0.0	
Z/D 0.0		Y/D 0.0		Z/D 0.0	
0.06		0.06		0.06	
0.33		0.30		0.72	
0.61		0.58		1.28	
0.89		0.85		2.39	
1.17		1.13		3.50	
3.0		8.7		4.61	
1.44		1.41			
1.72		1.69			
		1.97			
		3.4			

RUN 102		U_{∞} 30.5		U_j 13.89	
102/1		102/2		102/3	
X/D 4.25		X/D 10.86		X/D 60.61	
ρ_j/ρ_{∞} 3.01		ρ_j/ρ_{∞} 3.10		ρ_j/ρ_{∞} 3.01	
M 1.37		M 1.42		M 1.37	
Y/D 0.0		Z/D 0.0		Y/D 0.0	
Z/D 0.0		Y/D 0.0		Z/D 0.0	
0.06		0.06		0.06	
0.33		0.33		0.72	
0.61		0.85		1.83	
0.89		1.41		2.94	
1.17		1.97		4.05	
1.44		2.52		5.17	
1.72		3.08		6.28	
2.00		3.63			
2.28		0.9			
2.55					

RUN 103		U_{∞} 30.5		U_j 6.19	
103/1		103/2		103/3	
X/D 4.25		X/D 10.86		X/D 60.61	
ρ_j/ρ_{∞} 3.04		ρ_j/ρ_{∞} 3.11		ρ_j/ρ_{∞} 3.05	
M 0.62		M 0.63		M 0.62	
Y/D	0.0	Y/D	0.0	Y/D	0.0
Z/D	0.0	Z/D	0.0	Z/D	0.0
0.06	38.4	0.06	21.8	0.06	8.2
0.33	36.2	0.30	21.1	0.72	7.8
0.61	31.2	0.58	19.0	1.83	5.8
0.89	23.1	0.85	16.5	2.94	3.4
1.17	11.7	1.13	12.4	4.05	1.3
1.44	3.0	1.41	9.7	5.17	0.5
1.72	0.0	1.69	6.2	6.28	
		1.97	3.8		
		2.44	1.7		

RUN 104		U_{∞} 30.5		U_j 21.34	
104/1		104/2		104/3	
X/D 4.25		X/D 10.86		X/D 60.61	
ρ_j/ρ_{∞} 3.02		ρ_j/ρ_{∞} 2.99		ρ_j/ρ_{∞} 3.05	
M 2.12		M 2.10		M 2.14	
Y/D	0.0	Y/D	0.0	Y/D	0.0
Z/D	0.0	Z/D	0.0	Z/D	0.0
0.06	24.9	0.06	22.1	0.06	17.8
0.33	28.3	0.30	22.8	0.72	17.1
0.61	31.3	0.58	22.8	1.83	15.2
0.89	33.2	0.85	23.1	2.94	12.9
1.17	36.4	1.41	23.8	4.05	9.7
1.44	40.3	1.97	22.4	5.17	6.4
1.72	42.1	2.52	18.7	6.28	2.6
2.00	40.3	3.08	11.6	7.39	0.5
2.28	36.4	3.63	3.6		
2.55	25.6	4.19	0.9		
2.83	12.9				
3.11	5.0				
3.39	1.0				

RUN 105		U_{∞} 30.5		U_j 37.8	
105/1		105/2		105/3	
X/D 4.25		X/D 10.86		X/D 60.61	
ρ_j/ρ_{∞} 1.96		ρ_j/ρ_{∞} 1.97		ρ_j/ρ_{∞} 1.95	
M 2.42		M 2.44		M 2.46	
Y/D		Y/D		Y/D	
Z/D		Z/D		Z/D	
0.0		0.0		0.0	
0.06	11.8	0.06	15.6	0.06	18.0
0.33	16.1	0.33	17.1	0.72	18.0
0.61	20.3	0.58	18.1	1.28	17.5
0.89	21.9	0.85	19.1	2.34	15.9
1.17	25.4	1.41	21.0	3.50	14.2
1.44	28.9	1.97	22.0	4.61	11.5
1.72	33.7	2.52	22.4	5.72	7.6
2.00	36.0	3.08	21.0	6.83	3.5
2.28	38.8	3.63	15.6	7.94	1.3
2.55	37.9	4.19	9.1		
2.83	32.7	4.74	4.4		
3.11	25.9	5.3	1.7		
3.39	15.1				
3.67	7.5				
3.94	1.8				
4.22	0.1				

RUN 106		U_{∞} 30.5		U_j 25.81	
106/1		106/2		106/3	
X/D 4.25		X/D 10.86		X/D 60.61	
ρ_j/ρ_{∞} 2.05		ρ_j/ρ_{∞} 2.06		ρ_j/ρ_{∞} 1.97	
M 1.74		M 1.75		M 1.67	
Y/D		Y/D		Y/D	
Z/D		Z/D		Z/D	
0.0		0.0		0.0	
0.06	19.5	0.06	18.0	0.06	15.3
0.61	27.5	0.30	18.9	0.72	14.8
1.17	33.3	0.85	20.9	1.83	13.2
1.72	38.5	1.97	21.4	2.94	10.4
2.00	37.6	2.52	20.9	4.05	7.6
2.27	31.5	3.08	18.0	5.17	4.7
2.55	20.0	3.63	11.4	6.28	1.9
2.83	9.6	4.19	4.5	7.39	0.7
3.11	3.8	4.74	0.1	8.5	-
3.39	0.2				
3.67					

RUN No.120

U_i	18.14	ρ_i/ρ_∞	1.48
U_∞	25.9	M	1.03

X/D	Z/D	-0.44	0.0	0.44	0.88	1.32	1.76	2.20
1.5			31.4					
4.25		22.8	26.7	21.9	12.1	4.5	4.5	10.4
6.53		19.5	22.8	18.7	11.3	5.3	6.2	12.1
10.86		17.1	18.7	15.4	9.6	6.2	7.9	12.9
15.16		15.4	16.2	13.7	10.4	7.9	8.7	12.1
23.78		12.9	12.9	12.1	9.6	8.2	9.6	11.3
37.32		10.4	9.6		9.6	9.6	10.4	
54.64		8.7		8.7				8.7
73.72		8.7		8.7				7.9
91.23		7.9		7.9		7.0		7.9
108.56		7.0						7.0

RUN No.121

U_i	18.14	ρ_i/ρ_∞	1.96
U_∞	25.9	M	1.37

X/D	Z/D	-0.44	0.0	0.44	0.88	1.32	1.76	2.20
1.5			40.7					
4.25		30.1	33.1	29.1	19.3	9.4	8.8	19.3
6.53		26.1	27.6	24.5	17.7	9.9	11.1	18.2
10.86		22.4	23.0	20.3	15.5	12.2	13.8	17.7
15.16		19.3	20.3	18.7	15.5	13.3	13.8	16.6
23.78		17.1	17.1	16.0	14.4	13.8	14.4	16.0
37.32		14.4	14.4	13.8	13.3	13.3	13.8	13.8
54.64		12.7	12.2	12.2			11.6	
73.72		11.1	11.1		10.5			10.5
91.23		10.5	9.9		9.9			9.4
108.56		9.9	9.4					

RUN No.122

U_i	18.14	ρ_i/ρ_∞	2.5
U_∞	25.9	M	1.74

X/D	Z/D	-0.44	0.0	0.44	0.88	1.32	1.76	2.20
1.5			42.8					
4.25		29.9	33.7	29.9	20.9	10.0	10.9	20.5
6.53		25.7	28.3	25.4	19.2	12.7	13.1	19.7
10.86		23.0	24.2	21.3	18.0	14.9	15.8	19.7
15.16		20.5	21.3	20.1	17.5	16.7	16.7	18.8
23.78		18.4	18.4	18.0	17.1	16.7	16.7	17.5
37.32		15.8	15.8	15.8	15.8	15.8	15.8	15.8
54.64		13.6		13.6				13.6
73.72		12.2		12.2				12.2
91.23		11.3		11.3				11.3
108.56		10.9				10.9		10.9

RUN No.123

U_i	6.48	ρ_i/ρ_∞	1.96
U_∞	25.9	M	0.49

X/D	Z/D	-0.44	0.0	0.44	0.88	1.32	1.76	2.20
1.5			78.6					
4.25		45.4	48.0	37.8	27.8	11.3	15.0	32.7
6.53		33.6	35.0	28.8	21.3	12.4	15.0	25.3
10.86		23.9	24.3	20.8	15.6	10.7	14.0	19.2
15.16		18.7	19.2	16.7	13.4	10.2	11.8	15.6
23.78		14.0	13.4	11.8	10.2	9.1	10.7	12.4
37.32		10.2	9.6	8.5	8.0	8.0	8.5	9.6
54.64		8.0	7.4	6.9	6.9	6.9	6.9	7.4
73.72			6.3	5.8			6.3	6.3
91.23			5.8	5.8	5.8			5.8
108.56			5.2			5.2		5.2

RUN No.124

U_j	13.73	ρ_j/ρ_∞	1.96
U_∞	25.9	M	1.04

X/D	Z/D	-0.44	0.0	0.44	0.88	1.32	1.76	2.20
1.5			53.4					
4.25		34.0	39.5	34.0	24.8	12.9	12.9	25.8
6.53		28.7	32.6	28.7	21.2	13.4	14.0	22.3
10.86		23.8	25.8	22.8	17.1	13.4	15.5	20.2
15.16		20.2	21.8	19.7	16.1	13.4	14.5	17.6
23.78		16.6	16.6	15.0	13.4	12.9	14.0	15.5
37.32		12.9	12.9	11.8	11.8	11.8	11.8	12.3
54.64		10.7	10.7	10.2	10.2			10.2
73.72		9.1	9.1	9.1	9.1			9.1
91.23			8.5	8.5				8.5
108.56			8.0	8.0		8.0		8.0

RUN No.125

U_j	9.72	ρ_j/ρ_∞	1.96
U_∞	25.9	M	0.74

X/D	Z/D	-0.44	0.0	0.44	0.88	1.32	1.76	2.20
1.5			54.2					
4.25		38.2	40.4	33.5	19.7	7.4	10.7	27.3
6.53		30.7	32.1	26.8	18.2	9.1	12.9	23.8
10.86		23.3	23.3	20.2	14.5	9.6	12.9	19.2
15.16		18.2	18.7	17.1	13.4	10.2	11.3	15.5
23.78		14.5	14.0	12.3	10.7	9.6	11.3	12.9
37.32		10.7	10.2	9.6	8.0	8.5	9.6	10.2
54.64		8.5	8.5	8.0	7.4	7.4	8.0	8.0
73.72			7.4	7.4	6.9	6.9	7.4	7.4
91.23			6.3		6.3			6.3
108.56			5.8		5.8			5.8

RUN No.126

U_j	23.06	ρ_j/ρ_∞	1.95
U_∞	25.9	M	1.73

X/D	Z/D	-0.44	0.0	0.44	0.88	1.32	1.76	2.20
1.5			29.0					
4.25		19.9	23.0	19.3	10.8	4.7	4.7	12.5
6.53		18.8	20.4	17.8	11.3	6.9	7.5	13.5
10.86		16.7	17.8	15.1	11.9	9.7	10.3	14.1
15.16		15.7	16.7	15.1	13.0	11.9	11.4	14.1
23.78		15.1	15.1	14.6	13.5	13.5	13.5	14.6
37.32		14.1	14.1	13.5	13.5	13.5	13.5	14.1
54.64		13.0	12.4					13.0
73.72		11.9	10.8					11.9
91.23		10.8	10.3		10.3			10.3
108.56			9.7			10.3		9.7

RUN No.127

U_j	27.46	ρ_j/ρ_∞	1.94
U_∞	25.9	M	2.06

X/D	Z/D	-0.44	0.0	0.44	0.88	1.32	1.76	2.20
1.5			20.9					
4.25		13.0	16.2	13.6	8.1	3.5	3.0	7.5
6.53		13.6	14.6	12.5	8.6	5.8	5.8	9.2
10.86		13.6	14.1	12.5	10.3	9.2	9.7	10.8
15.16		14.1	14.1	14.0	12.3	11.4	12.0	12.5
23.78		14.6	14.6	14.1	14.1	14.1	14.1	14.1
37.32		14.6	14.6	14.6	14.6	14.6	14.6	14.6
54.64		14.1	14.1					14.1
73.72		13.0	13.0					13.0
91.23		12.5	12.5					12.5
108.56			12.0					12.0

RUN No.128

U_j	38.34	ρ_j/ρ_∞	1.97
U_∞	25.9	M	2.91

X/D	Z/D	-0.44	0.0	0.44	0.88	1.32	1.76	2.20
1.5		10.0		6.8	4.0	1.8	6.5	2.9
4.25		6.3	7.3	7.3	5.7	4.6	4.0	4.6
6.53		6.8	7.3	7.3	5.7	4.6	4.0	4.6
10.86		9.5	9.5	10.0	10.0	10.6	9.5	9.5
15.16		12.7	12.7	12.7	12.7	13.2	12.7	12.7
23.78		15.3	15.3	15.3	15.3	15.9	15.3	15.3
37.32		15.9	16.4	15.9				15.9
54.64		15.3	15.3					15.3
73.72		14.3	14.8		14.8			14.2
91.23		13.8	13.8			13.8		13.8
108.56		13.2						13.2

RUN No.130

U_j	18.14	ρ_j/ρ_∞	4.22
U_∞	25.9	M	2.95

X/D	Z/D	0.0
1.5		38.4
4.25		28.1
6.53		24.9
10.86		24.0
15.16		24.0
23.78		23.5
37.32		21.7
54.64		19.2
73.72		17.1
91.23		16.1
108.56		14.8

RUN No.129

U_j	32.13	ρ_j/ρ_∞	1.95
U_∞	25.9	M	2.42

X/D	Z/D	-0.44	0.0	0.44	0.88	1.32	1.76	2.20
1.5		14.4		5.7	2.4	2.4	5.7	
4.25		10.7	11.7	10.1	5.7	2.4	2.4	5.7
6.53		9.6	10.7	9.0	6.9	5.2	5.2	6.9
10.86		11.2	11.2	10.7	9.6	9.0	9.0	9.6
15.16		12.8	12.3	12.3	11.7	12.3	11.7	12.3
23.78		14.4	14.4	14.4	13.9	14.4	14.4	15.0
37.32		15.0	15.0	15.0				15.0
54.64		14.4	14.4					14.4
73.72		13.4	13.4		13.4			13.4
91.23		12.3	12.3					12.8
108.56		11.7				12.3		12.3

RUN No.131

U_j	18.14	ρ_j/ρ_∞	3.56
U_∞	25.9	M	2.49

X/D	Z/D	-0.44	0.0	0.44	0.88	1.32	1.76	2.20
1.5		41.4		28.6	20.4	11.6	11.2	19.4
4.25		28.3	31.3	28.6	20.4	11.6	11.2	19.4
6.53		25.2	27.4	25.2	19.7	16.1	15.7	20.1
10.86		23.6	24.3	23.0	20.4	19.1	19.1	20.7
15.16		22.7	23.0	22.0	20.7	20.4	20.1	21.1
23.78		21.1	21.1	21.1	20.4	20.4	20.1	20.4
37.32		19.1	19.1	19.1	18.4	18.8	18.8	18.8
54.64		17.1	17.1	16.4	16.4			16.4
73.72		15.1	15.1					14.7
91.23		14.0	14.0					13.7
108.56		13.0						12.6

RUN No.132

U_i	18.14	ρ_i/ρ_∞	3.04
U_∞	25.9	M	2.13

X/D	Z/D	-0.44	0.0	0.44	0.88	1.32	1.76	2.20
1.5			41.8					
4.25		28.9	31.8	28.3	20.1	11.6	10.9	19.4
6.53		25.6	27.6	24.6	19.0	14.2	14.2	19.4
10.86		22.9	23.6	21.8	19.0	17.2	17.6	20.1
15.16		21.5	21.5	20.8	19.0	18.3	18.3	19.7
23.78		19.7	19.7	19.0	18.3	18.3	18.3	18.6
37.32		17.2	17.2	17.2	16.8	16.8		17.2
54.64		15.0	15.4	15.0	15.0			15.0
73.72		13.5	13.5					13.5
91.23			12.8					
108.56			11.6		11.2			11.6

[illegible]

RUN No. 141		U_j 6.48		U_∞ 25.9	
Run No. 141/1		Run No. 141/2		Run No. 141/3	
X/D 4.25		X/D 15.16		X/D 60.61	
ρ_j/ρ_∞ 1.95		ρ_j/ρ_∞ 2.34		ρ_j/ρ_∞ 2.33	
M 0.49		M 0.59		M 0.58	
Z/D		Z/D		Z/D	
Y/D	0.0	Y/D	0.0	Y/D	0.0
0.00	46.2	0.00	18.2	0.00	7.3
0.06	43.6	0.06	15.3	0.06	7.3
0.27	40.6	0.33	13.1	0.61	5.4
0.54	31.0	0.61	11.0	0.89	4.0
0.82	16.3	0.89	8.3	1.17	2.5
1.10	2.9	1.17	5.6	1.44	0.6
1.38	0.0	1.44	2.9	1.72	5.8
1.6		1.72	1.0		
		2.00	0.1		

RUN No. 142		U_j 11.81		U_∞ 25.9	
Run No. 142/1		Run No. 142/2		Run No. 142/3	
X/D 4.25		X/D 15.16		X/D 60.61	
ρ_j/ρ_∞ 3.00		ρ_j/ρ_∞ 2.99		ρ_j/ρ_∞ 3.00	
M 1.37		M 1.37		M 1.37	
Z/D		Z/D		Z/D	
Y/D	0.0	Y/D	0.0	Y/D	0.0
0.00	43.2	0.00	22.3	0.00	11.8
0.06	43.5	0.06	20.9	0.06	11.8
0.28	43.8	0.33	19.5	0.33	11.0
0.42	44.0	0.61	18.5	0.61	9.9
0.55	44.0	0.89	17.1	0.89	8.7
0.69	43.2	1.17	14.9	1.17	7.5
0.83	41.5	1.44	12.0	1.44	6.3
1.11	37.1	1.72	9.4	1.72	4.6
1.39	25.3	2.00	6.0	2.00	3.4
1.67	9.6	2.28	2.9	2.28	2.2
1.81	4.5	2.55	1.3	2.55	1.4
1.94	2.1	2.83	0.5	2.83	0.5
2.22	0.5			3.11	0.1

Run No. 143		U_j 5.26		U_∞ 25.9	
Run No. 143/1		Run No. 143/2		Run No. 143/3	
X/D	4.25	X/D	15.16	X/D	60.61
ρ_j/ρ_∞	3.03	ρ_j/ρ_∞	2.99	ρ_j/ρ_∞	3.04
M	0.61	M	0.61	M	0.62
Z/D	0.0	Z/D	0.0	Z/D	0.0
Y/D	0.0	Y/D	0.0	Y/D	0.0
0.00	41.6	0.00	20.4	0.00	7.5
0.06	44.0	0.06	15.7	0.06	7.8
0.33	43.6	0.33	13.5	0.33	7.0
0.61	28.0	0.61	10.9	0.61	5.8
0.89	13.7	0.89	8.3	0.89	4.2
1.17	25.7	1.17	5.2	1.17	3.0
1.44	0.1	1.44	2.9	1.44	1.8
		1.72	0.9	1.72	0.9
		2.00	0.4	2.00	0.1
		2.28	0.1		
		2.56	0.1		

Run No. 144		U_j 18.14		U_∞ 25.9	
Run No. 144/1		Run No. 144/2		Run No. 144/3	
X/D	4.25	X/D	15.16	X/D	60.61
ρ_j/ρ_∞	3.03	ρ_j/ρ_∞	3.05	ρ_j/ρ_∞	3.00
M	2.11	M	2.13	M	2.10
Z/D	0.0	Z/D	0.0	Z/D	0.0
Y/D	0.0	Y/D	0.0	Y/D	0.0
0.00	30.2	0.00	17.2	0.00	14.3
0.06	30.5	0.06	20.8	0.06	14.3
0.28	33.9	0.33	21.1	0.33	13.5
0.55	37.2	0.61	20.4	0.89	11.6
0.83	39.0	0.89	17.9	1.44	9.3
1.11	41.5	1.17	15.4	2.00	6.6
1.39	43.0	1.44	12.4	2.55	3.8
1.67	41.1	1.72	8.5	3.11	1.7
1.94	29.8	2.00	5.0	3.67	0.5
2.22	15.5	2.28	2.1		
2.50	4.9	2.55	0.5		
2.78	0.9	2.83	0.0		
3.06	0.1				

Run No.145		U_j 32.13		U_∞ 25.9	
Run No.145/1		Run No.145/2		Run No.145/3	
X/D 4.25		X/D 15.16		X/D 60.61	
ρ_j/ρ_∞ 1.96		ρ_j/ρ_∞ 1.98		ρ_j/ρ_∞ 1.97	
M 2.43		M 2.46		M 2.45	
Y/D 0.0		Y/D 0.0		Y/D 0.0	
Z/D 0.0		Z/D 0.0		Z/D 0.0	
Y/D 0.00		Y/D 0.00		Y/D 0.00	
Z/D 0.06		Z/D 0.06		Z/D 0.06	
Y/D 0.28		Y/D 0.33		Y/D 0.61	
Z/D 0.55		Z/D 0.61		Z/D 1.17	
Y/D 0.83		Y/D 0.89		Y/D 1.72	
Z/D 1.11		Z/D 1.17		Z/D 2.28	
Y/D 1.39		Y/D 1.44		Y/D 2.83	
Z/D 1.67		Z/D 1.72		Z/D 3.39	
Y/D 1.94		Y/D 2.00		Y/D 3.94	
Z/D 2.22		Z/D 2.28		Z/D 4.50	
Y/D 2.50		Y/D 2.55		Y/D 5.05	
Z/D 2.78		Z/D 2.83		Z/D 5.05	
Y/D 3.05		Y/D 3.11		Y/D 5.05	
Z/D 3.33		Z/D 3.39		Z/D 5.05	
Y/D 3.61		Y/D 3.67		Y/D 5.05	
Z/D 3.94		Z/D 3.94		Z/D 5.05	

Run No.146		U_j 25.91		U_∞ 25.9	
Run No.146/1		Run No.146/2		Run No.146/3	
X/D 4.25		X/D 15.16		X/D 60.61	
ρ_j/ρ_∞ 1.96		ρ_j/ρ_∞ 1.91		ρ_j/ρ_∞ 1.97	
M 1.66		M 1.61		M 1.67	
Y/D 0.0		Y/D 0.0		Y/D 0.0	
Z/D 0.0		Z/D 0.0		Z/D 0.0	
Y/D 0.00		Y/D 0.00		Y/D 0.00	
Z/D 0.06		Z/D 0.06		Z/D 0.06	
Y/D 0.28		Y/D 0.33		Y/D 0.61	
Z/D 0.55		Z/D 0.61		Z/D 1.17	
Y/D 0.83		Y/D 0.89		Y/D 1.72	
Z/D 1.11		Z/D 1.17		Z/D 2.28	
Y/D 1.39		Y/D 1.44		Y/D 2.83	
Z/D 1.67		Z/D 1.72		Z/D 3.39	
Y/D 1.94		Y/D 2.00		Y/D 3.94	
Z/D 2.22		Z/D 2.28		Z/D 4.50	
Y/D 2.50		Y/D 2.55		Y/D 5.05	
Z/D 2.78		Z/D 2.83		Z/D 5.05	
Y/D 3.06		Y/D 3.11		Y/D 5.05	
Z/D 3.33		Z/D 3.39		Z/D 5.05	
Y/D 3.61		Y/D 3.67		Y/D 5.05	
Z/D 3.94		Z/D 3.94		Z/D 5.05	

RUN No.160

U_j	13.73	ρ_j/ρ_∞	1.96
U_∞	25.9	M	1.04

X/D	Z/D	-0.44	0.0	0.44	0.88	1.32	1.76	2.20
1.5			49.6					
4.25		31.6	35.4	32.1	25.8	17.6	16.6	24.8
6.53		25.3	28.7	26.8	21.2	15.5	15.0	20.2
10.86		19.7	21.7	20.7	18.1	15.0	14.5	17.1
15.16		16.6	18.1	17.6	16.0	14.5	13.9	15.5
23.78		14.5	15.0	14.5	13.9	13.4	13.4	13.9
37.32		12.3	12.3	12.9	12.3	12.3	12.3	12.3
54.64		11.3	11.3	11.3		11.3	11.3	
73.72			10.7	10.7		9.6	10.2	
91.23			10.2				9.6	
108.56			9.6				9.1	

RUN No.161

U_j	9.72	ρ_j/ρ_∞	1.95
U_∞	25.9	M	0.73

X/D	Z/D	-0.44	0.0	0.44	0.88	1.32	1.76	2.20
1.5			42.5					
4.25		24.9	26.4	21.9	14.1	9.2	10.8	19.8
6.53		19.9	19.9	16.7	11.3	8.0	9.7	15.1
10.86		14.1	14.1	13.0	10.3	8.0	8.6	10.8
15.16		11.3	11.3	11.3	9.2	8.0	8.0	9.2
23.78		9.7	9.2	9.2	8.6	8.0	8.0	8.6
37.32		8.6	8.0	8.0	8.0	8.0	8.0	8.0
54.64		8.0	7.5				8.0	8.0
73.72			6.9	7.5				8.0
91.23			6.9		7.5			7.5
108.56			6.3					6.9

RUN No.161A

U_j	9.72	ρ_j/ρ_∞	1.97
U_∞	25.9	M	0.74

X/D	Z/D	-0.44	0.0	0.44	0.88	1.32	1.76	2.20
1.5			43.5					
4.25		25.5	28.4	24.0	16.9	11.1	13.3	21.5
6.53		20.0	21.5	18.4	13.3	9.5	11.7	17.4
10.86		14.3	14.8	13.8	11.1	9.0	9.5	12.2
15.16		11.6	12.2	11.6	10.6	8.4	7.9	10.0
23.78		9.5	9.5	9.0	9.0	8.4	7.9	7.3
37.32		8.4	8.4	8.4	7.9	7.9	7.9	8.4
54.64			7.3					7.9
73.72			7.3					7.3
91.23			6.8					6.8
108.56			6.2					6.2

RUN No.162

U_j	6.48	ρ_j/ρ_∞	1.95
U_∞	25.9	M	0.49

X/D	Z/D	-0.44	0.0	0.44	0.88	1.32	1.76	2.20
1.5			63.0					
4.25		40.9	45.4	38.7	30.2	18.2	17.1	29.2
6.53		28.7	32.1	27.3	20.7	14.5	13.9	20.7
10.86		18.7	20.7	18.7	14.5	10.7	10.2	13.9
15.16		14.5	16.1	14.5	11.8	9.6	9.6	11.3
23.78		11.3	11.8	10.7	9.6	8.5	8.5	9.6
37.32		9.1	9.1	8.5	8.0	8.0	8.0	8.0
54.64		8.0	8.0	7.4	7.4			6.9
73.72			6.9					6.3
91.23			6.9					5.8
108.56			6.3					5.8

RUN No.163

U_j	27.46	ρ_j/ρ_∞	1.97
U_∞	25.9	M	2.09

X/D	Z/D	-0.44	0.0	0.44	0.88	1.32	1.76	2.20
1.5		17.5						
4.25		13.2	15.9	13.2	8.2	3.1	1.8	7.1
6.53		13.2	14.8	12.6	9.9	6.5	11.0	8.7
10.86		14.8	15.4	14.3	12.6	11.5	13.7	12.1
15.16		16.4	16.4	15.4	14.8	14.3	15.9	14.8
23.78		18.0	17.5	17.0	15.9	15.9	15.9	16.4
37.32		17.5	17.5	17.0	16.4	15.9	15.9	17.0
54.64		16.4	16.4	15.9	15.9	15.4	15.4	16.4
73.72		15.4	15.4	15.4	14.8	14.8	14.8	15.9
91.23		14.8	14.3	14.3				
108.56		13.7						

RUN No.164

U_j	23.06	ρ_j/ρ_∞	1.97
U_∞	25.9	M	1.75

X/D	Z/D	-0.44	0.0	0.44	0.88	1.32	1.76	2.20
1.5		27.9						
4.25		18.3	22.9	18.8	12.4	6.3	5.2	10.2
6.53		16.7	19.8	17.2	13.0	9.1	5.8	11.3
10.86		16.2	17.8	16.2	14.6	13.0	12.4	13.5
15.16		16.7	17.2	16.7	15.6	15.1	14.6	14.6
23.78		17.2	17.2	16.7	16.2	16.2	16.2	16.2
37.32		16.7	16.7	16.2	16.2	16.2	16.2	16.2
54.64		15.6	15.6	15.1	15.1	15.1	15.1	15.1
73.72		14.6						
91.23		14.1						
108.56		13.5						

RUN No.165

U_j	18.14	ρ_j/ρ_∞	1.97
U_∞	25.9	M	1.38

X/D	Z/D	-0.44	0.0	0.44	0.88	1.32	1.76	2.20
1.5		40.2						
4.25		25.9	31.8	27.4	19.9	12.4	11.3	18.3
6.53		21.9	25.9	23.4	18.3	12.9	12.4	16.7
10.86		18.8	20.9	20.3	17.2	15.1	14.6	16.2
15.16		17.2	18.8	18.3	16.2	15.7	15.1	15.7
23.78		16.2	16.2	16.2	15.7	15.7	15.1	15.7
37.32		14.6	14.6	14.6	14.6	14.6	15.6	14.6
54.64		13.5	13.5					
73.72		12.5						
91.23		11.9						
108.56		11.3						

RUN No.166

U_j	32.13	ρ_j/ρ_∞	1.98
U_∞	25.9	M	2.45

X/D	Z/D	-0.44	0.0	0.44	0.88	1.32	1.76	2.20
1.5		8.9						
4.25		7.3	9.5	8.4	5.7	2.8	1.8	5.7
6.53		9.5	10.0	9.5	7.8	6.8	6.2	7.8
10.86		13.7	13.7	12.7	12.1	12.1	11.6	12.1
15.16		16.8	16.3	15.8	15.3	14.7	14.7	14.7
23.78		17.9	17.9	17.3	17.3	16.8	16.8	16.8
37.32		18.4	18.4	17.9	17.3	17.3	16.8	17.3
54.64		17.9	17.9	17.9	17.3	17.3	16.8	17.3
73.72		16.8	16.8	16.8	16.8	16.8	16.3	16.8
91.23		16.3						
108.56		15.8						

RUN No.167

U_j	38.34	ρ_j/ρ_∞	1.97
U_∞	25.9	M	2.91

$x/D \quad z/D$	0.0
1.5	5.2
4.25	6.3
6.53	8.5
10.86	13.8
15.16	17.5
23.78	18.4
37.32	18.4
54.64	18.4
73.72	18.0
91.23	17.5
108.56	16.4

RUN No.180		U_j		18.14		U_∞		25.9	
		RUN No.180/1							
		X/D 4.25 ρ_j/ρ_∞ 1.96 M 1.37							
		X/D 6.53 ρ_j/ρ_∞ 1.98 M 1.39							
		X/D 10.86 ρ_j/ρ_∞ 1.99 M 1.39							
		X/D 15.16 ρ_j/ρ_∞ 1.99 M 1.39							
	Z/D	-0.44	0.0	0.44	0.88	1.32	1.76	2.20	U/U_∞ 0.0
	Y/D	0.00	0.06	0.17	0.44	0.72	1.00	1.28	U/U_∞ 0.0
		22.6	28.0	27.5	20.2	11.5	12.0	18.2	-
		25.6	29.4	25.1	15.1	9.9	11.5	20.2	0.47
		26.1	30.3	26.1	17.2	9.9	10.9	19.7	0.52
		29.9	32.7	31.3	23.1	10.9	10.9	23.6	0.5
		31.7	33.6	33.6	27.5	10.9	13.1	26.5	0.49
		34.1	35.4	35.0	28.5	10.9	12.0	28.9	0.54
		35.0	36.8	35.4	27.0	8.3	8.3	26.5	0.68
		35.0	35.9	32.2	21.2	5.1	5.6	21.2	0.84
		24.1	28.5	24.6	12.5	2.3	2.3	13.1	0.95
		12.0	15.1	12.5	5.1	0.6	0.6	4.5	0.99
		3.4	5.6	4.0	1.2	0.2	0.2	1.2	0.1
		0.6	1.2	0.6	0.1	0.1	0.1	0.1	0.1

RUN No.182		U _j 13.73		U _∞ 25.9	
Run No.182/1		Run No.182/2		Run No.182/3	
X/D	4.25	X/D	15.16	X/D	60.61
ρ_j/ρ_∞	1.97	ρ_j/ρ_∞	1.97	ρ_j/ρ_∞	2.00
M	1.05	M	1.04	M	1.06
Y/D	0.0	Y/D	0.0	Y/D	0.0
Z/D	0.0	Z/D	0.0	Z/D	0.0
0.00	34.6	0.00	27.9	0.00	22.5
0.06	32.3	0.06	27.0	0.06	20.4
0.17	35.5	0.39	27.7	0.39	19.9
0.44	35.9	0.67	27.7	0.47	19.9
0.72	36.4	0.94	27.2	0.94	18.9
1.00	35.5	1.22	26.7	1.50	16.3
1.28	33.2	1.50	22.3	2.05	12.0
1.55	25.2	1.78	18.3	2.61	4.1
1.83	13.6	2.05	5.1	3.17	0.7
2.11	4.7	2.33	1.2		
2.39	0.7				

RUN No.183		U _j 9.72		U _∞ 25.9	
Run No.183/1		Run No.183/2		Run No.183/3	
X/D	4.25	X/D	15.16	X/D	60.61
ρ_j/ρ_∞	1.97	ρ_j/ρ_∞	1.97	ρ_j/ρ_∞	1.99
M	0.74	M	0.74	M	0.75
Y/D	0.0	Y/D	0.0	Y/D	0.0
Z/D	0.0	Z/D	0.0	Z/D	0.0
0.00	28.1	0.00	19.2	0.00	14.1
0.06	29.0	0.06	18.8	0.06	14.1
0.17	29.9	0.39	20.8	0.39	14.1
0.44	32.3	0.67	21.3	0.67	14.1
0.72	31.3	0.94	19.8	0.94	14.1
1.00	28.5	1.22	19.2	1.22	13.6
1.28	24.2	1.50	18.2	1.78	12.0
1.55	16.2	1.78	15.2	2.33	6.4
1.83	7.2	2.05	8.9	2.61	3.0
2.11	1.8	2.33	3.4	2.89	0.7
2.39	0.1	2.61	0.7		

[illegible]

RUN No.200

U_j	6.48	ρ_j/ρ_∞	1.94
U_∞	25.9	M	0.48

X/D	Z/D	-0.44	0.0	0.44	0.88	1.32	1.76	2.20
1.5	53.7							
4.25	34.2							
6.53	26.4							
10.56	18.8							
15.16	14.6							
23.78	10.8							
37.32	8.0							
54.64	6.9							
73.72	5.8							
91.23	5.2							
108.56	4.7							

RUN No.201

U_j	9.72	ρ_j/ρ_∞	1.97
U_∞	25.9	M	0.74

X/D	Z/D	-0.44	0.0	0.44	0.88	1.32	1.76	2.20
1.5	30.3							
4.25	26.5							
6.53	21.5							
10.86	16.9							
15.16	13.8							
23.78	11.1							
37.32	9.5							
54.64	7.9							
73.72	7.3							
91.23	6.8							
108.56	6.2							

RUN No.202

U_j	13.73	ρ_j/ρ_∞	1.96
U_∞	25.9	M	1.04

X/D	Z/D	-0.44	0.0	0.44	0.88	1.32	1.76	2.20
1.5	35.5							
4.25	26.1							
6.53	22.6							
10.56	19.5							
15.16	17.5							
23.78	15.4							
37.32	13.3							
54.64	12.2							
73.72	11.1							
91.23	10.6							
108.56	10.1							

RUN No.203

U_j	18.14	ρ_j/ρ_∞	1.97
U_∞	25.9	M	1.38

X/D	Z/D	-0.44	0.0	0.44	0.88	1.32	1.76	2.20
1.5	26.0							
4.25	21.0							
6.53	19.5							
10.86	18.0							
15.16	17.5							
23.78	16.4							
37.32	15.9							
54.64	14.3							
73.72	13.2							
91.23	12.7							
108.56	12.2							

RUN No.204

U_j	27.46	ρ_j/ρ_∞	1.96
U_∞	25.9	M	2.08

X/D	Z/D	-0.44	0.0	0.44	0.88	1.32	1.76	2.20
1.5		11.9	13.0	11.9	8.1	5.3	5.3	8.6
4.25		11.9	13.0	11.9	8.1	5.3	5.3	8.6
6.53		12.4	13.0	12.4	10.8	9.2	9.2	10.8
10.86		15.1	14.6	14.1	14.1	14.1	14.1	14.6
15.16		16.7	16.7	16.7	16.7	16.2	16.2	16.7
23.78		18.3	17.8	17.8	17.8	17.8	17.8	17.8
37.32		17.8	17.8	17.8	17.8	17.8	17.8	17.8
54.64		17.3	17.3	17.3	17.3	17.3	17.3	17.3
73.72		16.7	16.7	16.7	16.7	16.7	16.7	16.7
91.23		16.2	16.2	16.2	16.2	16.2	16.2	16.2
108.56		15.1	15.1	15.1	15.1	15.1	15.1	15.1

RUN No.205

U_j	23.06	ρ_j/ρ_∞	1.96
U_∞	25.9	M	1.75

X/D	Z/D	-0.44	0.0	0.44	0.88	1.32	1.76	2.20
1.5		15.7	17.8	16.2	11.4	6.9	6.9	11.4
4.25		15.7	17.8	16.2	11.4	6.9	6.9	11.4
6.53		15.2	16.7	15.7	13.0	10.8	11.4	13.5
10.86		16.7	16.7	16.7	15.7	15.2	15.2	15.7
15.16		17.3	17.3	17.3	16.7	16.7	16.7	16.7
23.78		17.8	17.8	17.8	17.8	17.8	17.3	17.3
37.32		17.3	17.3	17.3	17.3	17.3	17.3	17.3
54.64		16.7	16.7	16.7	16.7	16.7	16.7	16.7
73.72		16.2	16.2	16.2	16.2	16.2	16.2	16.2
91.23		15.7	15.7	15.7	15.7	15.7	15.7	15.7
108.56		15.2	15.2	15.2	15.2	15.2	15.2	15.2

RUN No.206

U_j	32.13	ρ_j/ρ_∞	1.96
U_∞	25.9	M	2.44

X/D	Z/D	-0.44	0.0	0.44	0.88	1.32	1.76
1.5		7.5	9.7	8.6	5.8	3.5	3.5
4.25		8.0	9.7	8.6	5.8	3.5	3.5
6.53		10.8	10.8	10.8	9.2	9.2	8.6
10.86		15.2	14.6	14.6	14.6	14.6	14.1
15.16		17.8	17.3	16.7	16.7	16.7	16.7
23.78		18.9	18.9	18.9	18.3	18.3	17.8
37.32		18.9	18.9	18.9	18.9	18.3	18.3
54.64		18.2	18.9	18.9	18.3	18.3	18.3
73.72		17.8	17.8	17.8	17.8	17.8	17.8
91.23		17.3	17.3	17.3	17.3	17.3	17.3
108.56		16.7	16.7	16.7	16.7	16.7	16.7

RUN No.207

U_j	38.34	ρ_j/ρ_∞	1.97
U_∞	25.9	M	2.92

X/D	Z/D	0.0
1.5		3.0
4.25		6.4
6.53		9.7
10.86		15.6
15.16		17.7
23.78		18.8
37.32		19.3
54.64		19.8
73.72		18.8
91.23		18.3
108.56		17.2

RUN No. 220

X/D	4.25	U_j	18.14	ρ_j/ρ_∞	1.96
		U_∞	25.9	M	1.37

Y/D	Z/D	
0.0	0.0	
0.056	20.5	
0.222	21.6	
0.389	22.6	
0.667	27.0	
0.944	29.9	
1.222	31.8	
1.5	34.6	
1.778	36.9	
2.055	36.0	
2.333	28.5	
2.611	17.4	
2.889	7.4	
3.167	1.8	
	0.1	

RUN No. 221

X/D	4.25	U_j	32.13	ρ_j/ρ_∞	1.98
		U_∞	25.9	M	2.46

Y/D	Z/D	
0.0	0.0	
0.056	7.8	
0.222	8.4	
0.389	12.1	
0.667	14.2	
0.944	18.8	
1.222	21.4	
1.5	23.8	
1.778	27.2	
2.055	32.0	
2.333	37.0	
2.611	39.3	
2.889	39.7	
3.167	36.6	
3.444	30.1	
3.722	21.4	
4.0	11.0	
4.278	4.6	
	0.6	

RUN No.240

U_j	6.48	ρ_j/ρ_∞	1.97
U_∞	25.9	M	0.49

X/D	Z/D	-0.44	0.0	0.44	0.88	1.32	1.76	2.20
1.5			56.2					
4.25		34.5	36.3	30.0	21.9	8.2	13.9	27.6
6.53		27.2	27.6	23.4	18.0	11.9	16.5	22.4
10.86		19.9	19.4	16.5	13.9	12.4	14.9	18.0
15.16		15.9	15.4	13.9	12.4	11.9	13.4	14.4
23.78		10.3	11.3	10.3	10.3	10.8	11.9	
37.32		8.7	8.7	8.7	8.7	8.7	8.7	
54.64			7.1					7.1
73.72			6.1					
91.23			5.5					
108.56			-					

RUN No.241

U_j	9.72	ρ_j/ρ_∞	1.98
U_∞	25.9	M	0.74

X/D	Z/D	-0.44	0.0	0.44	0.88	1.32	1.76	2.20
1.5			34.8					
4.25		27.1	29.4	24.7	17.4	6.6	8.7	20.8
6.53		23.3	24.2	20.8	15.3	9.2	12.3	18.9
10.86		18.4	18.4	15.9	12.8	11.3	13.3	16.4
15.16		15.3	15.3	13.8	12.3	11.3	12.8	14.4
23.78		12.3	12.3	11.3	11.3	11.3	11.8	12.3
37.32		10.3	10.3	9.7	10.3	10.3	10.3	
54.64		8.7	9.2	9.2	9.2	9.2	9.2	
73.72			8.2					
91.23			7.6					
108.56			7.1					

RUN No.242

U_j	13.73	ρ_j/ρ_∞	1.97
U_∞	25.9	M	1.05

X/D	Z/D	-0.44	0.0	0.44	0.88	1.32	1.76	2.20
1.5			36.6					
4.25		28.0	30.3	27.1	20.3	10.8	12.8	22.3
6.53		24.2	26.1	23.2	18.9	14.4	15.9	20.8
10.86		20.8	20.8	18.9	16.9	15.9	16.9	18.9
15.16		18.4	18.4	17.4	16.4	15.9	16.4	17.4
23.78		15.3	15.3	15.3	14.8	15.3	15.3	15.3
37.32		13.4	13.4	13.4	13.4	13.4	13.4	
54.64			11.8					
73.72			10.8					
91.23			9.7					
108.56			9.2					

RUN No.243

U_j	18.14	ρ_j/ρ_∞	1.97
U_∞	25.9	M	1.38

X/D	Z/D	-0.44	0.0	0.44	0.88	1.32	1.76	2.20
1.5			27.1					
4.25		21.8	23.8	21.3	14.9	8.7	9.7	16.9
6.53		19.9	21.3	18.9	14.9	12.3	13.4	16.4
10.86		17.4	18.4	16.9	15.4	14.9	15.9	16.9
15.16		15.9	16.9	16.4	15.9	15.9	16.4	16.9
23.78		15.9	15.9	15.9	15.9	15.9	16.4	16.4
37.32		14.9	14.9	14.9	14.9	14.9	14.9	
54.64		13.4	13.4	13.9				
73.72			12.3	12.9				
91.23			11.8					11.8
108.56			10.8					11.3

RUN No. 244

U_j	23.06	ρ_j/ρ_∞	1.92
U_∞	25.9	M	1.71

X/D	Z/D	-0.44	0.0	0.44	0.88	1.32	1.76	2.20
1.5		17.0						
4.25		14.4	16.0	13.8	9.5	5.2	5.7	10.1
6.53		13.8	14.4	13.3	10.6	9.0	9.5	11.7
10.86		14.9	14.9	13.8	13.3	12.8	13.3	13.8
15.16		15.5	14.9	14.9	14.9	14.9	15.5	15.5
23.78		16.5	16.0	16.0	16.0	16.0	16.0	16.5
37.32		16.0	16.0	16.0	16.0	16.0	16.0	16.0
54.64		14.9	14.9	15.5	15.5	15.5	15.5	15.5
73.72			14.4					14.4
91.23			13.8					13.8
108.56			13.3					13.3

RUN No. 245

U_j	27.46	ρ_j/ρ_∞	1.95
U_∞	25.9	M	2.07

X/D	Z/D	-0.44	0.0	0.44	0.88	1.32	1.76	2.20
1.5								
4.25		12.6						
6.53		11.0	12.6	11.0	7.2	4.0	4.0	7.8
10.86		11.5	12.0	11.0	8.9	8.3	7.8	9.4
15.16		13.6	13.6	13.1	13.1	12.6	12.6	13.1
23.78		15.2	15.2	15.2	15.2	15.2	15.2	15.2
37.32		16.7	16.7	16.7	16.7	17.2	16.7	16.7
54.64		16.2	16.2	16.7	17.2	17.2	17.2	17.2
73.72			15.7		15.7	15.7	15.7	15.7
91.23			15.2		15.2	15.2	15.2	15.2
108.56			14.7		14.7	14.7	14.7	14.7

RUN No. 246

U_j	32.13	ρ_j/ρ_∞	1.97
U_∞	25.9	M	2.44

X/D	Z/D	-0.44	0.0	0.44	0.88	1.32	1.76	2.20
1.5								
4.25		8.8	8.8	8.8	6.1	4.0	4.5	6.6
6.53		10.4	10.4	9.9	9.3	8.3	8.3	8.8
10.86		14.6	14.6	13.5	13.5	13.5	13.5	13.5
15.16		17.1	16.6	16.1	16.1	16.6	16.1	16.1
23.78		18.6	18.1	18.1	18.1	18.1	18.1	17.6
37.32		18.6	18.1	18.6	18.6	18.6	18.6	18.6
54.64		18.1	18.1	18.1	18.1	18.1	18.1	18.1
73.72			17.6					17.6
91.23			17.1					17.1
108.56			16.6					16.6

RUN No. 247

U_j	38.34	ρ_j/ρ_∞	1.97
U_∞	25.9	M	2.92

X/D	Z/D	0.0
1.5		5.1
4.25		6.2
6.53		8.3
10.86		13.6
15.16		16.2
23.78		17.8
37.32		18.3
54.64		18.3
73.72		17.7
91.23		17.3
108.56		16.7

RUN No.260			U _∞ 25.9			U _j 18.14		
260/1			260/2			260/3		
X/D	4.25		X/D	23.78		X/D	60.61	
ρ _j /ρ _∞	1.97		ρ _j /ρ _∞	1.98		ρ _j /ρ _∞	1.98	
M	1.38		M	1.38		M	1.39	
Y/D	Z/D	0.0	Y/D	Z/D	0.0	Y/D	Z/D	0.0
0.00	25.4		0.00	15.3		0.00	12.1	
0.06	23.4		0.06	15.8		0.06	11.6	
0.24	26.9		0.33	16.3		0.5	11.6	
0.52	28.8		0.61	16.3		1.05	11.0	
0.80	32.6		0.89	15.8		1.61	9.5	
1.08	35.3		1.17	15.3		2.17	8.4	
1.35	37.6		1.44	14.3		2.72	7.3	
1.63	36.7		1.72	13.7		3.28	5.6	
1.91	28.3		2.00	12.7		3.83	4.6	
2.19	17.9		2.28	11.6		4.39	2.3	
2.47	6.2		2.55	10.0		4.94	1.2	
2.74	2.3		2.83	8.4				
3.02	0.6		3.11	6.8				
			3.39	5.1				
			3.67	3.4				
			3.94	1.8				
			4.22	0.6				

RUN No.261			U _∞ 25.9			U _j 32.13		
261/1			261/2			261/3		
X/D	4.25		X/D	23.78		X/D	60.61	
ρ _j /ρ _∞	1.98		ρ _j /ρ _∞	1.98		ρ _j /ρ _∞	1.99	
M	2.45		M	2.45		M	2.46	
Y/D	Z/D	0.0	Y/D	Z/D	0.0	Y/D	Z/D	0.0
0.00	8.9		0.00	16.8		0.00	16.7	
0.06	10.0		0.06	16.8		0.06	15.7	
0.24	12.6		0.61	17.3		0.50	16.3	
0.52	17.4		1.17	17.8		1.05	15.2	
0.80	20.9		1.72	17.8		1.61	14.7	
1.08	23.9		2.28	16.8		2.17	14.2	
1.35	26.8		2.83	16.3		2.72	13.1	
1.63	30.6		3.37	14.3		3.28	12.0	
1.91	35.3		3.94	11.6		3.83	10.5	
2.19	39.8		4.50	7.3		4.39	8.9	
2.47	40.2		5.05	3.4		4.94	7.2	
2.74	38.4		5.61	1.2		5.50	5.1	
3.02	31.1					6.05	2.9	
3.30	22.9					6.61	1.2	
3.58	12.6							
3.85	5.7							
4.13	1.2							
4.41	0.1							

RUN No.280

U_j	6.48	ρ_j/ρ_∞	1.96
U_∞	25.9	M	0.49

X/D	Z/D	-0.44	0.0	0.44	0.88	1.32	1.76	2.20
1.5	70.9	79.3	62.5	22.7	1.2	0.1	41.6	
4.25	52.7	64.1	54.3	33.3	7.9	6.8	34.8	
6.53	40.3	49.0	38.5	27.1	9.6	13.3	31.0	
10.86	30.5	32.9	26.6	19.6	12.3	17.0	25.2	
15.16	23.2	25.2	21.1	16.5	12.8	15.4	19.6	
23.78	17.5	17.0	14.4	12.8	12.8	13.9	16.5	
37.42	12.3	11.8	11.2	10.7	11.2	11.8	12.3	
54.64	9.6	9.6	9.6	9.6	9.6	9.6	9.6	
73.72		7.9	7.9					
91.23		6.5						
108.56		6.3						

RUN No.281

U_j	13.73	ρ_j/ρ_∞	1.99
U_∞	25.9	M	1.05

X/D	Z/D	-0.44	0.0	0.44	0.88	1.32	1.76	2.20
1.5	18.7	19.7	19.7	2.9	0.1	0.1	3.4	
4.25	27.6	40.0	32.7	13.6	1.8	1.2	9.4	
6.53	27.6	39.5	30.9	15.7	4.0	3.4	13.6	
10.86	27.6	34.6	25.6	15.7	7.8	9.4	17.2	
15.16	24.2	29.0	23.2	15.7	11.5	12.0	17.7	
23.78	21.2	21.2	17.7	14.1	13.1	15.1	18.7	
37.32	16.7	16.2	14.7	14.1	14.7	15.1	16.7	
54.64	13.6	13.6	13.6	13.6	13.6	14.1	14.1	
73.72	12.0	12.0	12.0	12.0	12.0	12.6	12.6	
91.23		11.5						
108.56		11.0						

RUN No.282

U_j	18.14	ρ_j/ρ_∞	1.99
U_∞	25.9	M	1.39

X/D	Z/D	-0.44	0.0	0.44	0.88	1.32	1.76	2.20
1.5	3.4	5.1	4.0	0.1	0.0	0.0	0.1	
4.25	9.9	17.2	11.0	1.8	0.1	0.1	2.3	
6.53	12.6	19.7	12.6	3.4	0.6	0.6	3.9	
10.86	15.7	19.7	12.0	5.1	2.3	2.9	7.3	
15.16	15.1	18.2	12.6	7.3	4.5	5.1	8.9	
23.78	15.1	14.7	11.5	8.9	8.3	9.4	12.0	
37.32	13.6	12.6	12.0	11.5	11.5	12.0	13.1	
54.64	12.6	12.6	12.6	12.6	12.6	12.6	12.6	
73.72	12.0							
91.23	12.0							
108.56	11.5							

RUN No.283

U_j	32.13	ρ_j/ρ_∞	1.96
U_∞	25.9	M	2.43

X/D	Z/D	-0.44	0.0	0.44	0.88	1.32	1.76	2.20
1.5	0.7	0.7	0.7	0.1	0.1	0.1	0.1	
4.25	0.7	1.2	1.2	0.1	0.1	0.1	0.7	
6.53	1.2	2.4	1.8	0.7	0.1	0.1	0.7	
10.86	2.9	4.0	2.9	1.8	0.7	0.7	1.2	
15.16	4.0	4.6	4.6	2.9	2.4	2.4	2.4	
23.78	8.4	7.9	7.9	7.4	7.4	7.4	7.4	
37.32	12.8	11.7	12.8	12.8	13.3	13.3	12.8	
54.64	14.4	14.4	14.4	14.4	14.9	14.9	14.9	
73.72	14.9	14.9						
91.23	14.9							
108.56	14.9							

RUN No. 300			U_{∞} 25.9			U_j 18.14		
300/1			300/2			300/3		
X/D	4.25		X/D	23.78		X/D	60.61	
ρ_j/ρ_{∞}	1.99		ρ_j/ρ_{∞}	1.98		ρ_j/ρ_{∞}	1.98	
M	1.39		M	1.39		M	1.38	
Y/D	0.0	Z/D	Y/D	0.0	Z/D	Y/D	0.0	Z/D
0.00	17.4		0.00	13.8		0.00	12.8	
0.06	23.5		0.06	14.3		0.06	12.8	
0.30	37.6		0.50	16.4		0.61	12.3	
0.58	40.8		1.05	19.0		1.17	12.8	
0.85	45.1		1.61	20.0		1.72	11.2	
1.13	48.7		2.17	15.9		2.28	10.1	
1.41	40.8		2.72	9.0		2.83	7.4	
1.69	7.9		3.28	1.2		3.39	5.2	
1.97	0.7		3.83	0.1		3.94	2.4	
						4.50	1.8	

RUN No. 301			U_{∞} 25.9			U_j 32.13		
301/1			301/2			301/3		
X/D	4.25		X/D	23.78		X/D	60.61	
ρ_j/ρ_{∞}	1.94		ρ_j/ρ_{∞}	1.98		ρ_j/ρ_{∞}	2.07	
M	2.41		M	2.46		M	2.57	
Y/D	0.0	Z/D	Y/D	0.0	Z/D	Y/D	0.0	Z/D
0.00	0.7		0.00	8.4		0.00	14.7	
0.06	0.7		0.06	9.5		0.06	14.7	
0.30	3.5		0.50	13.3		0.61	15.2	
0.58	10.3		1.06	16.4		1.17	15.7	
0.85	19.4		1.61	19.0		1.72	15.2	
1.13	23.6		2.17	21.1		2.28	15.2	
1.41	36.3		2.72	20.5		2.83	14.2	
1.69	63.7		3.28	16.4		3.39	12.7	
1.97	60.3		3.83	9.0		3.94	9.6	
2.24	25.6		4.39	2.3		4.50	7.0	
2.52	0.1		4.94	0.7		5.06	3.9	
						5.61	2.2	
						6.17	1.2	

RUN No.320

U_j	6.48	ρ_j/ρ_∞	1.96
U_∞	25.9	M	0.49

X/D	Z/D	-0.44	0.0	0.44	0.88	1.32	1.76	2.20
1.5	63.3	72.2	52.1	14.6	0.6	11.5	46.7	
4.25	46.3	50.4	38.5	21.2	4.0	20.7	36.7	
6.53	35.8	37.6	28.9	18.7	9.4	21.2	30.3	
10.86	26.0	26.0	20.2	14.6	13.5	18.7	23.1	
15.16	20.7	20.2	16.7	13.6	13.0	15.1	18.7	
23.78	14.6	14.1	12.0	14.5	12.0	13.5	15.1	
37.32	10.4	9.9	9.9	9.9	9.9	10.4	10.9	
54.64	7.8	8.3	8.3	8.3	8.3	8.3	8.3	
73.72	6.7	7.7						
91.23		6.1						
108.56		5.6						

RUN No.321

U_j	13.73	ρ_j/ρ_∞	1.97
U_∞	25.9	M	1.04

X/D	Z/D	-0.44	0.0	0.44	0.88	1.32	1.76	2.20
1.5	29.0	34.9	18.4	2.3	0.6	1.7	13.9	
4.25	31.3	38.5	29.4	12.4	2.3	5.0	19.9	
6.53	28.5	34.9	27.1	15.4	6.1	10.0	21.9	
10.86	26.2	28.1	21.9	15.4	11.3	14.9	20.9	
15.16	22.4	24.3	20.4	15.9	13.9	15.4	18.9	
23.78	19.4	18.4	16.4	15.4	14.9	16.4	17.9	
37.32	15.9	14.9	14.4	14.4	14.4	14.9	15.9	
54.64		13.4	12.9	13.4	13.4	13.4	13.4	
73.72		11.8	11.8	11.8				
91.23		11.3						
108.56		10.2						

RUN No.322

U_j	18.14	ρ_j/ρ_∞	1.99
U_∞	25.9	M	1.39

X/D	Z/D	-0.44	0.0	0.44	0.88	1.32	1.76	2.20
1.5	13.4	17.1	6.8	0.1	0.0	0.0	4.6	
4.25	17.6	23.2	16.0	4.6	0.1	1.2	7.9	
6.53	17.6	23.2	16.0	6.8	2.4	3.5	10.7	
10.86	18.1	21.2	15.0	9.0	6.3	7.9	13.4	
15.16	16.5	19.1	15.8	11.8	9.6	10.7	13.9	
23.78	16.0	16.0	14.4	13.3	13.4	13.9	15.5	
37.32	15.5	15.5	15.0	15.0	15.0	15.0	15.5	
54.64	14.4	14.4	14.4		14.4		14.4	
73.72		13.4						
91.23		12.9						
108.56		12.3						

RUN No.323

U_j	32.13	ρ_j/ρ_∞	1.97
U_∞	25.9	M	2.45

X/D	Z/D	-0.44	0.0	0.44	0.88	1.32	1.76	2.20
1.5	0.7	1.3	0.1	0.1	0.1	0.1	0.1	
4.25	3.5	5.2	3.5	0.7	0.1	0.7	2.4	
6.53	5.2	6.3	5.2	1.8	1.3	1.8	3.5	
10.86	6.3	7.5	5.8	5.2	4.7	4.7	5.2	
15.16	8.6	9.1	9.1	9.7	9.7	9.7	9.1	
23.78	13.5	13.5	14.5	15.1	15.6	15.6	14.5	
37.32	16.7	16.7	16.7	17.2	17.7	17.7	16.7	
54.64	17.2	17.2	17.2	17.7	17.7	17.2	17.2	
73.72	16.7	17.2		17.2	17.2			
91.23		17.2						
108.56		16.1						

RUN No. 340			U _∞ 25.9			U _j 18.14		
340/1			340/2			340/3		
X/D	4.25		X/D	23.78		X/D	60.61	
ρ _j /ρ _∞	1.99		ρ _j /ρ _∞	1.98		ρ _j /ρ _∞	1.98	
M	1.39		M	1.39		M	1.38	
Y/D	0.0	0.0	Y/D	0.0	0.0	Y/D	0.0	0.0
Z/D			Z/D			Z/D		
0.00	25.0		0.00	15.9		0.00	14.9	
0.06	25.5		0.06	16.4		0.06	14.4	
0.33	37.0		0.33	16.9		0.67	13.8	
0.61	42.3		0.61	16.9		1.22	12.8	
0.89	44.9		0.89	17.4		1.78	11.7	
1.17	44.9		1.17	17.4		2.33	9.5	
1.44	42.3		1.44	16.9		2.89	7.9	
1.72	23.1		1.72	16.4		3.44	5.2	
2.00	7.7		2.00	14.9		4.0	2.9	
2.28	2.3		2.28	13.3		4.55	1.2	
			2.56	10.6				
			2.83	7.4				
			3.11	4.6				
			3.39	1.8				
			3.67	0.7				
			3.94	0.1				

RUN No. 341			U _∞ 25.9			U _j 32.13		
341/1			341/2			341/3		
X/D	4.25		X/D	23.78		X/D	60.61	
ρ _j /ρ _∞	1.95		ρ _j /ρ _∞	1.96		ρ _j /ρ _∞	1.96	
M	2.43		M	2.43		M	2.43	
Y/D	0.0	0.0	Y/D	0.0	0.0	Y/D	0.0	0.0
Z/D			Z/D			Z/D		
0.00	5.7		0.00	14.5		0.00	18.2	
0.06	5.7		0.06	15.0		0.06	18.2	
0.61	27.4		0.61	17.7		0.67	18.2	
0.89	35.4		1.17	19.2		1.22	17.7	
1.17	34.9		1.72	19.7		1.78	16.6	
1.44	34.9		2.28	19.7		2.33	15.6	
1.72	35.9		2.83	17.7		2.89	14.0	
2.00	38.1		3.39	14.0		3.44	11.8	
2.28	33.5		3.94	8.5		4.00	9.6	
2.56	21.5		4.50	2.9		4.55	6.9	
2.83	6.8		5.05	0.7		5.11	4.1	
3.11	1.8					5.67	2.4	
						6.22	1.2	

RUN No.360

U_j	6.48	ρ_j/ρ_∞	1.93
U_∞	25.9	M	0.48

X/D	Z/D	-0.44	0.0	0.44	0.88	1.32	1.76	2.20
1.5		60.0	84.4	56.4	29.5	9.0	13.3	26.1
4.25		48.5	65.7	49.0	21.6	9.0	9.0	31.9
6.53		39.3	49.0	38.9	25.1	12.2	15.4	31.0
10.86		25.1	29.0	23.1	15.4	11.2	13.3	21.1
15.16		18.0	20.6	17.0	12.8	10.1	11.2	15.4
23.78		13.3	13.3	11.7	9.6	9.0	10.6	12.2
37.32		9.6	9.6	9.0	8.4	8.4	9.0	9.6
54.64		7.9	7.9	7.9	7.3	7.3	7.9	7.9
73.72			6.8					
91.23			6.3					
108.56			5.7					

RUN No.361

U_j	13.73	ρ_j/ρ_∞	1.96
U_∞	25.9	M	1.04

X/D	Z/D	-0.44	0.0	0.44	0.88	1.32	1.76	2.20
1.5		38.1	44.7	31.8	8.8	1.8	4.0	21.7
4.25		34.0	46.4	36.3	17.2	5.6	7.8	24.1
6.53		30.4	39.9	31.3	18.2	7.8	10.9	22.7
10.86		26.1	30.8	24.1	15.1	9.9	13.1	20.7
15.16		20.7	25.6	21.7	15.1	11.5	13.1	17.2
23.78		18.2	19.2	17.2	14.1	12.5	13.6	16.7
37.32		14.6	15.1	14.6	13.1	12.5	13.6	14.6
54.64		13.1	13.1		12.5	12.0	12.5	13.1
73.72		12.0	12.0					12.0
91.23			10.9					10.9
108.56			10.4					

RUN No.362

U_j	18.14	ρ_j/ρ_∞	1.95
U_∞	25.9	M	1.37

X/D	Z/D	-0.44	0.0	0.44	0.88	1.32	1.76	2.20
1.5		19.3	24.7	14.7	1.8	0.1	0.6	7.3
4.25		18.8	30.5	19.8	5.1	0.6	1.2	9.9
6.53		18.2	29.1	20.8	7.3	1.8	2.9	11.5
10.86		18.8	24.7	17.8	8.9	4.5	7.3	14.2
15.16		16.2	21.3	18.2	11.5	7.8	9.4	13.6
23.78		15.7	17.8	15.7	12.6	11.0	12.1	14.7
37.32		14.7	15.2	14.7	13.6	13.6	14.7	
54.64		13.6	14.2	14.2	14.2	14.2	14.2	14.2
73.72		13.1	13.1					
91.23			12.6					
108.56			12.1					

RUN No.363

U_j	32.13	ρ_j/ρ_∞	1.96
U_∞	25.9	M	2.43

X/D	Z/D	-0.44	0.0	0.44	0.88	1.32	1.76	2.20
1.5		0.7	0.7	0.1	0.1	0.1	0.0	0.1
4.25		4.5	6.2	3.5	1.2	0.1	0.7	1.7
6.53		5.7	7.3	5.1	1.7	0.7	1.2	2.3
10.86		6.7	8.4	6.2	4.5	4.0	4.5	5.0
15.16		7.3	8.9	8.9	8.9	8.9	9.4	8.9
23.78		12.1	12.7	13.7	15.3	15.8	15.8	15.3
37.32		16.3	16.3	16.3	17.3	17.3	18.4	17.8
54.64		16.8	16.8	16.8	17.3	17.8	17.8	17.8
73.72		16.8	16.8	17.3	17.3	17.3	17.3	17.3
91.23			16.8					
108.56			16.3					16.8

[illegible]

RUN No.380 (continued)				U_j	18.14	U_∞	25.9								
<u>RUN No.380/3</u>				<u>RUN No.380/4</u>				<u>RUN No.380/5</u>				<u>RUN No.380/6</u>			
X/D		10.86		X/D		15.16		X/D		23.78		X/D		60.61	
ρ_j/ρ_∞		1.95		ρ_j/ρ_∞		1.97		ρ_j/ρ_∞		1.97		ρ_j/ρ_∞		1.96	
M		1.37		M		1.38		M		1.38		M		1.37	
Z/D	U/U $_\infty$	0.0	0.0	Z/D	U/U $_\infty$	0.0	0.0	Z/D	U/U $_\infty$	0.0	0.0	Z/D	U/U $_\infty$	0.0	0.0
Y/D	Y/D			Y/D	Y/D			Y/D	Y/D			Y/D	Y/D		
0.00	23.7	-		0.00	21.5	-		0.00	17.4	-		0.00	14.9	-	
0.06	24.2	0.67		0.06	21.0	0.68		0.06	18.0	0.68		0.06	14.3	0.71	
0.44	27.1	0.77		0.44	22.0	0.78		0.44	18.0	0.70		0.44	14.3	0.77	
0.72	29.1	0.76		1.00	23.5	0.78		1.00	18.5	0.82		1.00	13.3	0.85	
1.28	28.6	0.73		1.28	22.0	0.78		1.55	15.9	0.84		1.55	11.7	-	
1.55	25.7	0.79		1.55	21.0	0.80		2.11	12.7	0.91		2.11	9.6	0.93	
1.83	20.1	0.88		2.11	13.5	0.92		2.67	6.2	0.98		2.67	7.4	-	
2.39	5.2	0.99		2.67	2.4	0.99		3.22	1.2	1.00		3.22	4.0	0.98	
2.67	0.7	1.00		2.94	0.1	1.00		3.78	0.1	1.00		3.78	1.8	-	
2.94	0.1	1.00										4.33	0.7	0.98	
												4.89	0.1	1.00	

<div> <div>RUN No.381</div> <div>U_j 32.13</div> <div>U_∞ 25.9</div> </div>											
RUN No.381/1			RUN No.381/2			RUN No.381/3			RUN No.381/4		
<div> <div>X/D 4.25</div> <div>ρ_j/ρ_∞ 1.96</div> <div>M 2.43</div> </div>			<div> <div>X/D 6.53</div> <div>ρ_j/ρ_∞ 1.96</div> <div>M 2.43</div> </div>			<div> <div>X/D 10.86</div> <div>ρ_j/ρ_∞ 1.95</div> <div>M 2.42</div> </div>			<div> <div>X/D 15.16</div> <div>ρ_j/ρ_∞ 1.97</div> <div>M 2.44</div> </div>		
RUN No.381/5			RUN No.381/6			RUN No.381/7			RUN No.381/8		
<div> <div>X/D 23.78</div> <div>ρ_j/ρ_∞ 1.97</div> <div>M 2.44</div> </div>			<div> <div>X/D 23.78</div> <div>ρ_j/ρ_∞ 1.97</div> <div>M 2.44</div> </div>			<div> <div>X/D 23.78</div> <div>ρ_j/ρ_∞ 1.97</div> <div>M 2.44</div> </div>			<div> <div>X/D 23.78</div> <div>ρ_j/ρ_∞ 1.97</div> <div>M 2.44</div> </div>		
U/U _∞			U/U _∞			U/U _∞			U/U _∞		
0.0 0.0			0.0 0.0			0.0 0.0			0.0 0.0		
Z/D			Z/D			Z/D			Z/D		
0.00			0.00			0.00			0.00		
0.06			0.06			0.06			0.06		
0.25			0.44			0.44			0.44		
0.53			0.72			1.00			1.00		
0.81			1.00			1.55			1.55		
1.09			1.28			1.83			2.11		
1.37			1.56			2.11			2.67		
1.64			1.83			2.39			3.22		
1.92			2.11			2.67			3.78		
2.20			2.39			2.54			4.05		
2.48			2.67			3.22			4.61		
2.75			2.94			3.50			4.89		
3.03			3.22			3.78			5.44		
			3.50			4.05					
			1.2			0.0					
			1.00			1.00					
			1.01			1.00					
			2.4			2.4					
			8.0			8.0					
			16.5			16.5					
			22.7			22.7					
			26.6			26.6					
			28.6			28.6					
			28.1			28.1					
			0.92			0.92					
			0.86			0.86					
			0.83			0.83					
			0.88			0.88					
			0.92			0.92					
			0.97			0.97					
			0.96			0.96					
			0.99			0.99					
			0.95			0.95					
			0.93			0.93					
			0.78			0.78					
			0.80			0.80					
			10.1			10.1					
			9.0			9.0					
			-			-					
			0.78			0.78					
			0.96			0.96					
			0.97			0.97					
			0.98			0.98					
			0.78			0.78					
			0.77			0.77					
			11.0			11.0					
			6.7			6.7					
			0.00			0.00					

RUN No.400

		U_j 6.48		ρ_j/ρ_∞ 1.95	
		U_∞ 25.9		M 0.49	
X/D	Z/D	-0.44	0.0	0.44	0.88 1.32 1.76 2.20
1.5	72.1	89.3	85.0	46.9	2.9 11.6 16.4
4.25	46.9	78.4	50.3	17.4	8.4 5.7 13.8
6.53	52.3	71.8	52.3	23.5	10.6 7.3 30.3
10.86	37.2	42.6	33.6	22.0	14.3 11.6 28.3
15.16	23.0	28.3	23.5	15.9	12.2 13.2 17.9
23.78	15.9	16.4	14.3	11.6	10.6 11.6 13.8
37.32	10.6	11.1	10.6	9.5	9.5 10.0 10.6
54.64	8.4	8.9	8.4	8.4	8.4 8.4 8.4
73.72	7.3	7.3	7.9	7.3	7.3 7.3 7.3
91.23	6.2	6.8	6.8		
108.56		6.2			

RUN No.401

		U_j 13.73		ρ_j/ρ_∞ 1.96	
		U_∞ 25.9		M 1.04	
X/D	Z/D	-0.44	0.0	0.44	0.88 1.32 1.76 2.20
1.5	18.5				
4.25	34.6	24.6	21.6	4.0	0.6 1.2 4.6
6.53	34.2	50.5	36.5	10.6	1.8 1.2 11.1
10.86	31.3	50.9	35.5	17.5	2.9 1.8 14.3
15.16	25.5	40.1	28.0	14.9	4.6 6.3 17.5
23.78	21.1	33.2	26.5	16.4	7.9 7.3 14.9
37.32	15.9	24.6	19.5	13.3	9.5 9.5 15.4
54.64	12.8	17.0	14.9	12.2	11.1 11.1 13.8
73.72	11.7	13.3	12.8	12.2	11.7 12.2 12.2
91.23	11.1	12.2			
108.56	10.0	11.1			

RUN No.402

		U_j 18.14		ρ_j/ρ_∞ 1.96	
		U_∞ 25.9		M 1.37	
X/D	Z/D	-0.44	0.0	0.44	0.88 1.32 1.76 2.20
1.5	2.3	5.6	4.0	1.2	0.0 0.0 0.6
4.25	11.0	21.7	8.9	1.2	0.6 0.6 0.6
6.53	12.0	23.2	11.5	1.7	0.6 0.6 1.2
10.86	14.1	23.7	12.0	2.9	0.6 0.6 3.4
15.16	13.1	20.7	15.1	5.1	0.6 1.2 4.5
23.78	14.1	18.2	13.6	6.7	2.9 4.5 8.9
37.32	13.6	14.6	13.1	9.4	7.8 8.3 11.0
54.64	12.0	13.1	12.6	11.5	10.5 11.5 11.5
73.72	12.6	12.6	12.6	12.0	12.0 12.0 12.0
91.23	12.0				
108.56	12.0				

RUN No.403

		U_j 32.13		ρ_j/ρ_∞ 1.96	
		U_∞ 25.9		M 2.43	
X/D	Z/D	-0.44	0.0	0.44	0.88 1.32 1.76 2.20
1.5	0.6	1.2	0.6	0.1	0.1 0.1 0.1
4.25	0.1	0.6	0.6	0.1	0.1 0.1 0.1
6.53	0.6	2.3	1.7	0.6	0.1 0.1 0.1
10.86	2.3	3.9	3.4	1.2	0.6 0.6 0.6
15.16	1.7	5.0	5.5	2.8	1.2 1.2 1.7
23.78	5.0	6.6	7.1	5.0	5.0 5.0 5.0
37.32	9.2	8.7	9.7	9.7	10.8 10.3 10.3
54.64	11.8	11.8	11.8	11.8	12.8 12.8 12.3
73.72	12.3	12.3	12.3	13.3	13.3 13.3 12.8
91.23	12.3	12.3			
108.56	12.8				

Run No. 420		U_j	18.14	U_∞	25.9														
		Run No. 420/1																	
		X/D 4.25 ρ_j/ρ_∞ 1.97 M 1.38																	
Z/D Y/D	-0.44	0.0	0.44	0.88	1.32	1.76	2.20	2.65	3.09	3.53	3.97	U/U_∞ 0.0							
0.00	9.8	24.0	10.9	1.2	0.1	0.1	0.7	11.9	22.1	9.3	12.0	-	Y/D	Z/D					
0.06	26.4	32.5	32.1	7.7	0.1	0.7	15.5	32.5	33.5	33.0	6.1	0.67	0.00	U/U_∞					
0.17	33.9	35.7	37.0	10.9	1.2	0.7	19.1	39.2	40.1	41.4	8.8	0.75	0.06	0.76					
0.44	54.3	46.9	52.3	22.1	0.1	0.7	35.7	54.3	49.4	52.7	18.1	0.73	0.39	0.83					
0.72	55.8	50.6	53.5	25.5	0.1	2.3	42.3	52.7	50.3	54.6	19.1	0.65	0.67	0.73					
1.00	54.3	52.3	52.3	17.1	0.1	0.7	33.9	53.5	52.3	51.5	10.4	0.65	0.94	0.69					
1.28	46.9	51.9	39.7	4.5			13.0	46.9	49.0	34.3	2.3	0.88	1.22	0.75					
1.55	18.1	28.8	10.9	0.1			1.2	15.1	20.6	7.2	0.6	0.97	1.50	0.93					
1.83	1.2	2.3	0.6					1.2	1.2	1.2		1.00	1.78	0.98					
2.11	0.1	0.1								0.6		1.00	2.05	1.00					
												1.00	2.33	1.00					

Run No. 420/2															
X/D 6.53 ρ_j/ρ_∞ 1.98 M 1.39	Y/D Z/D	0.0	U/U_∞ 0.0												
0.00	27.0	-													
0.06	31.7	0.76													
0.39	43.3	0.83													
0.67	47.1	0.73													
0.94	47.6	0.69													
1.22	45.0	0.75													
1.50	34.5	0.93													
1.78	13.6	0.98													
2.05	1.7	1.00													
2.33	1.2	1.00													

Run No. 420/2

 X/D 6.53
 ρ_j/ρ_∞ 1.98
 M 1.39

Y/D	Z/D	U/U_∞
0.00	27.0	-
0.06	31.7	0.76
0.39	43.3	0.83
0.67	47.1	0.73
0.94	47.6	0.69
1.22	45.0	0.75
1.50	34.5	0.93
1.78	13.6	0.98
2.05	1.7	1.00
2.33	1.2	1.00

RUN No. 420 (continued) U_j 18.14 U_∞ 25.9											
Run No. 420/3				Run No. 420/4				Run No. 420/5			
X/D 10.86 ρ_j/ρ_∞ 1.97 M 1.38				X/D 15.16 ρ_j/ρ_∞ 1.97 M 1.38				X/D 23.78 ρ_j/ρ_∞ 1.97 M 1.38			
Y/D	Z/D		U/U_∞	Y/D	Z/D		U/U_∞	Y/D	Z/D		U/U_∞
	0.0	0.0	0.0		0.0	0.0	0.0		0.0	0.0	0.0
0.00	23.7	-	-	0.00	19.9	-	-	0.00	18.8	-	-
0.06	23.7	0.73	0.70	0.06	20.4	0.70	0.69	0.06	18.3	0.06	0.66
0.39	30.9	0.86	0.84	0.39	24.3	0.84	0.82	0.39	19.8	0.50	0.75
0.67	34.6	0.86	0.86	0.67	27.2	0.86	0.86	0.67	21.3	1.05	0.88
0.94	37.3	0.80	0.80	0.94	29.5	0.85	0.86	0.94	22.3	1.61	0.94
1.22	37.3	0.77	0.83	1.22	30.5	0.83	0.86	1.22	22.8	2.17	10.0
1.50	34.1	0.79	0.82	1.50	29.1	0.82	0.85	1.50	22.3	2.72	6.8
1.78	26.1	0.90	0.86	1.78	24.8	0.86	0.86	1.78	20.3	3.28	2.9
2.05	13.1	0.98	0.93	2.05	18.1	0.93	0.91	2.05	16.8	3.83	0.1
2.33	2.3	1.00	0.98	2.33	8.2	0.98	0.95	2.33	13.1	4.11	0.1
2.61	0.1	1.00	1.00	2.61	1.7	1.00	0.98	2.61	6.7		
				2.89	0.1	1.00	1.00	2.89	2.4		
				3.17	0.0	1.00	1.00	3.17	0.6		

[illegible]

RUN No. 440	
U_j	6.48
U_∞	25.9
ρ_j/ρ_∞	1.93
M	0.48

X/D	Z/D	0.0	0.88	1.76	2.64	3.52	4.41	5.29	6.17
4.25		58.4	57.3	54.3	52.7	53.5	53.5	55.5	55.5
6.53		46.9							
10.86		35.9							
15.16		29.9							
23.78		22.3		29.9	28.5	29.0	29.0	28.5	
37.32		18.7							
54.64		15.1							
73.72		13.0							
91.23		11.5							
108.56		11.0	11.5	11.5	11.5	11.0	11.5	11.5	11.0

RUN No. 441

U_j	13.73
U_∞	25.9
ρ_j/ρ_∞	1.96
M	1.04

X/D	Z/D	0.0	0.88	1.76	2.64	3.52	4.41	5.29	6.17
4.25		59.6	59.6	60.3	59.6	59.2	58.8	58.4	57.7
6.53		56.1							
10.86		51.4							
15.16		46.9		47.3	46.9	46.5	46.1	45.7	
23.78		39.7							
37.32		34.9							
54.64		29.9		29.9	30.3	29.9	29.4	28.0	27.6
73.72		25.7							
91.23		23.2							
108.56		20.9	21.8	21.3	20.9	20.9	20.4	19.9	19.4

RUN No. 442

U_j	18.14
U_∞	25.9
ρ_j/ρ_∞	1.95
M	1.36

X/D	Z/D	0.0	0.88	1.76	2.64	3.52	4.41	5.29	6.17
4.25		56.8	56.8	57.6	57.3	57.3	56.8	55.6	55.2
6.53		55.2							
10.86		52.1							
15.16		48.8		49.2	48.8	48.0	47.2	45.5	43.8
23.78		42.1							
37.32		38.2							
54.64		33.2		33.7	33.7	32.8	31.4	29.6	27.7
73.72		28.6							
91.23		26.3							
108.56		24.4	23.9	23.9	23.4	22.9	22.4	21.9	20.5

RUN No. 443

U_j	32.13
U_∞	25.9
ρ_j/ρ_∞	1.93
M	2.39

X/D	Z/D	0.0	0.88	1.76	2.64	3.52	4.41	5.29
4.25		36.3	36.7	37.2	37.6	37.2	37.2	37.2
6.53		37.2						
10.86		36.3						
15.16		34.9		34.9	34.0	33.1	31.7	28.9
23.78		32.7						
37.32		29.4						
54.64		26.5		26.5	26.1	25.1	24.1	23.1
73.72		24.1						
91.23		22.1						
108.56		20.6	20.6	20.2	19.7	18.1	17.7	

RUN No.460

		U _j 6.48		ρ_j/ρ_∞ 1.94			
		U _∞ 25.9		M 0.48			
X/D	Z/D	-0.37	0.0	0.37	0.73	1.10	1.47 1.84 5.00 12.5
4.25	34.4	38.1	35.4	30.2	26.9	27.3	32.6 38.1 38.6
6.53	25.4	27.3	25.4	21.9	19.4	20.4	23.9
10.86	17.9	18.4	16.8	15.3	14.2	15.3	16.8
15.16	14.2	14.2	13.7	12.7	12.7	13.7	14.2
23.78	10.6	11.1	11.1	10.6	10.0	10.6	11.1
37.32	8.9	8.9	8.9	8.9	8.9	8.9	7.3 7.3
54.64	7.3						7.9
73.72	6.2						6.2
91.23	5.7						5.7
108.56	5.1						4.0 4.0

RUN No.461

		U _j 18.14		ρ_j/ρ_∞ 1.93			
		U _∞ 25.9		M 1.02			
X/D	Z/D	-0.37	0.0	0.37	0.74	1.10	1.47 1.84
4.25	26.8	28.3	25.9	22.0	19.0	20.0	23.4
6.53	23.4	24.4	23.0	21.0	19.5	20.0	22.5
10.86	21.0	21.0	21.0	19.5	19.0	19.5	20.0
15.16	19.5	19.5	19.0	18.5	18.0	18.0	18.5
23.78	16.5		16.5	16.5	16.5	16.5	16.5
37.32	15.0		15.0	15.0	15.0	15.0	15.0
54.64	13.5						
73.72	12.4						
91.23	11.4						
108.56	10.8						

RUN No.462

		U _j 18.14		ρ_j/ρ_∞ 1.96			
		U _∞ 25.9		M 1.37			
X/D	Z/D	-0.37	0.0	0.37	0.73	1.10	1.47 1.84 2.50 3.75 5.00 6.25 7.50 8.75 10.0 12.5
4.25	22.6	24.6	23.1	19.1	15.9	16.4	19.6 24.1 12.5 22.6 13.3 23.6 11.8 22.1 24.1
6.53	22.1	23.1	22.6	20.6	19.6	19.6	20.6
10.86	22.6	23.1	22.6	21.6	21.6	21.6	21.6
15.16	22.1	22.1	22.1	21.6	21.6	21.6	21.6
37.32	18.5	19.1	19.1	18.5	19.6	18.5	19.1 18.5 17.5 18.0 18.0 17.5 18.0 17.5
54.64	17.0		17.0			17.0	
73.72	15.4					15.4	
91.23	14.4					14.4	
108.56	13.3					13.3	13.3 13.3 13.3 12.8 12.8 12.8 12.8 12.8 12.8

RUN No. 463

U_j	32.13	ρ_j/ρ_∞	1.95
U_∞	25.9	M	2.42

X/D	Z/D	-0.37	0.0	0.37	0.73	1.10	1.47	1.84	2.50	3.75	5.00	6.25	7.50	8.75	10.0	12.5
4.25		10.8	11.8	12.3	13.4	12.9	12.3	11.3	11.4	8.2	7.2	7.2	7.2	9.3	7.2	2.0
6.53		17.4	17.9	18.5	18.9	18.5	18.7	17.9								
10.86		20.4	20.9	20.9	20.9	20.9	20.9	21.4								
15.15		21.4	21.4	21.9	21.4	21.9	21.9	21.9								
37.32		21.4	21.4	21.9	21.9	21.9	21.9	21.9	22.0	21.5	21.5	21.0	20.0	20.5	21.0	20.5
54.64		20.9		20.9												
73.72		19.9						19.9								
91.23		18.9														
108.56		18.5						18.5	18.1	18.1	18.1	18.1	17.5	18.1	17.5	17.5

RUN No. 480

RUN No. 480									
		U_j		6.48		ρ_j/ρ_∞		1.94	
		U_∞		25.9		M		0.49	
X/D	Z/D	-0.55	0.0	0.55	1.10	1.65	2.20	2.75	11.25
4.25		31.5	36.5	33.3	23.1	13.2	13.2	22.6	37.3
6.53		22.6	26.4	24.0	16.3	11.2	11.2	17.8	
10.86		15.7	17.8	15.2	10.7	7.5	8.6	12.2	17.7
15.16		11.7	13.7	11.7	8.6	6.5	7.0	9.7	
23.78		9.1	9.7	8.1	5.5	5.5	6.5	8.1	9.1
37.32		6.5	6.5	6.0	5.5	5.0	5.5	6.5	
54.64		5.0	5.5	5.0	5.0	5.0	5.0	5.0	5.0
73.72		4.4	4.4	4.4	4.4	4.4	4.4	4.4	
91.23			4.4	4.4					4.4
108.56			3.9						

RUN No. 481

RUN No.481		U_j 13.73		ρ_j/ρ_∞ 1.94				
		U_∞ 25.9		M 1.03				
Z/D	X/D	-0.55	0.0	0.55	1.10	1.65	2.20	2.75
4.25		24.5	30.1	25.9	14.2	6.5	6.5	14.7
6.53		21.2	25.9	22.1	12.7	6.5	7.0	13.2
10.86		17.3	20.2	16.7	10.2	6.5	7.6	12.7
15.16		14.2	16.3	14.2	10.2	7.0	7.6	11.2
23.78		11.2	12.2	10.7	8.6	7.6	8.1	10.2
37.32		9.1	9.6	8.6	8.1	8.1	8.1	9.1
54.64		8.1	8.1	8.1	7.6	7.6	8.1	8.1
73.72			7.6		7.6	7.6	7.6	7.6
91.23			7.0					
108.56			6.5					

RUN No. 482

RUN No. 482		U_j 18.14		ρ_j/ρ_∞ 1.96				
		U_∞ 25.9		M 1.37				
X/D	Z/D	-0.55	0.0	0.55	1.10	1.65	2.20	2.75
4.25		18.1	24.7	20.0	9.1	2.8	3.3	10.1
6.53		16.1	21.0	17.1	8.5	3.3	3.8	10.1
10.86		14.1	17.1	13.6	8.0	4.9	5.9	10.6
15.16		12.1	14.1	12.1	9.1	5.9	6.5	10.1
23.78		10.6	11.1	10.1	8.5	7.5	7.0	9.5
37.32		9.5	9.5	9.5	9.1	9.1	9.1	9.5
54.64		9.1	9.1	9.1	9.1	9.1	9.1	9.1
73.72		8.5	8.5					
91.23		8.5						
108.56		8.0						

RUN No. 483

RUN No.483									
		U _j 32.13		ρ _j /ρ _∞ 1.95					
		U _∞ 25.9		M 2.42					
X/D	Z/D	-0.55	0.0	0.55	1.10	1.65	2.20	2.75	11.25
4.25		2.8	4.3	2.8	0.6	0.1	0.1	1.7	3.32
6.53		2.8	3.9	2.8	0.6	0.1	0.6	1.7	
10.86		2.8	3.3	2.8	1.7	1.2	1.7	2.8	4.30
15.16		3.3	3.9	3.9	3.3	2.8	3.3	4.3	
23.78		5.4	5.4	5.4	6.0	6.0	6.5	6.0	
37.32		8.0	8.0	8.0	8.6	8.6	9.1	9.6	
54.64		9.1	9.1		9.6	9.6	9.6	9.6	10.1
73.72		9.6	9.6		9.6				
91.23		10.1							10.6
108.56		9.6							

RUN No. 500				
U _j 6.48		ρ_j/ρ_∞ 1.92		
U _∞ 25.9		M 0.48		
X/D	Z/D	-0.73	0.0	0.73 1.47 2.20 2.94
4.25	27.9	36.5	30.2	14.8 1.2 1.7
6.53	20.2	26.5	21.7	11.7 2.8 2.8
10.86	14.8	18.3	14.3	8.1 2.8 2.8
15.16	11.2	13.7	11.2	6.5 2.8 3.3
23.78	8.7	7.6	7.0	4.4 2.2 3.3
37.32	6.5	6.5	5.5	3.9 2.8 3.9
54.64	5.5	4.9	4.4	3.3 3.3 3.9
73.72	4.4	4.4	4.4	3.3 3.3 3.9
91.23	3.9	3.9	3.3	3.3 3.3 3.3
108.56	3.3	3.3	3.3	3.3 3.3 3.3

RUN No. 502				
U _j 18.14		ρ_j/ρ_∞ 1.95		
U _∞ 25.9		M 1.37		
X/D	Z/D	-0.73	0.0	0.73 1.47 2.20 2.94 3.67
4.25	13.5	22.3	13.5	2.2 0.6 0.6 3.3
6.53	12.5	19.9	12.5	3.3 0.1 0.6 4.3
10.86	11.5	15.5	10.5	3.3 1.1 1.1 5.4
15.16	10.0	13.5	10.0	3.8 1.1 1.7 5.4
23.78	9.5	10.5	7.9	4.3 2.2 3.3 6.9
37.32	7.9	8.5	6.9	4.8 3.8 4.8 6.9
54.64	6.9	6.9	5.9	5.4 4.8 5.4 6.4
73.72	6.4	5.9	5.4	5.4 5.4 5.4 5.9
91.23	5.9	5.9	5.9	5.9 5.9 5.9 5.9
108.56	5.9	5.9	5.9	5.9 5.9 5.9 5.9

RUN No. 501				
U _j 13.73		ρ_j/ρ_∞ 1.93		
U _∞ 25.9		M 1.03		
X/D	Z/D	-0.73	0.0	0.73 1.47 2.20 2.94 3.67
4.25	22.0	30.4	23.0	8.0 2.2 1.7 9.1
6.53	19.1	25.3	19.1	8.0 2.8 2.8 9.1
10.86	16.1	20.1	15.7	7.0 2.8 3.3 10.6
15.16	13.6	16.7	13.2	7.5 3.3 3.8 8.6
23.78	10.6	10.6	9.6	5.9 3.3 4.9 8.6
37.32	9.1	9.6	8.0	5.9 4.9 5.9 8.0
54.64	7.5	7.5	6.5	5.9 5.4 5.9 7.5
73.72	6.5	6.5	5.9	5.9 5.9 6.5 6.5
91.23	5.9	5.9	5.9	5.9 5.9 5.9 5.9
108.56	5.4	5.4	5.4	5.9 5.4 5.4 5.4

RUN No. 503				
U _j 32.13		ρ_j/ρ_∞ 1.95		
U _∞ 25.9		M 2.42		
X/D	Z/D	-0.73	0.0	0.73 1.47 2.20 2.94 3.67
4.25	0.6	2.8	1.7	0.1 0.1 0.6 0.1
6.53	0.1	2.2	1.7	0.1 0.1 0.1 0.1
10.86	0.1	2.2	1.7	0.1 0.1 0.1 0.6
15.16	0.6	2.2	1.7	0.6 0.1 0.1 1.2
23.78	0.6	2.2	1.7	1.2 0.1 0.1 1.2
37.32	1.2	2.8	2.8	1.7 1.7 1.7 2.2
54.64	2.8	3.8	3.8	3.3 3.3 3.3 3.3
73.72	3.3	4.3	3.8	3.8 3.8 4.9
91.23	3.8	4.9	3.8	3.8 3.8 4.9
108.56	3.8	5.4	3.8	5.4 5.4 5.4 5.4

RUN No.520

U_j	6.48	ρ_j/ρ_∞	1.92
U_∞	25.9	M	0.48
X/D		Z/D	
	0.0	5.51	
4.25	51.6	49.5	
6.53	44.1		
10.86	34.3	32.5	
13.12			
15.16	29.7		
23.78	24.0	22.5	
28.43			
37.32	20.6	17.6	
50.11	18.1		
54.64	15.5	13.5	
73.72			
86.80			
91.23	14.5		
108.56	13.5		

RUN No.521

U_j	13.73	ρ_j/ρ_∞	1.96
U_∞	25.9	M	1.04
X/D		Z/D	
	0.0	5.51	
4.25	61.3	58.3	
6.53	57.5		
10.86	52.5	46.1	
13.12			
15.16	48.6		
23.78	42.4	35.0	
28.43			
37.32	36.3	27.8	
50.11	31.4		
54.64	26.8	21.6	
73.72			
86.80			
91.23	24.5		
108.56	22.1		

RUN No.522

U_j	18.14	ρ_j/ρ_∞	1.94
U_∞	25.9	M	1.36
X/D		Z/D	
	0.0	5.51	
4.25	58.0	55.5	
6.53	56.6		
10.86	53.3	47.1	
13.12			
15.16	49.6		
23.78	44.7	37.0	
28.43			
37.32	39.2	29.5	
50.11	33.5		
54.64	29.5	22.9	
73.72			
86.80			
91.23	26.2		
108.56	23.9		

RUN No.523

U_j	32.13	ρ_j/ρ_∞	1.92
U_∞	25.9	M	2.38
X/D		Z/D	
	0.0	5.51	
4.25	48.0	46.4	
6.53	48.0		
10.86	47.6	44.7	
13.12			
15.16	46.8		
23.78	42.2	37.9	
28.43			
37.32	36.6	30.4	
50.11	31.3		
54.64	27.2	24.4	
73.72			
86.80			
91.23	24.8		
108.56	22.9		